REMOVAL AND RECOVERY OF TOXIC METAL CONTAMINANTS FROM PROCESS EFFLUENTS USING INTEGRATED BIOSORPTION AND ELECTROPLATING

LI CHUN CHIU

Ph.D

The Hong Kong Polytechnic University

2010

THE HONG KONG
POLYTECHNIC UNIVERSITY
香港理工大學

DEPARTMENT OF APPLIED BIOLOGY AND CHEMICAL TECHNOLOGY

Removal and Recovery of Toxic Metal Contaminants from Process Effluents Using Integrated Biosorption and Electroplating

by

LI Chun Chiu

A thesis submitted in partial fulfillment of the requirements

for the degree of

DOCTOR OF PHILOSOPHY

October, 2007

Certificate of Originality

I hereby declare that this thesis is my own work that, to the best of my knowledge and belief, it reproduces no material previously published or written, nor material that has been accepted for the award of any other degree or diploma, except where due acknowledgement has been made in the text.

LI Chun Chiu

Abstract

The research study reported herein aimed to apply *Micrococcus luteus*, an activated sludge bacterial isolate, to the removal and recovery of copper ions from wastewater. The work included optimization of calcium-alginate/polyacrylamide beads for the immobilization of *M. luteus*; development of a fixed-bed biosorption column of the cell-immobilized beads for the treatment of copper-contaminated wastewater; regeneration of the copper-laden beads (copper desorption); characterization of the fixed-bed biosorption and desorption; and, recycling of the desorbed copper in electroplating.

In the optimization of the cell-immobilized beads, a rehydration treatment (40 ^{o}C oven-drying followed by re-immersion in distilled-deionized water) stabilized the beads in a constant volume throughout the sequential batch copper biosorption/desorption cycles. No significant differences were found between the biosorption characteristics of the rehydrated form of the immobilized *M. luteus* (RIM) and those of the untreated beads, including their biosorption capacities, kinetics, equilibrium isotherms and diffusion mechanisms.

Fixed-bed copper biosorption studies showed that the breakthrough (C_e = 4 mg-Cu/L) of the RIM column was deferred by increasing the bed depth and decreasing the influent concentration and the flow rate. The optimal

conditions were a 50 cm bed depth, a 50 mg-Cu/L influent concentration, and a 1 mL/min inlet upward flow rate. The RIM beads in the column revealed better biosorption performances and less shrinkage than the untreated beads. A greater copper removal and a larger treatment volume were demonstrated by the RIM beads in the column reactor, compared with those in the continuous-stirred-tank reactor at the breakthrough and the batch reactor at the equilibrium.

Binary-metal biosorption studies demonstrated the metal-binding preference of the RIM column as Pb(II) > Cu(II) >> Ni(II) > Zn(II). Converging with this order, the overshot biosorption profiles ($C_e/C_o > 1$) of nickel and zinc were observed in the presence of Cu(II) ions, whereas Pb(II) ions promoted the copper overshoot.

The Clark model, the Adams-Bohart model, the Yoon and Nelson model, and the Thomas model were applied to predict the breakthrough profiles of the fixed-bed copper(II) biosorption. The linearized form of the Thomas model provided the better simulations, with large r^2 values, small average percentages of errors, and low variances in the predictions of the process performances.

Of 11 common desorbing materials, $CaCl_2$ displayed a moderate copper desorption ability and a better reusability of the RIM beads in the batch studies. Similar desorption efficiencies were obtained in the fixed-bed studies under different $CaCl_2$ concentrations and inlet flow rates.

The optimal fixed-bed desorption conditions were a 1 M $CaCl_2$ concentration and a 1 mL/min inlet upward flow rate.

The reusability of the RIM column was examined by introducing both synthetic and industrial electroplating wastewater in 10 successive biosorption/desorption cycles. Both the results showed that the copper removal decreased at the initial cycle(s) and remained steady afterward. A lower efficiency was found in the treatment of the industrial wastewater.

The surface chemical composition of the RIM beads in the sequential fixed-bed biosorption and desorption was characterized by X-ray energy-dispersive analysis. The results coupled with the material balance calculation showed that the ion exchange between calcium and copper ions was one of the major mechanisms of the biosorption and desorption in the RIM column.

After a two-step purification process using Na_2SO_4 and Na_2HPO_4, the recovered copper was isolated from the desorption effluent and directly re-used in an acid-sulfate-copper-electroplating process. The study showed that the addition of the recycled copper did not significantly change the properties of the deposited workpieces, including their overall appearance, surface smoothness, deposit distribution, coverage, copper purity on the deposits, and electrical resistance.

In this research studies, the rehydrated form of the Ca-alginate/Polyacrylamide immobilized *Micrococcus luteus* was successfully applied in the fixed-bed column reactor with reasonable copper removal performance, desorption efficiency and biosorbent reusability. The desorbed copper after the purification could be reused in the electroplating process without any significant influence on the plating performances and the deposit characteristics. Thus, this integrated biosorption system could be developed as a promising technology for copper removal and recovery from industrial wastewater, and should be applied further in the practical treatment system.

Acknowledgements

I wish to express my sincere gratitude to Dr. LO Wai-hung, Thomas, for his kind guidance, supervision and suggestions throughout the entire period of this study.

I would like to thank my co-supervisor, Dr. LEUNG Yun-chung, and the Board of Examiners (Chairman; External examiners) for giving valuable comments and suggestions on my research.

I would like to thank Dr. NG Lau-mei, Dr. LAM Kim-hung and my research colleagues for their provisions of helps and academic suggestions.

I would also like to thank my family and friends for their supports and encouragements.

Finally, I would like to thank the Research Committee of the Hong Kong Polytechnic University and the Research Grants Council (RGC) of Hong Kong SAR (China) for funding this project.

Table of Contents

List of Abbreviations

A	Probability of sorbate adsorption
B_i	Biot number
b	Sorption affinity of sorbents (L/mg $_{sorbates}$)
C	Concentration of target sorbates in solution phase of the column (mg/L or mg m^{-3} or mol $_{sorbates}/L_{fluid}$)
C_b	Concentration of sorbates in bulk solution phase surrounding the sorbent particle (mol $_{sorbates}$/L $_{fluid}$) or Effluent concentration of sorbates at the breakthrough (mg/L or mg m^{-3})
C_e or C_∞	Equilibrium concentration of sorbates in the reaction mixture or effluent concentration of sorbates (mg/L or mg m^{-3})
C_o	Initial reactant concentration or influent sorbate concentration (mg/L or mg m^{-3})
C_f	Concentration of sorbates in the sorbent particle in the pore fluid phase (mol $_{sorbates}$/L $_{sorbents}$)
C_t	Reactant concentration at the time t (mg/L or mg m^{-3})
c	Concentration of reactant (mg/L or mg m^{-3})
D_M	Diffusion coefficient of particle in bulk solution phase (cm^2/s)
D_{app}	Apparent diffusion coefficient (cm^2/s)
D	Diffusion coefficient in pore space of the sorbent particle (cm^2/s)
d_p	Mean diameter of the adsorbent particle (cm)
E	Probability of sorbate elution from sorbents
F	Fractional uptake of adsorbates at the time t
G_s	Solution flow rate per unit of the cross-sectional area (m^3 h^{-1} m^{-2})
g	Gravitational acceleration (cm^2/s)

h	Half length of diffusion path (cm)
J	Mass-transfer rate per unit of the reactor volume (mg $_{sorbates}$ h^{-1} m^{-3})
J_p	Diffusion flux in pore space of the sorbent particle
J_μ	Diffusion flux in surface adsorbed phase of the sorbent particle
K	Freundlich constants (mg $_{bound\ sorbates}$/g $_{sorbents}$)
K	Linear isotherm constant (slope of the linear isotherm)
K’	Henry constant
K'_∞	Henry constant at the infinite temperature
k	Reaction rate constant
k_{AB}	Kinetic constant of the Adams-Bohart model (L mg^{-1} h^{-1})
k_{Th}	Rate constant of the Thomas model (L h^{-1} mg^{-1})
k_{YN}	Proportional constant of the Yoon and Nelson model (min^{-1})
k_f	External film diffusion coefficient at the boundary film layer (cm/s)
k^*_f	External film diffusion coefficient of the particles moving at their terminal velocity through the liquid (cm/s)
k_m	Mass transfer coefficient (h^{-1})
k_s	Mass transfer coefficient of sorbate for a stagnant film surrounding sorbent packed inside the fixed-bed column (cm/s)
k_1	Rate constant of first-order kinetic reaction (min^{-1})
k_2	Rate constant of second-order kinetic reaction ($mg^{-1} \cdot L \cdot min^{-1}$)
$k_{2'}$ & $k_{2''}$	Rate constants of ion-exchange processes
k*	Pseudo rate constant
k_1^*	Rate constant of pseudo-first-order reaction (min^{-1})
k_2^*	Rate constant of pseudo-second-order reaction ($g \cdot mg^{-1} \cdot min^{-1}$)
L_a	Mass velocity of sorbent to keep mass-transfer zone stationary (mg h^{-1} m^{-2})

M	Overall packing density of resins (kg m^{-3})
n	Freundlich constants (dimensionless) or number of experimental points
PIM	Primitive (untreated) immobilized *Mircococcus luteus*
Q	Inlet (volumetric) flow rate (L h^{-1})
Q'	Heat of adsorption
q	Sorption capacity of sorbents (mg $_{sorbates}$ or mg $_{sorbates}$/g $_{sorbents}$ or mg $_{sorbates}$/mL $_{sorbents}$)
q_e	Sorption capacity of sorbents at the equilibrium (mg $_{sorbates}$ or mg $_{sorbates}$/g $_{sorbents}$ or mg $_{sorbates}$/mL $_{sorbents}$)
q_o	Maximum sorption capacity of sorbents (mg $_{sorbates}$ or mg $_{sorbates}$/g $_{sorbents}$ or mg $_{sorbates}$/mL $_{sorbents}$)
q_t	Sorption capacity of sorbents at the time t (mg $_{sorbates}$ or mg $_{sorbates}$/g $_{sorbents}$ or mg $_{sorbates}$/mL $_{sorbents}$)
Re	Reynolds number
RIM	Rehydrated form of the immobilized *Mircococcus luteus*
r or r_s	Radius of the spherical sorbent (cm)
S	Cross-sectional area of the column (m^2)
Sc	Schmidt number
Sh	Sherwood number
s	Shape factor of the particle
T	Temperature (K)
t	Reaction time (min or h)
t_b	Service time or Breakthrough time (min or h)
t_e	Exhaustion time (min)
U_o	Linear velocity of the influent flow or linear flow rate of solution phase inside the column packing (m h^{-1} or cm min^{-1} or cm s^{-1})

u_T	Terminal velocity of particle moving through the liquid (cm/s)
V_b	Breakthrough volume (L)
V_e	Exhaustion volume (L)
V_{eff}	Volume of effluent (L)
V_z	Velocity of adsorption zone
v_o	Fractional void volume (porosity) inside the column
v%	Variance
X	Amount of sorbents used (g or mL)
Z	Column bed depth (cm or m)
α	Reaction order
τ	Time required to obtain 50% bed exhaustion (min)
ε	Porosity of the sorbent particle
ε%	Average percentage of errors
ρ	Density of solution (g/cm^3)
ρ_t or ρ	Particle density or density of the adsorbent (g/L or g/cm^3)
μ	Viscosity of solution (g/cm/s)
φ_n	Eigenvalue
ΔC_o (or dC_o)	Incremental change in the contaminant (sorbate) concentration ($mg\ m^{-3}$)
ΔZ (or dZ)	Differential column bed depth (m)
$\Delta c/\Delta t$ (or dc/dt)	Reaction rate (change of the reactant concentration with time during reaction)
C_e/C_t	Dimensionless sorbate concentration in effluent

List of Figures

List of Tables

Chapter 1. Introduction

1.1 Motivations

Heavy metal pollution is one of the most serious global environmental problems, especially when the metals are in the form of aqueous ions. Aqueous heavy metal ions are too highly toxic, non-biodegradable and mobile to disperse easily; they accumulate in organisms and their adverse effects magnify along the food chain through bioaccumulation and bioconcentration. As a result, the problems of heavy metal pollution become unpredictable and uncontrollable, with hundreds of acute and chronic hazards impacting on humans once the metal concentrations exceed normal levels. As indicated by the EPA (2006), an excessive uptake of copper, for instance, can cause Wilson's disease, gastrointestinal disturbance, kidney failure, liver damage and even death. Likewise, the World Health Organization (WHO, 2005) confirmed that nickel has a carcinogenic impact and can cause kidney failure and a list of acute effects, including nausea, vomiting, headaches and weakness. Permanent damage to the human nervous system, kidneys and reproductive system, which is particularly serious in children, has been found in clinical studies of lead (Sheng *et al.*, 2008). Mass zinc poisoning has also been reported by the WHO (2003), with fever, nausea, vomiting, stomach cramps and diarrhea recorded in patients.

These problems are further intensified by a rapid economic growth, especially in developing countries. China is a typical example, with an upsurge in all kinds of heavy metal related industries, including electroplating, the electronic and electrical industries, and battery

manufacturing, heavily supported by government policies in recent decades. Environmental conservation strategies are unable to keep pace with these developments. In particular, an excessive amount of metal-contaminated industrial wastewater is discharged without a proper treatment, resulting in serious heavy metal pollution. Mass poisoning by heavy metals and many related fatal incidents occur frequently. The Chinese government is now working closely with researchers to solve this pollution problem.

Some physico-chemical technologies, such as ion exchange, activated carbon adsorption and chemical precipitation, have been developed and extensively applied to remove heavy metal ions from sewage sources. Researchers believe that these methods can provide reliable performance of heavy metal removals in conditioned environments. The advantages and limitations of these physico-chemical methods are listed in Table 1.1.

Eccles (1995) stated that the general concerns of the treatment process are:

(i) the cost effectiveness of the system installation and operation;

(ii) the reliability of the treatment;

(iii) the robustness of the sequential operation;

(iv) the selectivity of target contaminants;

(v) the simplicity of the system configuration and operation;

(vi) the flexibility in handling fluctuations in both the quality and quantity of sewage;

(vii) the compatibility with existing operations.

Table 1.1. Advantages and limitations of conventional physico-chemical methods for heavy metal removals.

Treatment method	Advantage	Limitation	Reference
Activated carbon adsorption	- High removal efficiency	- Hard to regenerate	Han and Yun (2007)
	- Moderate metal selectivity	- Low tolerance to pH, suspended solids and organics - Narrow working range: above 10 ppm	Eccles (1995)
Ion exchange	- Easy to regenerate	- High cost	Han and Yun (2007)
	- High metal selectivity - Broad working range: below 100 ppm	- Low tolerance to pH, organics and suspended solids	Eccles (1995)
	- High uptake ability - A large volume of sewage can be handled	- High cost - Influences by organics - High sensitivity to solution pH	Ahluwalia and Goyal (2007)
Precipitation		- Slow process rate - Long contact time	Mack *et al.* (2008)
		- Poor separation (filtration) of sludge (suspended precipitate)	Santos *et al.* (2004)
	- Low material cost - High tolerance to suspended solids and organics	- Requires additional processes to meet discharge standards - Low tolerance to pH - Low metal selectivity (pH dependence) - Narrow working range: above 10 ppm	Eccles (1995)
	- Cost effective	- Low removal efficiency at low pH and in the presence of other salts - Produces a large amount of high water-content sludge - High cost of sludge disposal	Ahluwalia and Goyal (2007)

However, only some of these criteria can be met by physico-chemical methods due to their inherent deficiencies. As shown in Table 1.1, a large amount of expensive resins is required in ion-exchange processes; hence, the treatment cost is greatly increased. A poor adsorbent reusability and an ineffective metal regeneration are observed in the activated carbon systems. In view of the precipitation methods, additional processes and costs are necessary to fulfill the discharge standards and handle the toxic sludge. Furthermore, there is no removal preference for metal species in the precipitation process. These limitations draw our attention to the need to develop a new, effective and inexpensive technology for the treatment of heavy metals.

An alternative technology has been proposed that applies biological materials to heavy metal removals. This technique is called 'biosorption'. As reported by Volesky and Holan (1995), it depends on the chemical activities of functional groups (metal-binding sites) on the surface of biological materials. Biomasses, such as activated sludge (Bakkaloglu *et al*., 1998), industrial waste or by-products (Fourest and Roux, 1994) and microbes (Deng *et al*., 2007) are frequently recommended in the biosorption process since they are usually costless, with at least an order of magnitude cheaper than the commercial ion-exchange resin, and require little modification in their preparation (Volesky, 2003). When the metal uptake abilities of these inexpensive biomasses and conventional sorbents (resins and activated carbon) have been compared, similar performance has been found (Cochrane *et al*., 2006; Hawari and Mulligan, 2006a; Lu *et al*., 2007;

Tobin and Roux, 1998). This illustrates that the treatment performance of biosorption is comparable to those of the physico-chemical methods, but the treatment costs are much lower. Multiple-metal biosorption studies have also shown that the biomasses usually have metal-binding preferences, which can greatly promote the selectivity of the treatment processes (Diniz *et al.*, 2007; Zhang and Banks, 2006).

However, Çabuk *et al*. (2007) and Li *et al*. (2008) indicated that the suspended biomass is inefficiently separated from wastewater after the biosorption process. Expensive separation technologies, such as centrifugation and membrane filtration, are required to retain the biomass particles for further recovery of bound metal ions and for reuse in the sequential treatment process. To solve this problem, Chen *et al*. (2005b), Iqbal *et al*. (2007) and Vijayaraghavan *et al*. (2007) suggested that the biomass could be immobilized on inexpensive and/or natural solid supports. They found that the metal uptake ability, biomass-liquid separation and/or compatibility in reactor systems could be significantly enhanced by using immobilized biomass.

Calcium alginate is one of the widely-used immobilization agents because it can be extracted from low-cost algae and bacteria (Nestle and Kimmich, 1996; Pavez *et al*., 2005). Many researchers have found that this bio-polymer contains abundant active metal-binding functional groups (Pavez *et al*., 2005; Stokke *et al*., 1991; Torres *et al*., 2007). This can significantly enhance the ability to remove heavy metals, but the chemical

stability of Ca-alginate is low. Its giant polymer structure is easily destroyed in the presence of common components in the aqueous medium, such as sodium ions (Tanaka and Irie, 1988), magnesium ions (Smidsrød and Skjåk-Bræk, 1990), phosphate ions (Dainty *et al*., 1986) and complexing agents (Khoo and Ting, 2001). Hence, its ability to entrap biomass and the reusability of the immobilized biosorbent are lessened.

Polyacrylamide (PAA) is another common immobilization agent. Andrès *et al.* (1995) and Dos Santos *et al.* (1997) indicated that this polymer is insensitive to different categories of chemicals and has high mechanical strength and cell encapsulation ability. However, the low chemical sensitivity of PAA induces its poor metal uptake ability. Thus, no enhancement of the metal removal is found as comparing the PAA-immobilized biomass with the freely-suspended cells.

Some other concerns and limitations have been discovered also when other immobilization agents are used. This motivates the development of new biomass immobilization techniques for removal of heavy metals from wastewater. Grafting PAA with Ca-alginate gel for the immobilization is a novel and enlightening idea to compensate for the inherent limitations of the immobilization agents. This polymer-grafting immobilization approach certainly facilitates the biomass-liquid separation. Moreover, it may also enhance the ability of heavy metal removals, chemical stability and mechanical strength of the immobilized biosorbents. However, little empirical research has been conducted for removal of heavy metals by this

bi-polymer immobilized biomass in order to confirm these advantages. This stimulates us to further investigate and develop the Ca-alginate/PAA biomass-immobilized beads as an effective metal biosorbent for wastewater treatment.

Volesky (2003) suggested that the development of biosorbents should be directed to substitute expensive ion-exchange resins, the closest rival in the wastewater treatment process. This is due to their similar technological and underlying process principles. In order to introduce the biosorbent into the enormous environmentally-based market as the competitor of the ion-exchange resin, the feasibility of applying the biosorbent in wastewater treatment systems for heavy metal removals should first be assessed. A fixed-bed column system is advisable in this pilot study since this setup is widely used in scale-up ion-exchange processes. Also, it can provide several compelling advantages, for instance, a high process efficiency; a continuous flow operation; virtually unlimited scale-up (by using multiple columns with a parallel and/or serial configuration); no solid/liquid separation; and, in-situ regeneration and washing (Belter *et al*., 1988). Thus, the performance of the biosorbent in the continuous flow fixed-bed column system should be necessarily studied.

Further, desorption of the bound metal ions from the biosorbents should be investigated. Grimm *et al*. (2008) and Hammaini *et al*. (2007) indicated that the importance of the desorption process is its recovery of bound metal ions from biomasses, the concentration of the metal ions from

wastewater and the regeneration of biomasses for re-use in sequential treatment cycles. These are directly related to both reducing and saving the cost of industrial processes. Accordingly, a list of chemicals such as acids, complexing agents and counter cations was examined to determine their suitability in the desorption process. Most researchers are devoting to increase the desorption efficiency and the reusability of biosorbents in their recent investigations. Little experimental work focuses on the reuse of desorbed metals in industrial production processes. This should gain a considerable attention because the reuse of valuable metals from desorption eluant can reduce the resource wastage, the material cost and also the cost of disposing hazardous metal-laden waste products. Although Butter *et al*. (1998) demonstrated that electrolysis was highly feasible to recycle cadmium from desorption eluant, no advanced investigation has been further performed to examine the applicability of the recycled metal powder. Hence, it is worthwhile studying the recovered metal species and applying them to the industrial use.

Based on the aforementioned perspectives, the use of biomasses for removal and recovery of heavy metals could fulfill most requirements of the treatment process as stated by Eccles (1995). The biosorption approach should be further explored and applied in metal-laden wastewater treatment to reduce the adverse environmental impact of heavy-metal pollution. To maximize the treatment efficiency of the biosorption process, biomass immobilization using calcium-alginate/PAA matrix should be investigated and optimized. It would also be worthwhile to develop an efficient metal

recovery process for recycling the bound metal ions and regenerating the biomasses. To reduce the production cost, the reuse of the recovered metal ions in industrial processes should also be investigated.

1.2 Objectives

To develop a novel and economical biosorption process for removal and recovery of heavy metal ions from industrial wastewater, this study uses *Micrococcus luteus*, a Gram-positive bacterium. This bacterium was isolated from the activated sludge of a local sewage treatment works and confirmed to have a good ability to remove copper(II) ions (Wong, 2001). The copper(II) biosorption properties and characterizations of the suspended cells were fully investigated in the previous study. FTIR analysis showed that carboxyl, thiocarbonyl, phosphate, amine and amide functional groups were located on this biomass surface; these groups might be responsible for the copper(II) biosorption. This biomass could be a potent biosorbent for treating copper-contaminated wastewater. However, the suspended *M. luteus* was inefficiently separated from the solution phase after the biosorption. This limited the biomass for further recovery of the bound copper(II) ions and for reuse in sequential treatment processes. Accordingly, the immobilization of *M. luteus* was investigated and optimized in this study. The optimized form of the immobilized *M. luteus* was applied further for development of an integrated wastewater treatment system for copper removal and recovery.

The objectives of this study are as follows:

(i) to optimize the immobilized *M. luteus* and determine its biosorption properties so it can be applied in a fixed-bed copper(II) biosorption process;

(ii) to develop and optimize a fixed-bed column reactor packed with the

optimized biosorbents for maximizing copper removal in wastewater treatment;

(iii) to compare the treatment performance of the column and those of other reactor systems;

(iv) to examine the competitive and overshooting effects of binary metal systems on the fixed-bed biosorption;

(v) to screen a selection of inexpensive agents for desorbing copper(II) ions from the biosorbents and maximize their reusability;

(vi) to optimize the copper(II) desorption process in the column reactor (column regeneration) and maximize the reusability of the column packing for sequential copper removal and recovery;

(vii) to study the biosorption and desorption mechanisms of the fixed-bed column;

(viii) to evaluate the applicability of four mathematical models – the Clark model, the Adams-Bohart model, the Yoon and Nelson model and the Thomas model – commonly used for simulating fixed-bed copper biosorption processes and predicting the treatment performance;

(ix) to examine the applicability of an integrated process for removing and recovering copper from industrial electroplating wastewater using the column reactor, and evaluate its treatment performance and reusability;

(x) to reuse the desorbed copper in the acid copper electroplating process and evaluate the plating performance.

1.3 Organization of thesis

There are a total of six chapters in this dissertation. The chapters of the dissertation are organized as follows:

Chapter 1 Introduction: the current chapter.

Chapter 2 Literature Review: this presents the literature related to the processes of biosorption, desorption and electroplating, and reviews the work in earlier research.

Chapter 3 Materials and Methods: this describes the materials and instruments used in the experiment, and states the experimental procedures used for data collection.

Chapter 4 Results and Discussion: this presents, discusses and interprets the findings obtained in this study.

Chapter 5 Conclusions: this summarizes the major findings of this research.

Chapter 6 Future Studies: this lists the limitations of this research and gives recommendations for future studies.

Chapter 2. Literature Review

2.1 Properties and toxicity of copper

Copper is one of the most frequently used heavy metals. The Copper Development Association (CDA, 2007) reported that in the year 2006, over sixteen million tons of copper ores had been supplied to different areas of industries throughout the world, including electroplating, dyeing, paper-manufacturing, printed-circuit board, electronic and electrical manufacturing. This amount was almost the highest among other heavy metals.

The properties of copper are: atomic number 29; atomic weight 63.54; density 8.9 kg/m^3; melting point 1083.4 ^oC; boiling point 2595 ^oC; reddish metal cubic crystalline form (Aaseth and Norseth, 1986; Tripler, 1974). It is grouped as transition metal. It can exist in a stable form of its metallic state and in ionic forms of monovalent (cuprous) and divalent (cupric) cations. The World Health Organization (WHO, 2004) listed some common copper compounds as follows:

- Copper(II) acetate monohydrate ($Cu(C_2H_3O_2)_2 \cdot H_2O$)
- Copper(II) chloride ($CuCl_2$)
- Copper(II) nitrate trihydrate ($Cu(NO_3)_2 \cdot 3H_2O$)
- Copper(II) oxide (CuO)
- Copper(II) sulfate pentahydrate ($CuSO_4 \cdot 5H_2O$)

The WHO (2004) further suggested that copper concentration in drinking water should be limited to below 2 mg/L. Although the toxicity of copper does not induce any acute fatal effect, its hazards are maximized if

both the bioaccumulation and the highest global consumption of copper couple with each other (CDA, 2007). Excessive uptake of copper can cause Wilson's disease (i.e. symptoms of: kidney failure and liver damage), nausea, vomiting, gastrointestinal bleeding, haematuria, intravascular haemolysis and methaemoglobinaemia (EPA, 2006; WHO, 2004).

In Hong Kong, the major sources of copper contamination come from sewage discharge from electroplating industries, printed circuit board factories, textile and dyeing industries, etc. According to the annual report of the Environmental Protection Department (EPD, 2005), the copper content in the sediment of the Victoria Harbor has remained at a high level, with about 112 to 266 mg-Cu/kg-sediment. This has meant that aquatic life may face a great threat from copper contamination, further inducing a greater impact on humans through the bioaccumulation of copper.

2.2 Conventional technologies for heavy metal wastewater treatment

Physico-chemical technologies such as ion exchange, activated carbon adsorption and precipitation are currently applied for removal of heavy metals from wastewater. Ion exchange is based on displacement reactions between substitutive ions on resins and target metal ions in wastewater. In the case of activated carbon adsorption, the target metal ions can be bound on activated carbon adsorbents through the electrostatic attraction or other intermolecular forces. In precipitation processes, aqueous metal ions can be removed by changing their solubility.

All these methods can provide a reliable performance in removal of heavy metal ions from wastewater. However, Table 1.1 shows that most of these methods are very costly and/or do not completely solve the problem. A typical example is chemical precipitation. This method generates a large volume of toxic sludge and only changes the phase of metal contaminants from aqueous phase to sludge. Thus, additional treatment processes and a huge disposal cost are required.

Recently, many researchers and engineers have been greatly interested in using biological approaches for wastewater treatment. They believed that these technologies can avoid most weaknesses of the physcio-chemical methods. One of the typical examples is to develop biological materials as adsorbents for the heavy metal removal. This technique is called 'biosorption'. The material cost of biosorption is low since the biosorbents are usually acquired from nature, industrial wastes or by-products (Section 2.3.1). Moreover, researchers found that the biosorbents could bind metal ions following their own preference order (Diniz *et al.*, 2008; Zhang and Banks, 2006). Further, a high efficiency of the metal regeneration is demonstrated in the desorption studies of metal-laden biomasses, as shown in Table 2.10 (Section 2.4). By comparing metal (Cu, Cd, Cr(VI), Ni, Pb and Zn) uptake abilities between various biosorbents and conventional sorption materials, lists of reports in the literature are summarized in Tables 2.1 to 2.6. Among these sorbents, the metal uptake abilities of the biomasses are virtually identical to those of the commercial resins, and generally better than those of activated carbon adsorbents. All such data

strongly support the belief that the treatment performance of the biosorption can be comparable to that of the conventional physico-chemical technologies. Thus, the application of the biosorbents should be further explored in the treatment of metal-laden wastewater.

Table 2.1. Comparison of copper uptake capacity of different sorbents.

	Sorbent	Cu uptake (mg/g)	Reference
Activated carbon	*Ceiba pentandra* hull	20.80	Rao *et al.* (2008)
	Granular AC	0.08	An *et al*. (2001)
	Powder AC	0.07	
	Norit® granular AC	19.18	Cochrane *et al.* (2006)
	Rubber wood sawdust	5.73	Kalavathy *et al.* (2005)
Biomass	Crab carapace	19.66	Cochrane *et al.* (2006)
	F. vesiculosus (brown macroalgae)	18.60	
	Immobilized *Micrococcus luteus* (bacterium)	44.26	This study
Commercial resin	Dowex® 50WX4 Fine Mesh	19.80	Cochrane *et al.* (2006)

Table 2.2. Comparison of cadmium uptake capacity of different sorbents.

Sorbent		Cd uptake (mg/g)	Reference
Activated carbon	*Ceiba pentandra*	19.50	Rao *et al.* (2008)
	Granular AC	3.37	An *et al*. (2001)
	Peanut shell	48.70	Wilson *et al.* (2006)
	Powder AC	3.37	An *et al*. (2001)
Biomass	Activated sludge	68.57	Hammaini *et al*. (1999)
	Anaerobic biomass	59.58	Hawari and Mulligan (2006a)
	Ascophyllum nodosum	132.64	Thomas *et al*. (2003)
	Penicillium chrysogenum	56.21	Volesky and Holan (1995)
	Sargassum natans	131.52	Thomas *et al*. (2003)
Commercial resin	Duolite GT-73	105.67	Vaughan *et al*. (2001)

Table 2.3. Comparison of chromium(VI) uptake capacity of different sorbents.

	Sorbent	Cr(VI) uptake (mg/g)	Reference
Activated carbon	Coconut shell (CAC)	4.72	Babel and Kurniawan (2004)
	Coconut shell (CSC)	2.18	
	Coir pith (CPC)	3.60	Namasivayam and Sangeetha (2006)
	Coir pith (ZnCPC)	19.80	
Biomass	*Mucor meihi*	30	Tobin and Roux (1998)
	Pseudomonas sp.	95	Ziagova *et al.* (2007)
	Rhizopus nigricans	40	Bai and Abraham (2002)
	Staphylococcus xylosus	143	Ziagova *et al.* (2007)
Commercial resin	Amberlite strongly acidic cation exchange resin (IRA-200)	32	Tobin and Roux (1998)
	Amberlite weakly acidic cation exchange resin (IRC-50)	18	
	Amberlite strongly basic anion exchange resin (IRA-900)	4	
	Amberlite weakly basic anion exchange resin (IRA-93)	55	

Table 2.4. Comparison of nickel uptake capacity of different sorbents.

Sorbent		Ni uptake (mg/g)	Reference
Activated carbon	Peanut shell	26.40	Wilson *et al.* (2006)
Biomass	Activated sludge	18.19	Hammaini *et al.* (1999)
	Anaerobic biomass	25.82	Hawari and Mulligan (2006a)
	Ascophyllum nodosum	40.50	Thomas *et al.* (2003)
	Sargassum natans	24.06	
Commercial resin	Lewatit TP207	25.82	Brown *et al.* (2000)
	Duolite GT-73	56.93	Vaughan *et al.* (2001)

Table 2.5. Comparison of lead uptake capacity of different sorbents.

Sorbent		Pb uptake (mg/g)	Reference
Activated carbon	*Ceiba pentandra*	25.50	Rao *et al.* (2008)
	Granular AC	16.58	An *et al.* (2001)
	Peanut shell	195.40	Wilson *et al.* (2006)
	Powder AC	26.94	An *et al.* (2001)
Biomass	Activated sludge	89.10	Hammaini *et al.* (1999)
	Anaerobic biomass	259.00	Hawari and Mulligan (2006a)
	Ascophyllum nodosum	271.43	Thomas *et al.* (2003)
	Penicillium chrysogenum	122.25	Volesky and Holan (1995)
	Sargassum natans	252.78	Thomas *et al.* (2003)
Commercial resin	Lewatit TP207	198.91	Brown *et al.* (2000)
	Duolite GT-73	122.25	Vaughan *et al.* (2001)

Table 2.6. Comparison of zinc uptake capacity of different sorbents.

Sorbent		Zn uptake (mg/g)	Reference
Activated carbon	Activated carbons	4.61 – 33.56	Galiatsatou *et al.* (2002)
	Bagasse	31.11	Mohan and Singh (2002)
	C	4.01 – 18.53	
	Centaur HSL	10.08	Chu (2002)
	F-300	6.03	
Biomass	*Bacillus subtilis*	137	Volesky (2003)
	Bentonite	52.91	Mellah and Chegrouche (1997)
	Crab carapace	172.5	Lu *et al.* (2007)
	Fungal biomass	98	Volesky (2003)
	Lignin	95	Bailey *et al.* (1999)
	Scarp rubber	100	Mohan and Singh (2002)
Commercial resin	Amberlite IRC-718	156.89	Reddad *et al.* (2002)
	Amberlite 200	84.98	
	Duolite GT-73	55.56	
	Lewatit TP-207	89.56	

2.3 Biosorption

As discussed in Section 2.2, biosorption is a promising treatment technology for the removal of heavy metals. In the publication of Volesky and Holan (1995), 'biosorption' is defined as passive sorption, precipitation and/or complexation of heavy metal ions on the surface components of biomasses. The term "passive" represents the reactions that are metabolic independent. All the interactions are closely related to chemical activities of both biomass surface and metal ions (Volesky, 2001). Thus, dead cells and other non-living bio-materials can also be used for the metal uptake. Strandbergy *et al.* (1985) further regarded biosorption as an indirect physico-chemical attraction of metal ions on the biomass surface.

The technique of biosorption has been successfully developed as a novel environmental technology for removal of heavy metals from wastewater. It is widely applied in wastewater treatment systems of different industries (Table 2.7). The latest biosorption studies further focus on the removal of organic pollutants and even protein separation as shown in Table 2.8.

Table 2.7. Biosorption in wastewater treatment.

Source of wastewater	Biomass	Treatment performance (mg/g)	Reference
Contaminated harbour seawater and mixed wastewater (containing industrial effluent and agricultural drainage)	*Ulva lactuca* (Green alga)	Cr(VI) removal: 9.01 (the habour seawater); 8.91 (the mixed wastewater)	El-Sikaily *et al.* (2007)
Electroplating wastewater	Chitosan derivatives	Cd removal: 7.95 – 10.99	Sankararamakrishnan *et al.* (2007)
Industrial wastewater	*Cladophora fascicularis*	Cu removal: 13.3 Pb removal: 1.8 Cr removal: 2.8 Cd removal: 0.4	Deng *et al.* (2007)
Ghee industrial wastewater	*Cassia fistula*	Ni removal: 34.8	Hanif *et al.* (2007)
Nickel chrome plating sewage		Ni removal: 166.3	
Battery manufacturing wastewater		Ni removal: 21.2	
Tannery industrial wastewater		Ni removal: 45.2	
Textile wastewater		Ni removal: 31.1	

Table 2.8. Latest investigations of biosorption.

Area of investigation	Biomass	Uptake of target species (mg/g)	Reference
Organics removal	Activated sludge	Humic acid: 2.4 Fulvic acid: 0.24 Phenol: 0.06	Mohan *et al.* (2008)
	Bacillus subtilis	Humic acid: 4.9 Fulvic acid: 0.71 Phenol: 0.20	
	non-viable algal *Spirogyra I02*	Azo dye (Direct Brown 1:1): 3	
	Rhizopus arrhizus	Lindane (Pesticide): 2.7	Cliff *et al.* (2003)
Protein separation	Under investigation	Monoclonal antibodies	Volesky (2003)

2.3.1 Biosorbents

Inexpensive biomasses or biomaterials, such as algae (Deng *et al*., 2007), bacteria (Ansari and Malik, 2007), chaff (Han *et al.*, 2005), chitin (Zhou *et al.*, 2005), fungi (Yan and Viraraghavan, 2001), grape stalk waste (Martínez *et al.*, 2006) and yeast (Skountzou *et al.*, 2003), can all be used for the removal of metal pollutants under a conditioned environment. They are usually collected from activated sludge (Bakkaloglu *et al*., 1998), industrial wastes or by-products (Fourest and Roux, 1992) and nature (Murphy *et al*., 2007), in order to reduce the treatment costs. Wang (2002) further established that the biosorbents demonstrate an outstanding efficiency in the metal removal processes, especially in sewage with a low metal concentration.

In order to develop biomasses as effective metal biosorbents, Volesky (1987 and 2003) stated a list of criteria, as follows:

(i) the biomasses should be cheap and can be easily obtained so as to reduce the material cost and simplify the treatment procedures;

(ii) the biomasses should have appropriate size and form for the metal uptake and even the scale-up application;

(iii) the metal uptake ability of the biomasses should be high enough to perform the effective removal;

(iv) the biomasses should have a high metal selectivity in order to enhance the removal of specific metal species from multi-metal media;

(v) the metal uptake rate of the biomasses should be rapid so as to maintain an efficient treatment process;

(vi) the metal recovery of the biomasses should be economically feasible and should yield a concentrated metal eluent;

(vii) the reusability of the biomasses should be high without demoting the metal biosorption capacity.

2.3.2 Mechanisms of biosorption

In Section 2.3, the biosorption process is defined as a metabolic independent metal binding pathway. Accordingly, countless varieties of living and non-living biomasses should be capable of performing the metal uptake. Baik *et al.* (2002) believed that the biosorption should be contributed mainly from frequently-found bulk molecules on the cell walls and external surface of the biomasses, such as chitin, chitosan, glucan, mannan and some other natural polymers. All these molecules contain

abundant active metal binding sites, like carboxyl, amine, hydroxyl, phosphate and sulfhydryl groups. In the presence of these functional groups, four kinds of biosorption mechanisms have been proposed (Veglio' and Beolchini, 1997). They are ion-exchange, micro-precipitation, physical sorption and surface complexation.

(i) **Ion exchange** is the displacement reaction between ions on the external structure of the biomasses and target metal ions in solution phase. Some of the active sites on the biomass surface may exist in ionic forms attached with light cations like K^+, Na^+, Ca^{2+} and/or Mg^{2+}. These cations can exchange with aqueous-phase metal cations to achieve metal uptake. The ion exchange between aqueous metal ions (Cd^{2+} and Pb^{2+}) and hydrogen ions from protonated *Sargassum glaucescens* biomass (Naddafi *et al.*, 2007) and the release of Ca^{2+} ions from aerobic granules in the Ni^{2+} biosorption (Liu and Xu, 2007) are typical examples. A similar phenomenon is also found in the exchange of metal anions, but the active sites carry positive charges and bind with other anions (such as chloride, sulfate, phosphate and nitrate) before the biosorption, for example, the chromium(VI) ion-exchanges on *Microcystis* cell walls (Pradhan *et al.*, 2007) and saltbush (*Atriplex canescens*) biomass (Sawalha *et al.*, 2006).

(ii) **Mirco-precipitation** is a physical entrapment of precipitated metal species on the polymer matrix of the biomass surface (Šćiban *et al.*,

2006; Veglio' and Beolchini, 1997). This mechanism could be promoted as solution pH reaches the solubility limit of metal ions (Volesky, 2003).

(iii) **Physical sorption** is regarded as the attachment of metal ions on the biomass surface through electrostatic interaction and intermolecular forces (Kasan, 1993). This reaction approach has been identified by the X-ray Photoelectron Spectroscopy (XPS) analysis of C–F interactions in the fluoride biosorption using *Spirogyra IO2* (Mohan *et al.*, 2007).

(iv) **Surface complexation** is the interaction between metal ions and the active sites on the biomass surface. This mechanism is proposed in the surface complexation modeling study of Cr(III)-carboxyl complexes on *Chlorella miniata* biomass (Han *et al.*, 2006) and the X-ray diffraction analysis of heavy metal (Hg, Cu, Pb, Zn and Mn) complexes of chitosan and crosslinked chitosans (Trimukhe and Varma, 2008). The modes of such interaction can be either coordination or chelation. Coordination is the formation of dative covalent bonds between metal ions and lone-pair electrons of the active sites. Chelation is an advanced coordination in which several active sites interact with a single metal ion so as to form a heterocyclic ring.

2.3.3 Factors affecting biosorption

Biomass content, pretreatment of biomass, solution pH, metal concentration, counter cations, anions and organics are the frequently investigated factors in biosorption studies. Many scientists believe that all these factors have significant effects on metal uptakes. These factors would be introduced briefly below.

2.3.3.1 Effect of biomass content

Simmons and Singleton (1996) found that a smaller value of the metal uptake per unit of biomass (biosorption capacity) is obtained at a higher biomass content since the amount of metal ions is the limiting factor under this condition. Also, the electrostatic interaction between biomass particles and the interferences between the binding sites may limit the accessibility of binding sites to metal ions, resulting in a further demotion of the biosorption capacity. In the extreme case, aggregation of biomass particles occurs when an excessive dosage of biomasses is introduced. This results in a significant drop of the metal uptake and even induces settling of the aggregated biomasses from the reaction mixture (Esposito *et al.*, 2001). A lower biomass content is thus preferred in order to maintain a greater distance between the biomass particles and reduce the interaction between them. Then, more binding sites are freely available for the metal uptake (Gadd *et al.*, 1988).

2.3.3.2 Effect of biomass pretreatment

Many researchers usually believe that the biosorption capacity can be enhanced by the pretreatment of biomass. Thus, the scope of some studies has expanded to include the effect of different biomass treatment methods, such as acid treatment (Yetis *et al*., 2000), alkaline treatment (Selatnia *et al*., 2004), heat treatment (Akar *et al*., 2005) and hydrogen peroxide treatment (Pamukoglu and Kargi, 2006). These methods can be generally classified as chemical modifications and physical treatments.

In fact, the effect of the chemical treatments on the biosorption is unpredictable. Baik *et al.* (2002) reported that by using alkaline-treated *Mucor rouxii*, the copper biosorption was promoted. It was due to the exposure of chitosan after the treatment. In another copper biosorption study using chemically-treated *Saccharomyces cerevisiae*, the biosorption capacities of both methanol-treated and formaldehyde-treated biomasses decreased significantly since these chemical agents reduced the number of the active binding sites through esterification of carboxyl groups and methylation of amino groups (Wang, 2002).

A similar phenomenon was observed in the physical treatments. A destructive effect on the binding sites was demonstrated when the biomass was treated at a high temperature. This resulted in a lower metal uptake (Srikrajib *et al.*, 1999). However, Padmavathy *et al.* (2003) reported that the nickel biosorption capacity of baker's yeast increased after heat treatment.

2.3.3.3 Effect of solution pH

Solution pH could greatly change the dominant forms of metal binding sites on the biomass surface and solution chemistry of heavy metals, which would directly interfere with the biosorption performance (Romera *et al*., 2007 and Saeed *et al*., 2005). In an acidic medium, the amount of protons remains at a high level. Although the solubility of most metal ions increases under this condition, metal ions greatly compete with protons for the binding sites. Also, the binding sites are dominant in their protonated forms, such as –COOH, –OH and $–NH_3^+$, at a low pH. Thus, the formation of metal-biomass interaction and the metal uptake are inhibited. As the pH increases, the proton content and the competition reduce. The binding sites then dissociate the bound proton to expose their negative charges or lone-pair electrons (like $–COO^-$, $–O^-$ and $–NH_2$). All these factors promote the metal uptake. On the other hand, Romera *et al*. (2007) pointed out that as metal ions are precipitated at a high pH, the overall metal removal can thus significantly increase. However, it is hard to evaluate the metal removal performance contributed by pure biosorption.

2.3.3.4 Effect of metal concentration

Ansari and Malik (2007) reported that the biosorption capacity of biomasses would vary under different metal concentrations. A small value of the biosorption capacity is obtained at a low metal concentration since the amount of metal ions is the limiting factor. By increasing the concentration, the availability of metal ions together with the biosorption capacity could be enhanced. As the metal content increases further, most

binding sites would be saturated. The biomass content is thus considered as the limiting factor in this extreme condition. The biosorption capacity may remain at a constant value and become independent on the further increase in the metal concentration. This relationship usually can be presented as a plot of the biosorption capacity versus equilibrium metal concentrations, which is called 'equilibrium isotherm'. Two common mathematical models, the Langmuir and Freundlich isotherm models, are often used to simulate the isotherm with good agreements.

The Langmuir isotherm model is derived from a dynamic equilibrium of adsorbents and adsorbates. As mentioned by Şahin and Öztürk (2005) and Volesky (2003), it has several assumptions:

(i) reversible adsorption;

(ii) monolayer adsorption;

(iii) single molecule adsorption per adsorption site;

(iv) no change in properties of the bound adsorbates;

(v) no interaction between the bound adsorbates;

(vi) identical adsorption affinity of adsorption sites with the adsorbates.

The general equation of the Langmuir isotherm model can be expressed in both linearized (Equation 2.1) and non-linearized (Equation 2.2) forms.

$$\frac{C_e}{q} = \frac{1}{b q_o} + \frac{C_e}{q_o} \qquad \text{(Equation 2.1)}$$

$$q = \frac{b C_e q_o}{(1 + b C_e)} \qquad \text{(Equation 2.2)}$$

where q is the adsorption capacity of adsorbents (mg $_{\text{bound adsorbates}}$/g $_{\text{adsorbents}}$); b is the adsorption affinity of adsorbents (L/mg $_{\text{adsorbates}}$); C_e is the equilibrium concentration of adsorbates in reaction mixture (mg $_{\text{adsorbates}}$ L^{-1}); q_o is the maximum adsorption capacity of adsorbents (mg $_{\text{bound adsorbates}}$/g $_{\text{adsorbents}}$).

Fourest and Roux (1992) stated that the term q_o represents the content of the bound adsorbates within the saturated adsorbents under a high adsorbate concentration. The term b measures the effectiveness of the adsorption at a low adsorbate concentration. A higher b value implies a higher adsorption affinity at the low concentration. Also, this term can be regarded as the adsorbate concentration achieving the half-saturation of the adsorption sites.

The Freundlich isotherm model assumes that the adsorbates would first occupy the adsorption sites with a higher binding affinity and then bind those with a lower affinity until saturation. The Freundlich isotherm model is presented as follows:

Linearized model: $$\ln q = \ln K + \frac{1}{n} \ln C_e \qquad \text{(Equation 2.3)}$$

Non-linearized model: $$q = K C_e^{1/n} \qquad \text{(Equation 2.4)}$$

where K and n are the Freundlich constants (unit of K is 'mg $_{\text{bound adsorbates}}$/g $_{\text{adsorbents}}$' and n is dimensionless).

According to Davis *et al.* (2003), the constant K represents the amount of the bound adsorbates when the equilibrium concentration of adsorbates in the solution phase is in unity. It also evaluates the adsorption effectiveness in the solution containing a low adsorbate concentration. The constant n correlates to the intensity of adsorption.

2.3.3.5 Effect of counter cations

Apart from the target metal species, industrial wastewater usually contains a large amount of different counter cations. Similar to solution pH, Önal *et al*. (2007) reported that these cations are also competitors for the binding sites of biomasses. As a result, the biosorption capacity of the target metal ions by the biomasses is reduced. Such competition generally depends on both the concentration (Pagnanelli *et al*., 2001) and chemical nature (Arıca *et al*., 2004) of the counter cations. The uptake of the target metal ions would be greatly inhibited at a high concentration of the counter cations due to an increase in the competition. Also, each cationic species has its specific chemical nature that governs the interaction mode on the biomasses. For instance, light metal ions (like Na^{+}, K^{+}, Ca^{2+} and Mg^{2+}) only bind with the biomasses through electrostatic interaction, and heavy metal ions (like Pb^{2+} and Cu^{2+}) have a higher tendency to form complexes with the binding sites, which can enhance the binding strengths. Once the counter cations can strongly interact with the biomasses, stable metal-biomass intermediates would be formed, resulting in a high metal binding preference and further inducing a strong competition with the uptake of the target metal ions.

2.3.3.6 Effect of anions

Apart from metal cations, an abundance of various anions commonly co-exists in wastewater, such as chloride, nitrate, sulfate, cyanide and phosphate. Some of them may have a strong ability to coordinate with heavy metal ions, resulting in a large variety of complexes. For example, copper ions would coordinate with cyanide ions to form $Cu(CN)^{+}$, $Cu(CN)_2$, $Cu(CN)_3^{-}$ and $Cu(CN)_4^{2-}$ complexes (Ludwing, 2003); coordination of gold ions and chloride ions could form $AuCl^{2+}$, $AuCl_2^{+}$, $AuCl_3$ and $AuCl_4^{-}$ complexes (Tripler, 1974). There are significant differences in electrostatic characteristics, solubilities and chemical properties between these complexes and their core metal ions. The interaction between metal ions and the binding sites may thus be weakened or even converted to other interaction modes in the biosorption reactions. The metal removals by biomasses might then be demoted (Kuyucak and Volesky, 1989). In the worst cases, the complexes would repulse the binding sites or become insoluble in the aqueous medium. The biosorption is then inhibited and even no metal uptake can be carried out.

2.3.3.7 Effect of organics

As mentioned by Jeon *et al.* (2005), the organics in wastewater could also interact with both metal ions and biomasses. This might affect the heavy metal biosorption. Aksu *et al.* (1999) reported that the nickel biosorption using dried aerobic activated sludge was inhibited in the presence of phenol. They proposed that nickel ions may interact with phenol molecules in the solution phase. This reduced the availability of

nickel ions towards biomasses and then resulted in a drop of the nickel removal.

Another perspective was suggested by Sing and Yu (1998). Three organic solvents, acetone, trichloroethane and ethanol, were introduced into the reaction mixture of the copper biosorption process by using *Phanerochaete chrysosporium*. The results showed that the copper biosorption capacity decreased in the presence of acetone, but an enhancement of the copper removal was found in the reaction mixture containing either trichloroethane or ethanol. A possible reason was that the solvents acted as modifiers for the biomass pre-treatment (Section 2.3.3.2). Acetone may wash out the binding sites, whereas trichloroethane and ethanol may convert the functional groups on the biomass surface to active metal binding forms. Thus, these two extreme observations were exhibited.

2.3.4 Dynamics of biosorption

Volesky (2003) reported that cadmium biosorption by using *Sargassum* biomass could be divided into two stages. The rate of the biosorption in the first stage was fast, indicating that about 75% of the total cadmium uptake was obtained within a short period of time. In the second stage, the cadmium biosorption proceeded slowly until it reached the equilibrium (no net metal uptake). The time required in this stage was much longer. Similar patterns of the biosorption kinetics have been reported in literature. For instance, the biosorption of lead, copper, cadmium, zinc, and nickel by

marine algal biomass (Sheng *et al.*, 2004), the biosorption of copper(II) and cobalt(II) by using crab shell particles (Vijayaraghavan *et al.*, 2006) and the removal of heavy metal ions (Cd, Cu and Zn) by coffee husks (Oliveira *et al.*, 2008).

As explained by Crist *et al.* (1996), the initial rate of the metal biosorption is mainly attributed to the surface binding. It depends on the surface area of biomass and the active binding sites residing on the biomass surface. In view of the second stage, the slower biosorption rate would be attributed to the interior penetration of metal ions (intraparticle diffusion in pore space and surface adsorbed phase) and a lower metal concentration gradient. Since most of the surface binding sites are occupied in the initial stage, metal ions have to access the interior active sites through the intraparticle diffusion. This additional mass transfer would slow down the overall biosorption rate. Moreover, the metal concentration in the reaction mixture is significantly reduced after the initial stage, resulting in a decrease of the concentration gradient between the bulk solution phase and the biomass surface. The external film mass transfer rate would thus be reduced. Both the intraparticle and external film diffusions induced a large deceleration of the biosorption rate, hence a longer reaction time is required in the second stage. The mass transfer will be discussed in detail in Section 2.3.4.2.

Similar to the kinetics of chemical reactions, the biosorption kinetics can be described by some mathematical models. Pseudo-first-order and

pseudo-second-order kinetic models usually reveal a good simulation in the biosorption kinetic studies. Aksu and Balibek (2007) found that both the pseudo-first-order and pseudo-second-order models can obtain good fittings for the chromium(VI) biosorption kinetics by dried *Rhizopus arrhizus* with $r^2 > 0.91$. On the other hand, the biosorption kinetics of copper(II) and cobalt(II) using crab shell particles can be successfully simulated by the pseudo-second-order model with $r^2 > 0.99$ (Vijayaraghavan *et al.*, 2006). Also, Oliveira *et al.* (2008) reported that the kinetic profiles of heavy metal removals (Cd, Cu and Zn) by coffee husks can be well described by the pseudo-second-order model with $r^2 > 0.99$.

2.3.4.1 Pseudo-order kinetic models

In general, the rate equation can be written as:

$$\text{Rate} = \frac{\Delta c}{\Delta t} = -k[c]^{\alpha} \qquad \text{(Equation 2.5)}$$

where c is the concentration of reactant c (mg L^{-1}); t is the reaction time (min); k is the reaction rate constant; α is the reaction order; $\Delta c/\Delta t$ is the reaction rate (change of the reactant concentration with time during the reaction).

As proposed by Connors (1990) and Wright (2004), the rate equation (Equation 2.5) can be easily solved by either (i) logarithm method or (ii) integration method. In the logarithm method, the rate constant can be obtained from a simple linear plot of log (rate) versus log [reactant] (reactant concentration) as shown in Equation 2.6. On the other hand, the rate

constant can also be calculated through integration of the rate equation (Equation 2.5). The integrated equations are presented in Equations 2.7 and 2.8 with respect to the first-order and the second-order kinetic models.

Logarithm method: $$\log\left(\frac{\Delta c}{\Delta t}\right)=\alpha \log c - \log k \qquad \text{(Equation 2.6)}$$

Integration method (first-order kinetic model):

$$\frac{\Delta c}{\Delta t}=\frac{d c}{d t}=-k_1 c$$

$$\int_{C_o}^{C_t}\frac{d c}{c}=-k_1\int_0^t d t$$

$$\ln C_t - \ln C_o = -k_1 t \qquad \text{(Equation 2.7)}$$

Integration method (second-order kinetic model):

$$\frac{\Delta c}{\Delta t}=\frac{d c}{d t}=-k_2 c^2$$

$$\int_{C_o}^{C_t}\frac{d c}{c^2}=-k_2\int_0^t d t$$

$$\frac{C_o - C_t}{C_t \cdot C_o} = k_2 t \qquad \text{(Equation 2.8)}$$

where C_t is the reactant concentration at time t (mg L^{-1}); C_o is the initial reactant concentration (mg L^{-1}); k_1 is the rate constant of the first-order kinetic model (min^{-1}); k_2 is the rate constant of the second-order kinetic model ($L \cdot mg^{-1} \cdot min^{-1}$).

As the reaction involves two or more reactants with a large concentration difference, a complicated rate equation would be expressed

(Equation 2.9). The logarithm method then converted Equation 2.9 to a complex log function (Equation 2.10). The simple log/log plot cannot be directly applied. Also, a complicated function would be drawn after the integration (Equation 2.11). It is difficult to solve and determine the rate constant (Wright, 2004).

$$\text{Rate} = -k[c]^{\alpha}[d]^{\alpha'}\cdots\cdots[z]^{\alpha''} \qquad \text{(Equation 2.9)}$$

Logarithm method:

$$\log(\text{Rate}) = \alpha \log c + \alpha' \log d \cdots\cdots + \alpha'' \log z - \log k \qquad \text{(Equation 2.10)}$$

Integration method:

$$\int \text{Rate} = -k \int c^{\alpha} d^{\alpha'} \cdots\cdots z^{\alpha''} \qquad \text{(Equation 2.11)}$$

where terms c to z are the reactant concentrations (mg L^{-1}); α to α" are the reaction orders. The total reaction order is equal to the sum of α to α".

In order to solve this problem, Conners (1990) established that the effect of particular reactants on the reaction rate can be regarded as a constant factor when the concentration of those reactants is in excess (almost constant) throughout the reaction. The rate equation can be simplified as shown in Equation 2.12. Both the logarithm and integration methods can be applied directly to obtain the rate constant again. This approach is called 'Pseudo-order technique'. Table 2.9 summaries the rate equations modified with the pseudo-order approach.

$$\text{Rate} = -k^{*}[c]^{\alpha} \qquad \text{(Equation 2.12)}$$

where k* is the pseudo rate constant (= $k\,[d]^{\alpha'} \cdots\cdots [z]^{\alpha''}$).

Table 2.9. Pseudo-order rate equations.

Kinetic model	Original rate equation	Pseudo-order equation	Pseudo-order rate constant (k*)
Pseudo-first order	Rate = k [c] $[d]^{\alpha'} \cdots\cdots [z]^{\alpha''}$	Rate = k_1* [c]	k_1* = k $[d]^{\alpha'} \cdots\cdots [z]^{\alpha''}$
Pseudo-second order	Rate = k $[c]^2$ $[d]^{\alpha'} \cdots\cdots [z]^{\alpha''}$	Rate = k_2* $[c]^2$	k_2* = k $[d]^{\alpha'} \cdots\cdots [z]^{\alpha''}$

Further expressing the pseudo-order equations (shown in Table 2.9) in terms of the biosorption capacities q, the typical models of the pseudo-first-order and pseudo-second-order kinetics can be derived as shown in Equations 2.13 to 2.16.

Pseudo-first-order kinetic model:

$$\frac{dq_t}{dt} = k_1^* (q_e - q_t)$$

$$\int_0^t \frac{dq_t}{(q_e - q_t)} = k_1^* \int_0^t dt$$

$$-\ln (q_e - q_t) = k_1^* t + constant$$

when t = 0, q_t = 0.

i.e. constant = $-\ln q_e$.

Linearized form: $\ln (q_e - q_t) = \ln q_e - k_1^* t$ (Equation 2.13)

Non-linearized form: $q_t = q_e - \frac{q_e}{e^{k_1^* t}}$ (Equation 2.14)

Pseudo-second-order kinetic model:

$$\frac{dq_t}{dt} = k_2^* (q_e - q_t)^2$$

$$\int_0^t \frac{dq_t}{(q_e - q_t)^2} = k_2^* \int_0^t dt$$

$$\frac{1}{(q_e - q_t)} = k_2^* t + constant$$

when $t = 0$, $q_t = 0$.

$$\text{i.e.} \quad \text{constant} = \frac{1}{q_e} .$$

Linearized form: $$\frac{t}{q_t} = \frac{1}{k_2^* q_e^2} + \frac{t}{q_e}$$ (Equation 2.15)

Non-linearized form: $$q_t = \frac{k_2^* q_e^2 t}{k_2^* q_e t + 1}$$ (Equation 2.16)

where k_1^* is the rate constant of the pseudo-first-order model (min^{-1}); k_2^* is the rate constant of the pseudo-second-order model ($g \cdot mg^{-1} \cdot min^{-1}$); q_t is the biosorption capacity of the sorbent at the time t ($mg_{sorbates}/g_{sorbents}$ or $mg_{sorbates}/mL_{sorbents}$); q_e is the biosorption capacity of the sorbent at equilibrium ($mg_{sorbates}/g_{sorbents}$ or $mg_{sorbates}/mL_{sorbents}$).

2.3.4.2 Mass transfer

In microscopic view, when a sorbent particle is suspended in a metal solution, several zones would be identified. They include bulk solution, a boundary film layer and an internal particle partition (Fig. 2.1). The bulk solution is a reaction mixture surrounding the sorbent particle. In the boundary layer, a liquid film is developed between the sorbent and the bulk solution. A complex network, which is composed of pores and channels, is

observed inside the sorbent particle. The metal ions in the bulk solution would diffuse across the boundary layer and reach the sorbent surface. This mass transfer step is called “external film diffusion”. A part of the metal ions is then immobilized on the surface binding sites of the sorbent (surface bindings), whereas the remainder would further diffuse into the pores and the surface of the network structure (intraparticle diffusion) to access the interior binding sites. The two-step mass transfer, including the external film and intraparticle diffusions, together with the metal binding is generally regarded as the basis of the sorption dynamics (Al Duri, 1995 and Bilgili, 2006). They proceed concurrently throughout the metal uptake process until it reached equilibrium.

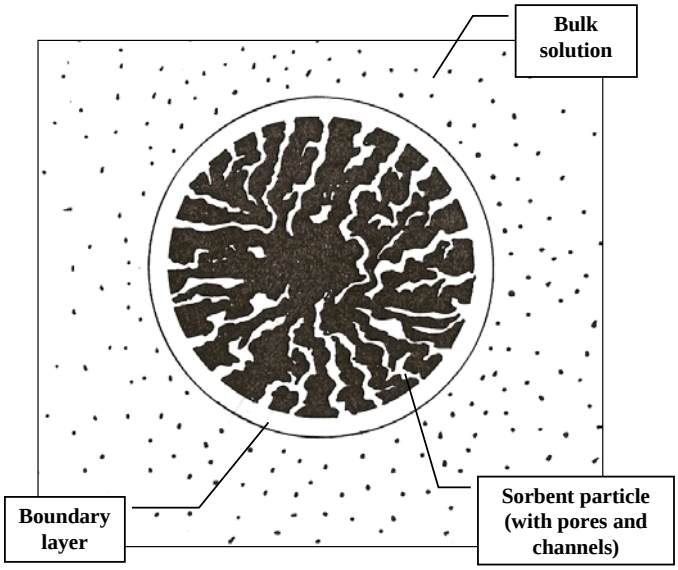

Figure 2.1. Sketch of adsorbent particle in solution. (Al Duri, 1995)

Helfferich (1995) pointed out that the film diffusion rate is proportional to the sorbate concentration and inversely proportional to the thickness of the boundary film layer. The film thickness further correlates to the solution agitation factor. A thicker film would be formed under an inefficient agitation. On the other hand, the rate of the intraparticle diffusion is inversely proportional to the radius of the sorbent particle but independent of the film thickness and the sorbate concentration. Volesky *et al.* (2003) explained that a larger sorbent particle with a larger radius (a longer diffusion path) usually has a more complex internal network structure, which is composed of many micropores, pores and channels. It may create a large intraparticle diffusion resistance and thus reduce the intraparticle diffusion rate. In the metal binding step, the factors affecting the metal uptake have been discussed in detail in Section 2.3.3.

Generally, the metal binding is an instantaneous reaction that is seldom considered in a rate determination of the sorption process. The critical rate-limiting factors should comprise the external film and intraparticle diffusions, which control the supply of metal ions to access the binding sites of the sorbent particles (Al Duri, 1995; Bilgili, 2006; Helfferich, 1995). In a well-agitated reaction mixture, the initial sorption rate is dominantly controlled by the intraparticle diffusion due to the presence of the large pore diffusion resistance. On the other hand, the film diffusion is not the limiting factor because the negligible film thickness under the sufficient agitation and the presence of the high metal content in the bulk solution can overcome the limitation of the film diffusion. After the initial phase, the

bulk metal concentration decreases. The effect of the film diffusion would become more significant. Both the intraparticle and film diffusions work together to control the mass transfer of the metal ions and the sorption rate.

2.4 Desorption

Recovery of heavy metals from the sorbents is usually studied in pairs with the metal biosorption process. It is also called 'desorption'. This step is important to recover bound metal species for recycling. Also, the metal-laden sorbents can be regenerated for reuse in further treatment cycles. Thus, the production cost and the treatment expense can be greatly reduced. Studies have provided several suggestions for selecting the optimal desorbing agent as summarized below:

(i) the desorbing agent should perform an effective regeneration of the sorbents as well as a high efficiency of the metal recovery (Park *et al.*, 2007);

(ii) the desorbing agent should be non-damaging to the sorbents, non-polluting and cheap (Davis *et al.*, 2000);

(iii) the desorbing agent should not demote the reusability of the sorbents in subsequent biosorption/desorption cycles (Hammaini *et al.*, 2007);

(iv) the ideal desorbing agent could improve the biosorption capacity of the sorbents after the desorption (Southichak *et al.*, 2006).

In practice, complexing agents, counter cations and acids are frequently applied as desorbing agents. Typical examples are listed in Table 2.10. The complexing agents can effectively chelate metal ions from the sorbents.

The counter cations can undergo ion-exchange to displace the bound metal species. Similar to the counter cations, acids can act as proton donors to displace the bound metal ions through ion exchange.

Table 2.10. Heavy metal recoveries using different desorbing agents.

Group	Desorbing agent	Biomass	Desorption efficiency	Reference
Complexing agent	EDTA (1 M)	Activated sludge	100% for Cd, Cu, Ni, Pb and Zn	Hammaini *et al.* (2007)
	NTA (0.01 M)	Carboxylated alginic acid	80% for Pb	Jeon *et al.* (2005)
Counter cation	NaCl (0.1 M)	*Spirogyra* species	~ 10% for Cu	Gupta *et al.* (2006)
	Sodium citrate (100 mM)	Gellan gum gel beads	65% for Ni	Lázaro *et al.* (2003)
	$NaHCO_3$ & Na_2CO_3 (0.01 N)	Immobilized *Rhizopus nigricans*	~ 90% for Cr(VI)	Bai and Abraham (2003)
	$CaCl_2$ (0.1 M)	*Cladophora fascicularis*	~ 30% for Pb	Deng *et al.* (2007)
	$Ca(NO_3)_2$ ($2\%_{w/v}$ concentration at pH 3)	*Sargassum* seaweed	92% for Cu	Davis *et al.* (2000)
Acid	HCl (0.1 M)	*Fucus vesiculosus*	96% for Cu	Grimm *et al.* (2008)
	HNO_3 (0.01 M)	Degreased coffee beans	96% for Cd	Kaikake *et al.* (2007)
	H_2SO_4 (0.1 M)	NaOH pre-treated activated sludge	94% for Cd	Al-Qodah (2006)
	Critic acid (1.0 M)	*Spirulina maxima*	75% for Pb	Gong *et al.* (2005)

2.5 Immobilization of biomass

As mentioned by Çabuk *et al.* (2007), although suspended biomasses can provide better contact with sorbates during biosorption, they are not suitable for large-scale treatment processes. It is because the suspended biomasses can only be well separated from the liquid phase by some expensive technologies, such as centrifugation and membrane separation (Li *et al.*, 2008). Thus, the immobilization of biomaterials has become an important scope in the recent biosorption studies. Apart from the enhancement of the biomass-liquid separation (Vijayaraghavan *et al.*, 2007), studies also showed that the biomass immobilization can provide many other advantages, such as:

(i) enhancing the biosorption capacity (Iqbal *et al.*, 2007);

(ii) promoting the selectivity and efficiency of biosorption, as well as the recycle of the biosorbents (Figueiredo *et al.*, 2008);

(iii) allowing a higher biomass loading inside the immobilized biosorbents and minimizing clogging in continuous flow treatments (Hu and Reeves, 1997);

(iv) producing the biosorbents with suitable size, mechanical strength, rigidity and porosity for applying in scale-up treatment operations (Önal *et al.*, 2007);

(v) improving the bioreactor efficiency, for instance, generating less biological sludge, increasing the treatment reliability and enhancing the level of tolerance to shock loading (Chen *et al.*, 2005b).

Agar (Khattar *et al.*, 1999), alginate (Al-Rub *et al.*, 2004), gellan gum gel (Lázaro *et al.*, 2003), loofa songe (Akhtar *et al.*, 2004), polyacrylaime (Texier *et al.*, 2002), polyacrylnitrile (Zouboulis *et al.*, 2003), polyethyleneimine (Deng and Ting, 2005), polysulfone (Beolchini *et al.*, 2003), silica gel (Rangsayatorn *et al.*, 2004) and zeolite (Figueiredo *et al.*, 2008) are used frequently as the biomass supports in the immobilization studies. These immobilization agents could attach the biomasses through covalent binding, cross-linking and/or mechanical entrapment (Velglio' and Beolchini, 1997).

2.5.1 Alginate

Alginate is one of common exopolymers on algal cell wall (Pavez *et al.*, 2005) and bacterial cell membrane (Nestle and Kimmich, 1996). It is mainly composed of D-mannuronic residues (M) and L-guluronic residues (G), which are linked up to form the alginate chain with different quantities and combinations as shown in Figs. 2.2 and 2.3. Usually, it exists as a single polymer chain after extraction of the cell surface by sodium salts. When sodium alginate is dissolved in water and further mixed with solution containing gelation agents, cross-linkages known as 'egg-box junctions' would be formed in between the polymer chains (Fig. 2.4). This results in a giant network structure (Ibáñez and Umetsu, 2002). Calcium ions, barium ions and other multi-valent cations are all commonly used as the gelation agents for developing the cross-linkages of alginate.

Studies demonstrated that the alginate network is effective for biomass entrapment (Aksu *et al.*, 1998; Al-Rub *et al.*, 2004; Arıca *et al.*, 2003; Li *et al.*, 2008; Lu and Wilkins, 1996; Önal *et al.*, 2007). Also, a large amount of branched M and G units containing free hydroxyl and carboxylate groups remains inside the network structure (Fig. 2.4). These functional groups have a strong affinity to metal ions, inducing an enhancement of the overall biosorption capacity (Stokke *et al.*, 1991; Yan and Viraraghavan, 2001). Moreover, alginate is inexpensive and easy to handle. All these advantages encourage the use of alginate as an immobilization agent.

However, the network structure and chemical properties of alginates are highly susceptible to solution compositions. The gelation cations would be easily chelated out from the cross-linkages of alginates in the presence of phosphate salts (Dainty *et al.*, 1986; Moreira *et al.*, 2006), EDTA (Khoo and Ting, 2001; Veglio' *et al.*, 2002), citrate and lactate (Smidsrød and Skjåk-Bræk, 1990). Moreover, a displacement reaction of the gelation cations is promoted under a high concentration of sodium ions (Tanaka and Irie, 1988) and Mg^{2+} anti-gelling agent (Smidsrød and Skjåk-Bræk, 1990), as well as in seawater or a high salinity environment (Moreira *et al.*, 2006). Further, Khoo and Ting (2001) found that alginate polymers cannot withstand a solution pH below 4.5 or above 9. All these conditions would alter the chemical and physical properties of alginate, and cause swelling and dissolution of the polymers. These may result in a serious biomass leaching.

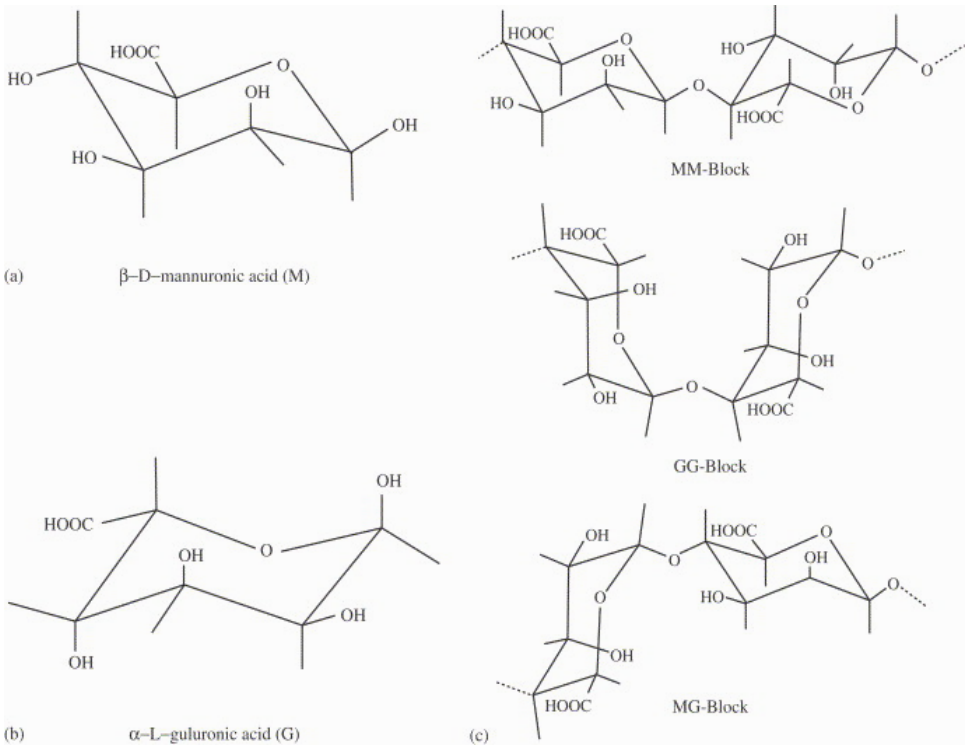

Figure 2.2. Basic components and structures of alginate: (a) D-mannuronic residue (M); (b) L-guluronic residue (G); (c) polysaccharide chains with three different possibilities of the residue bonding. (Pavez *et al.*, 2005)

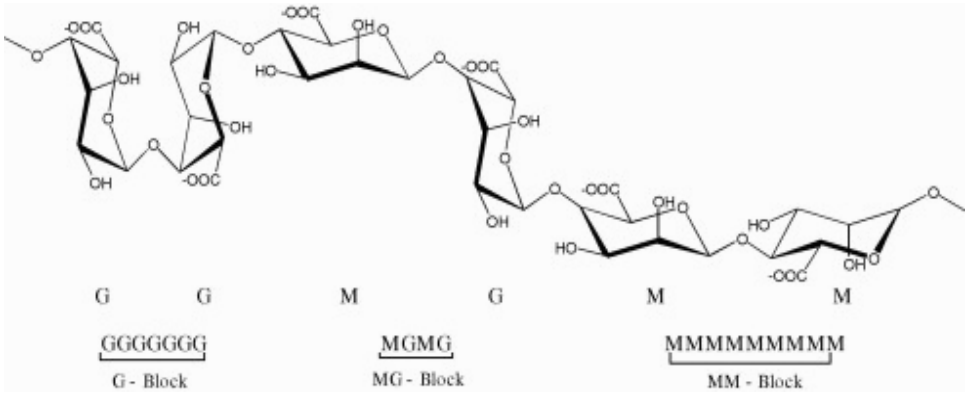

Figure 2.3. Fractions of alginate polymer chain. (Torres *et al.*, 2007)

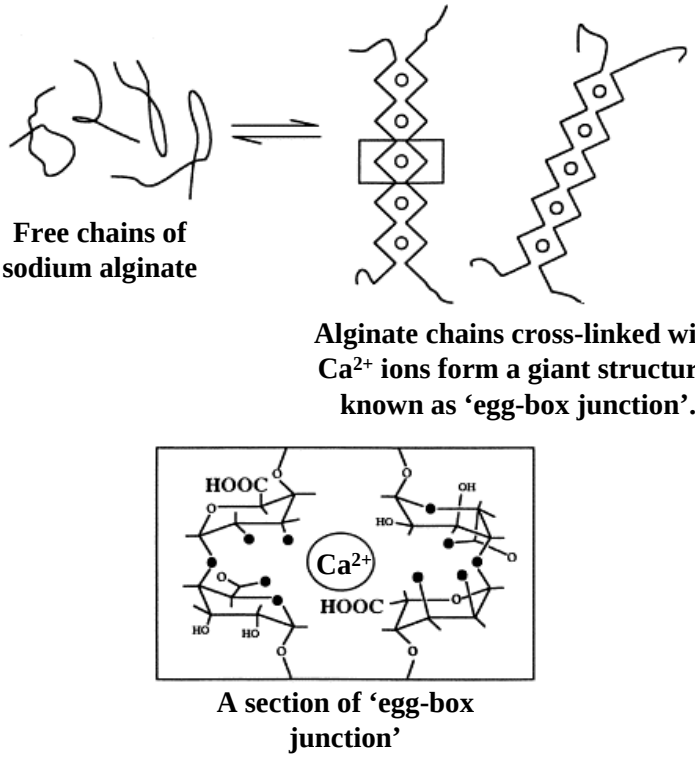

Figure 2.4. Schematic diagram of cross-linking of alginate chains by Ca^{2+} ions. (modified from Grant *et al*., 1973)

2.5.2 Polyacrylamide (PAA)

Polyacrylamide (PAA) is extensively used as an immobilization material of biomasses in both water/wastewater treatments and life-science applications. The typical examples are shown as follows:

(i) denitrification using immobilized *Alcaligenes eutrophus* (Chang *et al.*, 1999);

(ii) decolorization by immobilized *Pseudomonas luteola* (Chen *et al.*, 2005a);

(iii) removal of lanthanide ions using immobilized *Pseudomonas aeruginosa* (Texier *et al.*, 2002);

(iv) production of lipase by immobilized *Aspergillus niger* (Ellaiah *et al.*, 2004);

(v) nucleoside synthesis by immobilized bacterial cells (Trelles *et al.*, 2004);

(vi) protein analysis using Sodium-Dodecyl-Sulphate-PolyAcrylamide Gel Electrophoresis (SDS–PAGE) (Gouda *et al.*, 2007);

(vii) detection of chlorinated and brominated hydrocarbons by the polyacrylamide-based biosensor (Peter *et al.*, 1996).

The basic structure of polyacrylamide (PAA) contains a linear backbone chain with repeating units of acrylamide (vinyl carboxylic acid amide). Such polymer chain can connect to other backbones through cross-linking with N,N'-methylene-bis-acrylamide copolymers (bis). This results in a giant lattice structure with a high ability of the cell entrapment (Brady and Duncan, 1994). The overall equation of the polymerization is presented in Fig. 2.5. This reaction is initiated by tetramethylethylenediamine (TEMED) and ammonium persulfate. TEMED accelerates the rate of free radical formation from ammonium persulfate. The free radicals then catalyze a series of vinyl-addition polymerizations of both acrylamide and bis monomers. These produce many long polymer chains with random bis cross-linkages. Finally, a bulk lattice structure is obtained (Menter, 2000).

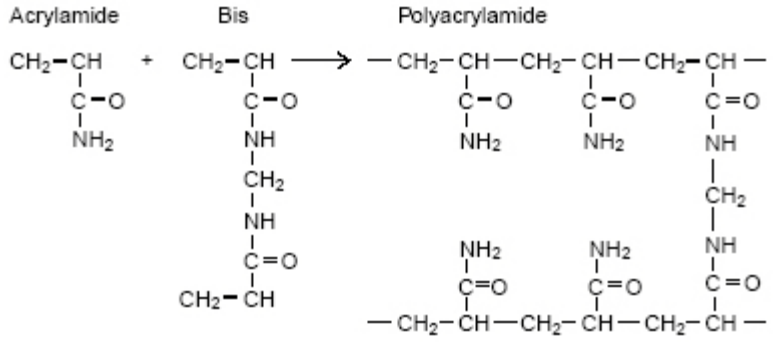

Figure 2.5. Polymerization of acrylamide. (Menter, 2000)

Texier *et al.* (2002) showed that a preference in using polyacrylamide as an immobilization agent is due to its simple experimental protocol and short reaction time. Also, this polymer does not affect the selective biosorption behaviour of biomasses (Andrès *et al.*, 1995). Furthermore, a small pore size and a high mechanical strength of the lattice structure can provide a high ability of the cell encapsulation (Dos Santos *et al.*, 1997). However, both the monomers of polyacrylamide are highly neuro-toxic, which may limit the use in scale-up treatment processes (Macaskie *et al.*, 1986).

2.6 Wastewater treatment in fixed-bed column reactor

Fixed-bed column reactor is one of the most common scale-up systems for wastewater treatment. The term 'fixed-bed' represents the sorbents that are closely packed inside the reactor without fluidizing in the solution flow during the treatment process. A diagram of a typical fixed-bed system is presented in Fig. 2.6. Belter *et al.* (1988) and Volesky (2003) stated that the column system is simple and the operation is straightforward. The

contaminant removal, sorbent regeneration and column rinsing can all be performed within the same reactor. Beside, the whole column setup only involves several sets of pumping and piping units for transferring the influent (including wastewater, regeneration agent and rinsing water) into the column as well as discharging the eluent. Diniz *et al.* (2008) further believed that the fixed-bed column is the most preferable processing device for the sorption processes. It is because the system can effectively use the concentration gradient to maximize the uptake capacity of the sorbents, even at a low contaminant concentration level.

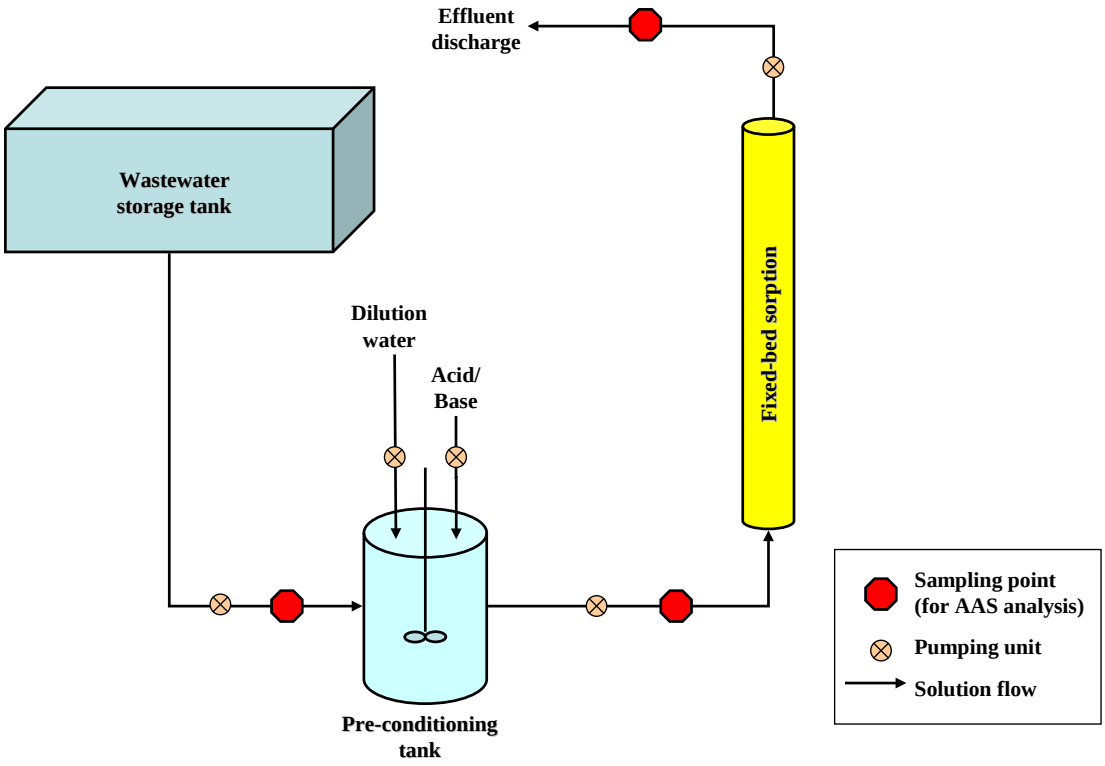

Figure 2.6. Process diagram of fixed-bed sorption column.

2.6.1 Biosorption in fixed-bed columns

In accordance to the benefits of using the column system for wastewater treatment as listed in Section 2.6, many researchers are particularly interested in applying this approach to biosorption studies. For instance, chromium(VI) biosorption by *Rhizopus arrhizus* (Preetha and Viruthagiri, 2007), copper(II) removal by *Sargassum wightii* (Vijayaraghavan and Prabu, 2006), zinc(II) uptake using crab carapace biosorbent (Lu *et al.*, 2007) and nickel(II) biosorption by immobilized *Chlorella sorokiniana* (Akhtar *et al.*, 2004). They also found that some well-established principles of conventional fixed-bed adsorption processes can be directly applied in the biosorption column. For example, mass transfer theory (Chu and Hashim, 2007) and ion-exchange mechanism (Naja and Volesky, 2006). These agreements further promote the application of the fixed-bed system in biosorption studies.

2.6.2 Breakthrough curve concept

Hatzikioseyian *et al.* (1999) established that biosorption dynamics in a fixed-bed column can be successfully described by a graphical expression called 'breakthrough curve'. It is usually plotted as the concentration ratio (C_e/C_o) versus time (or treatment volume). A typical sketch of a breakthrough curve is presented in Fig. 2.7 (for downflow operation mode), which reveals the biosorption performance as the area above the curve.

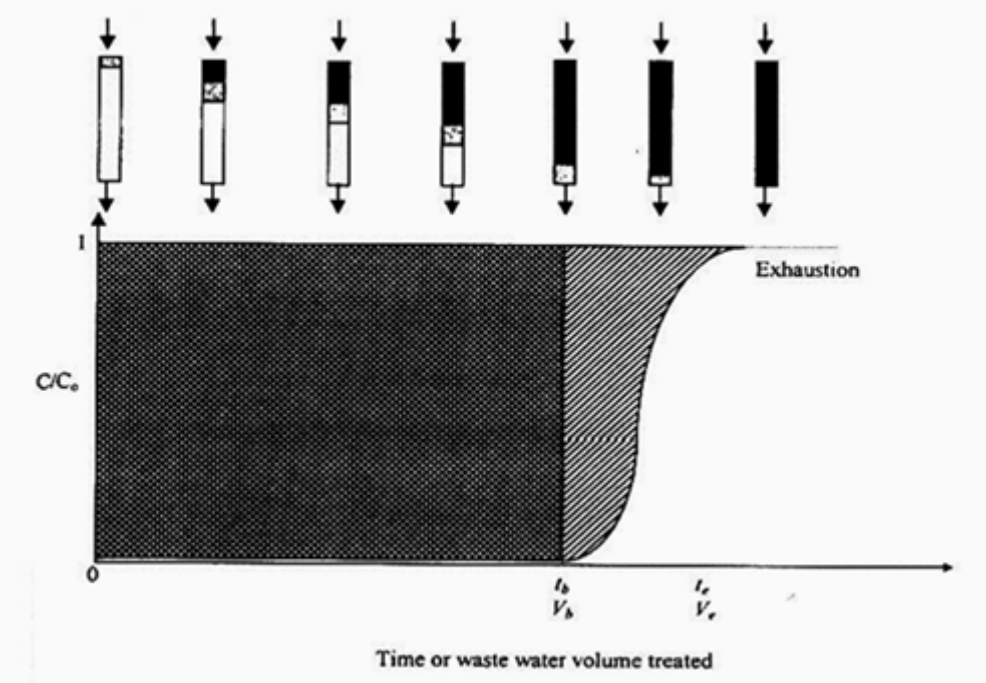

Figure 2.7. Typical breakthrough curve showing the movement of adsorption zone, breakthrough and exhaustion time. (Hatzikioseyian *et al.*, 1999)

Generally, the column can be divided into three sections during the biosorption process: unused bed, mass-transfer zone and saturated region. The unused bed is defined as the section containing the fresh biosorbents with no or little metal uptake. The mass-transfer zone (MTZ) represents the zone that biosorption of heavy metal ions occurs. On the other hand, the saturated region represents the section when the biosorbents are fully saturated with heavy metal ions. As shown in Fig. 2.7, metal ions are completely removed by the biosorbents at the top of the column and most biosorbents still remain unsaturated in the early stage of the biosorption. This develops a large unused bed region (white area). As the biosorption proceeds further, the MTZ (grey area) is developed. This zone would

move down and leave behind the saturated regions (black area). When the MTZ approaches the end of the column, the metal concentration in the effluent increases sharply to reach the level of influent metal concentration. Under this condition, all the biosorbents in the column would become almost saturated and no significant change in the effluent concentration is observed. This results in a plateau section of the breakthrough curve. A similar curve is also observed in an upward operation mode but all the zones move in the reverse direction (Hawari and Mulligan, 2006b; Jeon *et al.*, 2002; Saeed *et al.*, 2005; Vijayaraghavan *et al.*, 2005c).

In the breakthrough curve, the "breakthrough time" or "service time" represents the duration of ongoing biosorption until a predefined threshold sorbate concentration in the effluent is reached, and the point correlating with the column breakthrough is called "breakthrough point" (Volesky, 2003). Once all the biosorbents in the column are saturated with metal ions and the effluent concentration is almost the same as the influent concentration, this condition is known as the column (bed) exhaustion stage.

As shown in Fig. 2.8, the breakthrough profiles of fixed-bed adsorption can be generally divided into seven types. All of them have different morphologies. Bohart and Adams (1920) pointed out that the type of the breakthrough profile exhibited by a fixed-bed biosorption process depends on its operating conditions.

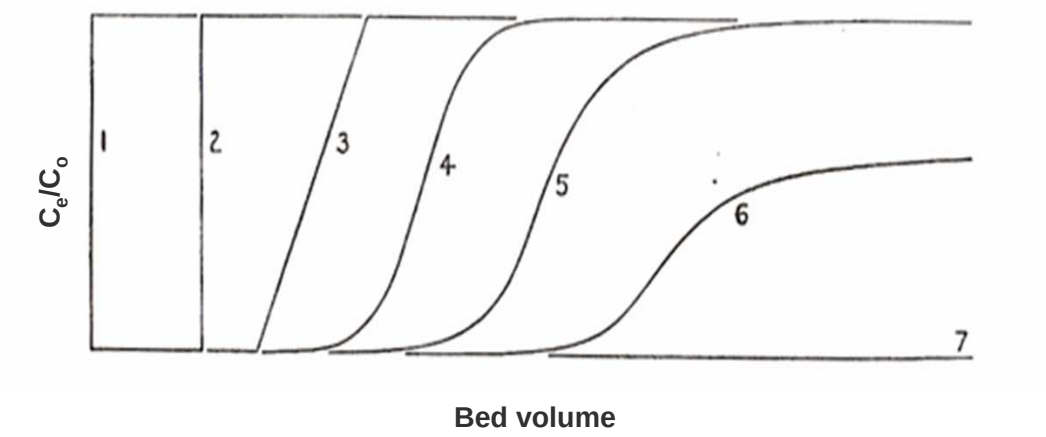

Figure 2.8. Types of breakthrough profiles of fixed-bed adsorption. (Bohart and Adams, 1920)

Type 1 in the figure represents the limit of adsorption approached by the breakthrough curve as the effectiveness of the adsorbents decreases, showing that the adsorbates saturate all the adsorbents in the column at once. Type 2 is exhibited by the adsorption in the presence of ideal adsorbents, which are infinitely fine grains and react with the adsorbates instantaneously. The area above the profile in the figure represents the adsorption capacity of the adsorbent bed. If the uniformity of adsorbent packing varies in different column sections, Type 3 would occur. By making assumptions that (i) an instantaneous adsorption exists in the column; (ii) the rate of adsorption is proportional to the adsorption capacity of the column and the concentration of the adsorbates; (iii) the adsorption is specifically performed with a mono-adsorbate species; and, (iv) the adsorbents are perfectly uniform, a highly-symmetrical profile with the point of inflection at 50% adsorption ($C_e/C_o = 0.5$) can be developed (Type 4). If the adsorption rate drops more rapidly than the rate of change of the residual adsorbent capacity or more than one type of adsorption sites with unequal reactivity are present

in the adsorbents, an asymmetrical curve (Type 5) would occur. When the adsorbents also act as a catalyst for further conversion of the adsorbates, the values of C_e/C_o would always be smaller than unity, resulting in Type 6. In an extreme case, the rate of a catalytic reaction is much faster than the adsorption rate. All the adsorbates are completely converted to other compounds. No adsorbate could be found in an effluent, inducing a flatten breakthrough profile (Type 7).

2.6.3 Mass transfer in biosorbent packing of columns

Before the metal binding takes place in a fixed-bed column, three major mass-transfer steps are involved in transporting metal sorbates from a bulk solution phase to specific binding sites on the surface or within the interior of biosorbents. The steps are: (i) interparticle mass transfer, (ii) interphase mass transfer, and, (iii) intraparticle mass transfer.

The interparticle mass transfer relates to the diffusion of the metal sorbates in the solution occupying the void space between the biosorbent particles inside the column packing. This type of the mass transfer is usually caused by the concentration gradient of the sorbates and the uneven solution flow. As mentioned by Tien (1994), such effect would further result in axial and radial dispersions of the sorbates. The axial dispersion takes places along the direction of the main solution flow, whereas the direction of the radial dispersion is transverse to the main flow direction. Mutlu *et al.* (1997) indicated that the radial factor could be neglected if the ratio of the particle diameter to the column diameter is below one-tenth.

Interphase and intraparticle mass transfers both involve the individual particles in the column. The interphase mass transfer, which is also called film diffusion, is the transfer of the sorbates between the bulk solution phase and the external surface of the particles. On the other hand, the intraparticle mass transfer is related to the diffusion properties of the sorbates from the outermost particle surface to micro-pores of the particle and even on the surface of the pore spaces. The details of both the interphase and intraparticle diffusions have been discussed in Section 2.3.4.2.

2.6.4 Factors affecting fixed-bed biosorption

In view of the adsorption column system, there are several critical factors affecting the treatment performance and the development of the mass transfer zone, including: (i) size of biosorbents, (ii) column bed depth, (iii) influent concentration, (iv) influent flow rate, and, (v) influent composition.

2.6.4.1 Effect of biosorbent size

Undoubtedly, more biosorbents can be packed in a column with a fixed bed depth as their size decreases. This may increase the overall metal removal capacity of the column. Ko *et al.* (2000) and Volesky *et al.* (2003) also believed that large biosorbents usually contain complex internal network structures, which are composed of many micropores, pores and channels. This may create a large intraparticle diffusion resistance. Moreover, as mentioned by Slejko (1985), the rate of sorbate uptake highly depends on the biosorbent size. A smaller size can provide a greater

overall surface area for the mass transfer. This speeds up the rate of the mass transfer and also the biosorption. All these advantages encourage the utilization of small biosorbents. However, Slejko (1985) also indicated that a dense column packing filled with extremely small particles may reduce the void space inside the biosorbent bed. This would induce poor contact between the influent solution and the biosorbents, and further increase the risk of clogging. These would result in a poor mass transfer and even cease the column operation.

2.6.4.2 Effect of column bed depth

Column bed depth is defined as the length of column packing filled with the biosorbents. It is usually considered as one of the critical factors in a fixed-bed process. This parameter is also frequently introduced in fixed-bed sorption models, such as the Adams-Bohart model (Malkoc *et al.*, 2006), the Bed-Depth-Service-Time model (Han *et al.*, 2007) and the Wolborska model (Quintelas *et al.*, 2008). Many researchers reported that a longer bed depth can increase the contact time between the biosorbents and the contaminants. It can also provide a larger surface area for the mass transfer and develop a broader mass transfer zone. All these, in turn, enhance the efficiency of a contaminant removal, allow a longer service time and handle a larger volume of wastewater (Kratochvil *et al.*, 1997; Low *et al.*, 1999; Sharma and Forster, 1995; Texier *et al.*, 2002; Vijayaraghavan *et al.*, 2005a; Wu and Yu, 2008; Zulfadhly *et al.*, 2001). However, as the bed depth increases up to a certain level, a greater head loss may be developed inside the column, resulting in the column clogging.

2.6.4.3 Effect of influent concentration

Çabuk *et al.* (2006), Han *et al.* (2006), Sağ and Aktay (2001), Texier *et al.* (2002) and Wu and Yu (2008) reported that a shorter service time and a smaller treatment volume can be obtained in a fixed-bed biosorption operating at a higher influent concentration. It is because a higher sorbate concentration can provide a larger amount of sorbates in the solution phase. Most binding sites of the biosorbents may be occupied in a short period of time, resulting in a faster column breakthrough and a steeper breakthrough profile.

2.6.4.4 Effect of inlet flow rate

Influent flow rate is usually optimized together with the column bed depth and the influent concentration in fixed-bed studies. Many studies showed that the service time decreased as the flow rate increased (Chang and Huang, 1998; Dursun and Aksu, 2000; Han *et al.*, 2007; Texier *et al.*, 2002; Valdman *et al.*, 2001; Vijayaraghavan *et al.*, 2005b). Under a faster flow rate, the retention time of sorbates in the column is shortened. Such a short period of time may be insufficient for transferring all sorbates to the binding sites of the biosorbents because the mass transfer rate is usually considered as the rate-limiting factor (Aksu *et al.*, 1998). Most sorbates thus first accumulate in the bulk solution, which is surrounding the biosorbents, and then are eluted out the column by following the effluent flow. As a result, a faster breakthrough and a steeper breakthrough curve may occur. By contrast, a longer service time and a more gentle

breakthrough profile can be obtained under a slower flow rate. However, the overall process becomes more time-consuming and less efficient.

2.6.4.5 Effect of influent composition

In fixed-bed biosorption studies with multiple components in the influent, Naddafi *et al.* (2007) found that the removals of all these components were inhibited. Both the service time and treatment volume of the process were also reduced. These might be due to the competition between the components for the limited binding sites within the column packing. Similar phenomena are observed in the following cases: the multiple-metal (lead, cadmium and mercury) biosorption (Chen *et al.*, 2005b); the zinc removal in the presence of copper and lead (Lu *et al.*, 2007); the lead uptake from multi-metal (Cd, Cu, Ni, Zn) solution (Saeed *et al.*, 2005); the competitive metal (copper, lead, zinc and nickel) biosorption studies (Zhang and Banks, 2006). In view of the breakthrough curve, the slope becomes much steeper as the influent contains more than one sorbate component. Also, an overshoot effect ($C_e/C_o > 1$) is displayed in the biosorption profile. Diniz *et al.* (2008) pointed out that this effect should be attributed to the sorbates with a lower binding affinity. Such sorbates occupy the binding sites together with the stronger binding species at the beginning of the biosorption. The weaker binding components could then be displaced by the incoming stronger binding sorbates as the binding sites are almost saturated. Thus, the effluent concentration of these weaker binding species becomes higher than that in the influent. An overshooting peak is then displaced in the biosorption breakthrough profile.

2.6.5 Fixed-bed biosorption models

2.6.5.1 Adams and Bohart model

As mentioned in Section 2.6.2, Bohart and Adams (1920) considered seven different types of breakthrough curves. Three of the curves (Types 1 to 3) were linear. Type 4 exhibited a symmetrical morphology with the point of inflection at 50% adsorption. Types 5 to 7 were similar to that of the Type 4 but they had a lower degree of symmetry (Mckay *et al.*, 1998).

Based on the Type 4, Bohart and Adams (1920) further established a fundamental equation to describe the relationship between C_e/C_o and time in a fixed-bed adsorption of chlorine gas by using the activated charcoal. This model assumes that the adsorption rate is proportional to both the residual adsorption capacity of the adsorbents and the concentration of the adsorbates (Section 2.6.2). The mass transfer rate correlated with the change in the residual adsorption capacity (Equation 2.17) and the adsorbate concentration (Equation 2.18) can then be defined.

$$\frac{\partial q}{\partial t} = -k_{AB} q C_o \qquad \text{(Equation 2.17)}$$

$$\frac{\partial C_o}{\partial Z} = -\frac{k_{AB}}{U_o} q C_o \qquad \text{(Equation 2.18)}$$

where q is the adsorption capacity of the adsorbents in terms of the concentration of the bound adsorbates per unit mass of the adsorbents (mg $_{\text{bound adsorbates}}$/g $_{\text{adsorbents}}$); k_{AB} is the kinetic constant of the Adams-Bohart model (L mg^{-1} h^{-1}); C_o is the influent contaminant concentration (mg m^{-3}); Z is the column bed depth (m); U_o is the linear velocity of the influent flow (m h^{-1}).

By solving these two differential equations, the Adams-Bohart model equation can be obtained as Equation 2.19 (linearized form) and Equation 2.20 (non-linearized form). The derivation of these mathematical equations was listed by Bohart and Adams (1920).

Linearized form: $$\ln\left(\frac{C_e/C_o}{q/q_o}\right) = k_{AB} C_o t - q_o Z \frac{k_{AB}}{U_o} \quad \text{(Equation 2.19)}$$

Non-linearized form: $$\frac{C_e}{C_o} = \frac{1}{1+e^{\left[k_{AB}\left(\frac{q_o}{U_o}Z - C_o t\right)\right]}} \quad \text{(Equation 2.20)}$$

where C_e is the contaminant concentration in the effluent (mg m^{-3}); q_o is the maximum adsorption capacity of the adsorbents in terms of the saturation concentration of the bound adsorbates per unit mass of the adsorbents (mg $_{\text{bound adsorbates}}/g_{\text{ adsorbents}}$).

Since most binding sites of the adsorbents are still unoccupied at the initial phase of the adsorption, i.e. $q \ll q_o$ and $q/q_o \rightarrow 1$. The model equations can then be modified as:

Linearized form: $$\ln\left(C_e/C_o\right) = k_{AB} C_o t - q_o Z \frac{k_{AB}}{U_o} \quad \text{(Equation 2.21)}$$

Non-linearized form: $$\frac{C_e}{C_o} = e^{\left(k_{AB} C_o t - k_{AB} q_o \frac{Z}{U_o}\right)} \quad \text{(Equation 2.22)}$$

By applying these model equations to the fixed-bed adsorption studies, Aksu and Gönen (2004), Malkoc *et al.* (2006) and Preetha and Viruthagiri (2007) found that the initial part of the breakthrough curves could be successfully simulated.

2.6.5.2 Clark model

Clark (1987) developed a mathematical model to simulate the breakthrough profiles of the organic contaminant removal using different granular activated carbon (GAC) columns in a water supply system. The study found that this model could successfully characterize the removal performances and provide a mean of extrapolation to the other operating conditions. These perspectives were also supported by the phenol biosorption study (Aksu and Gönen, 2004), the defluoridation treatment (Ayoob and Gupta, 2007) and the chromium(VI) removal process (Sağ and Aktay, 2001).

As described by Clark (1987), this model is derived from the liquid-phase mass balance in combination with the mass-transfer concept and the Freundlich isotherm. The liquid-phase mass balance of the adsorption process was first performed within a differential element in a fixed-bed reactor as expressed in following equations:

$$J = \frac{G_s S C_o - G_s S\left(C_o - \Delta C_o\right)}{S \Delta Z}$$

$$J = \frac{G_s \Delta C_o}{\Delta Z} = \frac{G_s dC_o}{dZ} \qquad \text{(Equation 2.23)}$$

where J is the mass-transfer rate per unit reactor volume (mg $_{adsorbates}$ h^{-1} m^{-3}); G_s is the solution flow rate per unit of the cross-sectional area (m^3 h^{-1} m^{-2}); S is the column cross-sectional area (m^2); C_o is the influent contaminant concentration (mg m^{-3}); ΔC_o (or dC_o) is the incremental change in the contaminant concentration (mg m^{-3}); ΔZ (or dZ) is the differential column bed depth (m).

This equation can further correlate with the mass-transfer concept and then yield:

$$J = \frac{G_s \, dC_o}{dZ} = k_m \left(C_o - C_e\right) \qquad \text{(Equation 2.24)}$$

where k_m is the mass transfer coefficient (h^{-1}) and C_e is the contaminant concentration in the effluent (mg m^{-3}).

On the other hand, the Freundlich isotherm model (Equation 2.4) between the adsorbents and the reaction mixture can be expressed as:

$$q = K\left(C_e\right)^{1/n}$$

$$C_e = \left(\frac{q}{K}\right)^n \qquad \text{(Equation 2.25)}$$

where q is the adsorption capacity of the adsorbents in terms of the concentration of the bound adsorbates per unit mass of the adsorbents (mg $_{\text{bound adsorbates}}$/g $_{\text{adsorbents}}$); K and n are the Freundlich constants.

As all the contaminants are completely removed by the adsorbents inside the column bed, the ideal mass balance of the fixed-bed adsorption is:

$$G_s C_o = L_a \, q$$

$$q = \frac{G_s C_o}{L_a} \qquad \text{(Equation 2.26)}$$

where L_a is the mass velocity of the adsorbent to keep the mass-transfer zone stationary (mg h^{-1} m^{-2}).

By further introducing the Freundlich isotherm (Equation 2.25) and the column mass balance (Equation 2.26) into Equation 2.24, the equation can be modified as:

$$\frac{G_s\, dC_o}{dZ} = k_m\left[C_o - C_o{}^n \left(\frac{G_s}{K L_a} \right)^n \right] \qquad \text{(Equation 2.27)}$$

As the velocity of the adsorption zone (V_z) is defined as dZ/dt, Equation 2.27 can be written as:

$$\frac{G_s}{V_z}\frac{dC_o}{dt} = k_m\left[C_o - C_o{}^n \left(\frac{G_s}{K L_a} \right)^n \right] \qquad \text{(Equation 2.28)}$$

Equation 2.28 can be further simplified to:

$$\frac{dC_o}{C_o - \Lambda C_o{}^n} = R\, dt \qquad \text{(Equation 2.29)}$$

where $$\Lambda = \left(\frac{G_s}{K L_a} \right)^n \qquad \text{(Equation 2.30)}$$

and $$R = \left(\frac{G_s k_m}{V_z} \right) \qquad \text{(Equation 2.31)}$$

By integrating Equation 2.29 subject to constant boundary conditions of the concentration (C_o) and the time (t), Equation 2.32 can be obtained.

$$\int_{C_b}^{C_e} \frac{dC_o}{C_o - \Lambda C_o{}^n} = R \int_{t_b}^{t} dt$$

$$C_e{}^{n-1} = \frac{C_b{}^{n-1}}{\Lambda C_b{}^{n-1} + \left(1 - \Lambda C_b{}^{n-1}\right) e^{-R(n-1)(t-t_b)}} \qquad \text{(Equation 2.32)}$$

where C_b is the contaminant concentration at the breakthrough (mg m^{-3}); C_e is the effluent contaminant concentration at the time t (mg m^{-3}); t_b is the breakthrough time (h).

If R (n – 1) = θ, then

$$C_e^{n-1} = \frac{1/\Lambda}{1+\left(\frac{1}{\Lambda C_b^{n-1}}-1\right)e^{\theta t_b-\theta t}} \qquad \text{(Equation 2.33)}$$

As $t \rightarrow \infty$, $C_e \rightarrow C_o$ (or $C_e^{n-1} \rightarrow C_o^{n-1}$)

i.e. $1/\Lambda = C_o^{n-1}$

Equation 2.33 can be rewritten as:

$$\frac{C_e}{C_o} = \left\{\frac{1}{1+\left[\left(\frac{1}{\Lambda C_b^{n-1}}-1\right)e^{\theta t_b-\theta t}\right]}\right\}^{1/n-1} \qquad \text{(Equation 2.34)}$$

2.6.5.3 Thomas model

The Thomas model was initially developed for the fixed-bed water softening process using the zeolite ion-exchange resin (Thomas, 1944). This comprises the concepts of the Langmuir isotherm and the second-order kinetic model as well as the ion-exchange theory. It is now widely used in column studies, for example, chromium(VI) biosorption study of *Rhizopus arrhizus* (Preetha and Viruthagiri, 2007), copper and lead removals by sericite (Tiwari *et al.*, 2007), cadmium adsorption onto granular red mud

(Zhu *et al.*, 2007) and adsorption of methylene blue using natural zeolite (Han *et al.*, 2007).

Thomas (1944 and 1948) first derived the model from the rate of the ion-exchange reaction. It could be characterized by an equation describing the concentrations of the exchangeable ions in solution and the resins as shown in Equation 2.35.

$$\frac{\partial q}{\partial t} = F(C, q) \qquad \text{(Equation 2.35)}$$

where q is the exchange capacity of the resins in terms of the concentration of the target ions in the resin ($mg_{\text{bound ions}}/g_{\text{resins}}$); C is the concentration of the target ions in the solution phase of the column (mg m^{-3}). Both the terms q and C are considered at the time t (h) after the entry of the solution into the column and at the distance Z (m) from the inlet point of the column (bed depth).

This exchange reaction is supposed to be the rate-limiting step of adsorption process, which is assumed to be a significantly slower rate than any inter-particle diffusion steps in the overall process. It assumes that the diffusion processes, such as the axial and radial dispersions, are relatively minor and even negligible. Thus, the second-order kinetic model can be directly introduced into the rate equation, yielding:

$$\frac{\partial q}{\partial t} = k_{2'}(q_o - q)C - k_{2''}(C_o - C)q \qquad \text{(Equation 2.36)}$$

where q_o is the maximum (initial) exchange capacity of the resins in terms of the saturation concentration of the target ions in the resin ($mg_{\text{bound ions}}$/g

resins); C_o is the concentration of the target ions in the influent (mg m^{-3}); $k_{2'}$ and $k_{2''}$ are the rate constants of the ion-exchange process.

To obtain the fundamental equation for this process, the mass balance of the ion exchange is further defined as shown in Equation 2.37. It includes the rate equation (Equation 2.36) as well as several critical column operation factors: the fractional void volume (porosity) inside the column (v_o); the overall packing density of the resins (M, kg m^{-3}); and the linear flow rate of the solution phase inside the packing (U_o, m h^{-1}).

$$U_o \frac{\partial C}{\partial Z} + \frac{\partial C}{\partial t} + \frac{M}{v_o} \frac{\partial q}{\partial t} = 0 \qquad \text{(Equation 2.37)}$$

As the term q in this differential equation is correlated with the Langmuir isotherm model, this differential mass balance can be successfully solved as presented by Thomas (1944 and 1948). As a result, the Thomas model is established and expressed as follows:

Linearized form: $$\ln\left(\frac{C_o}{C_e} - 1\right) = \frac{k_{Th} q_o X}{Q} - \frac{k_{Th} C_o}{Q} V_{eff} \qquad \text{(Equation 2.38)}$$

Non-linearized form: $$\frac{C_e}{C_o} = \frac{1}{1 + e^{\left[\frac{k_{Th}}{Q}(q_o X - C_o V_{eff})\right]}} \qquad \text{(Equation 2.39)}$$

where C_e is the contaminant concentration in the effluent (mg m^{-3}); k_{Th} is the rate constant of the Thomas model (L h^{-1} mg^{-1}); Q is the solution flow rate (L h^{-1}); X is the mass of the resin in the column (g); V_{eff} is the effluent volume (L).

2.6.5.4 Yoon and Nelson model

Based on the principles of gas adsorption kinetics, Yoon and Nelson (1984) developed a mathematical model addressing the adsorption and breakthrough of vapours or gases in a fixed-bed column. The breakthrough profiles could be successfully simulated by applying this model in the adsorption of different contaminant vapours and gases, which include toluene, vinyl chloride, ethyl acetate, trichlorinated hydrocarbon (Yoon and Nelson, 1984) and 1,1-dichloro-1-fluoroethane (Tsai *et al.*, 1999). Recently, this model has been applied to the fixed-bed adsorption of aqueous-phase contaminants, such as copper ions (Vijayaraghavan and Prabu, 2006), arsenite ions (Kundu and Gupta, 2007), fluoride ions (Ayoob and Gupta, 2007) and reactive dyes (Aksu *et al.*, 2007).

In view of the model theory, the rate of decrease in the probability of adsorption for each adsorbate molecule is assumed to be proportional to the probability of the adsorbate adsorption (A) and the probability of the adsorbate elution from the adsorbents (E) as shown in Equation 2.40.

$$-\frac{dA}{dt} \alpha A E \qquad \text{(Equation 2.40)}$$

Since the sum of the probabilities A and E is in unity, the model equation can be written as follows:

$$-\frac{dA}{dt} \alpha A (1 - A) \qquad \text{(Equation 2.41)}$$

Yoon and Nelson (1984) observed that the rate of decrease in the probability of the adsorption is also directly proportional to the influent contaminant concentration (C_o) and the inlet flow rate (Q), but inversely proportional to the amount of the adsorbent (X). Thus, Equation 2.41 can be expressed as follows:

$$-\frac{dA}{dt} \alpha \frac{C_o Q}{X} A(1-A)$$

$$-\frac{dA}{dt} = \frac{k' C_o Q}{X} A(1-A)$$

$$-\frac{dA}{dt} = k_{YN} A(1-A) \qquad \text{(Equation 2.42)}$$

where $k_{YN} = k' \frac{C_o Q}{X}$;

C_o is the influent contaminant concentration (mg m^{-3}); Q is the inlet flow rate (m^3 h^{-1}); X is the mass of the adsorbent (g); k' is a dimensionless constant of proportionality; k_{YN} is proportional constant of the Yoon and Nelson model (min^{-1}).

Since the constant k_{YN} is independent of time (t), Equation 2.42 can then be solved in the following expression:

$$-\frac{dA}{dt} = k_{YN} A(1-A)$$

$$\int \frac{dA}{A} + \int \frac{dA}{(1-A)} = -\int k_{YN}\, dt$$

$$-\ln \frac{A}{1-A} = k_{YN}(\tau - t) \qquad \text{(Equation 2.43)}$$

where τ is the time required to reach 50% bed exhaustion (min).

Accordingly, A = 1/2 (or E = 1/2), when t = τ. Similarly,

$$\ln\frac{E}{1-E} = k_{YN}(\tau - t) \qquad \text{(Equation 2.44)}$$

As previously defined, the term E is the probability of the adsorbate elution. Thus, E is equal to C_e/C_o, where C_e is the adsorbate concentration in the effluent (mg m^{-3}). The Yoon and Nelson model can be finally defined as follows:

$$\ln\frac{C_e}{C_o - C_e} = k_{YN}(\tau - t) \qquad \text{(Equation 2.45)}$$

This linearized model (Equation 2.45) can also be also rearranged to the non-linearized expression (Equation 2.46).

$$\frac{C_e}{C_o} = \frac{1}{1 + e^{k_{YN}(\tau - t)}} \qquad \text{(Equation 2.46)}$$

2.7 Electroplating of copper

Because of its good electrical conductivity, high ductility, relatively noble potential and favourably red colour, copper has been used in countless areas of technology and industry. Electroplating (electrodeposition) of copper is one of the most common and efficient ways to manufacture products with these desirable characteristics. It is usually performed in both alkaline cyanide and acid sulphate copper plating baths. As mentioned by Igel and Streup (2003), the applications of copper deposits include: (i) functional coatings in electrical and electronics industries (printed circuit boards and electrical contacts); (ii) adhesion promoting coatings (undercoating in plating zinc-based diecasts); (iii) intermediates coatings for improving brightness and leveling effects in decorative/corrosion-protective systems (copper-nickel); and, (iv) decorative uses for enhancing product appearances (lamps, vases and candleholder).

2.7.1 Electroplating using alkaline cyanide copper plating baths

Copper(I) cyanide is the copper source in alkaline cyanide copper plating solutions. Once copper ions were mixed with cyanide salts of sodium or potassium in the plating solution, the soluble copper(I) cyanide complexes can be readily formed as shown in Equations 2.47 to 2.49. By applying an electric field, decomposition of all these alkalicyanocuprous(I) complexes occurs near the cathode. Cuprous(I) ions, the final products of the decomposition, are then reduced on the cathode surface, resulting in a layer of copper deposits (Silman *et al.*, 1978).

$$CuCN + CN^- \rightarrow [Cu(CN)_2]^- \quad \text{(Equation 2.47)}$$

$$[Cu(CN)_2]^- + CN^- \rightarrow [Cu(CN)_3]^{2-} \quad \text{(Equation 2.48)}$$

$$[Cu(CN)_3]^{2-} + CN^- \rightarrow [Cu(CN)_4]^{3-} \quad \text{(Equation 2.49)}$$

On the other hand, there are several reactions undergoing at the anodes as listed in Equations 2.50 to 2.53. During the plating, Equations 2.50 to 2.52 are dominant and rapid to produce cuprous(I) ions. Since the plating solutions contain a large amount of cyanide ions, the formation of the alkalicyanocuprous(I) complexes is promoted. This completes the circuit of the whole electroplating bath (Ludwig, 2003).

$$Cu \rightarrow Cu^+ + e^- \quad \text{(Equation 2.50)}$$

$$Cu \rightarrow Cu^{2+} + 2e^- \quad \text{(Equation 2.51)}$$

$$Cu + Cu^{2+} \rightarrow 2\ Cu^+ \quad \text{(Equation 2.52)}$$

$$4\ OH^- \rightarrow 2\ H_2O + O_2 + 4e^- \quad \text{(Equation 2.53)}$$

The cyanide plating solutions are now widely used in the copper deposition of different substrates (workpiece), particularly in the plating of printed circuit boards. The main advantages are:

(i) inexpensive material cost (Silman *et al.*, 1978);

(ii) easy to handle and prepare (Silman *et al.*, 1978);

(iii) possible to produce adherent copper deposits on the workpieces made of materials with more electronegative potentials such as zinc-based diecasts, steels and copper alloys (Dini, 2000);

(iv) possible to provide a higher throwing power than other copper plating solutions; hence, these solutions are more suitable for plating the

workpieces with complex shape, such as holes of printed circuit boards (Ludwig, 2003);

(v) capable of performing an efficient plating with a large value of the weight of copper deposited per ampere since the deposition occurs through the discharge of monovalent cuprous(I) ions (Silman *et al.*, 1978).

2.7.2 Electroplating using acid sulfate copper plating baths

The electrodepostion in copper sulfate plating solutions is performed in an acidic environment. The basic compositions of these solutions are copper sulfate and sulfuric acid. As mentioned by Dini (2000) and Silman *et al.* (1978), this plating bath can provide many attractive benefits, including:

(i) the bath can produce deposits with good coverage and leveling properties;

(ii) the bath operating at a high plating rate can produce thicker deposits for electroforming applications;

(iii) the process is easy to operate and it performs a high plating efficiency;

(iv) the costs of chemicals and power consumption are low;

(v) the plating solution is less susceptible to impurities compared with the cyanide plating solution;

(vi) the plating effluent is less toxic.

Accordingly, it is frequently applied to produce a wide range of surface-finishing products such as plated wires, steel rolls, stainless steel

heating vessels, corrosion-protective overmachined parts, optical surfaces and even decorations (Igel and Streup, 2003).

2.7.2.1 Working principle

The working principle of the acid sulfate copper plating is much simpler than that of the alkaline cyanide bath. Copper(II) ions, sourced from copper sulfate in the solution, are reduced and deposited on the cathode surface under a rich supply of high-energy electrons as shown in Equation 2.54. A part of copper(II) ions may also perform an indirect deposition. They are first reduced to cuprous(I) ions and then deposited afterward (Equation 2.55).

$$Cu^{2+} + 2\ e^- \rightarrow Cu \qquad \text{(Equation 2.54)}$$

$$Cu^{2+} + e^- \rightarrow Cu^+ + e^- \rightarrow Cu \qquad \text{(Equation 2.55)}$$

At the anode, copper would dissolve in the plating solution as both copper(II) and cuprous(I) ions as shown in Equations 2.56 and 2.57. Both forms of copper ions replenish the deposited copper in order to maintain a constant copper content in the bath (Ludwig, 2003).

$$Cu \rightarrow Cu^{2+} + 2\ e^- \qquad \text{(Equation 2.56)}$$

$$Cu \rightarrow Cu^+ + e^- \qquad \text{(Equation 2.57)}$$

However, a side reaction of cuprous(I) ions may occur on the anode surface as depicted in Equation 2.58. This is known as disproportionation (Silman *et al.*, 1978). A fine copper sludge may form in the solution phase and randomly attach on the cathode workpiece, resulting in a rough deposit

surface. In order to minimize this sludge formation, phosphor-deoxided copper electrode is often used as the anode in the acid copper plating bath. It can effectively inhibit the disproportionation reaction and also promote the anode dissolution (ASTM, 2003; Dini, 2000; Durney, 1984; Hahn, 2003).

$$2\ Cu^{+} \rightarrow Cu^{2+} + Cu \qquad \text{(Equation 2.58)}$$

2.7.2.2 Compositions of acid sulfate copper plating baths

The basic compositions of acid sulfate copper plating solutions are copper sulfate and sulfuric acid. In modern acid copper electroplating processes, some other components are also used in order to achieve some desirable deposit requirements. For example, a shiny deposit appearance can be obtained by introducing chloride ions and organic brighteners. Also, a leveling coating can be produced in the presence of leveling agents. Such components reported in the literature are listed in Table 2.11.

Copper(II) sulfate pentahydrate ($CuSO_4 \cdot 5H_2O$) is usually used as a copper source in the plating bath. Table 2.11 shows that the optimal concentration of this salt is usually around 150 to 250 g/L. Under an insufficient copper supply, a low current efficiency is found in the bath (Dini, 2000). This means that the electric current supply for the plating is not fully utilized in the copper deposition. The excessive electropotential may thus accumulate on the cathode surface. This induces many uncontrollable side reactions, such as electrolysis of water molecules, resulting in a rough deposit layer. As the copper content increases, the

bath can be operated with nearly 100% current efficiency (Ludwig, 2003). All the current and applied electropotential can participate in the copper plating, resulting in a desirable deposit layer. Ludwig (2003) also pointed out that the deposits may become rough and highly porous if the bath is operated near the solubility limit of pure copper(II) sulfate due to local precipitation.

Sufluric acid is another basic component in acid sulfate copper plating baths. Dini (2000) believed that the acid can promote a grain refinement of the copper deposits and increase conductivity of the plating solution and electrodes. It can also increase the hardness of the deposit layers (ASTM, 2003); reveal a high macro-throwing power (Ludwig, 2003); enhance uniformity of the deposit layer; hydrolyze the copper sulfate salts; prevent cuprous(I) oxide formation; and, inhibit dendrite (rough and treed deposits) formation (Silman *et al.*, 1978). All these features and advantages can be demonstrated under the recommended acid concentration ranging from 25 to 110 g/L (Table 2.11). However, Dini (2000) showed that as the acid concentration further increases, a poor copper deposition is observed due to a dramatic decrease in solubility of copper sulfate.

Chloride ions are often introduced into the acid copper plating. They are generally supplied from either sodium chloride or hydrochloric acid. The main function of chloride ions is to bind copper ions as various forms of copper-chloride complexes. Through the formation of these complexes, the copper deposition rate and the rearrangement of the copper deposit

lattices can be successfully controlled so as to further modify the deposit layers, producing the desirable appearance, brightness, crystallographic orientation, internal stress and microhardness (Dini, 2000). Table 2.11 shows that the chloride content in the acid copper plating baths is usually in the range of 30 to 100 mg/L. If the concentration is below 30 mg/L, the amount of chloride ions is insufficient to function properly. On the other hand, there is a high tendency towards the dendrite formation under a high chloride concentration. In the presence of excess chloride ions, chlorine gas is formed by electrolysis and the anode is even hindered by a white film of copper(I) chloride. The copper deposition may then be terminated (Ludwig, 2003).

The components of the acid sulfate copper plating baths usually include one or several organic compounds based on the results of thorough experimental studies. As shown in Table 2.11, there is a long list of frequently-used organic additives. They can be classified into the following categories: brightener, leveling agent, hardness modifier, smoothness promoter and grain refiner (Rehim *et al.*, 2000). Generally, the working principle of these organics is similar to that of chloride ions discussed above. The organics would chelate the copper ions, resulting in a slower deposition rate. The deposits with the desirable properties can then be formed (Dini, 1993).

Table 2.11. Compositions of acid copper sulfate bath in current electroplating processes.

Composition	Range	Reference
$CuSO_4 \cdot 5H_2O$	• 210 – 214 g/L; • 150 – 250 g/L; • 195 – 248 g/L; • 160 – 230 g/L; • 87 – 275 g/L; • 160 – 220 g/L.	ASTM (2003) Dini (2000) Durney (1984) Ludwig (2003) Safranek (1986) Silman *et al.* (1978)
H_2SO_4	• 52 – 75 g/L; • 45 – 110 g/L; • 30 – 75 g/L; • 40 – 100 g/L; • 25 – 74 g/L; • 50 – 75 g/L.	ASTM (2003) Dini (2000) Durney (1984) Ludwig (2003) Safranek (1986) Silman *et al.* (1978)
Cl^-	• 30 – 100 mg/L; • 60 – 100 mg/L; • 30 – 150 mg/L.	Dini (2000) Durney (1984) Ludwig (2003)
Organic additives	• Sodium gluconate; • Glue, dextrose, phenolsulfonic acid, molasses, thiourea, polyalkylene glycol type polymers, alkane surfactants containing sulfonic acid, etc. • Gelatin, glycine, thiourea, dextrin, molasses, lignosulfonate, mercaptobenzimidazoles, naphthalene sulfonic acid, tribenzlamine, phenol polycols, etc. • Polyethylene glycol compounds, polypropylene glycol compounds, polyvinyl alcohol, polymeric phenazonium compounds, derivatives of thiourea, derivatives of dithiocarbamic acid, organic sulphur compounds, organic phosphorous compounds, organic dyestuffs (e.g., Janus Green and Crystal Violet), etc. • Sulphaguanidine • 3-*N*,*N*-dimethylaminodithiocarbamoyl-1-propanesulphonic acid (DPS) and polyethylene glycol (PEG).	Rehim *et al.* (2000) Dini (1993) Dini (2000) Ludwig (2003) Subramanian and Nageswar (1980) Vas'ko *et al.* (2004)

2.7.2.3 Operating conditions of acid sulfate copper plating

Apart from the compositions of the plating solution, the properties and appearance of copper deposits can also reveal a large variation under different operating conditions of the acid copper plating process. Current density, agitation and processing temperature are all crucial factors of the copper deposition among other parameters. Table 2.12 summarizes the preferred levels of these operating conditions in current acid sulfate copper electroplating processes.

Dini (2000) demonstrated that an increase in current density usually initiates a faster copper deposition rate in the acid copper plating. This may reach the limit of the copper diffusion. The cathode workpiece becomes depleted in copper ions, resulting in a poor configuration of copper deposits. When the current density increases further, the deposition rate would be accelerated exceedingly. The supply of copper ions by diffusion becomes extremely rare. An intensive formation of the dendrite deposits is induced together with vigorous release of hydrogen gas, which is produced from the side reactions of the deposition, such as proton reduction and electrolysis of water molecules. Highly porous and dispersive copper deposits are then obtained (ASTM, 2003; Dini, 2000; Nikolić *et al.*, 2006). By contrast, a low current density may be insufficient to maintain a reasonable process efficiency and produce a good deposit coverage. The preferred current density in current acid copper plating processes is listed in Table 2.12.

Both air agitation and mechanical stirring are common agitation modes in the plating process (Table 2.12). Under a proper agitation, the plating defects such as burning and pitting can be successfully eliminated, especially under a high current density (ASTM, 2003). This is because agitation can facilitate an adequate solution movement on the cathode surface; accelerate the rapid mass transfer; promote uniform property of the coatings over a wide range of current densities; and, reduce the electrochemical consumption of organic additives (Ludwig, 2003). All these can prevent the deposition from reaching the limiting diffusion condition, or inhibit the side reactions during the plating as discussed above.

In Table 2.12, the practical working temperature ranges between 20 and 50 ^{o}C. Based on economical concern, Dini (2000) showed that the process should be operated without temperature regulation since heat can be generated from the chemical reactions inside the bath. No additional expense is thus required for the installation and operation of the heating and cooling systems. Undoubtedly, the deposition rate can be speeded up under a higher temperature. This may promote the overall conductivity of the plating solution; however, the degree of grain refinement decreases, resulting in a rough layer of copper deposits (Dini, 2000). Moreover, the ASTM study (2003) reported that the elongation and hardness of the deposits are demoted as the temperature increases. On the other hand, the efficiency and rate of the deposition would decrease under a lower working temperature. Based on the above consideration, the plating temperature is preferably processed at near room temperature.

Table 2.12. Operating conditions of acid copper sulfate bath in current electroplating processes.

Operating condition	Range	Reference
Current density	• 1 – 10 A/dm^2; • 16 – 22 A/dm^2 (with a general agitation) & 50 A/dm^2 (under a fast agitation); • 2 – 10 A/dm^2; • 2 – 8 A/dm^2 (for a general plating) & 10 – 100 A/dm^2 (for printing cylinders, strips, wire, tubes & Cu cladding); • 0.5 – 4 A/dm^2; • 1 – 6 A/dm^2.	ASTM (2003) Dini (2000) Durney (1984) Ludwig (2003) Safranek (1986) Silman *et al.* (1978).
Agitation	• Air or mechanical agitation; • Air agitation; • Air agitation.	ASTM (2003) Durney (1984) Ludwig (2003)
Temperature	• 21 – 32 ^{o}C; • 32 – 43 ^{o}C; • 21 – 49 ^{o}C; • 20 – 50 ^{o}C; • 30 – 45 ^{o}C; • Around 45 ^{o}C.	ASTM (2003) Dini (2000) Durney (1984) Ludwig (2003) Safranek (1986) Silman *et al.* (1978).

2.8 Surface analysis using physical methods

2.8.1 Scanning Electron Microscopy (SEM)

The Scanning Electron Microscope (SEM) is a type of electron microscopes, which are capable of producing a high-resolution image of a sample surface. It is used to examine surfaces of different materials, such as microbes (Das and Guha, 2007), polymer (Wang *et al.*, 2007), and deposit of electrodeposition (Nikolić *et al.*, 2006). To perform these studies, a raster pattern with a primary beam of high-energy electrons, thermionically emitted from a tungsten or lanthanum hexaboride cathode within an electron gun, scans across a sample surface (Fig. 2.9). When this primary electron beam interacts with the sample, the electrons lose their energy by repeated scattering and adsorption. The energy exchange between the electron beam and the sample would result in several types of signals. The signals include backscattered electrons, secondary electrons, Auger electrons, X-ray fluorescence photons and other photons with various energy levels. Only the backscattered and secondary electrons serve as the basis of the scanning electron microscopy. By determining the electromagnetic radiation emitted from these electrons, a SEM image can be produced (Skoog *et al.*, 1998).

2.8.2 X-ray Energy Dispersive Analysis (EDAX)

The X-ray Energy Dispersive Analysis (EDAX) is a type of spectroscopy for qualitative and quantitative determinations of elements. It is widely applied in electrodeposition studies (Li *et al.*, 2006; Kokate *et al.*, 2006; Zainal *et al.*, 2004), since it can provide a list of useful information

about deposit properties, such as grain distribution, metal purity and coverage (Kanani, 2003). This instrument is usually combined with the scanning electron microscope (SEM) as shown in Fig. 2.9, because both are developed from similar working principles. Both of them require a high-energy primary electron beam for scanning the sample surface. Such electron beam is produced by the same electron gun through the thermo-ionization. The major difference between these two analyses is their signal detections. As mentioned in Section 2.8.1, several signals can be produced during the surface scanning of the sample. A SEM image is produced by determining the signals of the backscattered and secondary electrons, whereas an EDAX spectrum is obtained by measuring the wavelengths and intensity of the X-ray fluorescence (Skoog *et al.*, 1998).

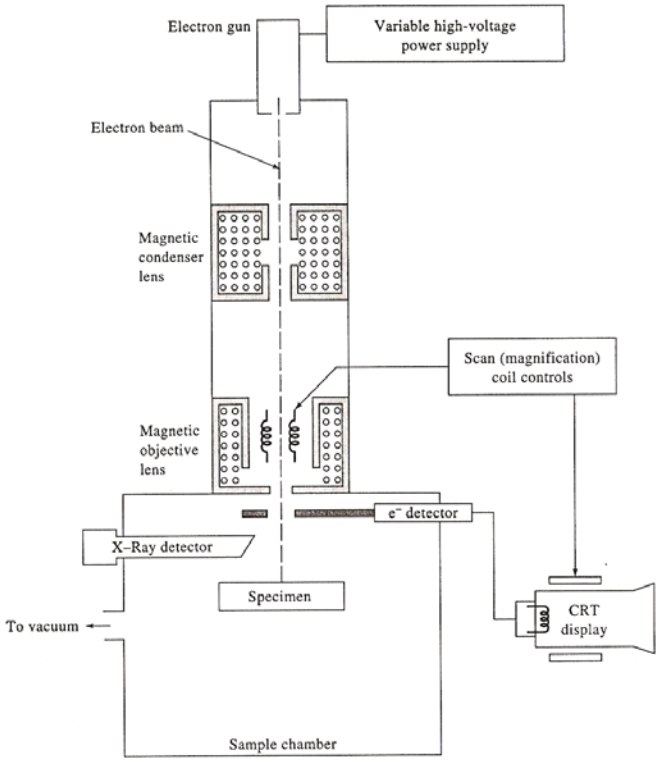

Figure 2.9. Schematic diagram of SEM and EDAX. (Skoog *et al.*, 1998)

2.8.3 Atomic Force Microscopy (AFM)

The Atomic Force Microscope (AFM) is one of the foremost instruments for imaging, measuring and manipulating sample surfaces at nanoscale. It can be considered as a modified scanning probe microscope with an extremely high resolution. As shown in Fig. 2.10, a sharp tip (probe) attached to a cantilever of the microscope is used for scanning the sample surface. As the tip scans across the surface, a force between the tip and the surface is induced, resulting in a deflection of the cantilever. Such deflection is monitored by a laser spot reflected from the top of the cantilever into a split photodiode detector. An AFM micrograph is then collected (West, 2007). Apart from the nanoscale surface morphology, the properties of samples, such as their microhardness and smoothness, can also be obtained through this measurement. Both silicon and silicon nitride probes are commonly used in the measurement. By employing other chemically-modified probes, the thermal and electrical conductivities as well as the magnetic property can be further determined (Thornton *et al.*, 2000). The atomic force microscope is widely used in material research studies (Khang *et al.*, 2007; Lafouresse *et al.*, 2007; Nichols *et al.*, 1992) and life-science (Eibl and Moy, 2005; Zhao *et al.*, 2007).

This instrument has also been used to examine biomass surface in some recent biosorption studies. Yin *et al.* (2008) found that particle-shaped crystals were attached on smooth biomass surface and aggregated with each other, resulting in a rough surface morphology. Similar observations were reported by Kazy *et al*. (2008), Majumda *et al*. (2008) and Pan *et al*. (2006).

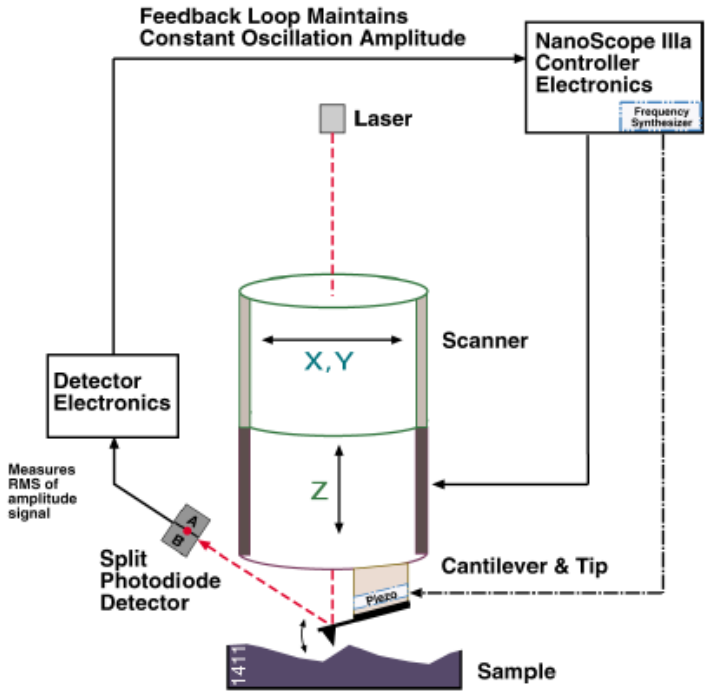

Figure 2.10. Schematic diagram of AFM. (Thornton *et al.*, 2000)

Chapter 3. Materials and Methods

3.1 Instrumentation

The agar plate inoculated with *Micrococcus luteus* was incubated in a LEEC GA2000 incubator operating at 37 ^{o}C. The cultivation of the bacterial cells in liquid broth medium was performed using a controlled-temperature orbital shaker (Unitwist model 400) and a 15-liter fermentor (B. Braun model BIOSTAT® C). The cell growth was monitored by the optical density measurement with an UV-visible spectrophotometer (Spectronic® model 20 Genesys™) at designated interval during the cultivation. The cells were harvested by centrifuges (Beckman model J2-M1 and J2-21) and lyophilized in a freeze dryer (Heto model FD8). All the media, solutions and glasswares for the cell cultivation were sterilized in autoclaves (Tokyo Hirayama model HA-30 and Sakura Finetechnical model ASV-3022) operating at 121 ^{o}C and 1.1 kgf/cm^{2}.

To perform the immobilization of the bacterial cells, the mixture containing the cells and polymer matrix was gelled in a gelation agent under gentle agitation using the orbital shaker. A part of the cell-immobilized beads was modified by drying in either an oven (Memmert model UFE 500) or the freeze dryer followed by re-hydrating under gentle agitation using the orbital shaker.

In the metal biosorption and desorption studies, all batch experiments were conducted in the orbital shaker operating at 25 ^{o}C and 250 rpm. A fixed-bed column and a continuous-stirred-tank reactor were used for the continuous studies. Both inlet and outlet flow rates of these reactors were

controlled by peristaltic pumps (Masterflux) and the effluent was collected by a fraction collector (Amersham model RediFrac). A Flame Atomic Absorption (AA) spectrophotometer (Perkin-Elmer Analyst model 100) and a Total Organic Carbon analyzer (Shimadzu model TOC-5000A) were used for analyzing the metal concentrations and organic contents of samples, respectively. The solution pH was monitored by a pH meter (Orion model 4-Star).

All of the above mixtures and solutions, including the cell cultivation broth, immobilization gel, metal stock solutions and analytical standards, were prepared by distilled and deionized (DDI) water, which was obtained from Fisons 'Fi-streem' Tanks. Moreover, all lab-wares for the metal biosorption and desorption were rinsed with DDI water after soaking overnight in 2 M nitric acid.

3.2 Preparation of biosorbents

3.2.1 Cultivation of *Micrococcus luteus*

Micrococcus luteus, a Gram-positive bacterium, was investigated throughout this study. It was previously isolated from an activated sludge process of a local sewage treatment plant (Leung *et al*., 2001). The colonies of *Micrococcus luteus* were maintained on nutrient agar (Oxoid) plates, which contained 1.0 g/L 'Lab-lemco' powder, 2.0 g/L yeast extract, 5.0 g/L peptone, 5.0 g/L NaCl and 15.0 g/L agar. To prepare inocula, the colonies were loop-inoculated into several 1-L Erlenmeyer flasks containing 500 mL of autoclaved liquid broth medium, which was composed of 16 g/L

trypone, 10 g/L yeast extract, 5 g/L NaCl and 10 g/L glucose. After incubating in the orbital shaker operating at 37 ^{o}C and 250-rpm for 20 h, the inocula were then transferred to the autoclaved fermentor containing 9 L of the broth medium with controlled growth conditions: pH 7.0; temperature 37 ^{o}C; pO_2 above 20%; stirring speed from 200 to 1000 rpm; air-flow from 2 to 26 L/min. Samples were taken from the fermentor at designated time intervals to monitor the cell growth through the optical density measurement using the UV-visible spectrophotometer operating at a wavelength of 600 nm. When the optical density did not increase further, the cells were harvested by centrifugation and then rinsed with DDI water twice. The harvested cells were then lyophilized and stored at 4 ^{o}C before use.

3.2.2 Immobilization of *Micrococcus luteus*

A cell suspension of *Micrococcus luteus* at 200 g/L was mixed with a solution containing 4% sodium alginate, 0.1% N,N,N',N'-tetramethylethylenediamide (TEMED), 18.2% acrylamide and 1.8% N,N'-methylene-bis-acrylamide (bis). The volume ratio of the cell suspension to the solution was 1:1. After a thorough mixing, the resulting mixture was syringed drop by drop into a gelation solution containing 4% calcium chloride and 0.1% ammonium persulfate. The drops gelled and formed spherical beads upon contact with the gelation solution. The beads immobilized with *M. luteus* were then re-suspended into the fresh gelation solution with constant and gentle agitation overnight in order to complete the gelation. The final concentration of *M. luteus* in the beads was about 0.3 g-cell/mL-beads. Eventually, the beads were washed with DDI water

and stored at 4 ^{o}C before use. These cell-immobilized beads without any further modification were labelled as 'primitive immobilized *Micrococcus luteus*' (PIM) in the following studies.

To optimize the immobilization of *M. luteus*, three modification approaches were studied. First, different grafting polymers were introduced into the cell-immobilized beads. Second, alternative gelation agents of alginate, namely, barium chloride, barium nitrate and calcium nitrate, were used instead of calcium chloride for preparing the beads according to the procedures described above. The molarity of these gelation agents was the same as that of the calcium chloride solution. Third, the PIM beads were dried overnight in the oven at 40 ^{o}C or in the freeze dryer, and then re-immersed in DDI water for five days with a constant and gentle agitation. This treatment was called 'rehydration treatment'. The beads prepared by this treatment were labelled as 'rehydrated form of immobilized *Micrococcus luteus*' (RIM).

3.3 Copper(II) biosorption studies

3.3.1 Batch system

The copper(II) biosorption experiments were performed by mixing different forms of the cell-immobilized beads (prepared according to the procedures described in Section 3.2.2) with 50 mL of 100 mg-Cu/L copper(II) nitrate solutions in a series of 500-mL Nalgene polypropylene bottles. One mL of the beads was introduced to each reactor bottle, whereas around 0.6 mL of the RIM beads, which was equivalent to 1 mL of

the PIM beads before the rehydration treatment, was used. The metal solutions with no biosorbent were used as controls. The reaction mixtures were then agitated on the orbital shaker operating at 250 rpm and 25 ^{o}C for 6 h. The solution pH was adjusted to 5.0 by dilute NaOH and HNO_3 at the start and after 3 h of the experiments. All the above experiments were performed in duplicates. At the end of each experiment, the copper(II) concentration of the supernatants was determined by the atomic absorption spectrophotometer at a wavelength of 324.8 nm, and the volume of the beads was re-measured.

3.3.1.1 Biosorption kinetics

The kinetic study was carried out for 26 h (1560 min) according to the procedures described in Section 3.3.1. The RIM beads with a volume of 2.5 mL were mixed with 250 mL of 100 mg-Cu/L copper(II) nitrate solution. The solution pH was adjusted to 5.0 at the start, and after 3 and 21 h of the experiment. Three mL of the supernatant was withdrawn from the reactors at designated intervals for analyzing the residual copper(II) concentration. The experiment was repeated by using 5 mL of the PIM beads, which was equivalent to 2.5 mL of the RIM beads after the rehydration treatment.

3.3.1.2 Equilibrium isotherm

To study the copper(II) biosorption isotherm, the experiment was conducted according to the procedures described in Section 3.3.1. The reactors were prepared by introducing 0.6 mL of the RIM beads into 50 mL of copper(II) nitrate solutions with concentrations ranging from 10 to 500

mg-Cu/L. The experiment was repeated by using 1 mL of the PIM beads, which was equivalent to 0.6 mL of the RIM beads after the rehydration treatment.

3.3.1.3 Effect of anions

The biosorption experiment was performed by mixing 0.6 mL of the RIM beads with 50 mL of 100 mg-Cu/L copper(II) solutions. The copper solutions were prepared by different copper salts including copper(II) nitrate, copper(II) chloride and copper(II) sulfate. The procedures and conditions were the same as described in Section 3.3.1.

3.3.1.4 Effect of organics

The biosorption experiment was performed by mixing 0.6 mL of the RIM beads with 50 mL of 2 mmol/L copper(II) nitrate solutions containing an organic additive at various concentrations. The organics and their concentrations used in this study are listed in Table 3.1. The procedures and conditions were the same as described in Section 3.3.1.

Table 3.1. A list of organic additives.

Type of organics	Concentration (mmol/L)
Coumarin	1.5; 3
Formaldehyde	1; 2
Urea	0.5; 1
4-butyne-1,2-diol	1; 2

3.3.2 Fixed-bed column

As depicted in Fig. 2.6, both the PIM and RIM beads were packed separately in polyacrylic cylindrical tubes (inner diameter = 1.08 cm) as fixed-bed column reactors. Fixed-bed biosorption experiments were carried out by continuously pumping an upward flow of copper(II) nitrate solutions from the bottom of the column through the stationary biosorbent bed at 25 ^{o}C. Throughout the experiment, the solution pH of the influent copper(II) solution was adjusted to 5.0 by dilute NaOH and HNO_3, and the inlet upward flow rate was regulated by a peristaltic pump. The effluent was collected at designated time intervals for the determination of the copper(II) concentration. The process was continued until a constant copper(II) concentration was obtained in the effluent. At the end of the process, the bed depth was re-measured and the packing was washed by DDI water.

3.3.2.1 Optimization of column biosorption conditions

To optimize the column biosorption process, several critical parameters, including (i) influent copper(II) concentration, (ii) inlet flow rate and (iii) column bed depth, were studied. In the study of the influent copper(II) concentration, 50 to 200 mg-Cu/L copper(II) nitrate solutions were introduced into the columns separately. The effect of inlet flow rate was investigated by introducing the copper(II) solution upwardly at flow rates of 1.0 to 3.0 mL/min. In order to determine the optimal bed depth, the biosorbents were packed in the columns with bed depths of 30 to 50 cm.

The procedures of the fixed-bed biosorption were the same as described in Section 3.3.2.

3.3.2.2 Binary-metal biosorption

The experiments of binary-metal biosorption were performed in the RIM columns by introducing copper(II) solutions in the presence of one additional metal species. The influent solutions were prepared by mixing nitrate salts of copper(II) with either nickel(II), lead(II) or zinc(II) at pH 5.0. The influent concentration of each species was fixed as 1 mM. The experiments were conducted according to the procedures described in Section 3.3.2 with the optimal conditions obtained in Section 3.3.2.1.

3.3.3 Continuous-stirred-tank reactor (CSTR)

The copper(II) biosorption experiment was carried out in a CSTR (inner diameter = 17 cm; maximum capacity = 5 L) as shown in Fig. 3.1. Copper(II) nitrate solution at 50 mg-Cu/L and pH 5.0 was continuously pumped into the reactor. Both the inlet and outlet flow rates were fixed at 1 mL/min in order to maintain a constant reaction volume of about 3.5 L. The reaction mixture was thoroughly mixed with 42 mL of the RIM beads by a magnetic stirrer (Heidolph model MR3001) operating at 250 rpm and 25 ^{o}C. The copper(II) concentration of the effluent was determined at designated time intervals. The experiment was continued until a constant copper(II) concentration of the effluent was obtained. The bead volume was re-measured at the end of the process.

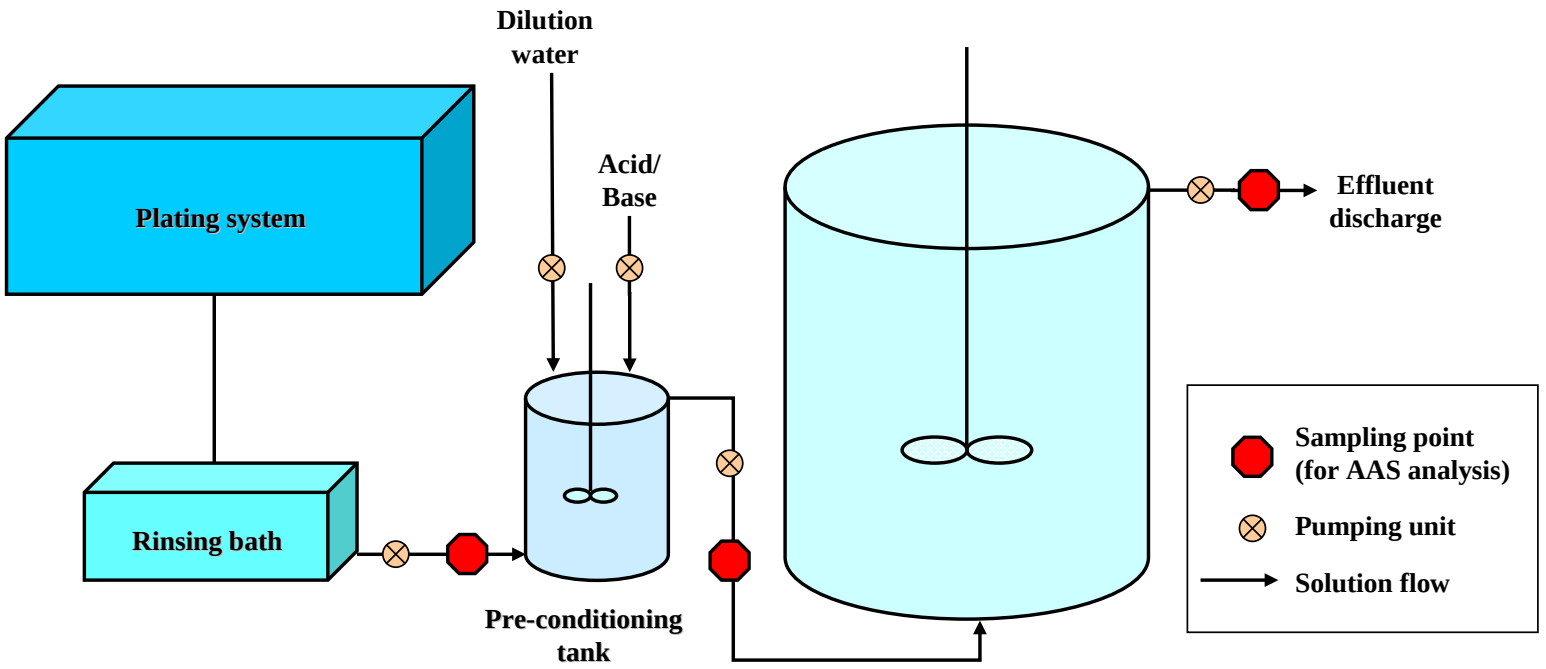

Figure 3.1. Process diagram of Continuous-stirred-tank reactor (CSTR).

3.4 Copper(II) desorption studies

3.4.1 Batch system

The biosorption processes were first performed in a series of batch reactors according to the procedures described in Section 3.3.1. In each reactor, 0.6 mL of the RIM beads was mixed with 50 mL of 100 mg/L copper(II) nitrate solution for 6 h. After the biosorption, 10 mL of the desorbing medium (listed in Table 3.2) was mixed with the copper-laden beads in the orbital shaker operating at 250 rpm and 25 ^{o}C for 6 h. At the end of the biosorption and desorption processes, supernatants were collected for the determination of the residual copper(II) concentration. The beads were washed twice with DDI water after each process and reused in the following biosorption/desorption cycles. The experiments were repeated by using 1 mL of the other bead forms obtained in Section 3.2.2.

Table 3.2. A list of desorbing agents.

Group	Desorbing agent	Concentration (M)
Complexing agents	Ethylenediaminetetraacetic acid disodium salt (Na_2(EDTA))	0.1; 0.5
	Nitrilotriacetic acid disodium salt (Na_2(NTA))	0.1; 0.5
	Sodium tripolyphosphate ($Na_5P_3O_{10}$)	0.1; 0.3
Counter cations	Sodium chloride (NaCl)	1; 2; 4
	Sodium nitrate ($NaNO_3$)	1; 2; 4
	Sodium sulphate (Na_2SO_4)	0.5; 1; 2
	Calcium chloride ($CaCl_2$)	0.2; 1; 2; 4
	Calcium nitrate ($Ca(NO_3)_2$)	0.2; 1; 2; 4
Proton exchangers	Hydrochloric acid (HCl)	0.2; 0.4; 2
	Nitric acid (HNO_3)	0.2; 0.4; 2
	Sulfuric acid (H_2SO_4)	0.1; 0.2; 1

3.4.2 Fixed-bed column

The biosorption experiments were first carried out in the RIM columns according to the procedures described in Section 3.3.2 with the optimal conditions obtained in Section 3.3.2.1. Once the biosorption processes reached the breakthrough point (C_e = 4 mg-Cu/L), various concentrations (1 to 4 M) of the desorbing agent ($CaCl_2$) were introduced upwardly through the column beds under different inlet flow rates (0.5 to 2.0 mL/min). The copper(II) concentration of the desorption effluent was determined at designated intervals. The desorption was continued until no more copper(II) ions could be found in the effluent. At the end of the biosorption and desorption processes, the biosorbent beds were rinsed with DDI water and the bed depths were re-measured.

To carry out consecutive biosorption/desorption cycles, the above procedures were repeated under the optimal conditions of the biosorption and desorption processes. The biosorption processes were conducted up to the breakthrough point (C_e = 4 mg-Cu/L), whereas the desorption processes were continued until 85% of copper content inside the column beds was desorbed. Besides the copper(II) concentration of the effluent, the calcium concentration, the total organic carbon content and the effluent pH were determined.

3.5 Removal and recovery of copper from industrial electroplating wastewater

3.5.1 Compositions of industrial electroplating wastewater

The industrial wastewater was collected from a research laboratory of a local electroplating material supplier. It was a mixture containing the acid copper sulfate plating wastewater, which was collected from different product development studies. To analyze the metal concentrations in the wastewater, the flame atomic absorption (AA) spectrophotometer was used. Moreover, the total organic carbon content was measured by the TOC analyzer, and several common anions such as sulfate, chloride and nitrate were determined by the universal methods (Foulke, 1975; Hillman, 1995).

3.5.2 Integrated wastewater treatment

Integrated treatment process for removal and recovery of copper(II) ions from the industrial wastewater was performed by using the RIM column in ten consecutive biosorption/desorption cycles. The fixed-bed experiment was carried out according to the procedures described in Sections 3.3.2 and 3.4.2 under the optimal conditions of the biosorption and desorption. The setup is shown in Fig. 3.2. The wastewater was first conditioned to 50 mg-Cu/L and pH 5.0, and then pumped upwardly into the column with a bed depth of 50 cm. After reaching the column breakthrough point (C_e = 4 mg-Cu/L), the desorbing agent (1 M $CaCl_2$) was introduced to regenerate the copper-laden RIM packing until 85% of copper content inside the column bed was desorbed. The inlet upward flow rates of both the biosorption and desorption were fixed at 1 mL/min. At

designated time intervals, pH and different compositions (copper, calcium and total organic carbon) in the effluent were determined. The column was rinsed with DDI water at the end of the biosorption and desorption processes. The regenerated column was then reused for further nine cycles.

3.6 Re-use of desorbed copper by electroplating

3.6.1 Conventional precipitation methods

To conduct the chemical precipitation experiments, 50 mL of the industrial wastewater at 50 mg-Cu/L was mixed with either sodium hydroxide pellets or disodium hydrogen phosphate salts under 250-rpm stirring. Both the chemicals were added until there was no further precipitation. The precipitate was then collected by using filtration and then rinsed with excess DDI water. After overnight drying in the oven at 100 ^{o}C, the weight of the precipitate was recorded. The copper contents in the supernatant and the precipitate were determined.

3.6.2 Purification of regenerated copper from desorption effluent

As shown in Fig. 3.2, the desorption effluent was first transferred to tank A of the purification unit after the integrated treatment (Section 3.5.2). Sodium sulfate salt was introduced into the tank until there was no further precipitation. The intermediate supernatant was then pumped into tank B for the second stage of the purification using 1 M disodium hydrogen phosphate solution. The final supernatant was discharged. In these two purification steps, the pH of the reaction mixtures was adjusted to about 5.0. Sedimentation of the precipitate was performed before the supernatant was

discharged or transferred to the next unit. The copper contents of the precipitate and the supernatants were determined. The settled precipitate in tank B was collected to prepare the copper electroplating solution (Section 3.6.3).

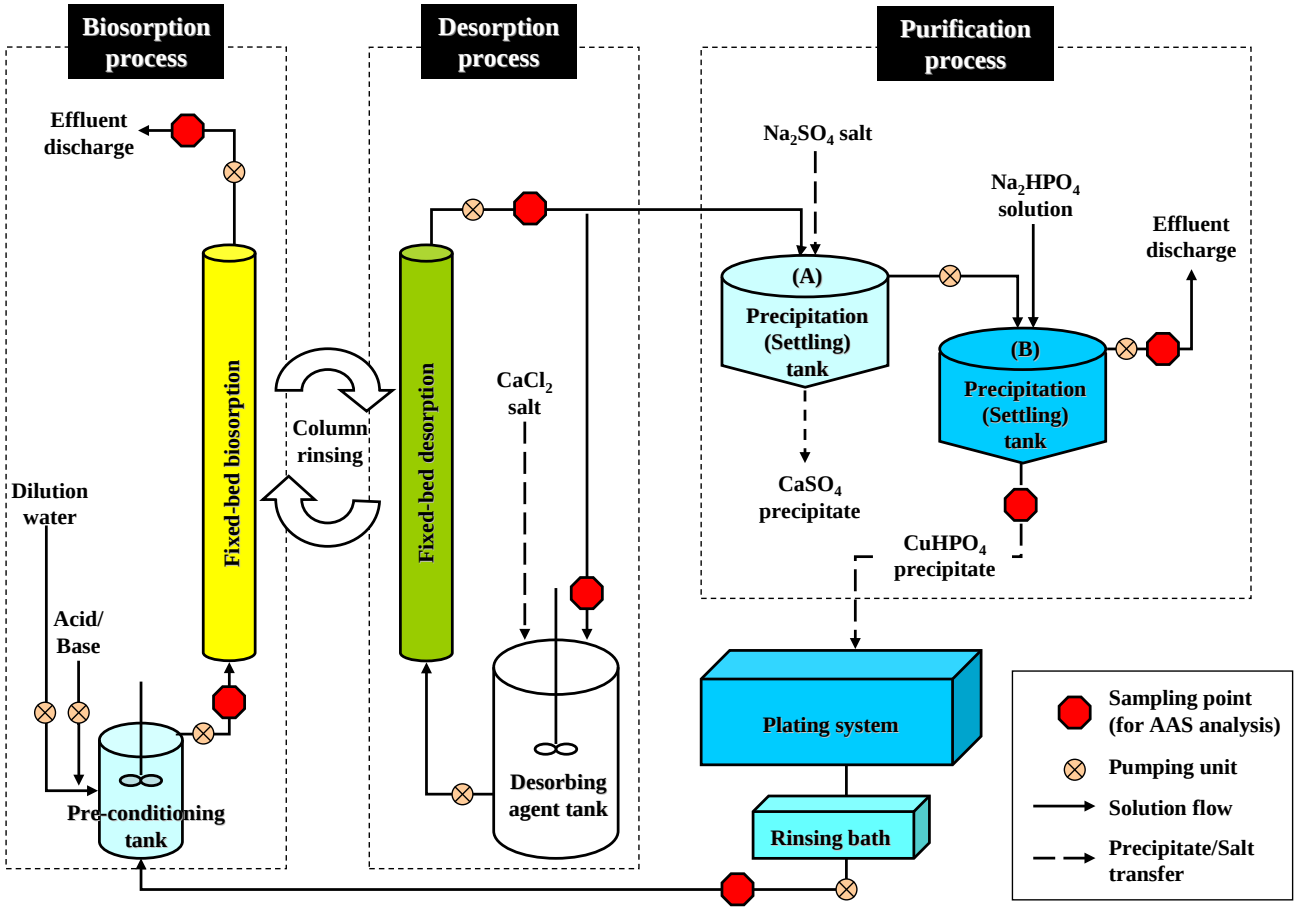

Figure 3.2. Process diagram of integrated wastewater treatment system comprising a copper(II) biosorption column, a column regeneration (copper(II) desorption) process, and a copper recycle (purification) system.

3.6.3 Electroplating of copper

An electroplating bath was first constructed using the following components: (i) a 267-mL lucite Hull cell (Kocour model A267); (ii) a DC-regulated power supply (Manson model MPA-1850); (iii) a polished brass cathode (workpiece); (iv) a corrugated phosphated copper anode; (v) electrical wires. The setup is shown in Fig. 3.3. Before introducing the electrodes into the bath, the cathode was degreased by reagent-graded acetone in an ultrasonic cleaner (Branson model 5510) for 15 min; the anode was first washed by 18 M sulfuric acid and then by DDI water. After the cleaning steps, the cathode was hooked at the inclined wall of the Hull cell and connected to the negative (-) terminal of the power supply, whereas the anode was held at the opposite side of the cathode and connected to the positive (+) terminal. The plating experiments were performed by introducing various compositions of copper plating solutions under different operating conditions as listed in Table 3.3. At the end of the plating process, the cathode was rinsed thoroughly with DDI water and the anodes were again re-immersed in 18 M sulfuric acid followed by DDI water rinsing. The plating performances of different bath compositions and operating conditions were evaluated by comparing the characteristics of the copper deposits on the workpieces (cathodes), which were determined by a Scanning Electron Microscope (Leica model Stereoscan 440), a X-ray Energy Dispersive Analyzer (Jeol model JSM-6490) and a resistance multitester (Sanwa model YX-360TR).

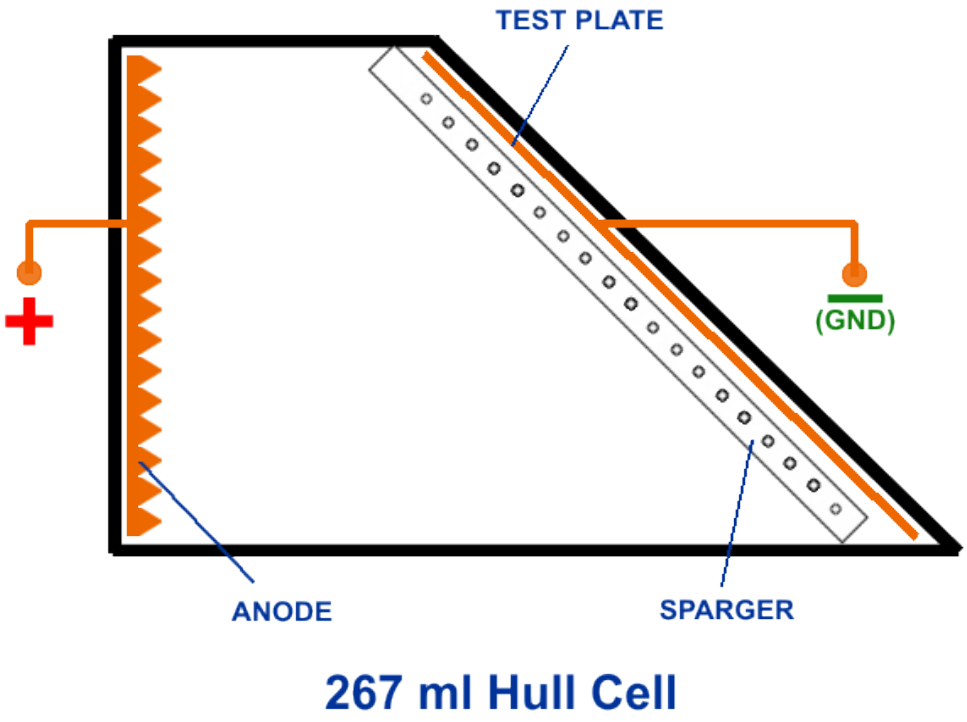

Figure 3.3. Configuration of Hull cell in copper plating. (Think & Tinker Ltd., 2007)

Table 3.3. Compositions of plating solutions and operating conditions of electroplating.

Parameter	Bath components						Plating conditions [a]		
	$CuSO_4 \cdot 5H_2O$ (g/L)	$CuHPO_4$ ($\%_{mole}$)	Recycled Cu [b] ($\%_{mole}$)	H_2SO_4 (g/L)	Cl^- (mg/L)	PVA ($\%_{wt}$)	Current (A)	Agitation (rpm)	Plating time (min)
Copper content	50 – 350	0	0	0	0	0	2	200	10
Acid concentration	200	0	0	0 – 200	0	0	2	200	10
Chloride (from NaCl)	200	0	0	50	0 – 300	0	2	200	10
PVA[c] (Organic additives)	200	0	0	50	75	0.01 – 1.0	2	200	10
Current	200	0	0	50	75	0.1	1 – 5	200	10
Agitation speed	200	0	0	50	75	0.1	5	0 – 300	10
Plating time	200	0	0	50	75	0.1	5	200	1 – 20
$CuHPO_4$ addition [d]	100 – 200 (50 – 100$\%_{mole}$)	0 – 50	0	50	75	0.1	5	200	5
Recycled $CuHPO_4$ addition [d]	195 (97.5$\%_{mole}$)	0	2.5	50	75	0.1	5	200	5

[a] All experiments were carried out at room temperature, and the voltage was automatically regulated by the power supply;
[b] Recycled Cu salt in form of $CuHPO_4$ was obtained as described in Section 3.6.2;
[c] Organic additives – PVA (Polyvinyl alcohol): Molecular weight = 30000 – 70000;
[d] $CuHPO_4$ addition (g/L) = (200 g/L $CuSO_4 \cdot 5H_2O$/ Molecular weight of $CuSO_4 \cdot 5H_2O$) × ($\%_{mole}$ of $CuHPO_4$ added) × (Molecular weight of $CuHPO_4$)/ (Purity of $CuHPO_4$).

3.7 Scanning Electron Microscopy and X-ray Energy Dispersive Analysis

The samples were dried in the oven at 45 ^{o}C overnight and then mounted on aluminum stubs by double-sided tapes. The stubs were further fixed in a sample holder and placed into a sample chamber of the Scanning Electron Microscope (SEM) equipped with the X-ray Energy Dispersive Analyzer (EDAX) (Leica Stereoscan model 440; Jeol model JSM-6490). Both the SEM photographs and EDAX spectra could be obtained after the chamber was flushed full of argon gas under 0.02 to 0.04 mbar. To avoid the accumulation of electrons on the surface of the samples with low electrical conductivity, a thin layer of gold was coated on the samples by a polaron SC502 Sputter Coater before the SEM scanning.

Chapter 4. Results and Discussion

4.1 Preparation of immobilized *Micrococcus luteus*

Although freely suspended biomaterials can provide a better contact with metal ions during biosorption, their use in the biosorption process presents serious problems, including difficulty in biomaterial-liquid separation, low rigidity, low mechanical strength, and unsuitability in large-scale applications. Immobilization of biomaterials can overcome these disadvantages in the use of suspended biomaterials. Biomass immobilization offers the following major advantages:

(i) facilitating the biomass-liquid separation;

(ii) allowing a higher biomass loading;

(iii) enhancing the biosorption capacity;

(iv) producing biosorbents with a suitable size, mechanical strength, rigidity and porosity for applying in scale-up treatment operations;

(v) improving the efficiency, reliability and level of tolerance to shock loading of the biosorption process.

Calcium alginate is commonly employed to immobilize biomaterials. However, this material has a low rigidity and mechanical strength. In this study, in order to enhance the mechanical properties but without demoting the copper(II) biosorption ability, the immobilization method of *Micrococcus luteu*s on Ca-alginate support was studied and modified. Three approaches were used to modify the immobilized biosorbents. These included (i) grafting the immobilization gel with other synthetic polymers; (ii) preparing the beads with other alginate gelation agents; and, (iii) fixing the size of the beads through rehydration processes. The

immobilized *M. luteus* was modified as mentioned in Section 3.2.2. Characteristics of the modified and primitive (without any modification) beads were then studied and compared in copper(II) biosorption experiments as described in Sections 3.3.1 and 3.4.1.

4.1.1 Effect of grafting polymers

To improve the mechanical properties of calcium alginate, different grafting polymers such as polyacrylamide (PAA), polyvinyl alcohol (PVA) and phosphorylated polyvinyl alcohol (P-PVA) were introduced respectively into the alginate matrix for the immobilization of bacterial cells in the previous work of our research group. It was found that a better mechanical strength and a higher uniformity of the cell-immobilized beads were demonstrated by introducing polyacrylamide (PAA) into the alginate beads. These two advantages were important for applying the beads in scale-up treatment processes.

The batch copper(II) biosorption study was performed by mixing 1 mL of the cell-immobilized Ca-alginate/PAA gel beads with 50 mL of 100 mg-Cu/L copper(II) stock solution at pH 5.0 and under 250 rpm shaking for 6 h. The result in Table 4.1 shows that the cell-immobilized Ca-alginate/PAA gel beads exhibited a high copper(II) uptake ability, which was about 81.30 ± 0.13% of copper removal (equivalent to 3.87 ± 0.12 mg of copper). Also, by carrying out a simple filtration step, the biosorbent can be easily separated from solution phase. However, shrinkage of the beads was observed after the copper(II) biosorption in the batch system.

As shown in Table 4.1, about 30% decrease in the bead volume was found in the batch system. It might be caused by the re-arrangement of the alginate cross-linkage and/or change of its linking strength.

The shrinkage was further found in the fixed-bed columns of different bed depth (30 – 50 cm). At the exhaustion stage of the fixed-bed copper(II) biosorption, the percentage decrease of the bead volume was very significant and a notable decline of the bed depth was resulted (Table 4.1). This shrinkage problem would limit the application of the biosorbent and deteriorate the copper(II) biosorption performances in the scale-up system.

In order to retain the advantages of PAA grafting polymer but without the shrinkage problem, the cell-immobilized Ca-alginate/PAA gel beads were further modified in the following studies.

Table 4.1. The characteristics of the cell-immobilized Ca-alginate/polyacrylamide gel beads in the copper(II) biosorption of different reactor systems.

		Batch reactor [*] (Equilibrium)	**Fixed-bed column [#] (Exhaustion)**		
Bed depth	(cm)	-	30	40	50
Copper removal	(mg-Cu)	3.87 ± 0.12	210.08	286.60	387.04
	(%)	81.30 ± 0.13	-	-	-
Bead volume					
Initial	(mL)	1.01 ± 0.12	28.95	39.30	47.80
Final	(mL)	0.70 ± 0.07	18.40	23.73	27.60
|% change|		30.77 ± 1.48	36.44	39.63	42.26
Bed depth					
Initial	(cm)	-	30.0	40.0	50.0
Final	(cm)	-	28.8	37.5	37.2
|% change|		-	4.00	6.25	25.60

Remarks:

[*] Experimental conditions of the batch reactor: Volume of the cell-immobilized beads used = 1 mL; [*Micrococcus luteus*] = 0.066 g-cell/mL-beads; Initial copper(II) concentration = 100 mg-Cu/L; Solution pH = 5.0; Volume of reaction mixture = 50 mL; Contact time = 6 h; Agitation speed = 250 rpm.

[#] Experimental conditions of the fixed-bed column: Column bed depths = 30 – 50 cm; Influent copper(II) concentration = 50 mg-Cu/L; Influent pH = 5.0; Influent upward flow rate = 1 mL/min; [*Micrococcus luteus*] = 0.066 g-cell/mL-beads.

4.1.2 Effect of alginate gelation agents

Salts of strontium, barium and calcium can be used as agents for alginate gelation (Bajpai *et al*., 2006; Moreira *et al*., 2006; Sakurai and Sakakibara, 1999). They could bind water-soluble alginate chains together to form a giant polymer structure through formation of cross linkage (Fig. 2.4). Such bulk polymer is insoluble and effective for biomass entrapment.

Actually, strontium salts are seldom utilized to prepare the alginate polymer for scale-up applications, due to their expensive cost. Another reason is the toxicity of strontium ions. According to the US standard (ATSDR, 2004), strontium ions are strictly limited below 4 μg-Sr/L in drinking water so as to minimize their environmental impact. Due to the cost and safety concerns of strontium salts, they were excluded in this study. Only barium chloride, barium nitrate, calcium chloride and calcium nitrate were used to prepare the immobilized *Micrococcus luteus* for further investigation.

The sizes of the cell-immobilized beads prepared by these gelation agents were similar to each other. The diameters were 3.00 ± 0.03 mm, 3.01 ± 0.03 mm, 3.07 ± 0.03 mm and 3.06 ± 0.03 mm with respect to the beads gelled by barium chloride, barium nitrate, calcium chloride and calcium nitrate.

In order to study the effect of the gelation agents on the copper(II) biosorption capacity, the immobilized *M. luteus* prepared by different

gelation agents was used as the copper biosorbents in the sequential biosorption/desorption cycles. The biosorption process was performed by mixing 1 mL of the cell-immobilized beads with 50 mL of 100 mg-Cu/L copper(II) stock solution at pH 5.0 and under 250 rpm shaking for 6 h. The copper-laden beads were then introduced into 10 mL of 0.2 M hydrochloric acid for the copper(II) desorption. The desorption process was conducted for 6 h. The copper removal and recovery of different kinds of immobilized beads in the sequential biosorption/desorption cycles are presented in Figs. 4.1 (a) and (b).

In the consecutive biosorption/desorption study, the results in Figs. 4.1 (a) and (b) show that the copper removals and recoveries were similar between different kinds of beads. However, the volume of all the beads decreased dramatically from initial 1 mL to about 0.6 mL after the five biosorption/desorption cycles (Fig. 4.1(a)). Fig. 4.2 further illustrates that no improvement of the bead stability was found even using different gelation agents. Thus, this approach could not reduce the shrinkage of the beads during the biosorption/desorption cycles. Calcium salts were preferred to barium salts because barium salts are more toxic than calcium ions. The US standard (ASTDR, 2005) reported that the concentration of barium ions should be limited to 4 mg-Ba/L in drinking water. Of the different calcium salts, calcium chloride was preferably used for the bead preparation in the following studies since calcium chloride was satisfactorily used in our previous work (Lo *et al*., 2002).

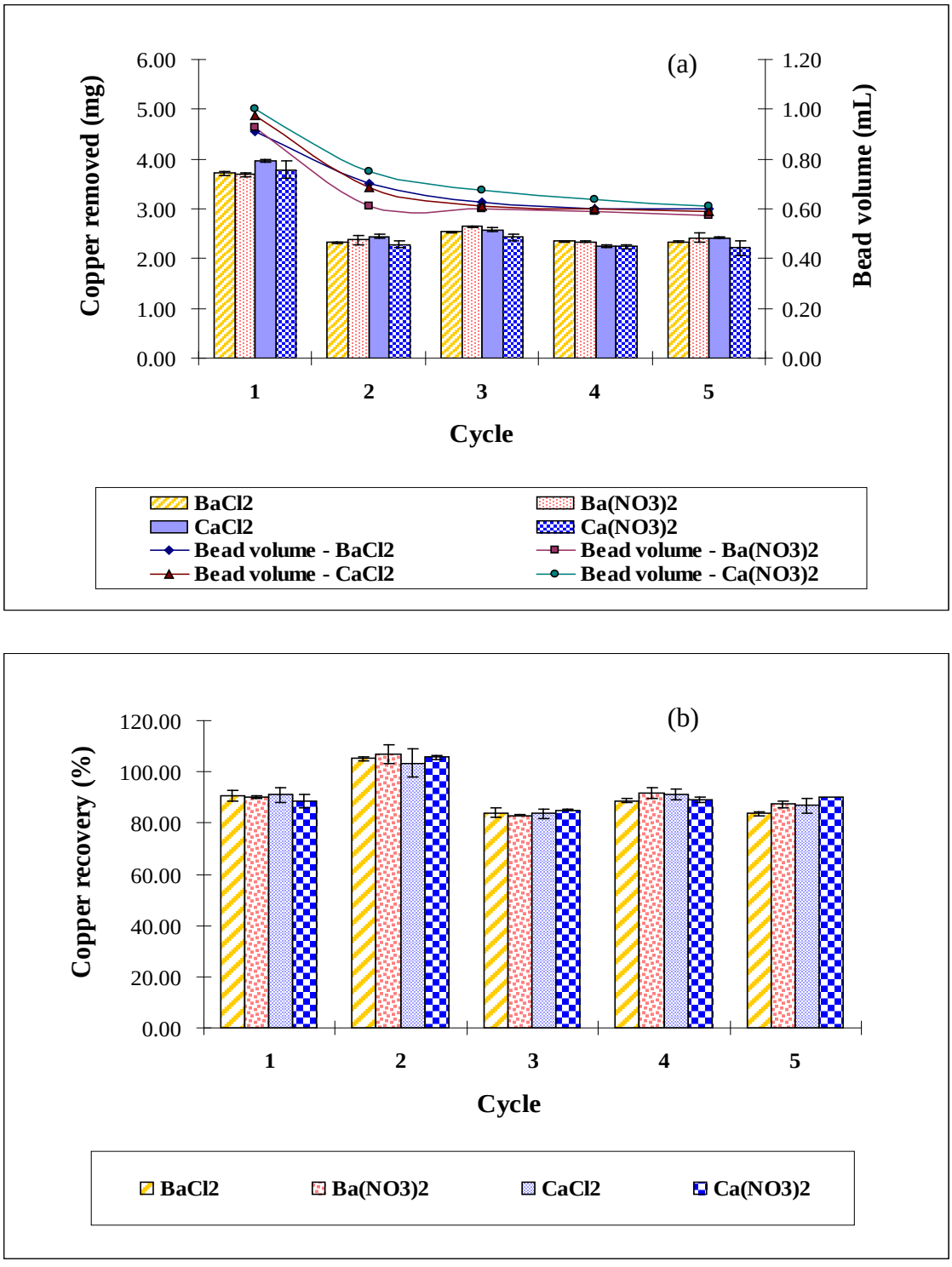

Figure 4.1. Effect of alginate gelation agents on characteristics of immobilized *Micrococcus luteus* in five batch biosorption/desorption cycles: (a) Biosorption; (b) Desorption.

* Experimental conditions are listed in Table 4.2.

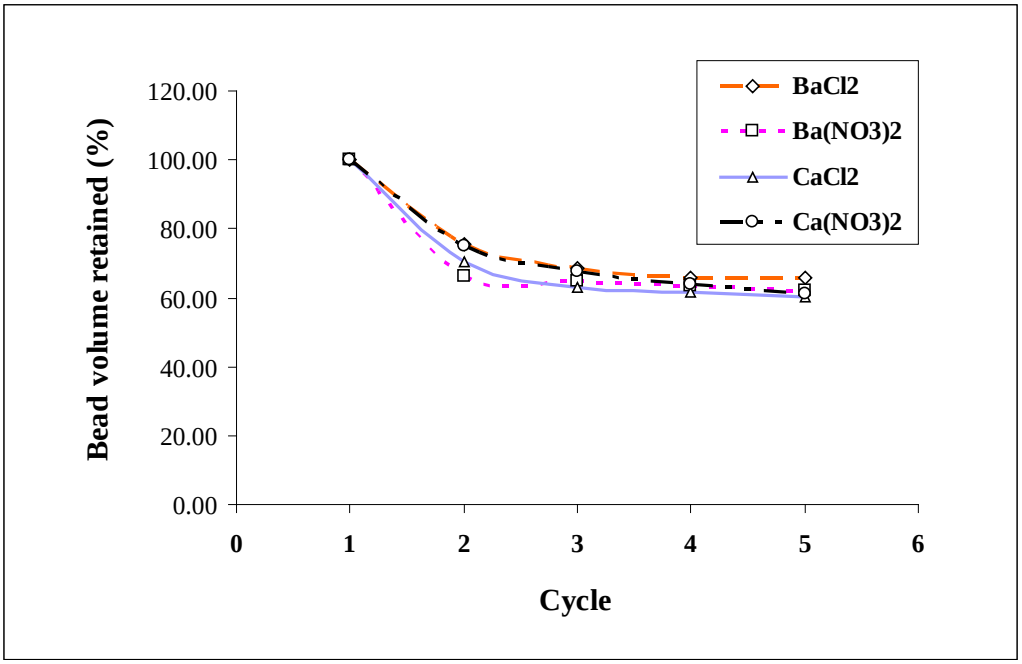

Figure 4.2. Volume change of immobilized *Micrococcus luteus* prepared by different alginate gelation agents in five batch biosorption/desorption cycles.

* Experimental conditions are listed in Table 4.2.

Table 4.2. Experimental conditions of the copper(II) biosorption/desorption cycles using the immobilized *Micrococcus luteus* prepared by different alginate gelation agents (correlated to Section 4.1.2).

Biosorption	**Desorption**
– Volume of cell-immobilized beads used = 1 mL (for all forms of the beads); – Concentration of *Micrococcus luteus* in the beads = 0.066 g-cell/mL-beads; – Initial copper(II) concentration = 100 mg-Cu/L; – Solution pH = 5.0; – Volume of reaction mixture = 50 mL; – Contact time = 6 h; – Agitation speed = 250 rpm.	– Desorbing agent used = 10 mL of 0.2 M HCl; – Contact time = 6 h; – Agitation speed = 250 rpm.

4.1.3 Effect of rehydration treatment

The immobilized *Micrococcus luteus* prepared by the $CaCl_2$ gelation agents were divided into two groups. One group was dried in the freeze-dryer and the second group was dried in the oven at 40 ^{o}C. After the overnight drying, the dehydrated beads were then re-immersed in DDI water for five days. This process is called 'rehydration treatment'. The details of the treatment are described in Section 3.2.2. High-temperature drying should be avoided since surface cracking and destruction of the biosorbents might occur (Bajpai and Sharma, 2004).

Fig. 4.3 shows the volume change of the beads during the rehydration treatment. After the drying processes, the bead volume in these two groups decreased significantly from 1.00 mL to about 0.20 mL and 0.15 mL for the freeze-drying and the oven-drying, respectively. Swelling of these two bead groups was observed when the biosorbents were re-immersed into DDI water. The bead volume was stabilized to about 0.6 mL after the five-day rehydration process. This observation may be due to the presence of polyacrylamide (PAA) matrix inside the beads. It might promote the reconstruction of the bead internal lattice, resulting in the swelling. However, the volume of these rehydrated beads was smaller than that of the untreated species. This might be related to the rearrangement of the alginate configuration during drying. This would strengthen the cross-linkage and shorten the distance between the polymer chains. Thus, the swelling of the beads was restricted, inducing the smaller bead volume.

The shapes of the beads prepared by the two different drying methods were examined and compared. The beads could maintain their spherical shape after the oven drying and also in the following rehydration step. By contrast, a serious collapse and an irregular shape were observed in the freeze-dried beads and their rehydrated forms. Such distorted morphology was unsuitable for scale-up applications. It might induce clogging in a fixed-bed process when these irregular beads were packed into the column. Thus, the oven-drying method is preferred to the freeze-drying method.

To study the effect of the rehydration on the copper(II) biosorption and desorption, the rehydrated beads of the oven-dried immobilized *M. luteus* were applied to the five sequential copper(II) biosorption/desorption cycles. As shown in Figs. 4.4 (a) and (b), the untreated immobilized *M. luteus* and the rehydrated beads could perform similar copper removals and recoveries in all the cycles. The differences were almost less than 10%. In view of the bead stability, the volume of the untreated beads significantly decreased with about 40% over the cycles (Fig. 4.4 (a)). However, the volume of the rehydrated beads remained almost constant. All these results showed that the oven-drying process with rehydration could produce highly stable Ca-alginate/PAA gel beads with unaffected copper(II) biosorption and desorption properties.

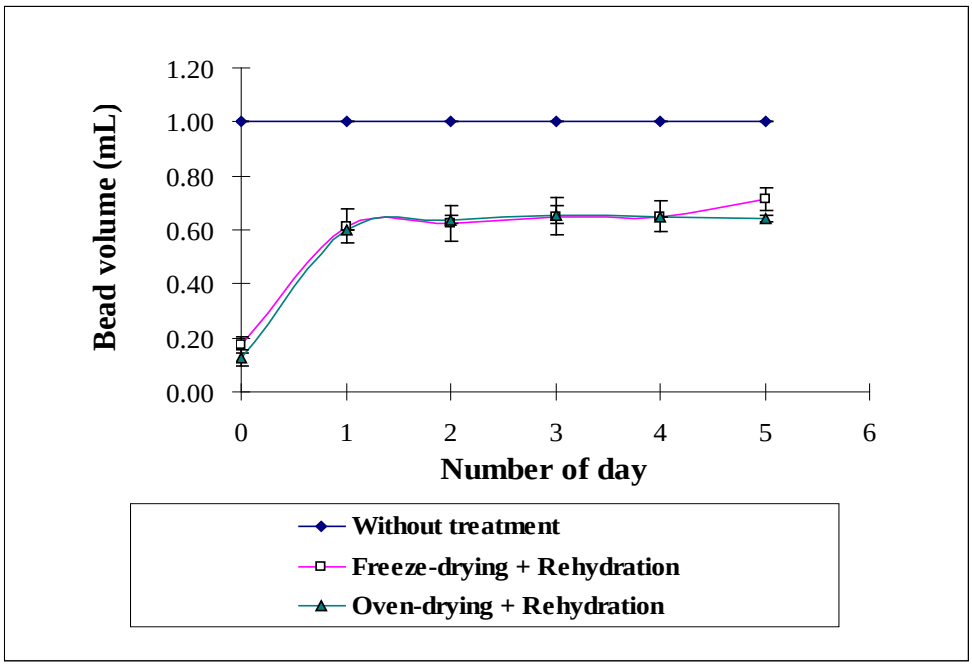

Figure 4.3. Volume change of immobilized *Micrococcus luteus* during rehydration treatment.

* Treatment conditions are listed in Table 4.3.

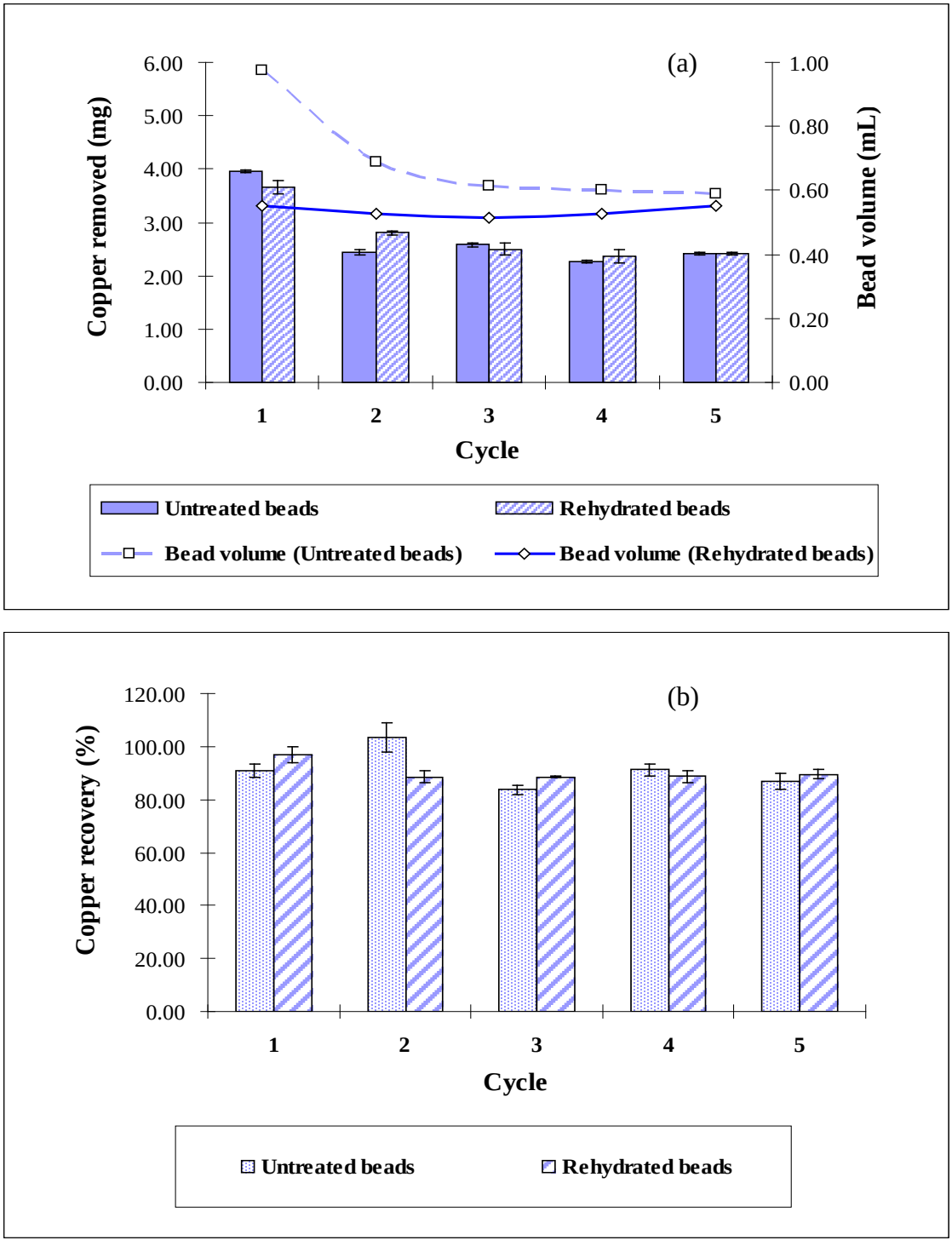

Figure 4.4. Effect of rehydration treatment (40 ^{o}C oven-drying with rehydration) on characteristics of immobilized *Micrococcus luteus* in five batch biosorption/desorption cycles: (a) Biosorption; (b) Desorption.

* Experimental conditions are listed in Table 4.3.

Table 4.3. Treatment conditions of rehydration processes of the immobilized *Micrococcus luteus* and experimental conditions of the copper(II) biosorption/desorption cycles (correlated to Section 4.1.3).

Treatment conditions	
Freeze-drying with rehydration	**Oven-drying with rehydration**
– Volume of cell-immobilized beads used = 1 mL (using $CaCl_2$ gelation agent); – The beads were dried overnight in the freeze-dryer and then re-immersed in DDI water for 5 days.	– Volume of cell-immobilized beads used = 1 mL (using $CaCl_2$ gelation agent); – The beads were dried overnight in the 40 ^{o}C oven and then re-immersed in DDI water for 5 days.
Experimental conditions	
Biosorption	**Desorption**
– Volume of cell-immobilized beads used = 0.6 mL (the beads with the oven-drying-rehydration treatment) and 1 mL (the beads without the treatment); – Concentration of *Micrococcus luteus* in the beads = 0.133 g-cell/mL-beads (the beads with the oven-drying-rehydration treatment) and 0.066 g-cell/mL-beads (the beads without the treatment); – Initial copper(II) concentration = 100 mg-Cu/L; – Solution pH = 5.0; – Volume of reaction mixture = 50 mL; – Contact time = 6 h; – Agitation speed = 250 rpm.	– Desorbing agent used = 10 mL of 0.2 M HCl; – Contact time = 6 h; – Agitation speed = 250 rpm.

4.2 Batch copper(II) biosorption studies

The results in Section 4.1.3 show that the stability of the immobilized *Micrococcus luteus* could be enhanced by the rehydration treatment. To further examine the effect of this treatment on the copper(II) biosorption characteristics, studies on biosorption kinetics, biosorption isotherms, diffusion properties and effect of anions were carried out. In the following section, the rehydrated form of the immobilized *M. luteus* will simply be called 'RIM' beads and the primitive (untreated) cell-immobilized beads will be termed as 'PIM' beads.

4.2.1 Effect of contact time

The time required for copper uptake to reach equilibrium by the RIM and PIM beads was studied. As described in Section 3.3.1.1, the experiment was carried out by introducing an equivalent weight of the RIM and PIM beads into 250 mL of 100 mg-Cu/L copper(II) solution at solution pH 5.0, respectively. The reaction mixtures were mixed well on the orbital shaker operating at 250 rpm at 25 ^{o}C. The copper concentration of the reaction mixtures was determined at designated time intervals.

Fig. 4.5 compares the copper(II) biosorption capacity of the RIM and PIM beads as a function of contact time. The kinetic profiles for copper removal by the two immobilized biosorbents showed a similar trend. The copper uptake rate of both the RIM and PIM beads at the first 180 min was relatively rapid. Then, the copper uptake rate was reduced gradually after 180 min and the biosorption reached equilibrium at 720 min.

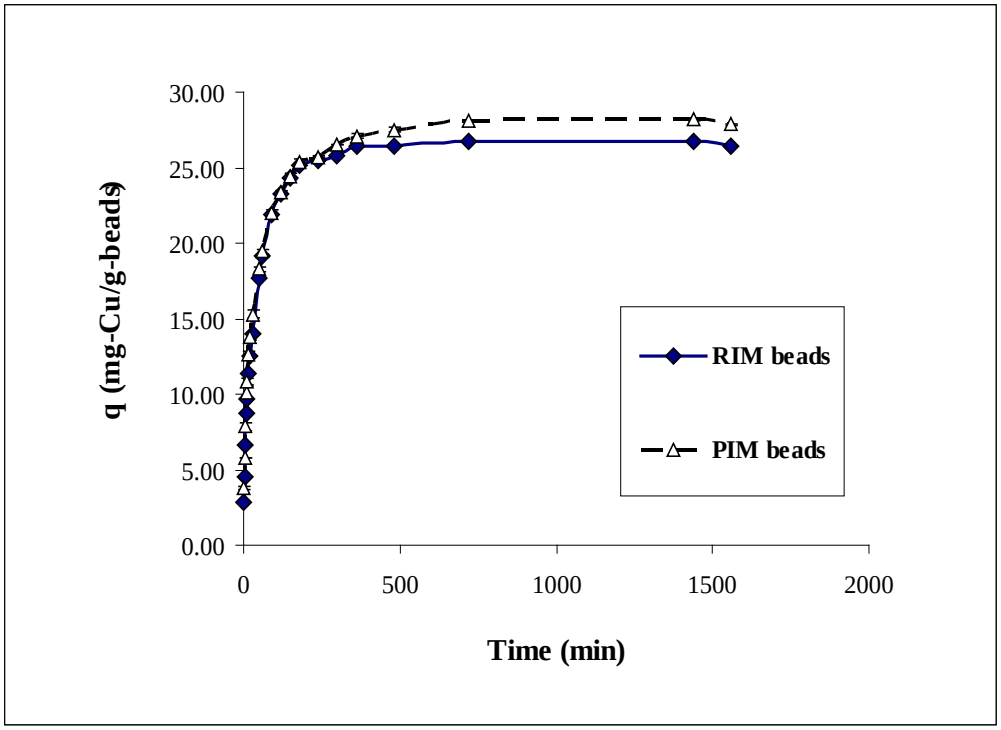

Figure 4.5. Kinetic profiles of copper(II) biosorption using different forms of immobilized *Micrococcus luteus*: Rehydrated beads (RIM) and Primitive form (PIM).

* Experimental conditions: Volume of cell-immobilized beads used = 2.5 mL (for RIM beads) and 5 mL (for PIM beads); Density of cell-immobilized beads = 0.2916 ± 0.0035 g/mL (for RIM beads) and 0.1456 ± 0.0003 g/mL (for PIM beads); [*Micrococcus luteus*] = 0.133 g-cell/mL-beads (for RIM beads) and 0.066 g-cell/mL-beads (for PIM beads); Initial copper(II) concentration = 100 mg-Cu/L; Solution pH = 5.0; Volume of reaction mixture = 250 mL; Agitation speed = 250 rpm.

4.2.2 Biosorption kinetics

The aim of this part of research was to investigate the effect of rehydration treatment on the copper(II) biosorption kinetics. The biosorption kinetic profiles of both the RIM and PIM beads were obtained by following the experimental procedures stated in Section 3.3.1.1. These profiles are displayed in Fig. 4.5.

The kinetic study has demonstrated that the kinetic profiles of copper(II) biosorption by both the RIM and PIM beads were similar (Fig. 4.5). The copper removals increased rapidly at the initial phase and then gently rose to equilibrium. The equilibrium time was almost the same at about 720 minutes. These two kinetic profiles overlapped with each other in the time period up to 240 min. However, at the equilibrium, the copper removal by the PIM beads was slightly larger than that by the RIM beads. This might be related to change of the internal bead structure after the rehydration. The cross linkage of alginate inside the beads might be re-arranged during rehydration, inducing pore blockage and channel narrowing inside the beads. A greater internal diffusion resistance inside the RIM beads was then developed. The diffusion of copper(II) ions was thus restricted in the beads. Fewer or no copper(II) ions could access the blocked interior binding sites, causing the lower copper removal by the RIM beads at the equilibrium.

The experimental data were further simulated by the pseudo-first-order and pseudo-second-order kinetic models with both the linear and non-linear

regressions. Table 4.4 lists the model parameters, while Figs. 4.6 (a) and (b) display the simulated profiles. The results show that the pseudo-second-order model achieved larger correlation coefficient (r^2) and smaller root mean square errors (RMSE) than the pseudo-first-order model. This validated that the pseudo-second-order model was more representative than the pseudo-first-order model for simulating the kinetic data of both the RIM and PIM beads.

Regarding the pseudo-second-order kinetic constants (k_2*), Table 4.4 shows that the constants k_2* for both the RIM and PIM beads were similar, with less than 18% difference. This indicates that the kinetics of copper(II) biosorption by the RIM beads was similar to that by the PIM beads.

To summarize, the rehydration treatment of the Ca-alginate/PAA immobilized *Micrococcus luteus* did not significantly influence the copper(II) biosorption rate. The biosorption of copper(II) ions by both the RIM and PIM beads was better simulated by the pseudo-second-order kinetics.

Table 4.4. Calculated parameters of pseudo-first-order and pseudo-second-order kinetic models for copper(II) biosorption using different forms of immobilized *Micrococcus luteus*.

	Rehydrated cell-immobilized beads (RIM)				**Primitive cell-immobilized beads (PIM)**			
Pseudo-first-order kinetic model								
	k_1* (min^{-1})	q_e (mg-Cu/g-beads)	r^2	RMSE	k_1* (min^{-1})	q_e (mg-Cu/g-beads)	r^2	RMSE
Linear form	$9.65\times10^{-3} \pm 7.07\times10^{-5}$	16.13 ± 0.09	0.9406 ± 0.0024	10.54 ± 0.17	$7.90\times10^{-3} \pm 4.24\times10^{-4}$	16.60 ± 0.08	0.9529 ± 0.0087	11.70 ± 0.07
Non-linear form	$3.11\times10^{-2} \pm 7.21\times10^{-4}$	25.43 ± 0.03	0.9616 ± 0.0003	1.68 ± 0.01	$3.55\times10^{-2} \pm 1.19\times10^{-3}$	25.92 ± 0.03	0.9263 ± 0.0015	2.28 ± 0.02
Pseudo-second-order kinetic model								
	k_2* (g-beads · mg-C u^{-1} · min^{-1})	q_e (mg-Cu/g-beads)	r^2	RMSE	k_2* (g-beads · mg-C u^{-1} · min^{-1})	q_e (mg-Cu/g-beads)	r^2	RMSE
Linear form	$2.12\times10^{-3} \pm 9.33\times10^{-5}$	26.95 ± 0.00	0.9998 ± 0.0001	1.19 ± 0.06	$1.75\times10^{-3} \pm 4.31\times10^{-5}$	28.45 ± 0.06	0.9998 ± 0.0000	1.21 ± 0.00
Non-linear form	$1.61\times10^{-3} \pm 3.75\times10^{-5}$	27.48 ± 0.01	0.9907 ± 0.0001	0.83 ± 0.00	$1.79\times10^{-3} \pm 6.22\times10^{-5}$	27.99 ± 0.02	0.9906 ± 0.0134	1.15 ± 0.00

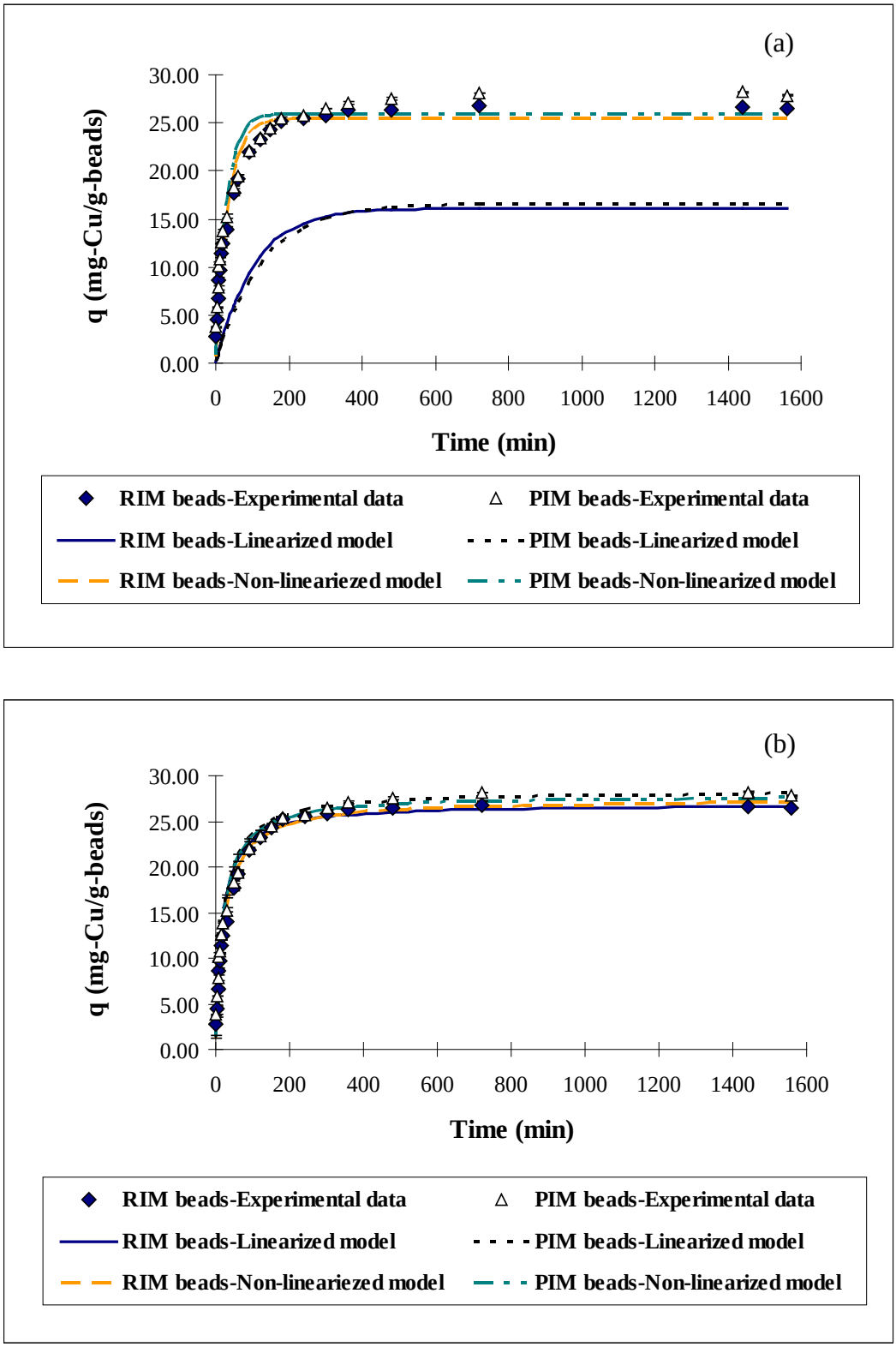

Figure 4.6. Simulated kinetic profiles of copper(II) biosorption using different forms of immobilized *Micrococcus luteus* (Rehydrated beads – RIM and Primitive form – PIM): (a) Pseudo-first-order model; (b) Pseudo-second-order model.

4.2.3 Biosorption isotherms

As stated by Bilgili (2006), biosorption isotherm is a simple method to understand the metal biosorption behavior of the biosorbents under different metal concentrations in aqueous environment. To collect such information on both the RIM and PIM beads, the experiment was conducted by introducing an equivalent weight of these two bead forms into 50 mL of copper solution with concentrations ranging from 10 to 500 mg-Cu/L for 6 h (described in Section 3.3.1.2). The Cu(II) biosorption isotherms of the RIM and PIM beads are presented in Fig. 4.7.

Fig. 4.7 shows that the equilibrium isotherms of both the RIM and PIM beads increased sharply at low Cu(II) equilibrium concentrations (C_e). When the C_e was above 20 mg-Cu/L, the isotherm profiles became much less steep. This implied that the binding sites became saturated at this stage.

The copper removal by the RIM beads was similar to that by the PIM beads at low Cu(II) equilibrium concentrations (C_e). As the C_e increased further, the copper removal by the RIM beads was lower than that by the PIM beads (Fig. 4.7). The lower copper removal may be caused by the change of the internal bead structure after rehydration treatment. This created a greater mass transfer resistance inside the RIM beads. As a result, a lower mass transfer and uptake of copper(II) ions by the RIM beads were resulted.

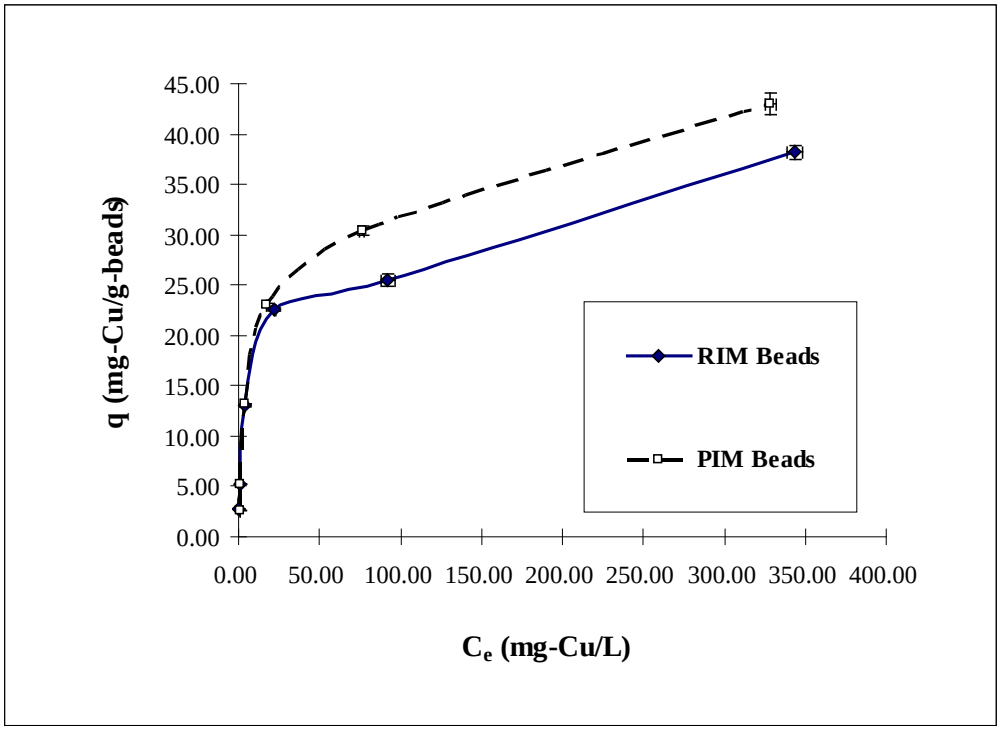

Figure 4.7. Equilibrium isotherms of copper(II) biosorption using different forms of immobilized *Micrococcus luteus*: Rehydrated beads (RIM) and Primitive form (PIM).

* Experimental conditions: Volume of cell-immobilized beads used = 0.6 mL (for RIM beads) and 1 mL (for PIM beads); Density of cell-immobilized beads = 0.3037 ± 0.0127 g/mL (for RIM beads) and 0.1694 ± 0.0050 g/mL (for PIM beads); [*Micrococcus luteus*] = 0.133 g-cell/mL-beads (for RIM beads) and 0.066 g-cell/mL-beads (for PIM beads); Solution pH = 5.0; Volume of reaction mixture = 50 mL; Contact time = 6 h; Agitation speed = 250 rpm.

Langmuir and Freundlich isotherm models were applied to simulate the isotherm data of the RIM and PIM beads. The model equations are listed in Section 2.3.3.4. Both linear and non-linear regression analyses were employed to fit the isotherm data to these two isotherm models. Table 4.5 lists the calculated model parameters. The simulated profiles are displayed in Figs. 4.8 (a) and (b).

As shown in Table 4.5, the correlation coefficients (r^2) of all the isotherm model simulations (both the linear and non-linear regressions) were close to unity, and reasonably-small root mean square errors (RMSE) were found. These results indicate that the copper(II) biosorption isotherms could be described well by both the Langmuir and Freundlich models. The Langmuir parameter "b" represents the Cu(II) binding affinity of the biosorbent, and the Freundlich parameter "K" represents the amount of sorbed copper when the solution concentration in the equilibrium is unity. Both the parameters "b" and "K" measure the effectiveness of Cu(II) biosorption at low C_e. Table 4.5 shows that both the parameters "b" and "K" obtained for the RIM beads were close to those for the PIM beads, indicating that both types of beads had similar Cu(II) biosorption ability at low C_e. Moreover, a lower Langmuir "q_o" value was obtained for the RIM beads. All these observations from the modeling matched the experimental results that the Cu(II) biosorption data of the RIM beads overlapped with that of the PIM beads at low Cu(II) levels and the Cu(II) biosorption capacity of the RIM beads was lower than that of the PIM beads at high C_e (Fig. 4.7).

Table 4.5. Calculated parameters of Langmuir and Freundlich isotherm models for copper(II) biosorption by different forms of immobilized *Micrococcus luteus*.

	Rehydrated cell-immobilized beads (RIM)				**Primitive cell-immobilized beads (PIM)**			
Langmuir model								
	q_o (mg-Cu/g-beads)	b (L/mg-Cu)	r^2	RMSE	q_o (mg-Cu/g-beads)	b (L/mg-Cu)	r^2	RMSE
Linear form	38.84 ± 0.75	6.95×10^{-2} ± 7.07×10^{-4}	0.9843 ± 0.0017	5.20 ± 0.07	44.46 ± 1.12	6.45×10^{-2} ± 2.12×10^{-3}	0.9941 ± 0.0003	3.99 ± 0.16
Non-linear form	33.16 ± 0.84	1.36×10^{-1} ± 9.97×10^{-3}	0.9157 ± 0.0028	4.36 ± 0.02	40.44 ± 1.01	8.47×10^{-2} ± 2.21×10^{-3}	0.9601 ± 0.0021	3.47 ± 0.17
Freundlich model								
	K (mg-Cu/g-beads)	n	r^2	RMSE	K (mg-Cu/g-beads)	n	r^2	RMSE
Linear form	5.65 ± 0.00	2.78 ± 0.04	0.9194 ± 0.0060	5.49 ± 0.08	4.77 ± 0.01	2.33 ± 0.03	0.8995 ± 0.0040	8.30 ± 0.16
Non-linear form	8.00 ± 0.05	3.71 ± 0.05	0.9570 ± 0.0055	3.11 ± 0.13	7.95 ± 0.02	3.36 ± 0.05	0.9524 ± 0.0008	3.79 ± 0.06

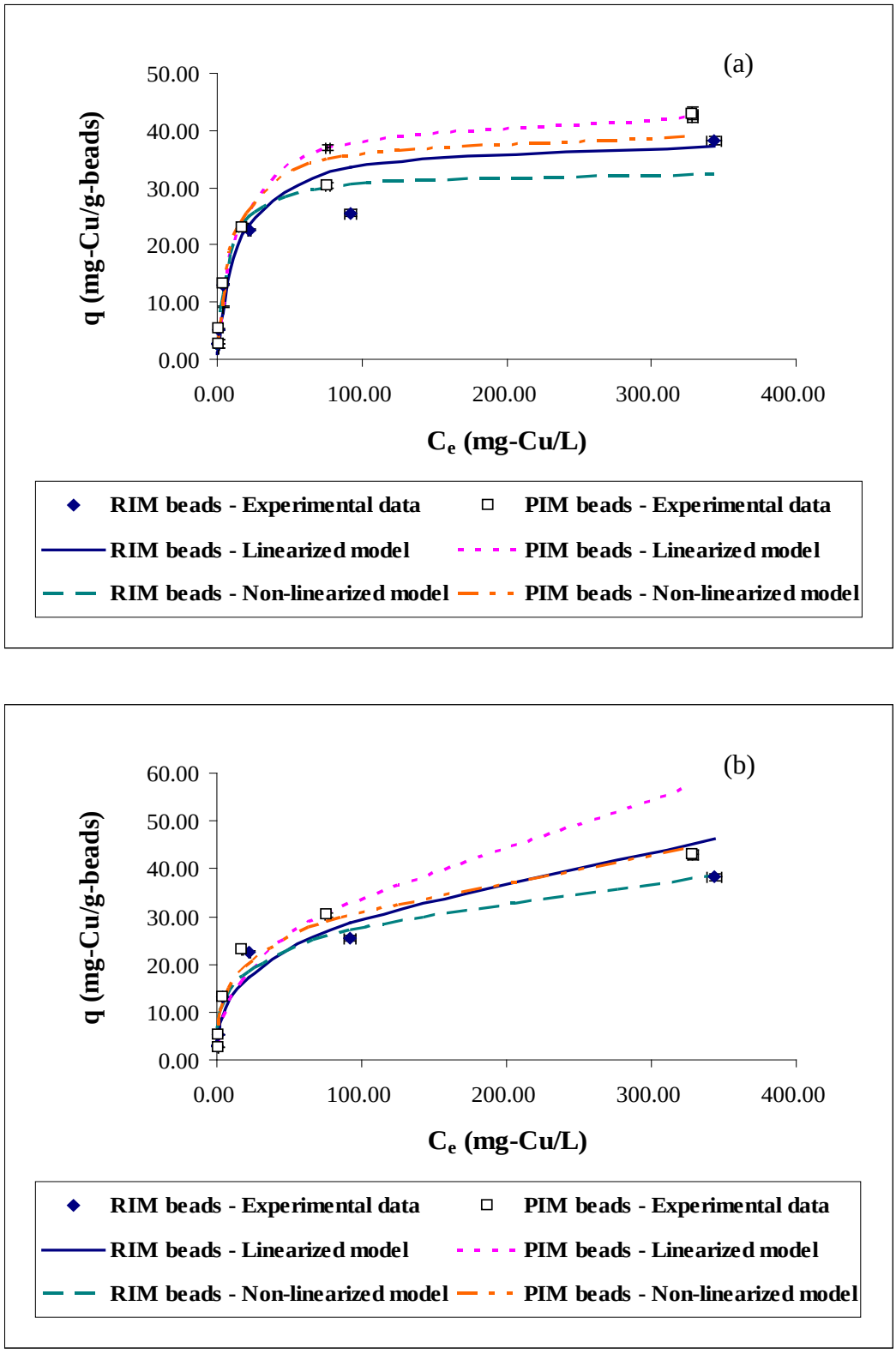

Figure 4.8. Simulated isotherm profiles of copper(II) biosorption using different forms of immobilized *Micrococcus luteus* (Rehydrated beads – RIM and Primitive form – PIM): (a) Langmuir isotherm model; and (b) Freundlich isotherm model.

4.2.4 Diffusion properties

The rehydration treatment might affect the structural arrangement of the immobilized *M. luteus*, which would, in turn, affect the diffusion properties of copper(II) ions surrounding and inside the cell-immobilized beads. Both the intraparticle diffusion coefficients and the external film diffusion coefficients for copper(II) ions in the RIM and PIM beads were calculated in this sub-section to investigate the effect of rehydration treatment on the diffusion properties.

4.2.4.1 Intraparticle diffusion coefficient

The mass transfer within an adsorbent particle (intraparticle diffusion) is generally attributed by pore diffusion and surface diffusion. In this study, both the RIM and PIM beads are highly porous, with porosity (ε) equal to 0.75 and 0.89, respectively. Thus, the pore diffusion should be the dominant factor in the intraparticle diffusion, whereas the surface diffusion could be neglected. Based on this assumption, the intraparticle diffusion coefficient could be simply calculated by using the pore diffusion model derived from Fick's law. This model regards concentration gradient as the driving force of diffusion. The equation of the pore diffusion model associated with its initial and boundary conditions are expressed as follows:

$$\varepsilon \frac{\partial C_f}{\partial t} + (1-\varepsilon)\,\rho \frac{\partial q}{\partial t} = \frac{\varepsilon D}{r^2} \frac{\partial}{\partial r}\left(r^2 \frac{\partial C_f}{\partial r} \right) \qquad \text{(Equation 4.1)}$$

As $C_f(r, t)$ is based on the solution volume within the pores,

the initial condition is:

$$C_f = 0 \qquad (t = 0) \qquad \text{(Equation 4.2)}$$

and the boundary conditions are:

$$\frac{\partial C_f}{\partial r} = 0 \qquad (r = 0, t > 0) \qquad \text{(Equation 4.3)}$$

$$\varepsilon D \frac{\partial C_f}{\partial r} = k_m (C_b - C_f) \qquad (r = h, t > 0) \qquad \text{(Equation 4.4)}$$

where ε is the porosity of the adsorbent particle; C_f is the concentration of the adsorbates in the pore fluid phase (mol $_{adsorbates}$/L $_{fluid}$); C_b is the concentration of the adsorbates in the bulk surrounding the adsorbent particle (mol $_{adsorbates}$/L $_{fluid}$); ρ is the density of the adsorbent (g/L); q is the concentration of metal ions in the adsorbed phase (mg $_{adsorbate}$/g $_{adsorbent}$); D is the diffusion coefficient in the pore space (cm^2/s); r is the radius of the spherical particle (cm); h is the half length of diffusion path (= radius of the spherical object (r), cm); k_f is the external mass transfer coefficient (cm/ s).

With the assumption of linear adsorption isotherm, Equation 4.1 can be modified and solved by Laplace transform. The solution for the concentration distribution within the particle is given below:

$$\frac{C(x,\tau) - C_o}{C_b - C_o} = 1 - \sum_{n=1}^{\infty} a_n K_n(x) \cdot \exp\left(-\varphi_n^2 \tau\right) \qquad \text{(Equation 4.5)}$$

where $x = \frac{r}{h}$, $\tau = \frac{D_{app}\, t}{R^2}$, $a_n = \frac{2(\sin\varphi_n - \varphi_n \cos\varphi_n)}{\varphi_n^2 \left(1 + \frac{\cos^2 \varphi_n}{B_i - 1}\right)}$, $K_n(x) = \frac{\sin(\varphi_n x)}{x}$,

$\varphi_n \cos\varphi_n = (1 - B_i) \cdot \sin\varphi_n$, $B_i = \frac{k_m R}{\varepsilon D}$,

n is the number of experimental points, φ_n is the eigenvalue, B_i is the Biot number, D_{app} is the apparent intraparticle diffusion coefficient ($D_{app} = \frac{\varepsilon D}{\varepsilon + (1-\varepsilon)K\rho}$) and K is the slope of the linear isotherm.

By introducing the fractional uptake of the adsorbate molecules at the time t (Equation 4.6) into Equation 4.5, Equation 4.7 is resulted.

$$F = \frac{q_t}{q_e} = \frac{C_o - C_t}{C_o - C_\infty} \qquad \text{(Equation 4.6)}$$

$$F = 1 - \sum_{n=0}^{\infty} b_n \cdot \exp\left(-\varphi_n^2 \tau\right) \qquad \text{(Equation 4.7)}$$

where $b_n = \frac{6\left(\sin\varphi_n - \varphi_n \cos\varphi_n\right)^2}{\varphi_n^4\left(1 + \frac{\cos^2\varphi_n}{B_i - 1}\right)}$.

When the film resistance becomes negligible compared to the internal diffusion resistance ($B_i \rightarrow \infty$), Equation 4.7 can be simplified to:

$$F = 1 - \frac{6}{\pi^2}\sum_{n=0}^{\infty}\left(\frac{1}{n}\right)^2 \exp\left\{\frac{-D_{app} n^2 \pi^2 t}{h^2}\right\} \qquad \text{(Equation 4.8)}$$

Aharoni and Suzin (1982) suggested that in the early stage of the adsorption process (t is relatively small), Equation 4.8 can be reduced to Equation 4.9. Then, the apparent intraparticle diffusion coefficient (D_{app}) can be determined directly from the slope of the plot of F versus $t^{1/2}$.

$$F = \frac{6}{\pi^{1/2}} \frac{D_{app}^{\ 1/2}}{h} t^{1/2} \qquad \text{(Equation 4.9)}$$

As discussed above, this equation is based on the assumption of linear adsorption isotherm. In this study, Fig. 4.7 shows that the biosorption isotherm of the RIM and PIM beads could be regarded as linear when the Cu(II) biosorption capacity was up to 15 mg-Cu/g-beads. Only the kinetic data (Section 4.2.2) taken within the initial time period of 3 – 20 min were applied to plotting F versus $t^{1/2}$ to determine the apparent intraparticle diffusion coefficients (D_{app}) for copper(II) ions in the RIM and PIM beads.

The plots of F Vs $t^{1/2}$ are depicted in Fig 4.9 for copper(II) biosorption using the RIM and PIM beads. Both the plots of the RIM and PIM beads were linear with large r^2 values (above 0.98). By determining the slope of the plots, the intraparticle diffusion coefficients for copper(II) ions in the RIM beads and PIM beads could be determined. They were $2.04 \times 10^{-7} \pm 4.15 \times 10^{-9}$ and $3.80 \times 10^{-7} \pm 1.44 \times 10^{-8}$ cm^2/s, respectively. The coefficient in the RIM beads was smaller than that in the PIM beads, illustrating that a greater diffusion resistance existed in the RIM beads. This was caused by the compression of the beads' internal structure during the rehydration treatment. The relative volume occupied by the bacterial cells inside the beads was thus greatly increased to about 50% with 16% decrease in the bead's porosity. This resulted in a greater intraparticle diffusion resistance in the RIM beads. Consequently, a lower copper(II) removal by the RIM beads was resulted, as discussed in Section 4.2.3.

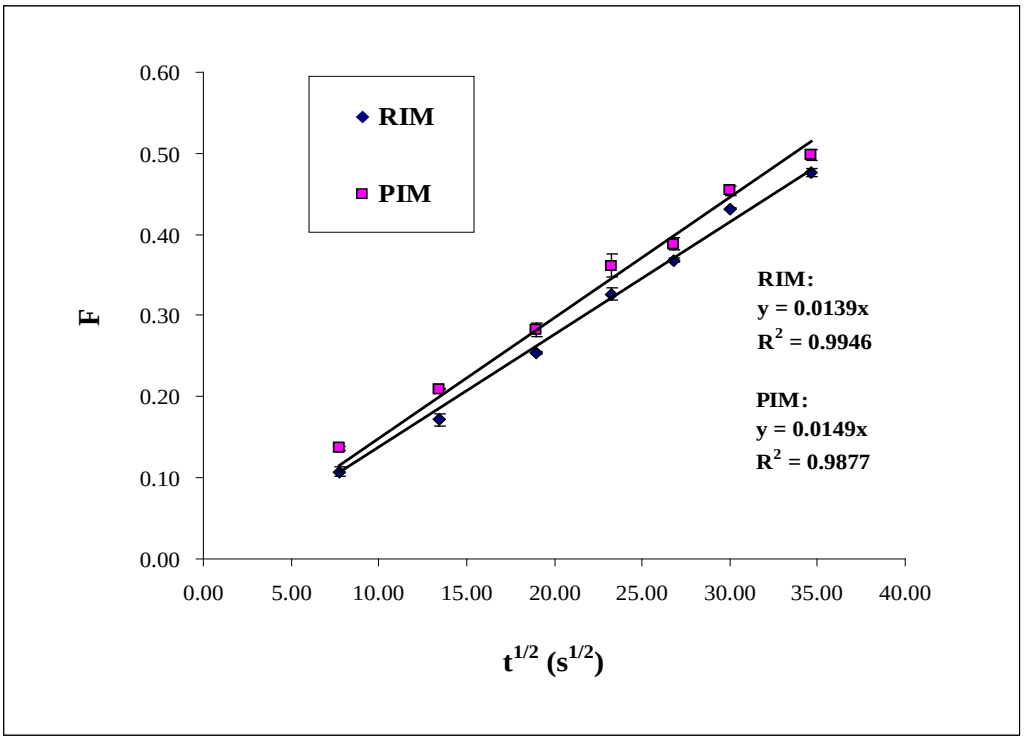

Figure 4.9. The F Vs $t^{1/2}$ plots of copper(II) biosorption by RIM and PIM beads.

* Experimental conditions: Volume of cell-immobilized beads used = 2.5 mL (for RIM beads) and 5 mL (for PIM beads); Density of cell-immobilized beads = 0.2916 ± 0.0035 g/mL (for RIM beads) and 0.1456 ± 0.0003 g/mL (for PIM beads); [*Micrococcus luteus*] = 0.133 g-cell/mL-beads (for RIM beads) and 0.066 g-cell/mL-beads (for PIM beads); Initial copper(II) concentration = 100 mg-Cu/L; Solution pH = 5.0; Volume of reaction mixture = 250 mL; Agitation speed = 250 rpm; Time period = 3 – 20 min (36 – 240 s).

4.2.4.2 External film diffusion coefficient

Choy *et al.* (2004) reported that the external film diffusion coefficient between liquid and sorbent particles under a well agitation condition, k_f, and the external film diffusion coefficient with the same particles moving at their terminal velocity (u_T) through the same liquid, k^*_f, was approximately regarded as

$$\frac{k_f}{k_f^*} \approx 2.0 \qquad \text{(Equation 4.10)}$$

As described by Tien (1994), the term k^*_f can be estimated from the Harriott model (Equation 4.11).

$$\frac{k_f^*(d_p)}{D_M} = 2.0 + 0.6 \left[\frac{d_p\,(u_T)}{\mu}\right]^{0.5} \left[\frac{\mu}{\rho\, D_M}\right]^{0.33}$$

(Equation 4.11)

where d_p is the mean diameter of the adsorbent particle (cm); D_M is the diffusion coefficient of copper(II) ions in bulk copper(II) nitrate solution (= 1.26×10^{-5} cm^2/s); μ is the liquid viscosity (g/cm/s); ρ is the liquid density (g/cm^3).

The correlation used to calculate the terminal velocity is expressed as:

$$u_T = \frac{0.153\, g^{0.71} d_p^{1.14}\, \Delta\rho^{0.77}}{\rho^{0.29}\, \mu^{0.43}} \qquad \text{(Equation 4.12)}$$

where g is the gravitational acceleration (cm^2/s); $\Delta\rho = (\rho_t + \varepsilon^*\rho)$ is the density difference between the particle and liquid (g/cm^3); ρ_t is the particle density (g/cm^3).

The calculated values of the parameters in Equation 4.12 are shown as follows:

	RIM beads	PIM beads
d_p (cm)	0.22 ± 0.01	0.31 ± 0.01
ρ_t (g/cm^3)	1.05 ± 0.02	1.07 ± 0.04
ε	0.75	0.89
ρ (g/cm^3)	0.997	0.997
$\Delta\rho = (\rho_t + \varepsilon^*\rho)$ (g/cm^3)	1.79 ± 0.02	1.96 ± 0.04
μ (g/cm/s)	8.94×10^{-2}	8.94×10^{-2}
u_T (cm/s)	18.35 ± 0.22	29.30 ± 0.64

By using Equations 4.10 to 4.12, the external film diffusion coefficients (k_f) in the RIM and PIM beads were found to be about $8.85 \times 10^{-3} \pm 5.10 \times 10^{-5}$ and $4.48 \times 10^{-3} \pm 4.68 \times 10^{-5}$ cm/s, respectively. The k_f values in the RIM and PIM beads obtained were similar to those obtained from using the single-external-mass-transfer-resistance model developed by Furusawa and Smith (1973) and the external mass transfer model described by Choy *et al*. (2004).

To further clarify the rate-controlling step in the mass transfer of the copper(II) biosorption process, the Sherwood number was calculated by Equation 4.13.

$$Sh = k_f (d_p) / D_{app} \qquad \text{(Equation 4.13)}$$

where Sh is the Sherwood number.

As Do (1998) discussed in his article, a large value of the Sherwood number indicates that the resistance of the intraparticle diffusion is more important than the film diffusion resistance. The Sherwood numbers obtained for RIM and PIM beads are 9546 ± 194 and 3621 ± 120, respectively. This showed that the intraparticle diffusion should be the rate-controlling step in the copper(II) biosorption of both the RIM and PIM beads.

To conclude, the rehydration treatment did not significantly change the mass transfer mechanism of the immobilized *M. luteus* in the copper(II) biosorption process. The mass transfer of copper(II) ions in both the RIM and PIM beads was under the intraparticle diffusion control. The rehydration treatment caused a greater diffusion resistance and a lower mass transfer of copper(II) ions inside the RIM beads, as demonstrated by comparing the calculated values of intraparticle diffusion coefficients between the RIM and PIM beads.

4.2.5 Effect of anions

The effect of anions on the copper(II) biosorption was investigated in the batch system by mixing the RIM beads with 100 mg-Cu/L of copper(II) solutions separately prepared by nitrate, chloride and sulfate of copper(II) salts. The details of the experiment were described in Section 3.3.1.3. The results are presented in Fig. 4.10. It shows that the co-existing anions had no significant effect on the copper(II) biosorption by the RIM beads. Among the biosorption mixtures in the presence of these three anionic species, the copper removals were almost the same (about 3.5 mg-Cu), with less than 7% difference.

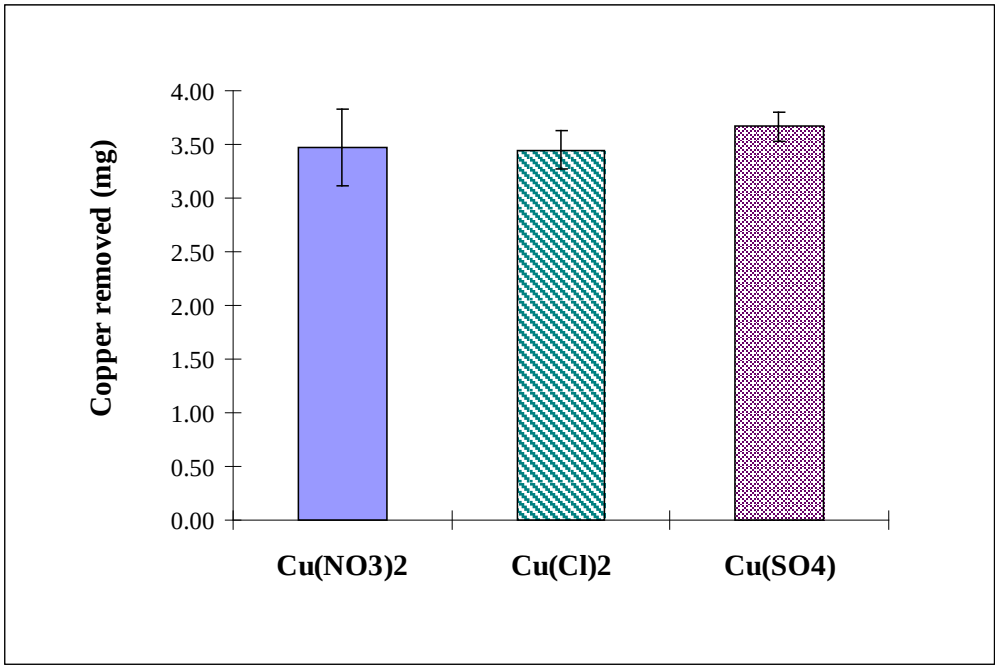

Figure 4.10. Effect of anions on copper(II) biosorption by RIM beads in batch system.

* Experimental conditions: Volume of the RIM beads used = 0.6 mL; [*Micrococcus luteus*] = 0.133 g-cell/mL-beads; Initial copper(II) concentration = 100 mg-Cu/L (prepared by different copper salts); Solution pH = 5.0; Volume of reaction mixture = 50 mL; Contact time = 6 h; Agitation speed = 250 rpm.

4.3 Copper(II) biosorption in fixed-bed column

One of the objectives of this project was to develop a metal-laden wastewater treatment system. A fixed-bed column reactor packed with the RIM Ca-alginate/PAA beads may be one of the desirable choices, attributing to its high treatment efficiency, maximized utilization of sorbent materials, simple configuration and limited working space. To apply the RIM beads in a fixed-bed reactor for copper(II) biosorption, several critical column parameters such as influent copper(II) concentrations (C_o), inlet upward flow rates (Q) and column bed depths (Z) were studied. The experimental procedures and conditions were stated in Section 3.3.2.

In the following sections, the treatment volume is expressed as 'bed volume' (BV = cumulative volume of treated solution/volume of biosorbents inside the reactor), and the effluent metal concentration is expressed as 'dimensionless concentration' ($C_e/C_o = [M^{n+}]_{effluent}/[M^{n+}]_{influent}$). The breakthrough level of Cu(II) ions was set at 4 mg-Cu/L, which is the maximum discharge limit of copper in wastewater according to the regulation of the Hong Kong Special Administrative Region (EPD, 2004).

4.3.1 Effect of influent copper(II) concentration

The fixed-bed biosorption was performed by feeding the copper(II) influent with various copper(II) concentrations (C_o): 50, 100 and 200 mg-Cu/L. The inlet upward flow rate of the influent and the bed depth of the column were fixed at 1 mL/min and 50 cm, respectively. The results are presented in Fig. 4.11 and Table 4.6.

Fig. 4.11 shows that all the breakthrough profiles exhibited a 'S' shape, which converged with the breakthrough concept described in Section 2.6.2. At the lowest influent concentration (C_o = 50 mg-Cu/L), the most dispersive breakthrough curve was displayed, whereas the slope of the curve at the highest concentration (200 mg-Cu/L) was the steepest. Similar trend was also reported in the column studies using immobilized *C. vulgaris* (Aksu *et al*., 1998) and immobilized *Pseudomonas aeruginosa* (Texier *et al*., 2002).

In view of the breakthrough stage, Table 4.6 shows that the copper removals and the treatment volume decreased dramatically as the copper(II) concentrations increased. The drops can be up to about 66% and 91%, respectively. At a high copper(II) concentration, the excess copper(II) ions accumulated in the bulk solution phase and could not be removed by the gel beads. This increased the effluent copper(II) concentration, resulting in the earlier breakthrough as well as the lower copper removal and the smaller treatment volume.

During the bed exhaustion stage, the treatment volume decreased significantly (over 77%) as the copper(II) concentrations increased. The decrease might also relate to the mass transfer of copper(II) ions. At the higher concentration (200 mg-Cu/L), the faster mass transfer could promote the rapid occupation and saturation of the binding sites of the beads. This thus induced the column exhaustion within a smaller volume of the influent. However, the total copper removals at the exhaustion stage were quite similar, with less than 14% difference, under different influent copper(II) concentrations. It was because all the columns were packed with a similar amount of the RIM beads.

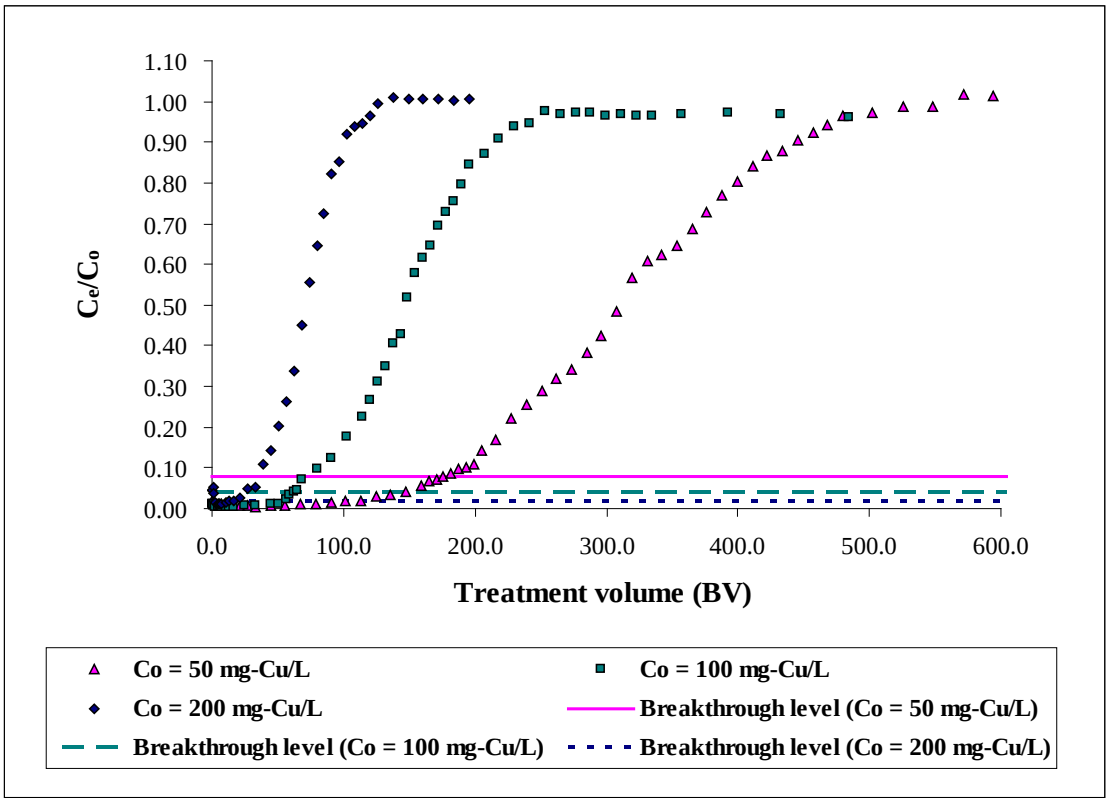

Figure 4.11. Breakthrough curves of copper(II) biosorption using RIM columns under different influent concentrations (C_o).

* Experimental conditions: Q = 1 mL/min; Z = 50 cm; Influent pH = 5.0; Breakthrough level = 4 mg-Cu/L; [*Micrococcus luteus*] = 0.133 g-cell/mL-beads.

Table 4.6. Copper(II) biosorption performances of RIM columns operating under different influent copper(II) concentrations (C_o).

Influent copper(II) concentration (mg-Cu/L)	**50**	**100**	**200**
Volume of bead used (mL)	41.90	41.45	41.43
Breakthrough stage (4 mg-Cu/L)			
Copper removal* (mg-Cu)	363.21	251.24	125.18
Treatment volume[#] (BV)	178.28	62.58	16.25
Exhaustion stage			
Copper removal* (mg-Cu)	649.77	610.12	561.85
Treatment volume[#] (BV)	548.45	288.06	126.01

* The copper removals of the column systems were calculated by integration of area above the breakthrough curves.

[#] The treatment volume with unit 'bed volume (BV)' was calculated by 'cumulative volume of treated solution/volume of the biosorbents packed in the reactor'.

4.3.2 Effect of inlet flow rate

Chang and Huang (1998) and Vijayaraghavan *et al*. (2005b) reported that the column biosorption performance exhibited an inversely proportional relationship with the inlet flow rate. To investigate such phenomenon, different inlet upward flow rates (Q) from 1 to 3 mL/min were applied respectively in the RIM columns with fixed bed depth (Z = 50 cm) and influent copper(II) concentration (C_o = 50 mg-Cu/L) at pH 5.0. The results are presented in Fig. 4.12 and Table 4.7.

The results in Table 4.7 show that an inverse trend of the treatment performance was observed at the column breakthrough when the flow rate increased. The amounts of copper removal and the treatment volume decreased by about 23% and 19%, respectively. These observations could be explained by the retention time of copper(II) ions and mass transfer inside the column packing. A faster flow rate would shorten the retention time of copper(II) ions inside the column that might be insufficiently long for the mass transfer and the biosorption reaction of Cu(II) ions. Many copper(II) ions would then directly pass through the column packing without any interaction with the biosorbents. This also increased the effluent copper level, resulting in early breakthrough and poor treatment performance. As a result, the copper removal and the treatment volume decreased at the breakthrough point when the inlet flow rate increased.

During the exhaustion stage, the amounts of copper removal at the three different flow rates were almost the same, with less than 4% difference.

This was because all the columns were packed with a similar amount of RIM beads. Fig. 4.12 shows that all the three breakthrough curves were close together at different flow rates. It indicates that the influence of flow rate did not have a significant effect on the fixed-bed copper(II) biosorption.

To estimate the mass-transfer property inside the RIM column, the Sherwood numbers (Sh) of copper(II) biosorption by the RIM column at different flow rates were first determined by using Equation 4.14.

$$Sh = 2.0 + 1.1 \left[\frac{d_p\,(U_o)\,\rho}{\mu}\right]^{0.6} \left[\frac{\mu}{\rho\, D_M}\right]^{0.33}$$

(Equation 4.14)

where Sh is the Sherwood number; Re is the Reynolds number; Sc is the Schmidt number; U_o is the flow velocity around the RIM beads (the linear flow rate of the solution phase inside the column packing, cm/s); d_p is the diameter of the RIM beads (= 0.22 cm); ρ is the density of the influent solution (~ the density of water = 0.997 g/cm^{-3}); μ is the viscosity of the influent solution (~ the viscosity of water = 8.937 × 10^{-3} g/cm· s^{-3}); and D_M is the diffusion coefficient of copper(II) ions in bulk copper(II) nitrate solution (= 1.26 × 10^{-5} cm^2/s).

By applying the Sherwood number and the intraparticle diffusion coefficient (Section 4.2.4.1) into Equation 4.15, the mass transfer coefficients (k_s) of copper(II) ions for a stagnant film surrounding a RIM bead packed inside the fixed-bed column at different flow rates could be obtained.

$$k_s = \frac{Sh\ (D_i)}{d_p} \qquad \text{(Equation 4.15)}$$

Table 4.7 shows that both the Sherwood numbers and the mass transfer coefficients (k_s) increased with increasing flow rates. This means that the transfer of copper(II) ions in the stagnant film was accelerated when the flow rate increased. However, all the k_s values obtained were smaller than that obtained in batch system (8.85×10^{-3} cm/s, presented in Section 4.2.4.2). The possible reason was related to the flow velocity (U_o) of the solution in the reactor. The flow velocities in the RIM columns at 1 to 3 ml/min of influent flow rates were about 16.37 to 49.10 cm/s (Table 4.7), whereas the flow velocity in the batch reactor was much faster, with about 90.32 cm/s. The slower flow velocity in the column decreased the transfer of copper(II) ions from the bulk solution phase to the stagnant film layer. Thus, smaller k_s values were obtained in the fixed-bed system.

Table 4.7 also shows that all the Sh values at different flow rates were significantly large. The large values of the Sherwood number indicate that intraparticle diffusion should be the rate-controlling step in the copper(II) biosorption. Therefore, liquid flowrate had a minor influence on the overall rate of copper(II) biosorption.

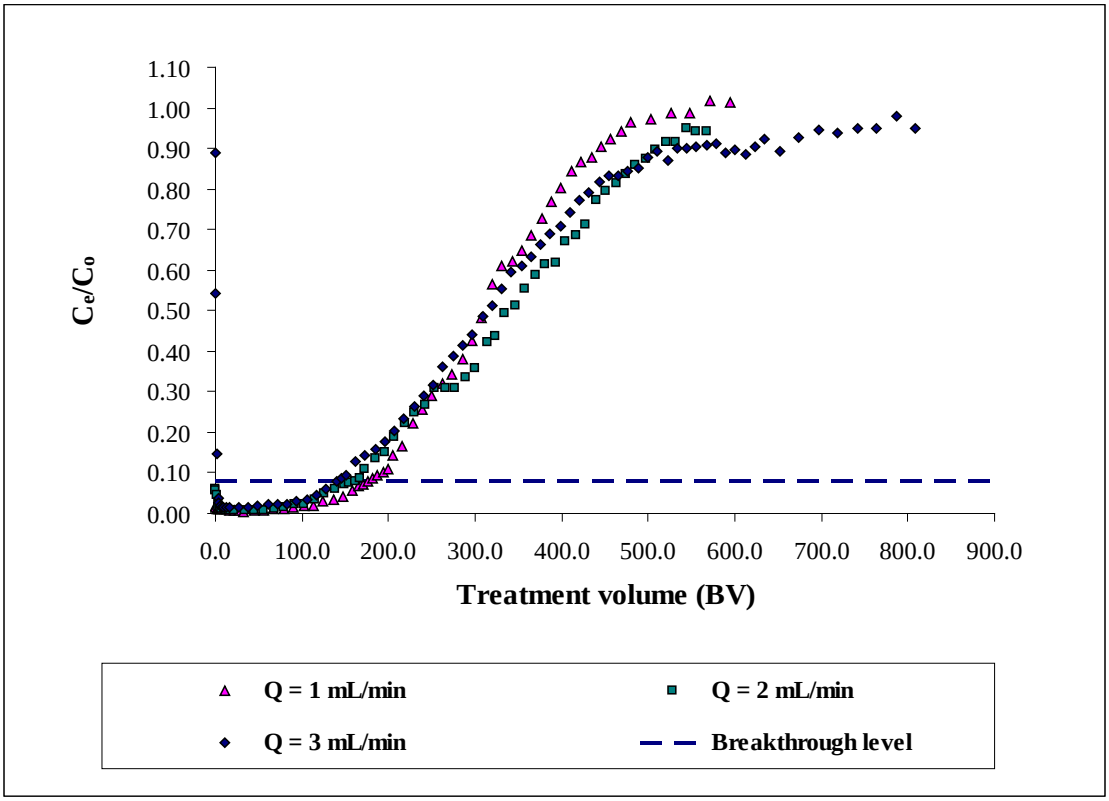

Figure 4.12. Breakthrough curves of copper(II) biosorption using RIM columns with different inlet upward flow rates (Q).

* Experimental conditions: C_o = 50 mg-Cu/L; Z = 50 cm; Influent pH = 5.0; Breakthrough level = 4 mg-Cu/L; [*Micrococcus luteus*] = 0.133 g-cell/mL-beads.

Table 4.7. Biosorption performances and mass transfer of copper(II) ions in RIM columns operating under different inlet upward flow rates (Q).

Inlet flow rate (mL/min)	**1**	**2**	**3**
Volume of bead used (mL)	41.90	41.38	42.65
Breakthrough stage (4 mg-Cu/L)			
Copper removal* (mg-Cu)	363.21	319.91	281.68
Treatment volume[#] (BV)	178.28	164.57	142.44
Exhaustion stage			
Copper removal* (mg-Cu)	649.77	675.34	666.16
Treatment volume[#] (BV)	548.45	543.81	600.70
Mass transfer of copper(II) ions for a stagnant film surrounding a RIM bead packed inside the column			
Flow velocity, U_o (cm/s)	16.37	32.73	49.10
Reynolds number, Re	401.70	803.41	1205.11
Schmidt number, Sc	711.42	711.42	711.42
Sherwood number, Sh	352.70	533.56	679.97
Mass transfer coefficient for the stagnant film, k_s (cm/s)	3.27×10^{-4}	4.95×10^{-4}	6.31×10^{-4}

* The copper removals of the column systems were calculated by integration of area above the breakthrough curves.

[#] The treatment volume in unit 'bed volume (BV)' was calculated by 'cumulative volume of treated solution/volume of the biosorbents packed in the reactor'.

4.3.3 Effect of column bed depth

In this study, the RIM beads were packed in the columns with bed depth (Z) ranging from 30 to 50 cm. The influent copper(II) concentration and the inlet upward flow rate in the fixed-bed biosorption were fixed at 50 mg-Cu/L and 1 mL/min, respectively. The breakthrough curves are displayed in Fig. 4.13 and the results of the biosorption performances are summarized in Table 4.8.

Fig. 4.13 and Table 4.8 show that an increase in column bed depth promoted the copper removal and treatment volume of the RIM column. The biosorption performances at both the breakthrough and exhaustion stages of the column operations were enhanced as the bed depth increased (Table 4.8). The enhancement was particularly significant at the column breakthrough with about 75% increase in both the copper removals and the treatment volume.

One obvious explanation was the presence of a larger quantity of the biosorbents in the column with a longer bed depth (Table 4.8). This certainly increased the number of the binding sites and promoted the copper uptake as well as the treatment volume. Also, a longer bed depth could extend the retention time of copper(II) ions inside the column packing. This provided a sufficient time for the mass transfer and the biosorption of Cu(II) ions. The copper uptake can thus become more efficient, resulting in the better treatment performance.

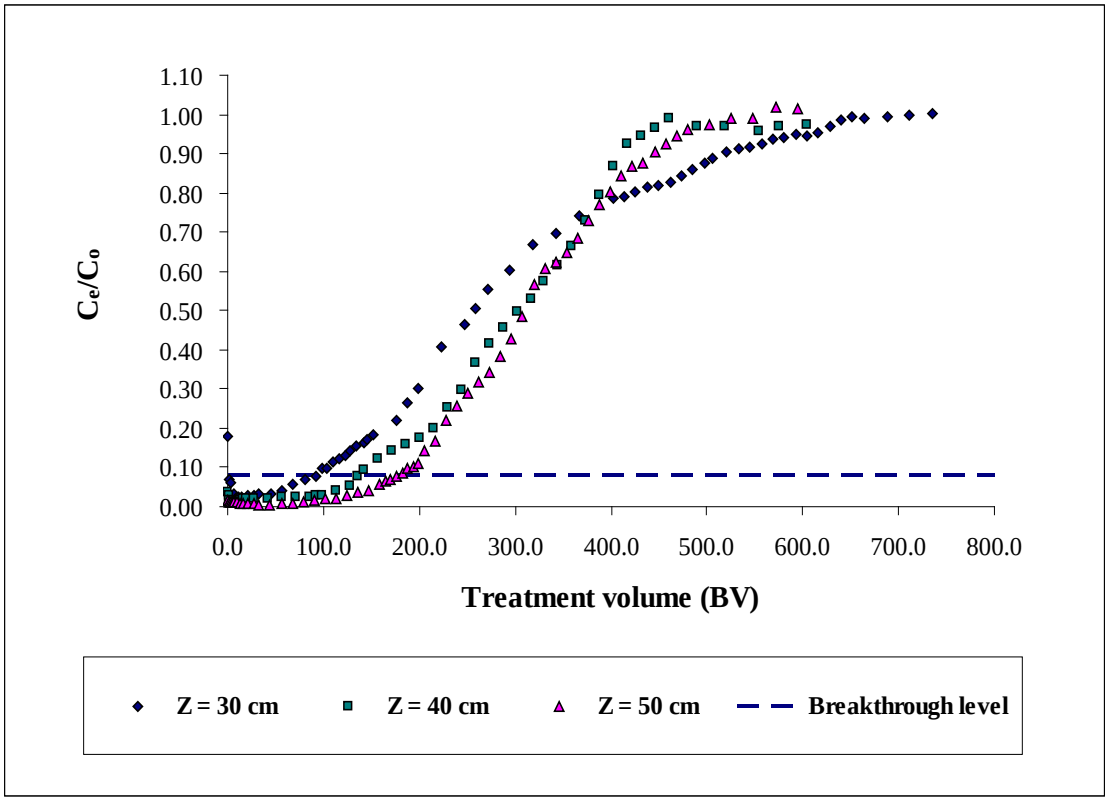

Figure 4.13. Breakthrough curves of copper(II) biosorption using RIM columns with different bed depths (Z).

* Experimental conditions: C_o = 50 mg-Cu/L; Q = 1 mL/min; Influent pH = 5.0; Breakthrough level = 4 mg-Cu/L; [*Micrococcus luteus*] = 0.133 g-cell/mL-beads.

Table 4.8. Copper(II) biosorption performances of RIM columns operating with different bed depths (Z).

Bed depth (cm)	**30**	**40**	**50**
Volume of bead used (mL)	20.15	33.23	41.90
Breakthrough stage (4 mg-Cu/L)			
Copper removal* (mg-Cu)	88.32	217.15	363.21
Treatment volume[#] (BV)	93.21	136.60	178.28
Exhaustion stage			
Copper removal* (mg-Cu)	283.82	481.51	649.77
Treatment volume[#] (BV)	652.11	460.50	548.45

* The copper removals of the column systems were calculated by integration of area above the breakthrough curves.

[#] The treatment volume in unit 'bed volume (BV)' was calculated by 'cumulative volume of treated solution/volume of the biosorbents packed in the reactor'.

4.3.4 Optimal conditions of copper(II) biosorption in fixed-bed column

From the above studies, the RIM beads were successfully applied in the column system for the copper(II) biosorption. Also, the effects of the critical process parameters (C_o, Q and Z) on the treatment performances of the RIM columns (the copper removals and the treatment volume) were investigated in detail. The results show that a lower influent concentration, a slower inlet flow rate and a longer column bed depth could enhance the copper removals at the breakthrough stage (Tables 4.6 to 4.8). Similar observation was found in the results of the treatment volume as well.

The breakthrough level was defined as 4 mg-Cu/L, which is the Cu(II) legal discharge limit of wastewater in the Hong Kong SAR. This is one of the most important criteria in the process design of the fixed-bed column for Cu(II) removal. The results obtained in Sections 4.3.1 to 4.3.3 indicated that the best treatment performances of the RIM column at the breakthrough stage were achieved under the conditions of: 50 mg-Cu/L influent concentration, 1 mL/min inlet upward flow rate, and 50 cm column bed depth. Thus, these experimental conditions were selected as the optimal process conditions of copper(II) biosorption using the RIM columns and were further applied in the subsequent fixed-bed studies.

4.3.5 Applicability of modified biosorbent for copper(II) biosorption in fixed-bed column

In order to understand the effect of the bead rehydration on the fixed-bed biosorption, the biosorption performances between the RIM and PIM beads in the column system were compared. The studies were performed by using the PIM beads with the same process parameters and procedures of the RIM column experiments (Sections 3.3.2 and 3.3.2.1). The breakthrough profiles are presented in Figs. 4.14 to 4.16 and the treatment performances are summarized in Tables 4.9 to 4.11.

These figures and tables show that the trends obtained from the PIM columns were similar to those of the RIM columns. The copper removals and the treatment volume of the PIM columns at the breakthrough stage were promoted by increasing the bed depths and decreasing the copper(II) concentration as well as the flow rate. However, no breakthrough result could be obtained from the PIM columns under the conditions of the highest influent concentration (200 mg-Cu/L), the fastest flow rate (3 mL/min) and the shortest bed depth (30 cm).

Further comparing the RIM and PIM column systems, significant differences in their treatment performances and stabilities were found. The copper removals and the treatment volume of the RIM columns both were much better than those of the PIM columns under all the different process conditions (Tables 4.9 to 4.11). A possible reason was related to their bead volume. Since the volume of the immobilized beads was reduced after the

rehydration treatment, more RIM beads can be packed inside the columns. This then enhanced the copper uptake and the treatment volume of the RIM columns. On the other hand, Tables 4.12 to 4.14 show that a serious bead shrinkage (about 40% shrinkage) and a significant shortening of the bed depth (up to 26% shortening) were found in the PIM columns after the fixed-bed biosorption. By contrast, the RIM columns were highly stable with less than 8% reduction in the bead volume and the bed depth. The results indicate that the RIM beads had much higher rigidity and mechanical strength than the PIM beads. Also, the fixed-bed columns packed with the RIM beads had superior Cu(II) biosorption performance compared with the columns packed with the PIM beads under the equivalent experimental conditions.

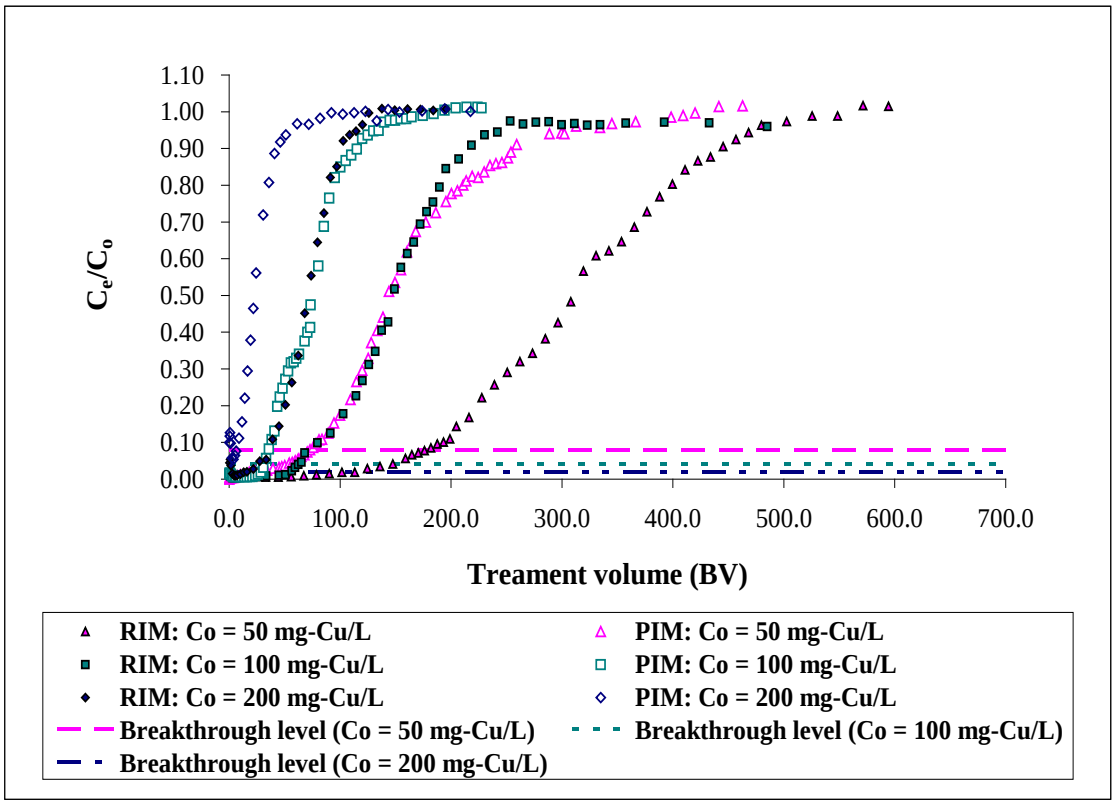

Figure 4.14. Breakthrough curves of copper(II) biosorption using RIM and PIM columns under different influent copper(II) concentrations (C_o).

* Experimental conditions: Q = 1 mL/min; Z = 50 cm; Influent pH = 5.0; Breakthrough level = 4 mg-Cu/L; [*Micrococcus luteus*] = 0.133 g-cell/mL-beads (for RIM beads) and 0.066 g-cell/mL-beads (for PIM beads).

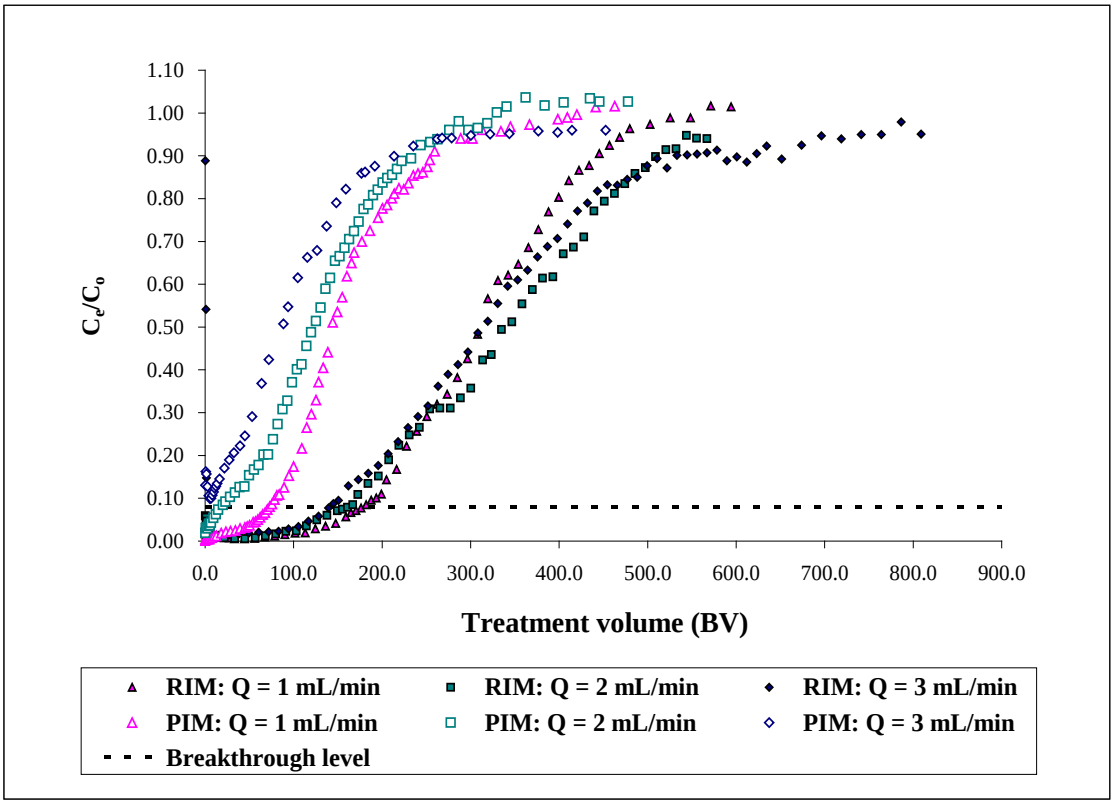

Figure 4.15. Breakthrough curves of copper(II) biosorption using RIM and PIM columns under different inlet upward flow rates (Q).

* Experimental conditions: C_o = 50 mg-Cu/L; Z = 50 cm; Influent pH = 5.0; Breakthrough level = 4 mg-Cu/L; [*Micrococcus luteus*] = 0.133 g-cell/mL-beads (for RIM beads) and 0.066 g-cell/mL-beads (for PIM beads).

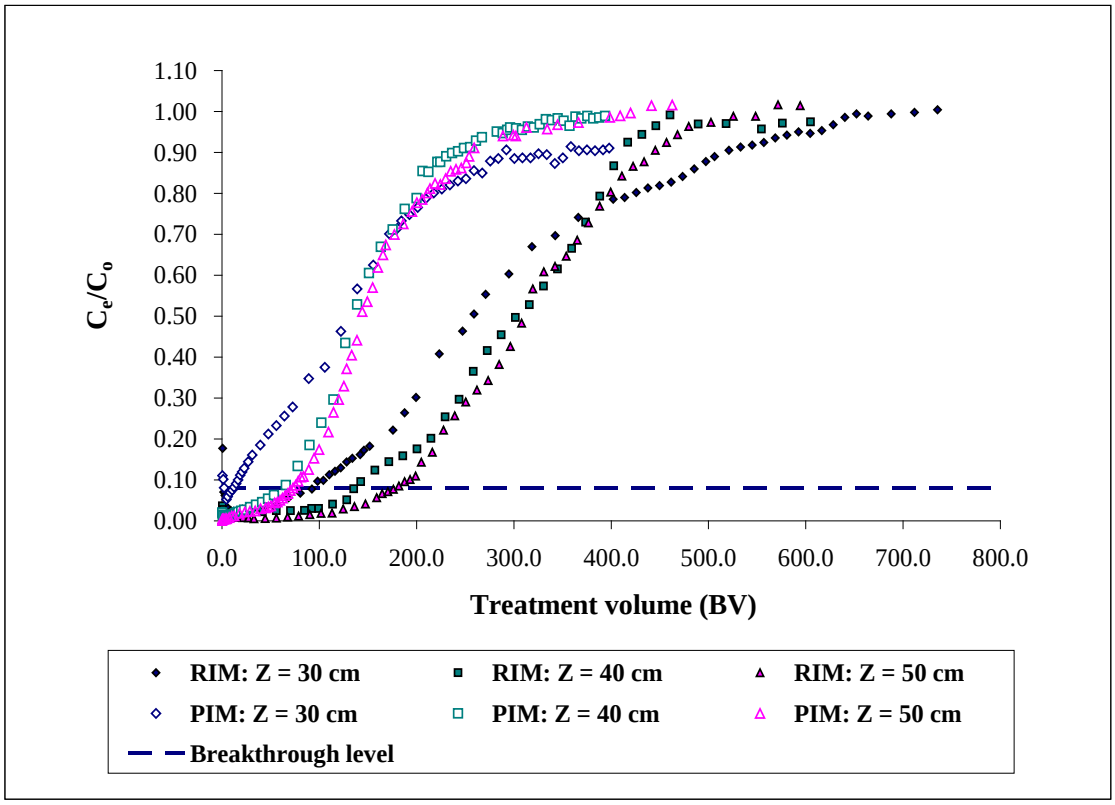

Figure 4.16. Breakthrough curves of copper(II) biosorption using RIM and PIM columns with different column bed depths (Z).

* Experimental conditions: C_o = 50 mg-Cu/L; Q = 1 mL/min; Influent pH = 5.0; Breakthrough level = 4 mg-Cu/L; [*Micrococcus luteus*] = 0.133 g-cell/mL-beads (for RIM beads) and 0.066 g-cell/mL-beads (for PIM beads).

Table 4.9. Copper(II) biosorption performances of RIM and PIM columns operating under different influent copper concentrations (C_o).

	RIM column			**PIM column**		
Influent copper(II) concentration (mg-Cu/L)	**50**	**100**	**200**	**50**	**100**	**200**
Volume of bead used (mL)	41.90	41.45	41.43	47.80	48.50	46.90
Breakthrough stage (4 mg-Cu/L)						
Copper removal* (mg-Cu)	363.21	251.24	125.18	170.20	147.70	~
Treatment volume[#] (BV)	178.28	62.58	16.25	72.22	31.86	~
Exhaustion stage						
Copper removal* (mg-Cu)	649.77	610.12	561.85	387.04	351.92	238.28
Treatment volume[#] (BV)	548.45	288.06	126.01	419.92	194.23	143.28

* The copper removals of the column systems were calculated by integration of area above the breakthrough curves.

[#] The treatment volume in unit 'bed volume (BV)' was calculated by 'cumulative volume of treated solution/volume of the biosorbents packed in the reactor'.

~ No breakthrough result can be obtained from this experimental condition.

Table 4.10. Copper(II) biosorption performances of RIM and PIM columns operating under different inlet upward flow rates (Q).

	RIM column			**PIM column**		
Inlet flow rate (mL/min)	**1**	**2**	**3**	**1**	**2**	**3**
Volume of bead used (mL)	41.90	41.38	42.65	47.80	47.55	44.15
Breakthrough stage (4 mg-Cu/L)						
Copper removal* (mg-Cu)	363.21	319.91	281.68	170.20	38.86	~
Treatment volume[#] (BV)	178.28	164.57	142.44	72.22	16.98	~
Exhaustion stage						
Copper removal* (mg-Cu)	649.77	675.34	666.16	387.04	312.50	235.92
Treatment volume[#] (BV)	548.45	543.81	600.70	419.92	329.76	452.55

* The copper removals of the column systems were calculated by integration of area above the breakthrough curves.
[#] The treatment volume in unit 'bed volume (BV)' was calculated by 'cumulative volume of treated solution/volume of the biosorbents packed in the reactor'.
~ No breakthrough result can be obtained from this experimental condition.

Table 4.11. Copper(II) biosorption performances of RIM and PIM columns with different bed depths (Z).

	RIM column			**PIM column**		
Bed depth (cm)	**30**	**40**	**50**	**30**	**40**	**50**
Volume of bead used (mL)	20.15	33.23	41.90	28.95	39.30	47.80
Breakthrough stage (4 mg-Cu/L)						
Copper removal* (mg-Cu)	88.32	217.15	363.21	~	116.30	170.20
Treatment volume[#] (BV)	93.21	136.60	178.28	~	62.14	72.22
Exhaustion stage						
Copper removal* (mg-Cu)	283.82	481.51	649.77	210.08	286.60	387.04
Treatment volume[#] (BV)	652.11	460.50	548.45	358.5	345.04	419.92

* The copper removals of the column systems were calculated by integration of area above the breakthrough curves.

[#] The treatment volume in unit 'bed volume (BV)' was calculated by 'cumulative volume of treated solution/volume of the biosorbents packed in the reactor'.

~ No breakthrough result can be obtained from this experimental condition.

Table 4.12. Change in bed depth and bead volume of RIM and PIM columns after copper(II) biosorption under different influent copper(II) concentrations (C_o).

	RIM column			**PIM column**		
Influent copper(II) concentration (mg-Cu/L)	**50**	**100**	**200**	**50**	**100**	**200**
			Bed depth			
Initial (cm)	50.0	50.0	50.0	50.0	50.0	50.0
Final (cm)	49.7	49.8	49.5	37.2	47.5	46.7
|% change|	0.60	0.40	1.00	25.60	5.00	6.60
			Bead volume			
Initial (mL)	41.90	41.45	41.43	47.80	48.50	46.90
Final (mL)	39.70	40.93	41.96	27.60	28.90	26.30
|% change|	5.25	1.27	1.29	42.26	40.41	43.92

Table 4.13. Change in bed depth and bead volume of RIM and PIM columns after copper(II) biosorption under different inlet upward flow rates (Q).

	RIM column			**PIM column**		
Inlet flow rate (mL/min)	**1**	**2**	**3**	**1**	**2**	**3**
			Bed depth			
Initial (cm)	50.0	50.0	50.0	50.0	50.0	50.0
Final (cm)	49.7	49.0	48.5	37.2	47.5	44.4
|% change|	0.60	2.00	3.00	25.60	5.00	11.20
			Bead volume			
Initial (mL)	41.90	41.38	42.65	47.80	47.55	44.15
Final (mL)	39.70	42.30	43.33	27.60	29.00	23.60
|% change|	5.25	2.24	1.58	42.26	39.01	46.55

Table 4.14. Change in bed depth and bead volume of RIM and PIM columns with different bed depths (Z) after copper(II) biosorption.

	RIM column			**PIM column**		
Bed depth (cm)	**30**	**40**	**50**	**30**	**40**	**50**
			Bed depth			
Initial (cm)	30.0	40.0	50.0	30.0	40.0	50.0
Final (cm)	29.0	39.3	49.7	28.8	37.5	37.2
|% change|	3.33	1.75	0.60	4.00	6.25	25.60
			Bead volume			
Initial (mL)	20.15	33.23	41.90	28.95	39.30	47.80
Final (mL)	21.63	35.33	39.70	18.40	23.73	27.60
|% change|	7.32	6.32	5.25	36.44	39.63	42.26

4.3.6 Comparison of copper(II) biosorption performances in different reactor systems

After the biosorption performance of the RIM column was optimized, its performance was further compared with those of two other conventional treatment systems: batch reactor and continuous-stirred-tank reactor (CSTR). The experiments were performed as stated in Sections 3.3.1, 3.3.2 and 3.3.3. The copper(II) stock solution with 50 mg-Cu/L at pH 5.0 was introduced into these systems containing the RIM beads for the biosorption. The results are presented in Figs. 4.17 to 4.19. Table 4.15 summarizes the experimental conditions and performance of the three reactor systems.

In view of the batch system, the residual copper(II) concentration in the biosorption equilibrium was about 3.97 mg-Cu/L, which could meet the legal discharge limit (4 mg-Cu/L). However, the treatment performance was improper for scale-up applications. As shown in Fig. 4.17, a low copper removal (4.09 mg-Cu/mL-beads) was demonstrated. It only attained about a quarter of the copper uptake of the continuous systems (the RIM column and the CSTR) at the exhaustion stage (equilibrium). Also, a large difference of the treatment volume was found between the batch and continuous systems. The batch system could only treat about 17% and 11% of the treatment volume of the fixed-bed column and the CSTR, respectively (Fig. 4.18). A good explanation of such large differences was that a fresh copper(II) influent was continuously supplied to the column and the CSTR, which induced a further shift of the equilibrium position to the right in the copper(II) biosorption (Equation 4.16). This promoted the

copper uptake by the biosorbents. By contrast, no fresh copper(II) stock was added in the batch system during the experiment, so that a smaller concentration gradient was resulted. Thus, the treatment performance of the batch reactor system was lower than that of the continuous systems.

$$Cu^{2+}(aq) + Ca-Biosorbent(s) \xleftrightarrow{\text{Sorption Equilibrium}} Cu-Biosorbent(s) + Ca^{2+}(aq)$$

(Equation 4.16)

Fig. 4.19 shows that the copper(II) biosorption profiles of both the CSTR and the fixed-bed column displayed a 'S' shape. The effluent concentration of the CSTR was kept below the breakthrough level (4 mg-Cu/L) at the initial phase and then rose gently until the RIM beads became saturated with Cu(II) ions. Similar trend was also observed in the profile of the column system, but it presented a steeper slope and a faster exhaustion. Further comparing the treatment performances between these two continuous systems, superior copper removal and treatment volume were found in the column reactor at the breakthrough point, whereas the better results were attained by the CSTR at the exhaustion stage (Figs. 4.17 and 4.18; Table 4.15).

Up to the breakthrough level, the treatment performance of the CSTR was poorer than that of the column. Volesky (2003) indicated that the poor performance might be caused by the mixing of the reaction suspension in the CSTR. This inevitably diluted the influent copper(II) concentration

once the influent solution was introduced into the tank. The concentration gradient of copper(II) ions between the biosorbent phase and the bulk solution then was diminished. As a result, the treatment performance of the CSTR is inferior to that of the column reactor at the breakthrough.

Since the process objective was to treat the copper level of wastewater below the legal discharge limit, which was the defined breakthrough point, the process performance would only be evaluated at the breakthrough point rather than the exhaustion stage. The results show that the column reactor was much more effective and applicable than the CSTR at the breakthrough point. This demonstrates that the RIM column reactor should be a more promising system for treating copper-laden wastewater.

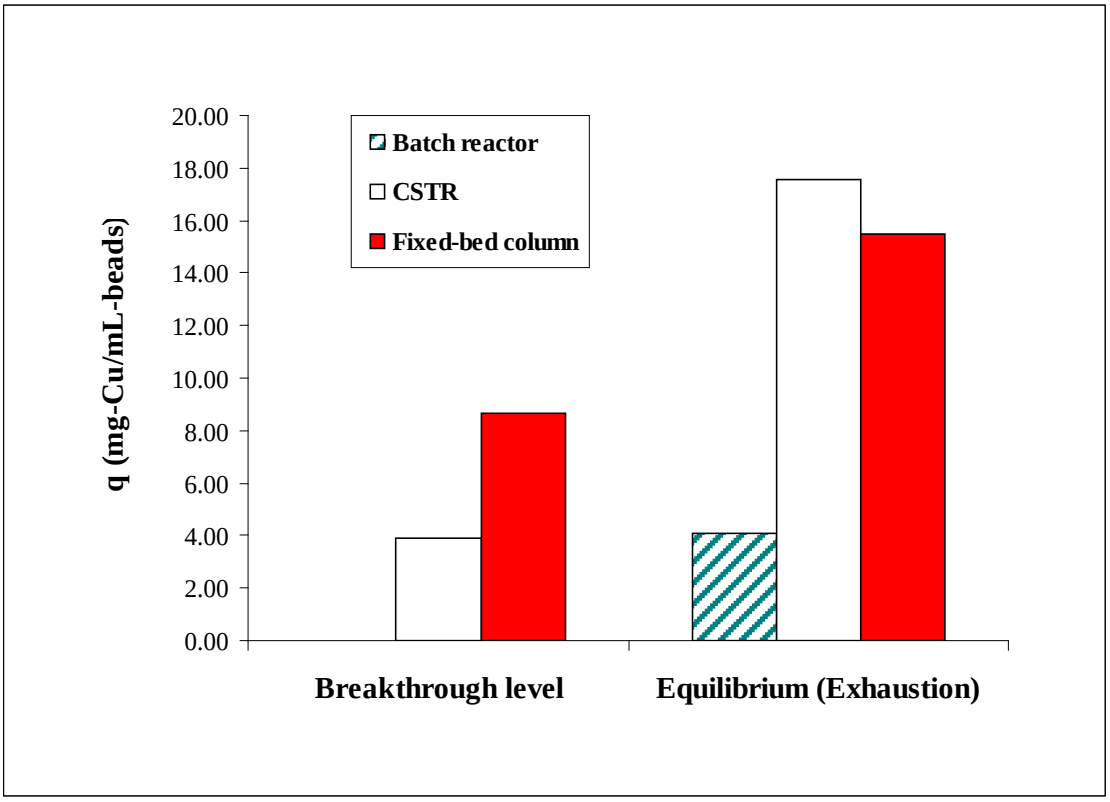

Figure 4.17. Copper removals in different treatment systems.

* Experimental conditions are listed in Table 4.15.

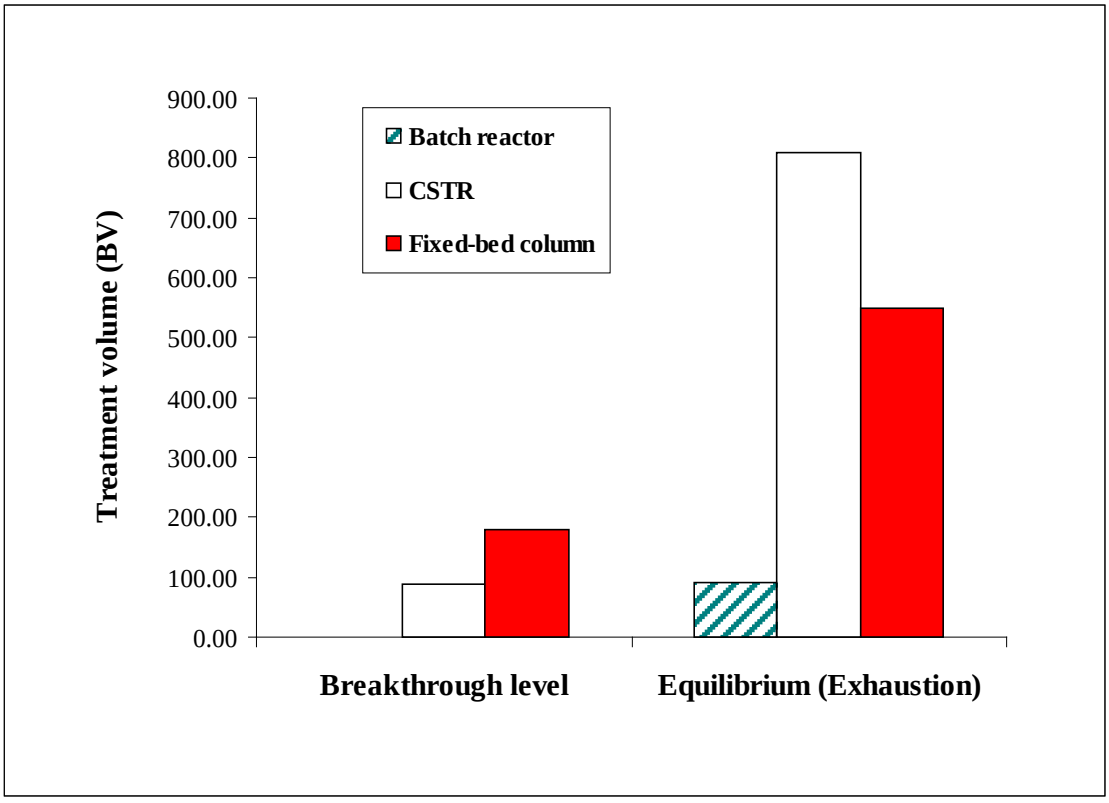

Figure 4.18. Treatment volume of different treatment systems.

* Experimental conditions are listed in Table 4.15.

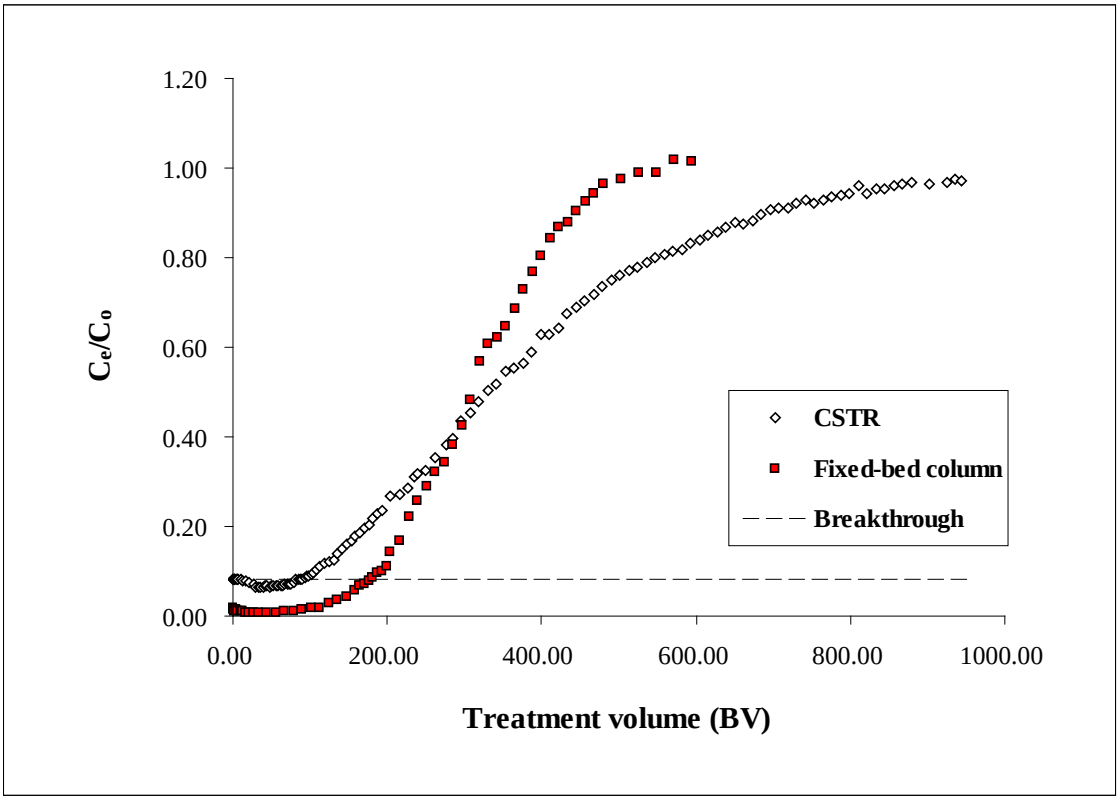

Figure 4.19. Breakthrough curves of copper(II) biosorption in different treatment systems.

* Experimental conditions are listed in Table 4.15.

Table 4.15. Copper(II) biosorption performances of different reactor systems.

Reactor systems		Batch	CSTR	Fixed-bed column
Volume of bead used (mL)		0.55	42.00	41.90
Experimental conditions		- C_o = 48.60 mg-Cu/L; - pH 5.0; - Reaction volume = 50 mL; - Agitation = 250 rpm; - Reaction time = 6 h; - [*Micrococcus luteus*] = 0.133 g-cell/mL-beads.	- C_o = 48.81 mg-Cu/L; - pH 5.0; - Q_{in} & Q_{out} = 1 mL/min; - Reaction volume = 3.5 L; - Stirring speed = 250 rpm; - [*Micrococcus luteus*] = 0.133 g-cell/mL-beads.	- C_o = 49.88 mg-Cu/L; - pH 5.0; - Q_{in} = 1 mL/min; - Z = 50 cm; - [*Micrococcus luteus*] = 0.133g-cell/mL-beads.
Breakthrough stage (4 mg-Cu/L)				
Copper removal (q)	(mg-Cu)	--	165.09*	363.21*
	(mg-Cu/ mL-beads)	--	3.93	8.67
Treatment volume[#] (BV)		--	87.14	178.28
Exhaustion or equilibrium				
Copper removal (q)	(mg-Cu)	2.24	738.59*	649.77*
	(mg-Cu/ mL-beads)	4.09	17.59	15.51
Treatment volume[#] (BV)		90.91	810.00	548.45

* The copper removals of the column system and the CSTR were calculated by integration of area above the breakthrough curves.

[#] The treatment volume in unit 'bed volume (BV)' was calculated by 'cumulative volume of treated solution/volume of the biosorbents packed in the reactor'.

4.3.7 Fixed-bed biosorption behaviour in binary-metal systems

The fixed-bed biosorption profiles in the binary-metal systems were further investigated. As described in Section 3.3.2.2, the experiments were carried out by introducing the binary-metal influent solutions into the RIM columns with 50 cm bed depth at 1 mL/min inlet upward flow rate. The influent solutions were prepared by mixing nitrate salt of copper(II) with either nickel(II), lead(II) or zinc(II) at pH 5.0. The concentration of each metal species was fixed as 1 mM. The profiles of the Cu-Zn, Cu-Ni and Cu-Pb systems are presented in Figs. 4.20 to 4.22 respectively.

These three figures illustrate that all the copper(II) biosorption processes reached the breakthrough and the bed exhaustion earlier compared with the single metal systems. This was due to the additional occupation of the binding sites by the counter metal ions apart from copper ions. Fig 4.20 shows that a Zn(II) peak was displayed in the breakthrough curve in the presence of Cu(II) ions during the fixed-bed biosorption. Similarly, Fig. 4.21 depicts that a Ni(II) peak was displayed in the breakthrough curve in the presence of Cu(II) ions. However, Fig. 4.22 illustrates that a Cu(II) peak was displayed in the breakthrough curve in the presence of Pb(II) ions. As mentioned by Figueira *et al*. (2000), these phenomena were called "overshooting", which described the effluent concentration of the less preferable species over its influent concentration ($C_e/C_o > 1$). Similar observation was reported in other studies. A La(III) peak was displayed in the breakthrough curve in the presence of Eu^{3+} ions during the fixed-bed biosorption using the protonated *Sargassum* sp. (Diniz *et al.*, 2008).

Overshoots of Ni(II) and Zn(II) ions was observed in the presence of Cu(II) and Pb(II) ions during the biosorption using the sunflower-seed-waste column (Zhang and Banks, 2006).

At the initial stage of the binary-metal biosorption, the selective biosorption and the competition between the two metal species were not significant due to the presence of an abundance of the un-occupied binding sites. The fresh biosorbent bed would bind both the metal species without specific preference. However, when the binding sites became almost fully occupied, the two different metal species would compete with each other for the binding sites. The preferred metal ions in the influent would displace the less preferable species from the biosorbents, since the interaction between the biosorbents and the less preferable ions was weaker. The displaced ions entered the solution flow in the column and then increased the concentration of the less preferable species in the effluent. The overshooting ($C_e/C_o > 1$) was thus resulted. After the overshooting peak, most of the less preferable ions were excluded from the biosorbent bed. The effluent concentration of the less preferable species would then decrease down to the level of the influent ($C_e/C_o = 1$). Moreover, the column was almost exhausted at this stage.

As discussed above, the metal binding preference can be established from the overshooting breakthrough profile. Thus, from Figs. 4.20 to 4.22, the metal binding preference of the RIM beads could be arranged as follows: Pb(II) > Cu(II) > Ni(II) > Zn(II).

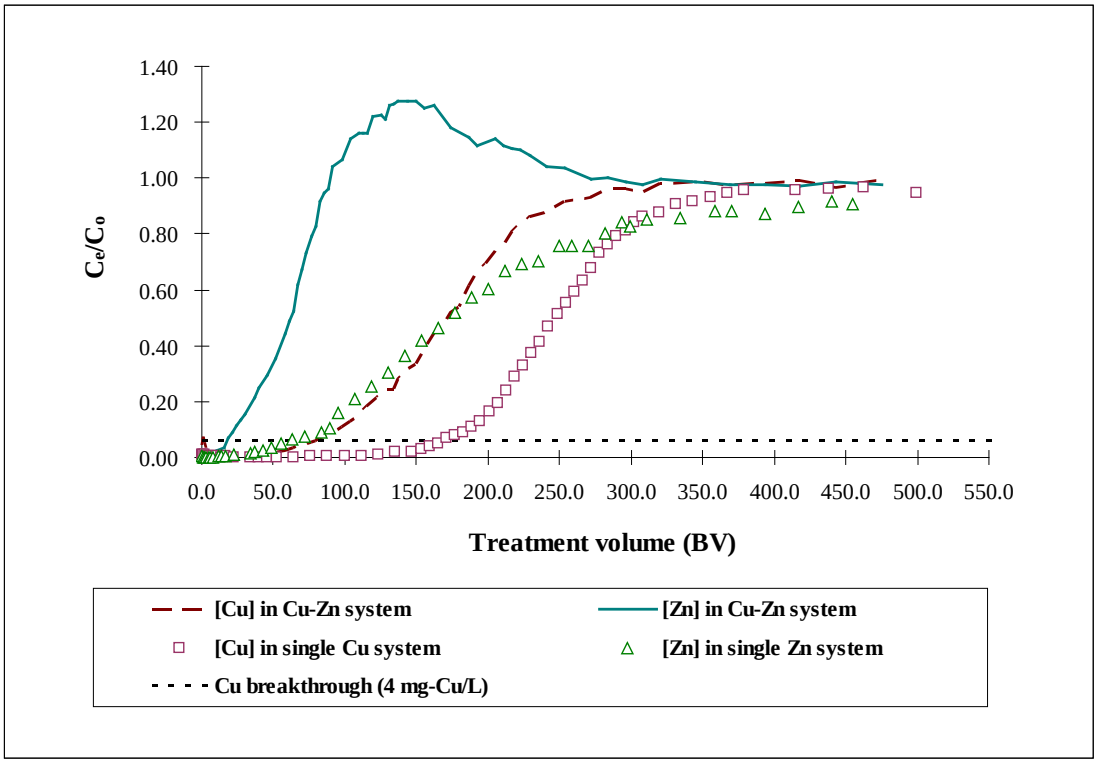

Figure 4.20. Breakthrough curves of biosorption of metal ions using RIM columns in copper-zinc system.

* Experimental conditions: C_o = 1 mM (for each metal ion); Q = 1 mL/min; Z = 50 cm; Influent pH = 5.0, Breakthrough level = 4 mg-Cu/L; [*Micrococcus luteus*] = 0.133 g-cell/mL-beads.

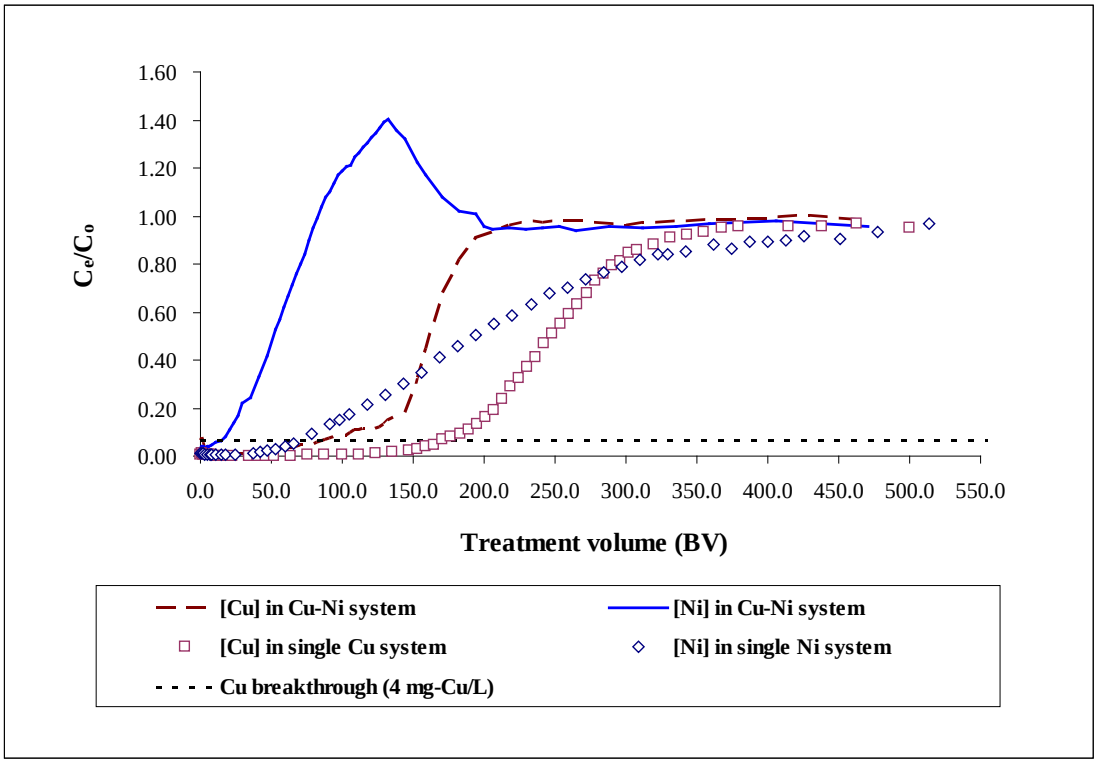

Figure 4.21. Breakthrough curves of biosorption of metal ions using RIM columns in copper-nickel system.

* Experimental conditions: C_o = 1 mM (for each metal ion); Q = 1 mL/min; Z = 50 cm; Influent pH = 5.0, Breakthrough level = 4 mg-Cu/L; [*Micrococcus luteus*] = 0.133 g-cell/mL-beads.

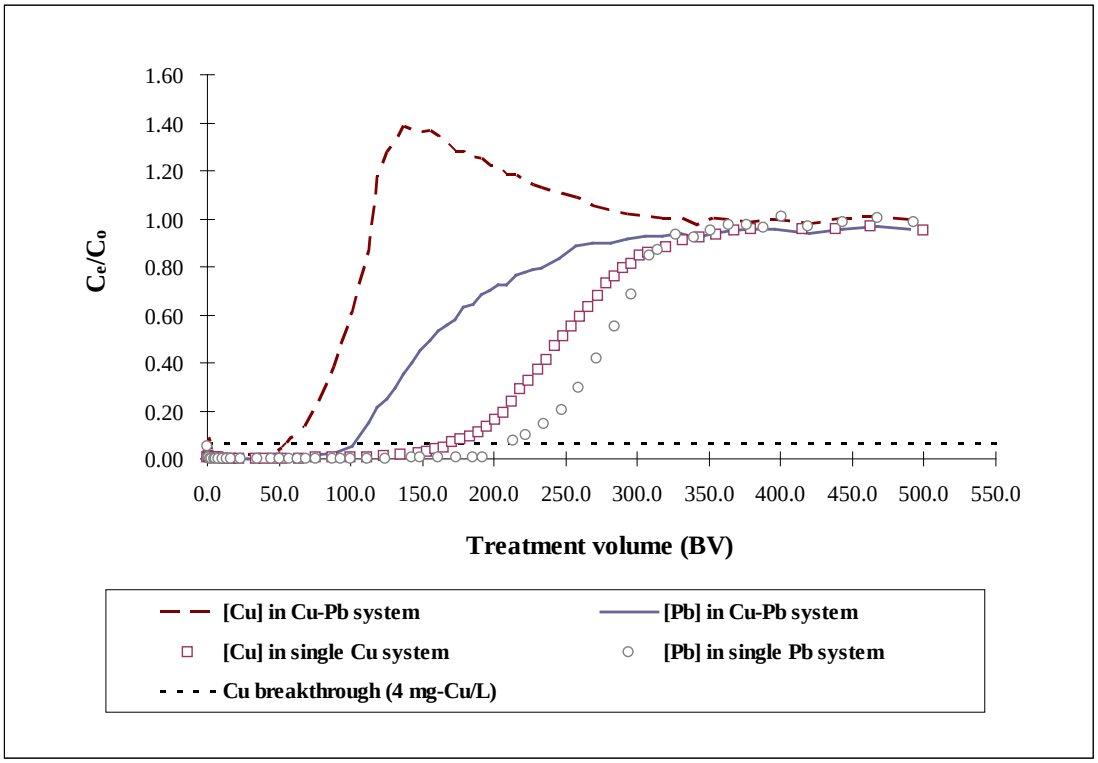

Figure 4.22. Breakthrough curves of biosorption of metal ions using RIM columns in copper-lead system.

* Experimental conditions: C_o = 1 mM (for each metal ion); Q = 1 mL/min; Z = 50 cm; Influent pH = 5.0, Breakthrough level = 4 mg-Cu/L; [*Micrococcus luteus*] = 0.133 g-cell/mL-beads.

4.3.7.1 Binding preference of metal ions

To further analyze the metal binding preference of the RIM beads, the uptake of metal ions (Fig. 4.23) and the percentage change of the metal biosorption capacities (Table 4.16) in the binary-metal systems were calculated from the fixed biosorption data. As shown in Fig. 4.23 and Table 4.16, the uptakes of Ni(II) and Zn(II) ions using the RIM beads were significantly inhibited in the presence of Cu(II) ions. The percentage decrease of the Ni(II) uptake was similar to that of the Zn(II) uptake with only about 4% difference (Table 4.16). However, the Ni(II) uptake is slightly higher than that of the Zn(II) uptake (Fig. 4.23). This indicated that the biosorption of Ni(II) ions by the RIM beads had a slightly higher binding preference than that of Zn(II). On the other hand, the Cu(II) biosorption was greatly suppressed in the presence of Pb(II) ions but not Zn(II) and Ni(II) ions. Table 4.16 shows that there was about 76% decrease of the copper uptake in the copper-lead system using the RIM beads. By contrast, the decrease in the lead removal using the RIM beads was about 31%. Based on these results, the biosorption preference of the RIM beads can be established as follows: Pb(II) > Cu(II) >> Ni(II) > Zn(II).

To explain the biosorption preference of the RIM beads, the metal-binding sites (functional groups) on the biosorbents and characteristics of the target metal ions should be reviewed in detail. The RIM bead is composed of *Micrococcus luteus*, calcium alginate and polyacrylamide. As shown in Fig. 2.5, the metal-binding activity of polyacrylamide was low or negligible. It was because only the carboxyl

(C=O) and amide ($–NH_2$) functional groups freely exist in this polymer. These two groups could only interact with metal cations through a weak intermolecular force. On the other hand, other studies indicated that a large quantity of carboxylic (COO^-) groups in alginate (Ibáñez and Umetsu, 2004) and on the surface of *Micrococcus luteus* (Wong, 2001) were active in the metal uptake reaction. The carboxylic groups generally have lone-pair electrons, which have a high bonding affinity towards low-energy vacant orbitals of metal cations. This promoted the bond formation between the biosorbents and metal cations. Thus, the binding sites, especially the carboxylic groups, of the RIM beads should mainly affect the biosorption capacity of metal ions, but not the selectivity of the metal cationic species.

Another factor affecting the binding preference is the characteristics of the target metal ions, which is related to the electron configuration of metal ions. Table 4.17 summarizes the electron configurations of Zn(II), Ni(II), Cu(II) and Pb(II) ions in orbitals. In view of Zn(II) ion, a highly-stable electron configuration is obtained by fully occupying all '3d' orbitals with ten outermost-shell electrons (Fig. 4.24). When lone-pair electrons in carboxyl groups of the beads were introduced into the electron shell of Zn(II) ion for Zn—O=C< bond formation, an extremely large energy should be required to re-arrange this stable configuration. It was highly unfavourble in energetics and limited the Zn-complex coordination. As a result, a low zinc uptake was found.

A similar situation was found in the case of Ni(II) ions. As shown in Fig. 4.24, eight outermost electrons of Ni(II) ion fully occupy the lower energy boundary of the '3d' orbitals (d_{xy}, d_{yz} and d_{xz}) and half fill the higher energy orbitals ($d_{x^2-y^2}$ and d_{z^2}). This electron configuration is also stable. The formation and strength of the Ni—O=C< bond would thus be reduced, resulting in a low nickel uptake.

Different from Zn(II) and Ni(II) ions, the electron configuration of Cu(II) ion is less stable since it is a d^9 electron system (Fig. 4.24). No half or fully orbital-filling stabilization could be found, resulting in a larger repulsion between the '3d' electrons. Less energy would be required to convert the electron configuration for accepting the lone-pair electrons from the carboxyl groups. This promoted the formation of a strong Cu—O=C< bond and induced a higher copper removal over the zinc and nickel removal.

In the case of Pb(II) ions, the outermost electron shell consists of three low-energy empty '6p' orbitals (Fig. 4.24). No great conversion of the electron configuration should be required to accept the electron pairs from the carboxyl groups. The Pb-biomass interaction would thus be highly favourable due to a lower energy requirement. This resulted in the highest binding preference in this study.

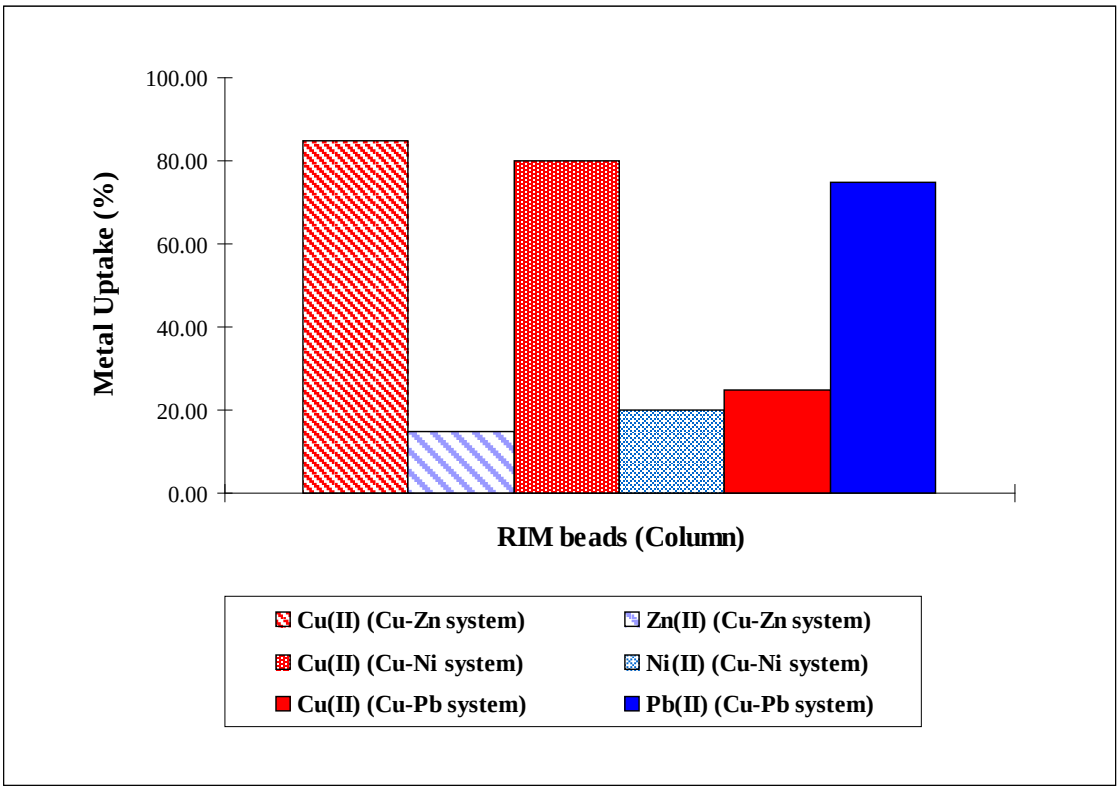

Figure 4.23. Metal uptakes by RIM beads in binary metal systems.

* Experimental conditions are listed in Table 4.16.

Table 4.16. Percentage decrease in biosorption of metal ions by RIM beads in binary-metal systems.

	RIM beads (Column)		
	Cu + Zn	Cu + Ni	Cu + Pb
Cu(II)	32.00%	36.00%	76.00%
Zn(II)	84.21%		
Ni(II)		81.82%	
Pb(II)			30.77%

- Experimental conditions: C_o = 1 mM (for each metal ion); Q = 1 mL/min; Z = 50 cm; Influent pH = 5.0, Breakthrough level = 4 mg-Cu/L; [*Micrococcus luteus*] = 0.133 g-cell/mL-beads.

Table 4.17. Electron configuration of heavy metal ions. (Housecroft and Sharpe, 2005)

Metal ion	Number of electrons	Electron configuration in orbitals
Zn(II)	28	1s 2 2s 2 2p 6 3s 2 3p 6 3d 10
Ni(II)	26	1s 2 2s 2 2p 6 3s 2 3p 6 3d 8
Cu(II)	27	1s 2 2s 2 2p 6 3s 2 3p 6 3d 9
Pb(II)	80	1s 2 2s 2 2p 6 3s 2 3p 6 3d 10 4s 2 4p 6 4d 10 4f 14 5s 2 5p 6 5d 10 6s 2 6p 0

(a) Zn(II) ion (3d orbitals)

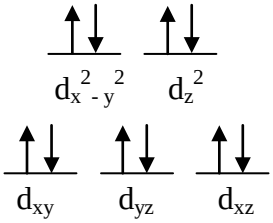

(b) Ni(II) ion (3d orbitals)

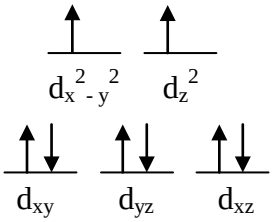

(c) Cu(II) ion (3d orbitals)

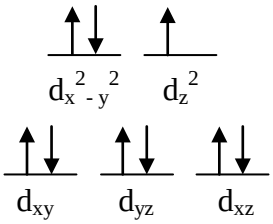

(d) Pb(II) ion (6p orbitals)

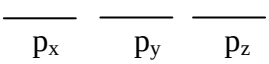

Figure 4.24. Electron configuration of heavy metal ions in outermost orbitals: (a) Zn(II) ion; (b) Ni(II) ion; (c) Cu(II) ion; and, (d) Pb(II) ion.

4.4 Copper(II) desorption studies

The development of metal biosorbents should not concentrate only on evaluating their biosorption characteristics. Regeneration and reuse of the biomaterials should be considered also. The performance of the biomass regeneration can be understood as how feasible the bound copper(II) ions can be recovered (desorbed) from the biomass. Accordingly, experiments were carried out to screen an effective desorbing agent for copper recovery from the RIM beads and to study the reusability of the RIM beads. These studies were carried out in both the batch reactors and the fixed-bed systems.

4.4.1 Batch desorption studies

Desorbing agents are generally classified into three major categories: (i) Complexing agents; (ii) Competing counter cations; and, (iii) Proton exchangers (Davis *et al.*, 2000; Gong *et al.*, 2005; Hammaini *et al.*, 2007; Park *et al.*, 2007). The metal desorption abilities of the complexing agents depend on their chelating power. Counter cations usually act as ion-exchangers to displace the bound metal cations from biosorbents. Similar to the counter ions, proton exchangers donate their protons to recover the bound metal species. Based on these three categories, a list of desorbing agents with various concentrations was selected to determine their abilities to recover copper(II) ions from the copper-loaded RIM beads in the batch reactors. The list is presented in Table 3.2, and the experiments were carried out as described in Section 3.4.1.

Fig. 4.25 shows the copper recoveries from the RIM beads using different desorbing agents with various concentrations. The figure shows that the copper(II) desorption ability (copper recovery) can be ordered as follows: Proton exchangers (HCl, HNO_3 and H_2SO_4) > Complexing agents (Na_2(EDTA), Na_2(NTA) and $Na_5P_3O_{10}$) > Counter calcium ions ($CaCl_2$ and $Ca(NO_3)_2$) >> Counter sodium ions (NaCl, $NaNO_3$ and Na_2SO_4). The results in Fig. 4.25 also shows that in most cases, the desorption abilities generally increased with the concentrations. This was because the concentration gradient and the displacement potential between the desorbing agent and the bound copper(II) ions were promoted under a higher concentration of the desorbing agents.

Regarding the sodium salts, Fig. 4.25 shows that the order of the copper(II) desorption ability can be arranged as: Na_2SO_4 >> NaCl > $NaNO_3$. Except $NaNO_3$, the abilities increased slightly with an increase of the sodium concentrations. All these three sodium salts displayed poor copper recoveries of around 60%, 30% and 20% with respect to Na_2SO_4, NaCl, and $NaNO_3$. Also, a destruction of the beads was found because sodium ions displaced the calcium ions from the alginate cross-linkage of the RIM beads. The alginate was then converted back to a soluble form of sodium alginate, resulting in swelling or dissolution of the beads. Thus, the counter sodium ions are not a good desorbing agent.

All three common complexing agents (Na_2(EDTA), Na_2(NTA) and $Na_5P_3O_{10}$) showed good desorption abilities with about 90%, 85% and 75%

for Na_2(EDTA), Na_2(NTA), and $Na_5P_3O_{10}$, respectively (Fig. 4.25). The concentration effect was minor since their chelating power was strong enough to recover most bound copper(II) ions even using lower concentrations. However, such excessive power also removed most calcium ions from the alginate cross-linkage in the beads, leading to a complete distortion of the beads. Hence, these complexing agents should not be used in the desorption process.

Excellent copper recoveries were observed using the acids as the desorbing agent (Fig. 4.25). HCl, HNO_3 and H_2SO_4 all displayed more than 90% recoveries. There was a minor or even no influence with an increase in the acid concentrations. This might be explained by the strong interaction between protons and the functional groups of the beads, resulting in a high displacement potential of the bound copper(II) ions by protons. A good desorption performance was then obtained even at low acid concentrations.

However, the acids were unfavourable to be applied in the biosorption/desorption cycles. A continuous decrease of the copper removals was displayed throughout the cycles (Figs. 4.26 (a) to (c)). The decrease was particularly serious in the cases using the highest acid concentrations. Only about 60% of the copper uptake could be retained at the end of the five cycles (Table 4.19). As suggested by some researchers, this may be due to an incomplete desorption (Bai and Abraham, 2003) and a loss of metal binding sites by acid deterioration (Figueira *et al*., 2000).

According to Figs. 4.27 (a) to (c), the effect of incomplete desorption should be minor since the copper recoveries in all the cycles were over 90%. The acid deterioration of the copper binding sites inside the RIM beads may be the dominant factor. This problem was further magnified in the sequential biosorption/desorption cycles of the fixed-bed process even using a low concentration of HCl (0.2 M) for the regeneration of the RIM column. This will be discussed in detail in Section 4.4.2.2. Therefore, the strong acids should not be used in the desorption process.

As for the calcium counter ions, two highly-soluble calcium salts ($CaCl_2$ and $Ca(NO_3)_2$) were chosen in this study. Fig. 4.25 shows that these two sources of calcium ions with various concentrations had moderate desorption abilities, with about 40 to 65% of the copper recoveries. The figure also indicates that the desorption abilities generally increased with the calcium concentrations owing to a higher displacement potential under a higher calcium concentration. However, lower copper recoveries were displayed in the cases using the highest concentration (4 M) of the calcium salts. This may be due to a high viscosity of these solutions, which reduced the mobility and diffusion of calcium ions on the bead surface or inside the beads. As a result, a poor mass transfer occurred, inducing a drop in the copper recoveries at the highest concentration.

These two calcium species were further investigated in five successive biosorption/desorption cycles. Their biosorption performances are presented in Figs. 4.28 (a) and (b). The copper removals dropped slightly

after the first cycle and then remained at a high level with minor fluctuations afterwards. After the five cycles, about 83 – 94% and 73 – 83% of the copper uptake could be maintained using different concentrations of $CaCl_2$ and $Ca(NO_3)_2$, respectively (Table 4.19). These results were different from the decreasing trend of the copper removals in the studies using the acids. The residual biosorption capacities using the calcium salts all were much higher than those using the acids. The incomplete desorption by the calcium salts should be the major cause of the decline of the biosorption performance, especially in the first two cycles. This was because the recoveries seldom reached 100%, as shown in Figs. 4.29 (a) and (b). The un-desorbed copper(II) ions accumulated inside the beads in each cycle would reduce the availability of the binding sites for copper(II) uptake in the next biosorption run.

As discussed above, the destructive effect on the RIM beads was observed when the sodium salts, complexing agents and acids were used as the desorbing agents. The calcium salts could exhibit moderate desorption abilities and a better maintenance of the biosorption performances in the sequential biosorption/desorption cycles. They were thus preferred to be used. Between $CaCl_2$ and $Ca(NO_3)_2$, $CaCl_2$ was chosen in the fixed-bed desorption process since it showed a slightly better performance in the copper removals and recoveries throughout the five cycles.

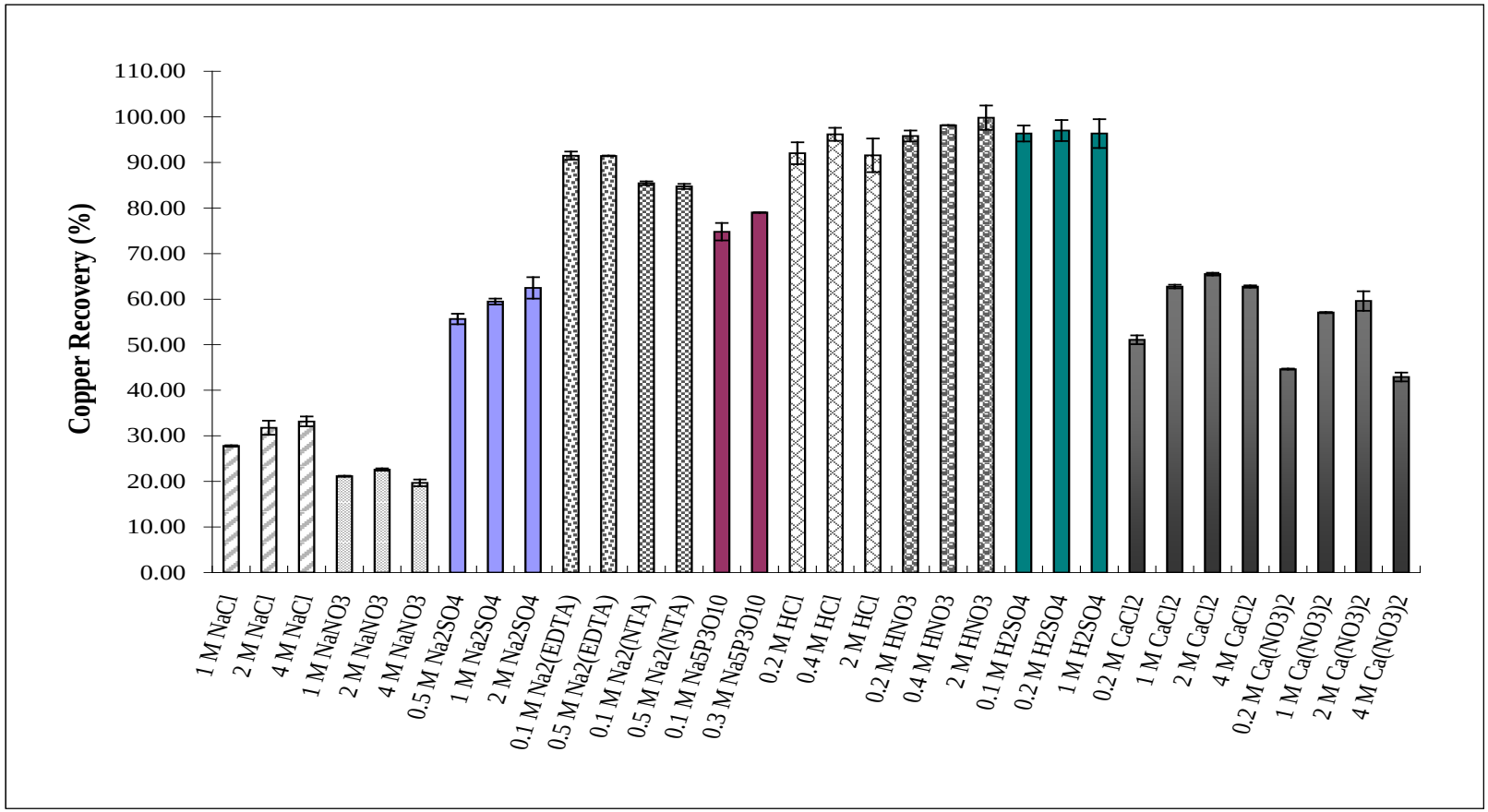

Figure 4.25. Copper recoveries from copper-laden RIM beads using different desorbing agents with various concentrations.
* Experimental conditions are listed in Table 4.18.

Table 4.18. Experimental conditions of the copper(II) biosorption and desorption using the RIM beads (correlated to Section 4.4.1).

Biosorption	**Desorption**
– Volume of RIM beads used = 0.6 mL; – Concentration of *Micrococcus luteus* in the RIM beads = 0.133 g-cell/mL-beads; – Initial copper(II) concentration = 100 mg-Cu/L; – Solution pH = 5.0; – Volume of reaction mixture = 50 mL; – Contact time = 6 h; – Agitation speed = 250 rpm.	– Volume of desorbing agent used = 10 mL; – Contact time = 6 h; – Agitation speed = 250 rpm.

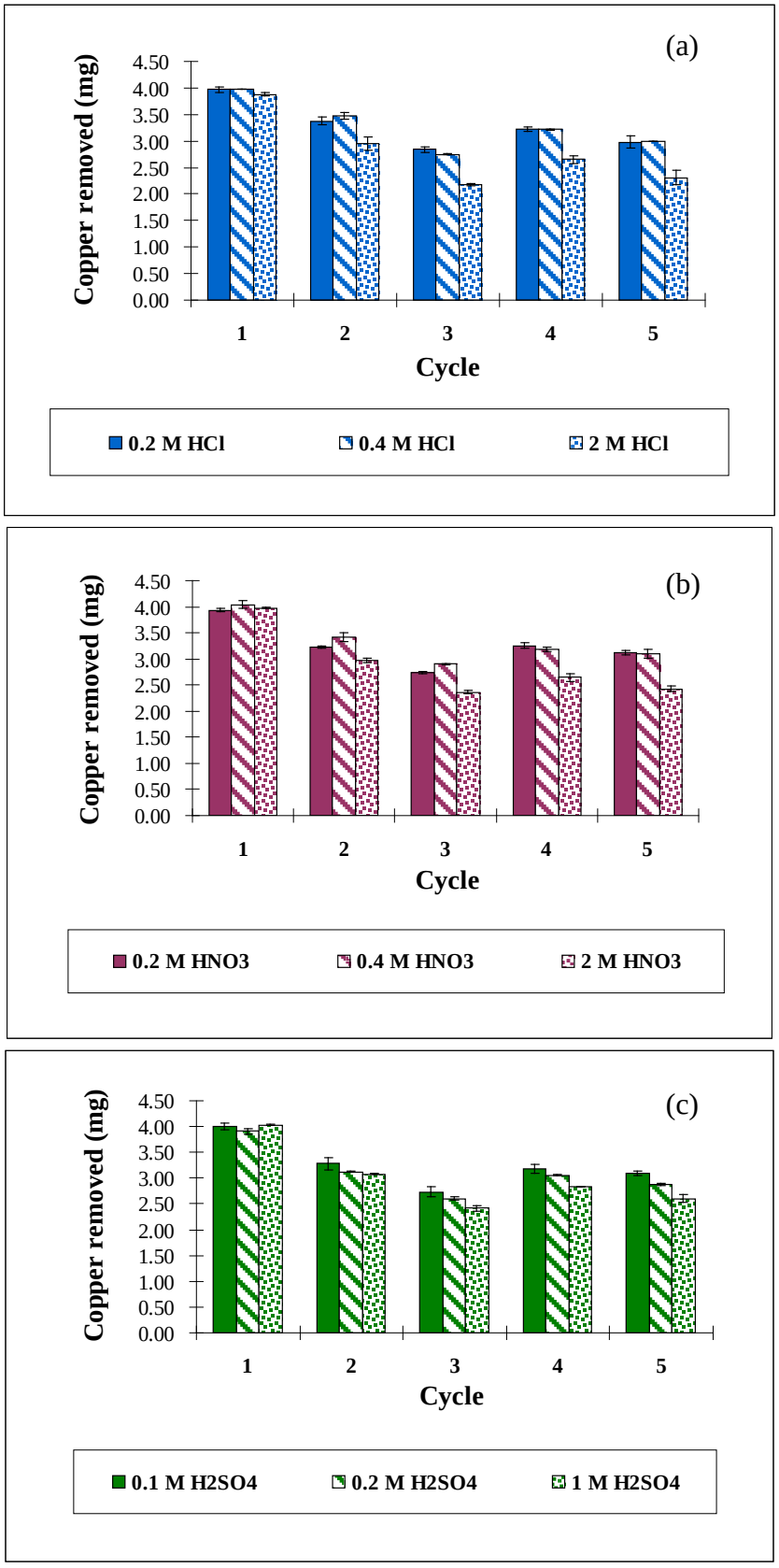

Figure 4.26. Copper removals of RIM beads in batch systems with five sequential biosorption/desorption cycles using various concentrations of different acids as desorbing agents: (a) HCl; (b) HNO_3; and, (c) H_2SO_4.
* Experimental conditions are listed in Table 4.18.

Table 4.19. Residual copper(II) biosorption capacities after five biosorption/desorption cycles using different desorbing agents.

Desorbing agent		Residual biosorption capacity (%)
Proton exchanger (Acid)	0.2 M HCl	73.52 ± 2.00
	0.4 M HCl	75.20 ± 0.18
	2 M HCl	61.71 ± 3.04
	0.2 M HNO_3	79.35 ± 0.44
	0.4 M HNO_3	79.35 ± 3.52
	2 M HNO_3	60.04 ± 1.40
	0.1 M H_2SO_4	77.55 ± 0.24
	0.2 M H_2SO_4	73.56 ± 0.39
	1 M H_2SO_4	63.16 ± 2.07
Competing counter cation (Calcium salt)	0.2 M $CaCl_2$	82.97 ± 0.03
	1 M $CaCl_2$	87.62 ± 1.09
	2 M $CaCl_2$	93.66 ± 0.70
	4 M $CaCl_2$	90.56 ± 2.20
	0.2 M $Ca(NO_3)_2$	73.32 ± 0.36
	1 M $Ca(NO_3)_2$	82.76 ± 0.61
	2 M $Ca(NO_3)_2$	82.60 ± 2.69
	4 M $Ca(NO_3)_2$	79.26 ± 2.22

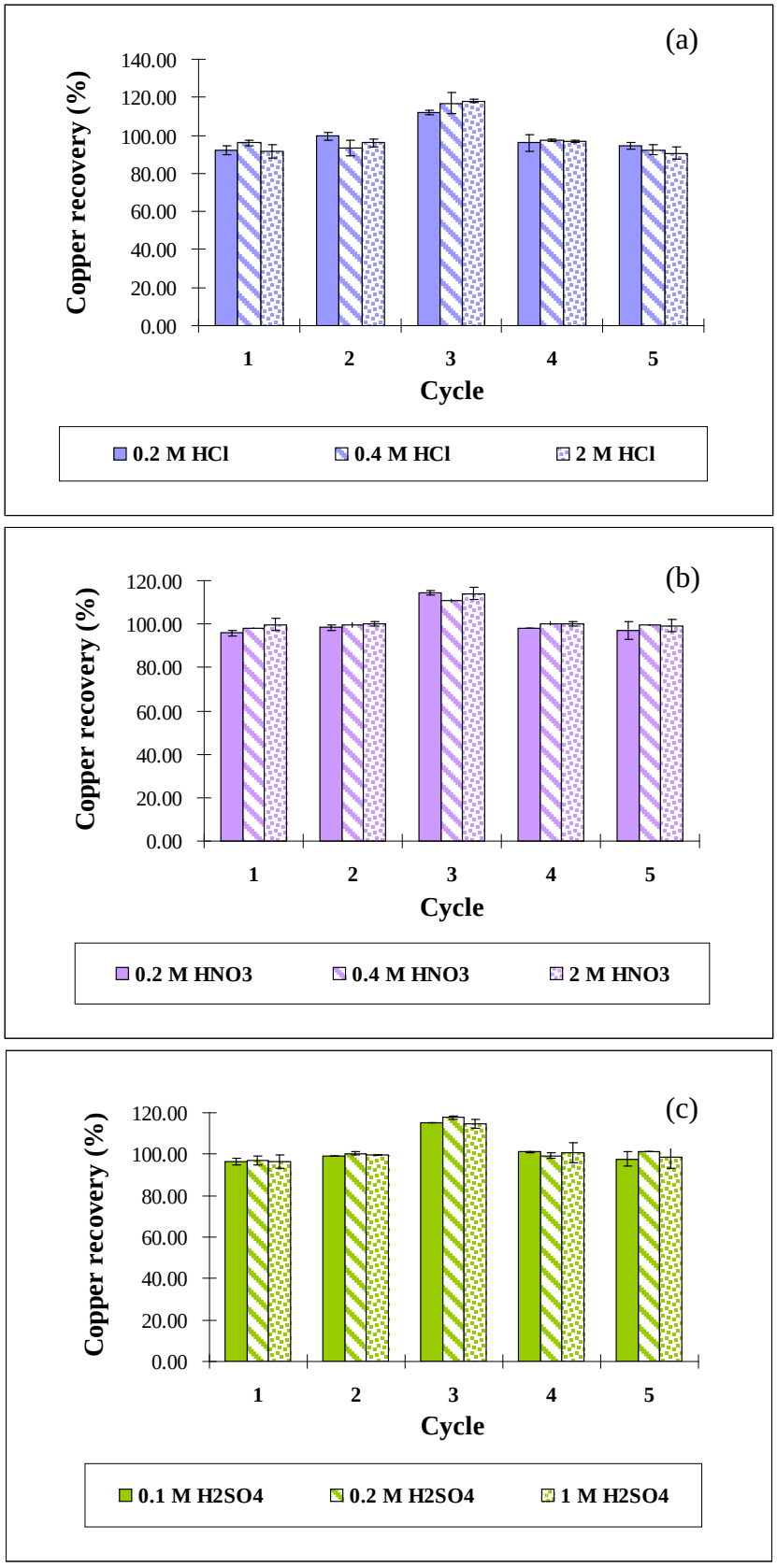

Figure 4.27. Copper recoveries from RIM beads in batch systems with five sequential biosorption/desorption cycles using various concentrations of different acid desorbing agents: (a) HCl; (b) HNO_3; and, (c) H_2SO_4.
* Experimental conditions are listed in Table 4.18.

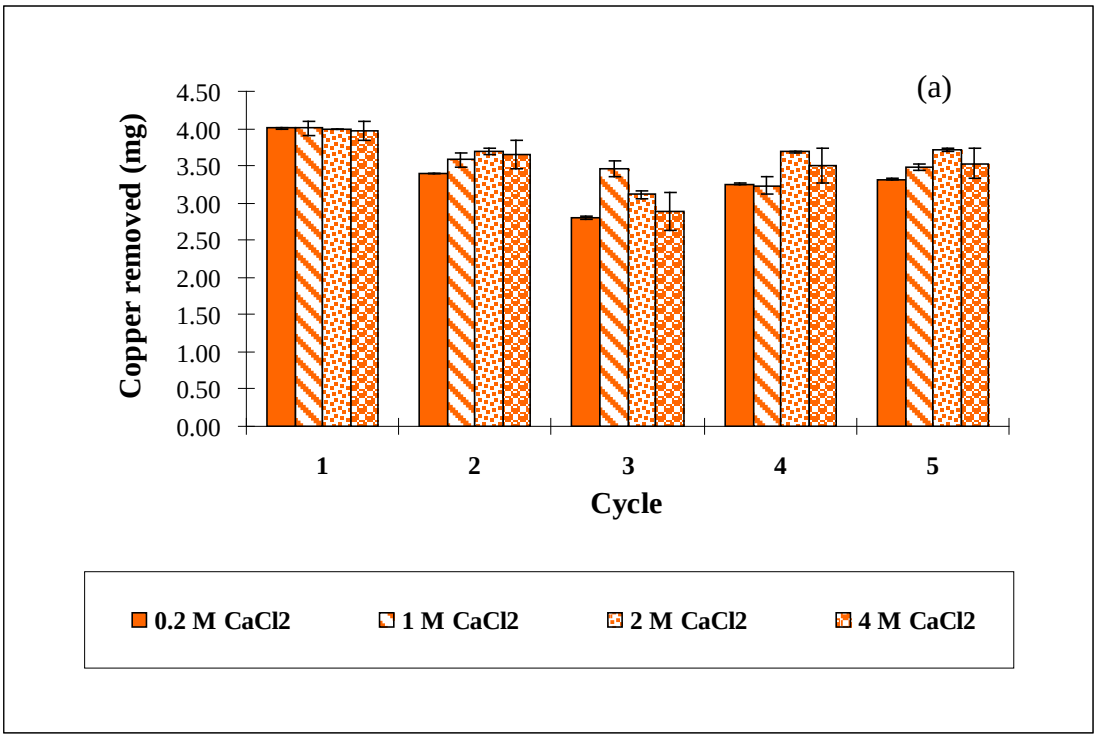

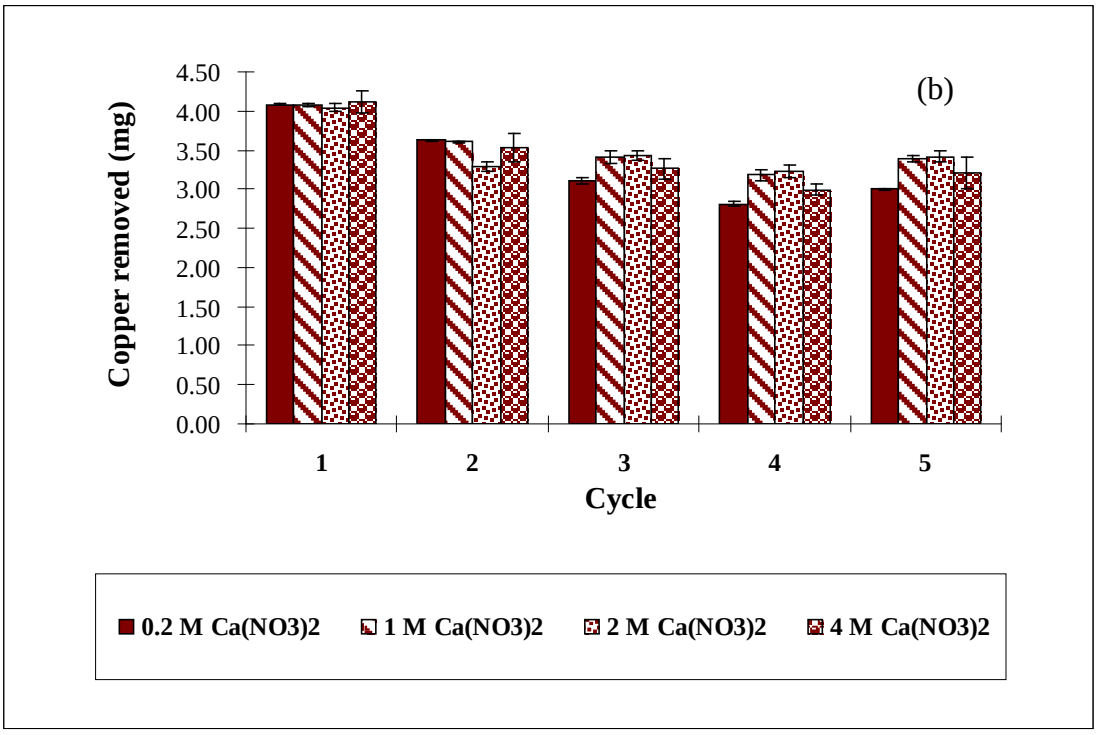

Figure 4.28. Copper removals of RIM beads in batch systems with five sequential biosorption/desorption cycles using various concentrations of different calcium salts as desorbing agents: (a) $CaCl_2$; (b) $Ca(NO_3)_2$.

* Experimental conditions are listed in Table 4.18.

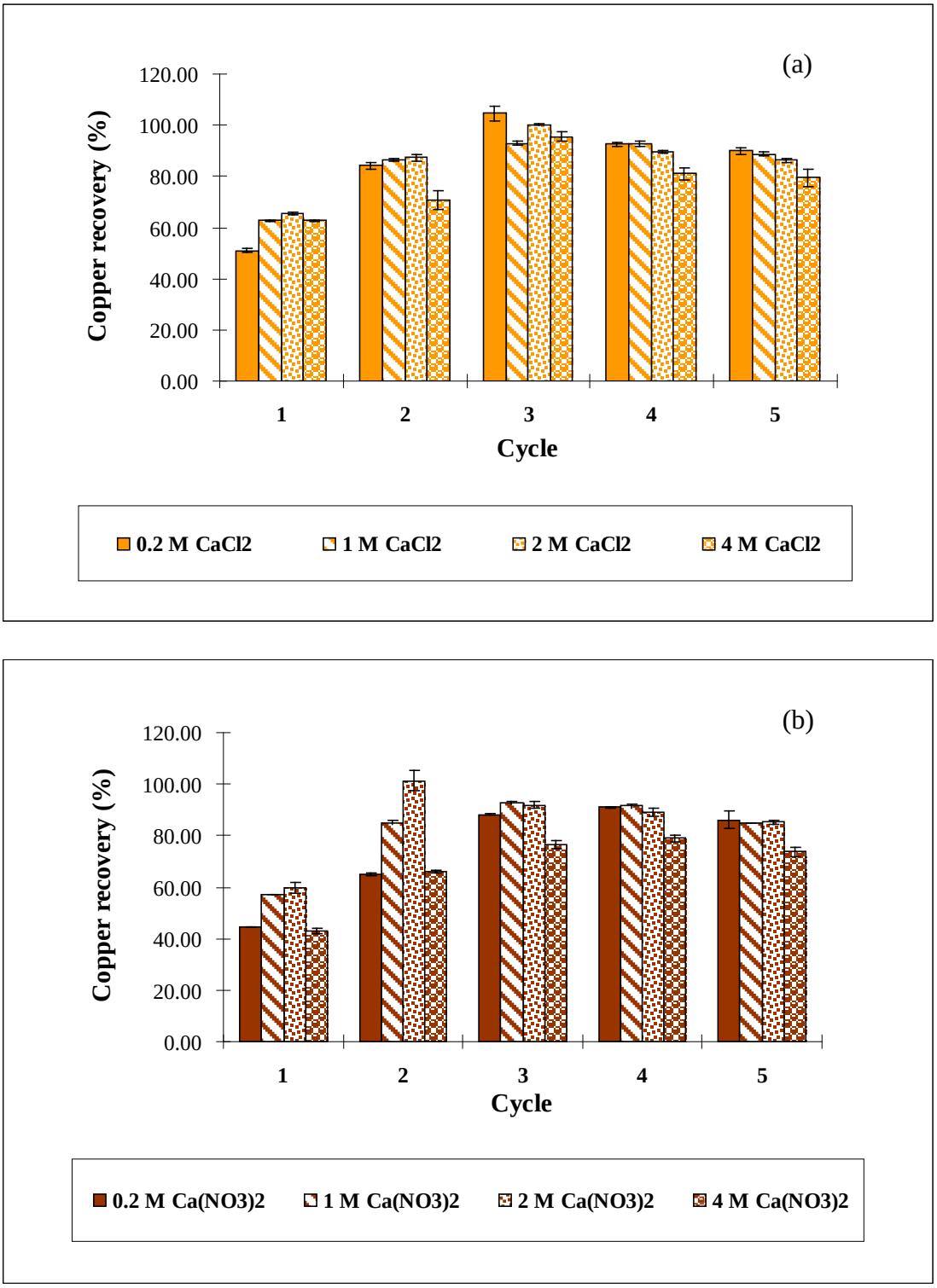

Figure 4.29. Copper recoveries from RIM beads in batch systems with five sequential biosorption/desorption cycles using various concentrations of different calcium salts as desorbing agents: (a) $CaCl_2$; (b) $Ca(NO_3)_2$.

* Experimental conditions are listed in Table 4.18.

4.4.2 Fixed-bed desorption studies

The previous section shows that using $CaCl_2$ solution as the desorbing agent could provide a better maintenance on the biosorption performance and a reasonable desorption ability in the sequential cycles of the batch system. Fixed-bed desorption studies were further carried out by introducing various concentrations of $CaCl_2$ solution as the desorbing agent into the copper-laden RIM column with different flow rates.

Generally, the desorption process could be considered as a reverse reaction of the copper(II) biosorption. Calcium ions of the desorbing agent may act as sorbates to displace the bound copper(II) ions from the beads (discussed in Section 4.4.3). Similar to other ion exchange reactions, the interchange between the bound copper(II) species and calcium ions of the desorbing agent depends on (i) the metal binding affinities of the sorbents and (ii) the concentration gradients between the displaced metal species and the substitute. *Micrococcus luteus* and alginate chains, the major bead components, have a great binding affinity towards copper(II) ions. This could lead to a strong copper binding and thus limit the displacement of the bound copper(II) species by the aqueous calcium ions in the desorption process. However, this limitation could be overcome by increasing the calcium concentration. With a sufficient and continuous supply of calcium ions in the fixed-bed system, a large concentration gradient between these two ions could be developed. The equilibrium position would be shifted to the right to recover more copper(II) ions (Equation 4.17). As referred to the previous fixed-bed studies (Section 4.3), the calcium supply in the

column desorption might be affected by the influent concentrations as well as the inlet flow rates. The effects of these two critical factors will be reported in the following sub-sections.

$$Ca^{2+}(aq) + Cu - Biosorbent(s) \xleftrightarrow{\text{Sorption Equilibrium}} Ca - Biosorbent(s) + Cu^{2+}(aq)$$

(Equation 4.17)

4.4.2.1 Effects of inlet flow rate and influent concentration

In order to perform fixed-bed desorption studies, the copper(II) biosorption of the RIM columns was conducted first under the optimal conditions as discussed in Section 4.3.4. When the column broke through, $CaCl_2$ solutions with 1, 2 and 4 M of initial concentrations were separately pumped into the copper-laden RIM columns for copper recovery at various inlet upward flow rates (0.5 to 2 mL/min). The experiments were continued until a constant concentration or an absence of copper(II) ions was found in the desorption effluent. The desorption profiles are presented in Figs. 4.30 (a) to (c), and the results are summarized in Table 4.20.

The results in Table 4.20 show that the copper removals in the preceding biosorption runs were close with less than 16% difference. The difference might be due to the variation of the bed packing, including the packing density and quantity of the beads. In view of the desorption profiles (Figs. 4.30 (a) to (c)), similar trends were observed in all the conditions of the influent $CaCl_2$ concentrations and the inlet flow rates. In the initial phase of the fixed-bed desorption, a rapid increase of the copper

recovery was observed. It was because a large amount of the bound copper(II) ions in the RIM columns was displaced instantaneously into the effluent in this phase. As the desorption proceeded to its equilibrium, the copper content in the column greatly decreased. The rate of the copper recovery thus slowed down and the desorption profile leveled off.

As shown in Fig. 4.31, most of the fixed-bed desorption operating at different influent $CaCl_2$ concentrations and inlet flow rates demonstrated similar desorption performances, attaining about 80% copper recovery. It indicates that the influent concentrations and inlet flow rates did not significantly influence the overall copper(II) desorption performances in the RIM column system. The similar copper recoveries obtained in the fixed-bed desorption were rendered by the presence of the continuous supply of calcium ions. This developed a large concentration gradient between calcium ions and the bound copper(II) ions, promoting the shift of the desorption equilibrium to the right to displace more copper(II) ions, as shown in Equation 4.17.

In view of the effect of the $CaCl_2$ concentrations on the desorption profiles, Figs. 4.30 (a) to (c) show that the pattern of the desorption profiles were similar under various concentrations of $CaCl_2$ (1 to 4 M) at the same flow rates. These data shows that $CaCl_2$ concentrations only had a minor influence on the fixed-bed desorption profile.

Regarding the effect of inlet flow rates (Q) on the column desorption profiles, Figs. 4.30 (a) to (c) show that the profiles became dispersive as the desorption processes were performed at the fastest flow rate (2 mL/min). This was because, at the fastest flow rate, a larger volume of the $CaCl_2$ solution was introduced into the column, diluting greatly the concentration of the recovered copper(II) ions in the effluent. This resulted in the dispersive desorption profile. On the other hand, the desorption curves were less dispersive and even overlapped with each other in the cases with slower flow rates (Q = 0.5 and 1 mL/min). At these flow rates, the desorption rate was governed by the calcium supply. More calcium ions would be supplied by the desorption runs operating at 1 mL/min, compared with 0.5 mL/min. This could promote the exchange of bound copper(II) ions and counteract the effect of dispersion. As a result, the overlapping of the desorption profiles was observed.

However, an exception was found in the desorption operating at 1 M $CaCl_2$ concentration and 0.5 mL/min. The overall copper recovery was about 72.29%, which was poorer than the others (Table 4.20). Also, an abnormal desorption profile was observed in this operation (Fig. 4.30 (a)). These observations can be explained by the fact that the supply of calcium ions was insufficient at such low influent $CaCl_2$ concentration and slow flow rate. The desorption ability thus became weaker, resulting in the suppression of the copper recovery and the abnormal desorption profile.

On the other hand, a better desorption performance was found in the fixed-bed operations, compared with that of the batch systems. The copper recoveries of the fixed-bed systems were about 72 to 83% (Table 4.20), whereas those of the batch systems were only 63 to 66% (Fig. 4.29(a). This enhancement was possible because a continuous supply of fresh calcium ions to the fixed-bed system could further shift the equilibrium position to the right (Equation 4.17).

To select the optimal desorption conditions for the following fixed-bed studies, both the desorption efficiency and the material cost were considered. The above results indicate that the influent $CaCl_2$ concentrations and flow rates had no significant influence on the overall copper recovery, but the abnormal suppression of the copper recovery was found in the desorption run operating at the lowest $CaCl_2$ concentration (1 M) and the slowest flow rate (0.5 mL/min). Therefore, a moderate flow rate (1 mL/min) together with 1 M $CaCl_2$ solution was chosen in the following column desorption processes to ensure an efficient desorption with minimum material consumption.

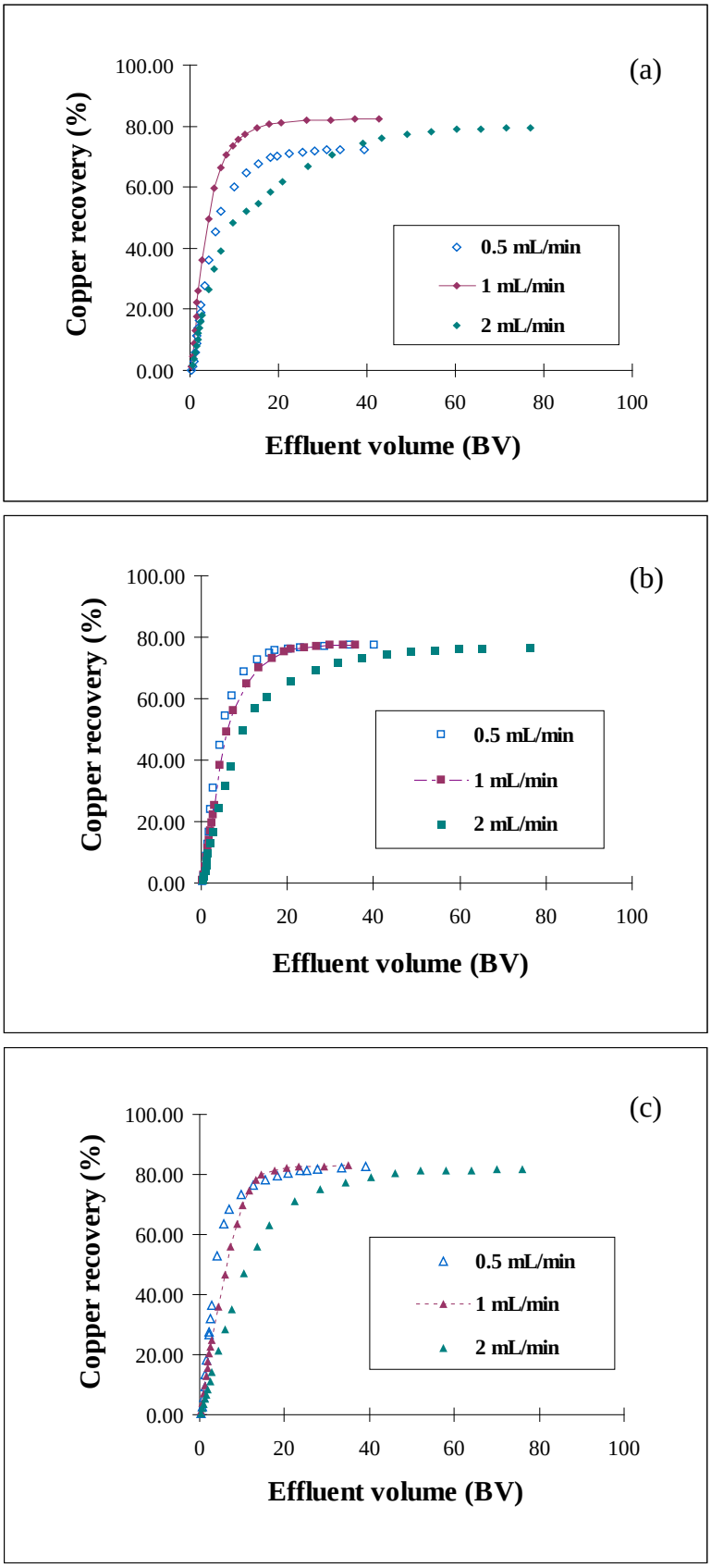

Figure 4.30. Desorption profiles of copper-laden RIM columns by introducing various concentrations of $CaCl_2$ solutions at different inlet upward flow rates: (a) 1M; (b) 2 M; and, (c) 4 M.
* Experimental conditions are listed in Table 4.20.

Table 4.20. Copper removals and recoveries of RIM columns using different $CaCl_2$ concentrations and inlet upward flow rates for fixed-bed desorption.

$CaCl_2$ concentration (M)	Inlet upward flow rate (mL/min)	Bead volume in the column (mL)	Copper removal (mg)	Copper recovery (%)
1.00	0.5	42.58	370.64	72.29
	1.0	43.45	338.39	82.25
	2.0	42.85	343.84	79.41
2.00	0.5	41.65	380.21	77.40
	1.0	40.10	348.32	77.36
	2.0	43.23	397.99	76.33
4.00	0.5	43.00	380.67	82.57
	1.0	41.00	335.47	82.94
	2.0	40.28	357.81	81.74

* Experimental conditions of the fixed-bed biosorption: C_o = 50 mg-Cu/L; Q = 1 mL/min; Z = 50 cm; Solution pH = 5.0; Breakthrough level = 4 mg-Cu/L; [*Micrococcus luteus*] = 0.133 g-cell/mL-beads.

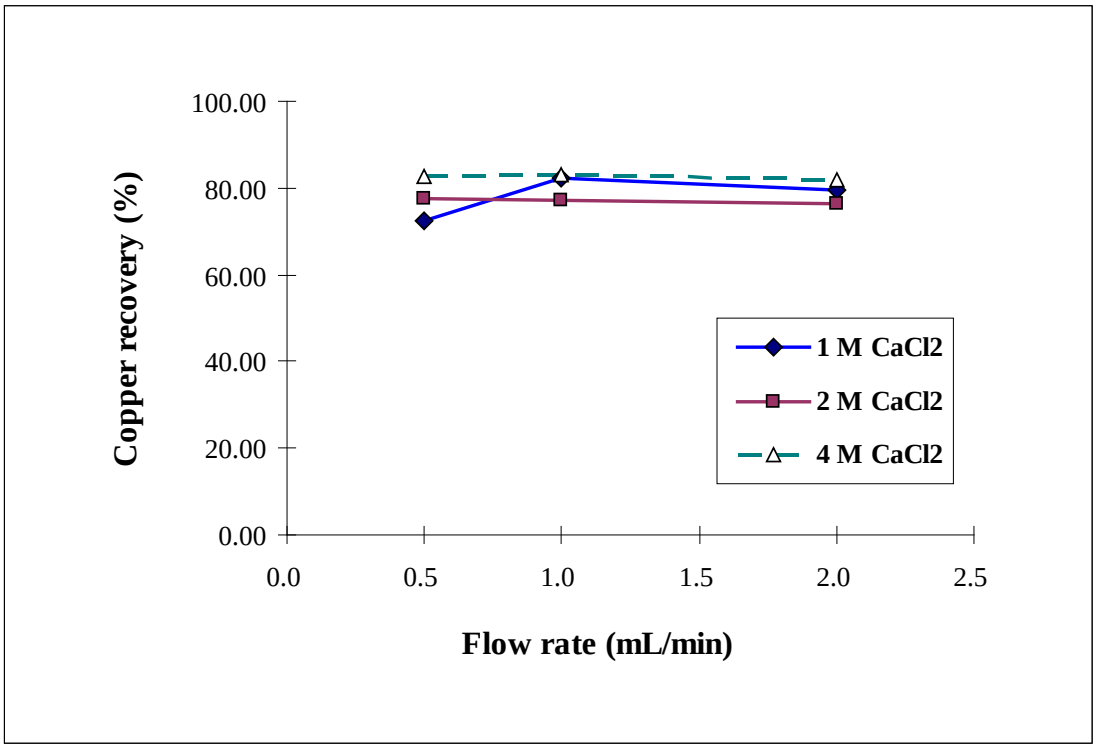

Figure 4.31. Copper recoveries of copper-laden RIM columns by introducing various concentrations of $CaCl_2$ solutions at different inlet upward flow rates.

* Experimental conditions are listed in Table 4.20.

4.4.2.2 Sequential removal and recovery of copper

The reusability of adsorption columns is another critical issue to be evaluated in the desorption process. This sub-section further reports the process performances of the RIM column in ten successive biosorption/desorption cycles. The biosorption process was carried out by pumping 50 mg-Cu/L copper(II) nitrate solution until the breakthrough point (C_e = 4 mg-Cu/L) was reached. After that, the desorption process was performed by introducing 1 M $CaCl_2$ solution until 85% of the copper coner inside the RIM column was desorbed. The inlet upward flow rate of both the processes was maintained at 1 mL/min. The details of the experiments are described in Section 3.4.2. The removals and recoveries of copper and the organic leakage were investigated throughout the cycles to evaluate the reusability of the RIM column.

Fig. 4.32 illustrates the copper removals and the treatment volume of the RIM column in ten biosorption/desorption cycles. The copper removals decreased gently in the first four cycles and then remained at a steady level. About 41% of the copper removal ability retained after the ten cycles (Table 4.21). A similar trend was observed in the results of the treatment volume (Fig. 4.32 and Table 4.22).

As suggested by Bai and Abraham (2003), the decrease of the copper removal ability could be regarded as an incomplete desorption of the bound metal ions from the biomass. Fig. 4.33 clearly shows a considerable amount of copper(II) ions accumulated inside the column because the

percentage of the copper recoveries was only between 80% and 90% throughout the cycles. By subtracting the amount of copper(II) ions recovered from that of copper removed in the same cycle, the copper accumulation was obtained and listed in Table 4.21. The results shows that the total amount of copper(II) ions accumulated in the biosorbents increased throughout the ten cycles. This strongly suggested that the loss of the copper removal abilities was mainly caused by the incomplete desorption.

A similar experiment was performed but 0.2 M HCl was used as the desorbing agent. All conditions and procedures were the same as the above experiment with 1 M $CaCl_2$ solution. The results are presented in Fig. 4.34 and Tables 4.23 to 4.24. A continuous decrease of both the copper removal and the treatment volume was observed in the case using 0.2 M HCl (Fig. 4.34). The drop was especially serious in cycle 2. Both the copper removal and treatment volume were only approximate half as compared with those using the $CaCl_2$ solution from cycles 2 to 10 (Fig. 4.34). Tables 4.23 and 4.24 further show that only about 17% of the copper removals and the treatment volume remained at the last cycle after the acid desorption, whereas 41% of the treatment performances could be maintained in the case using the $CaCl_2$ solution. All these results indicate that the column reusability was much better when the $CaCl_2$ solution was used as the desorbing agent.

The incomplete desorption was one of the major reasons to explain the continuous decline in the treatment performances of the column while using

acid as the desorbing agent. As showed in Table 4.23, the copper recoveries were around 80% to 90%, which were close to those using the $CaCl_2$ solution. This meant that there was about 10% to 20% of the bound copper accumulated inside the column throughout the cycles, inducing the decline of the copper removal abilities. This explanation could be validated by calculating the copper accumulation of each cycle. An increasing trend of the total amount of copper(II) ions accumulated in the biosorbents was exhibited throughout the ten biosorption/desorption cycles (Table 4.23).

Another reason might be related to the acid deterioration of the biosorbents (Figueira *et al*., 2000). This inference was investigated by measuring the amount of organics in the column desorption effluent. The organics might come from the cell leakage and/or the dissolution of the immobilization polymer matrices. As shown in Fig. 4.35, a larger amount of organics was released when HCl was used as the desorbing agent throughout the ten cycles. About a 60% higher total organic leakage TOC (173.7 mg) was found when HCl was used, compared with $CaCl_2$ solution (108.8 mg). As the acid diffused into the beads, it might induce the deterioration of the metal binding sites (organic functional groups) on the cells and the polymer matrices. The acid also promotes the dissolution of the alginate through the displacement of calcium ions, which were the gelation cations in the alginate matrix. All these would lower significantly the copper removal abilities and the treatment performances, especially so in cycle 2 (Fig. 4.34).

The above results show that the desorption process using 1 M $CaCl_2$ at 1 mL/min could obtain a superior treatment performance and column reusability than using 0.2 M HCl. Thus, 1 M $CaCl_2$ at 1 mL/min will be used to desorb Cu(II) ions from the RIM column in the integrated treatment process (Section 4.6.4).

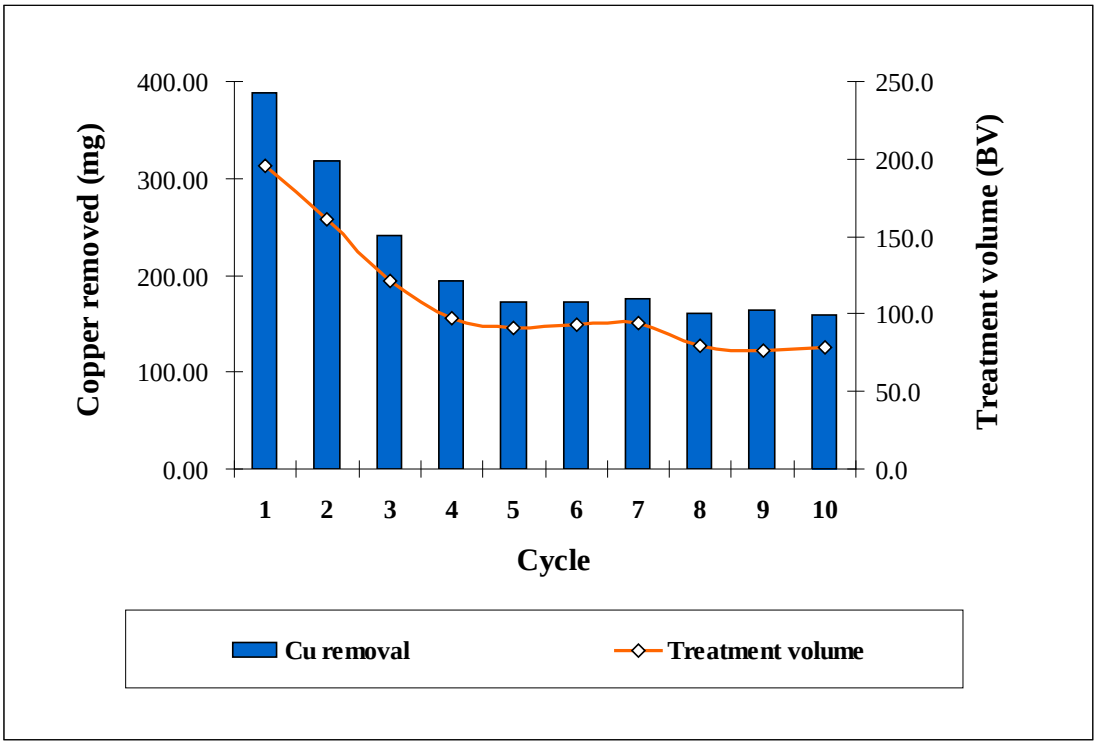

Figure 4.32. Copper removals and treatment volume of RIM column in 10 sequential biosorption/desorption cycles using 1 M $CaCl_2$ for column regeneration.

* Experimental conditions are listed in Table 4.21.

Table 4.21. Copper removals and recoveries of RIM column in ten sequential biosorption/desorption cycles using 1 M $CaCl_2$ for column regeneration.

Cycle	Biosorption		Desorption		Copper accumulation	
	Copper removal	Performance retained	Copper recovery		Copper retained	Net copper retained in biosorbents
	(mg) [(a)]	(%) [(b)]	(mg) [(c)]	(%) [(d)]	(mg) [(e)]	(mg) [(f)]
1	388.34		330.87	85.20	57.47	57.47
2	317.44	81.74	271.11	85.40	46.33	103.80
3	240.70	61.98	210.33	87.38	30.37	134.17
4	193.51	49.83	160.58	82.98	32.93	167.10
5	173.11	44.58	140.75	81.31	32.36	199.46
6	173.02	44.55	151.72	87.69	21.30	220.76
7	176.56	45.47	157.14	89.00	19.42	240.18
8	161.13	41.49	137.66	85.44	23.47	263.65
9	163.66	42.14	135.77	82.96	27.89	291.54
10	158.63	40.85	134.47	84.77	24.16	315.70

- Fixed-bed biosorption conditions: C_o = 50 mg-Cu/L; Q = 1 mL/min; Z = 50 cm; Solution pH = 5.0; [*Micrococcus luteus*] = 0.133 g-cell/mL-beads; The process was conducted up to the breakthrough level (4 mg-Cu/L);
- Fixed-bed desorption conditions: C_o = 1 M $CaCl_2$; Q = 1 mL/min; The process was continued until 85% of copper content inside the column bed was desorbed;
- Calculation:

(b) Biosorption performance retained (%) = (a) $_{\text{Cycle n}}$ / (a) $_{\text{Cycle 1}}$;

(d) Copper recovery (%) = (c) / (a);

(e) Copper accumulation (mg) = (a) – (c);

(f) Net amount of copper retained in biosorbents = $\sum_{n=1}^{10}(e)$.

Table 4.22. Treatment volume of RIM column in ten sequential biosorption/desorption cycles using 1 M $CaCl_2$ for column regeneration.

Cycle	Treatment volume (BV) [(a)]	Capacity retained (%) [(b)]	Capacity loss (%) [(c)]
1	195.5		
2	160.8	82.22	17.78
3	121.7	62.22	37.78
4	97.0	49.63	50.37
5	90.5	46.30	53.70
6	92.7	47.41	52.59
7	94.1	48.15	51.85
8	79.7	40.74	59.26
9	76.8	39.26	60.74
10	78.2	40.00	60.00

- Fixed-bed biosorption conditions: C_o = 50 mg-Cu/L; Q = 1 mL/min; Z = 50 cm; Solution pH = 5.0; [*Micrococcus luteus*] = 0.133 g-cell/mL-beads; The process was conducted up to the breakthrough level (4 mg-Cu/L);
- Fixed-bed desorption conditions: C_o = 1 M $CaCl_2$; Q = 1 mL/min; The process was continued until 85% of copper content inside the column bed was desorbed;
- Calculation:

(b) Capacity retained (%) = (a) $_{\text{Cycle n}}$ / (a) $_{\text{Cycle 1}}$;
(c) Capacity loss (%) = 100% – (b).

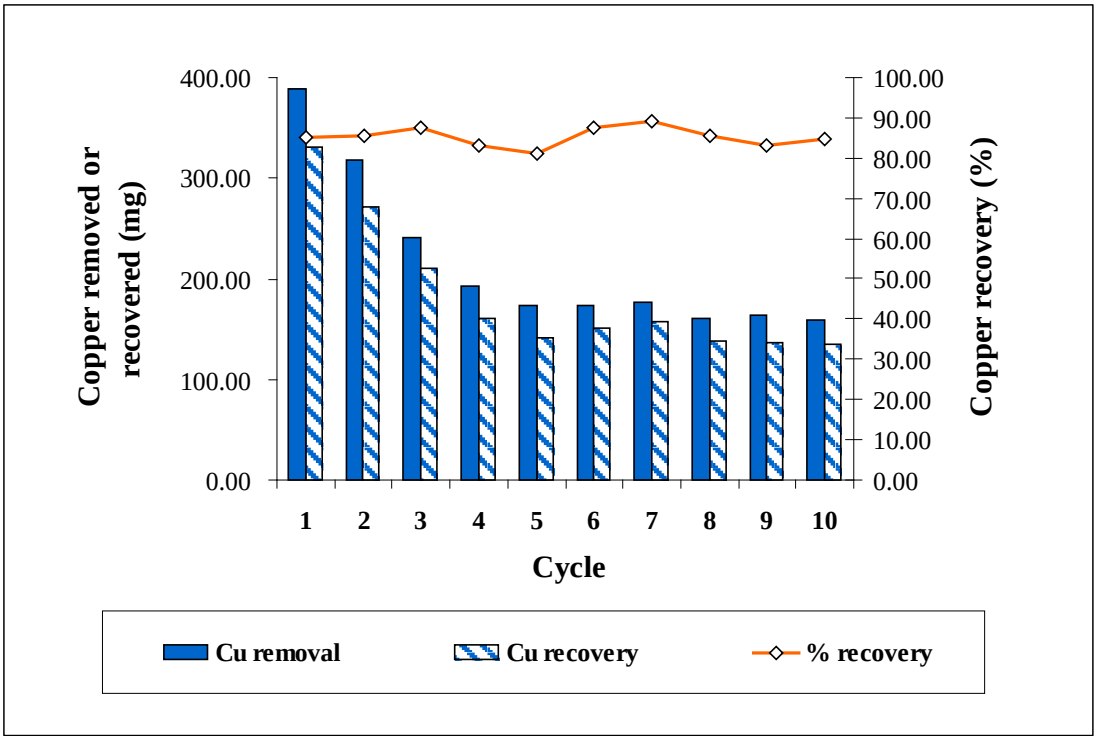

Figure 4.33. Copper removals and recoveries of RIM column in ten sequential biosorption/desorption cycles using 1 M $CaCl_2$ for column regeneration.

* Experimental conditions are listed in Table 4.21.

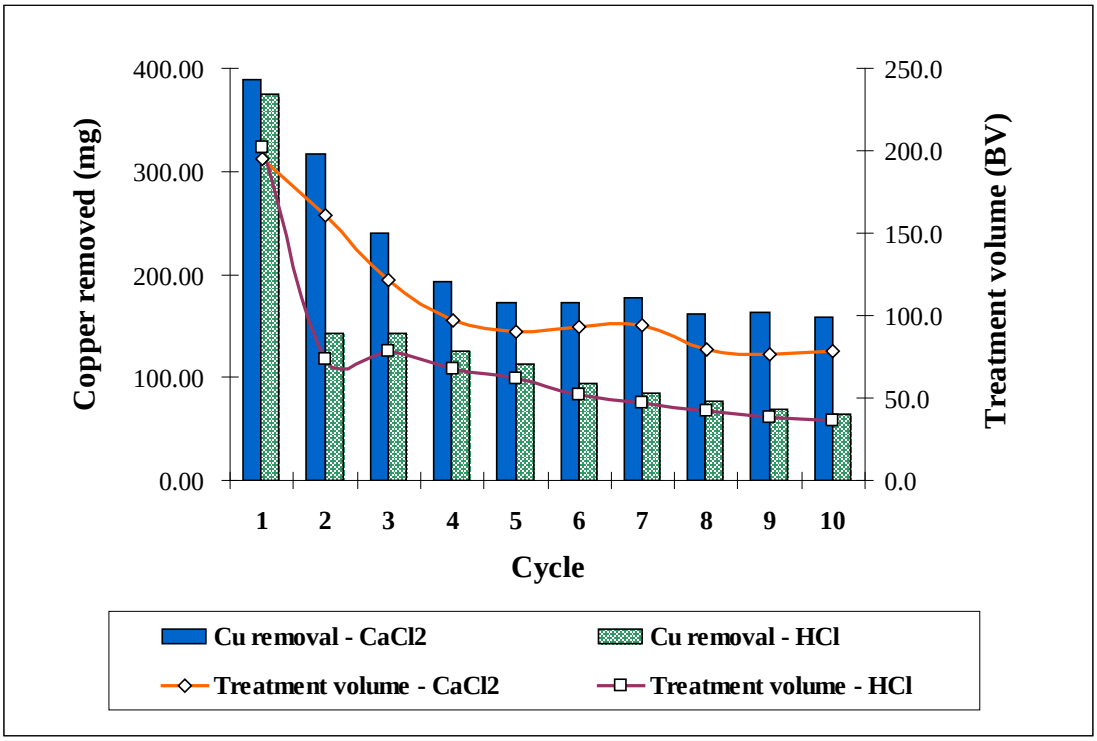

Figure 4.34. Copper removals and treatment volume of RIM columns in ten sequential biosorption/desorption cycles using 1 M $CaCl_2$ or 0.2 M HCl for column regeneration.

* Experimental conditions are listed in Tables 4.21 and 4.23.

Table 4.23. Copper removals and recoveries of RIM column in ten sequential biosorption/desorption cycles using 0.2 M HCl for column regeneration.

Cycle	Biosorption		Desorption		Copper accumulation	
	Copper removal	Performance retained	Copper recovery		Copper retained	Net copper retained in biosorbents
	(mg) [(a)]	(%) [(b)]	(mg) [(c)]	(%) [(d)]	(mg) [(e)]	(mg) [(f)]
1	375.46		304.59	81.12	70.87	70.87
2	142.19	37.87	119.54	84.07	22.65	93.52
3	143.31	38.17	121.93	85.08	21.38	114.90
4	126.18	33.61	106.30	84.24	19.88	134.78
5	113.43	30.21	92.88	81.88	20.55	155.33
6	94.15	25.08	77.80	82.10	16.35	171.68
7	84.66	22.55	69.78	82.43	14.88	186.56
8	76.37	20.34	62.79	82.22	13.58	200.14
9	69.48	18.51	60.39	86.93	9.09	209.23
10	63.58	16.93	53.60	84.30	9.98	219.21

- Fixed-bed biosorption conditions: C_o = 50 mg-Cu/L; Q = 1 mL/min; Z = 50 cm; Solution pH = 5.0; [*Micrococcus luteus*] = 0.133 g-cell/mL-beads; The process was conducted up to the breakthrough level (4 mg-Cu/L);
- Fixed-bed desorption conditions: C_o = 0.2 M HCl; Q = 1 mL/min; The process was continued until 85% of copper content inside the column bed was desorbed;
- Calculation:

(b) Biosorption performance retained (%) = (a) $_{\text{Cycle n}}$ / (a) $_{\text{Cycle 1}}$;

(d) Copper recovery (%) = (c) / (a);

(e) Copper accumulation (mg) = (a) – (c);

(f) Net amount of copper retained in biosorbents = $\sum_{n=1}^{10}(e)$.

Table 4.24. Treatment volume of RIM column in ten sequential biosorption/desorption cycles using 0.2 M HCl for column regeneration.

Cycle	Treatment volume (BV) [(a)]	Capacity retained (%) [(b)]	Capacity loss (%) [(c)]
1	201.6		
2	74.0	36.72	63.28
3	78.7	39.06	60.94
4	67.7	33.59	66.41
5	61.4	30.47	69.53
6	52.0	25.78	74.22
7	47.2	23.44	76.56
8	42.5	21.09	78.91
9	37.8	18.75	81.25
10	36.2	17.97	82.03

- Fixed-bed biosorption conditions: C_o = 50 mg-Cu/L; Q = 1 mL/min; Z = 50 cm; Solution pH = 5.0; [*Micrococcus luteus*] = 0.133 g-cell/mL-beads; The process was conducted up to the breakthrough level (4 mg-Cu/L);
- Fixed-bed desorption conditions: C_o = 0.2 M HCl; Q = 1 mL/min; The process was continued until 85% of copper content inside the column bed was desorbed;
- Calculation:

(b) Capacity retained (%) = (a) $_{\text{Cycle n}}$ / (a) $_{\text{Cycle 1}}$;
(c) Capacity loss (%) = 100% – (b).

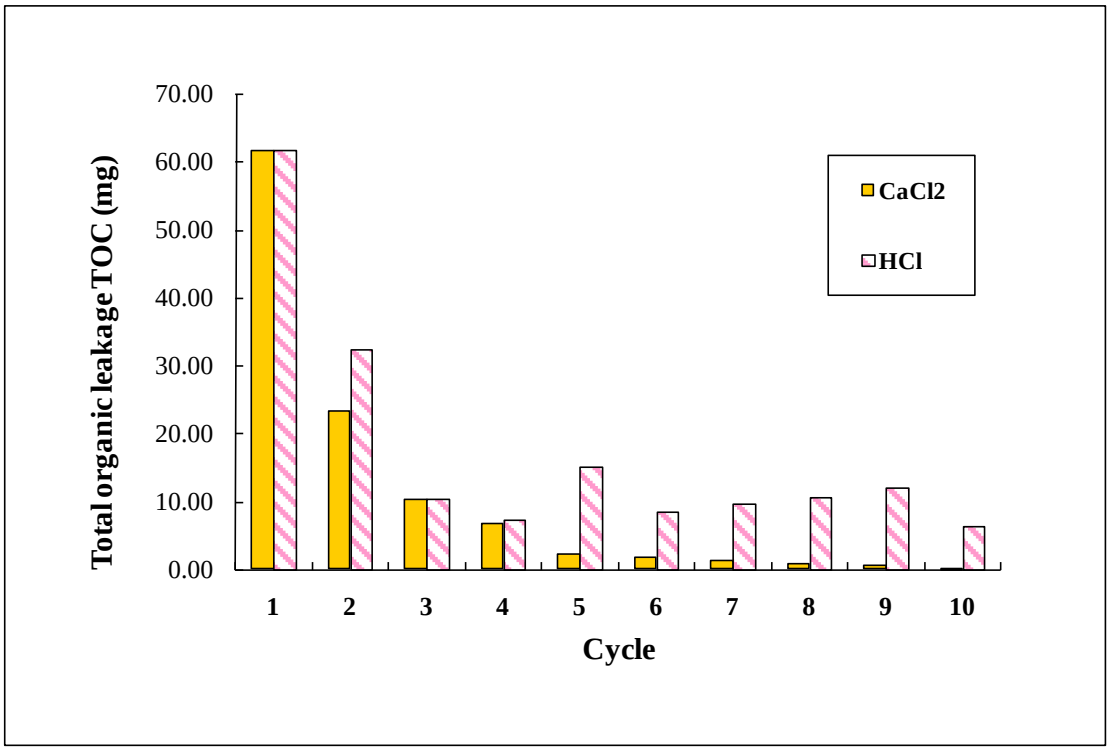

Figure 4.35. Organic leakage of RIM columns in ten sequential biosorption/desorption cycles using 1 M $CaCl_2$ or 0.2 M HCl for column regeneration.

* Experimental conditions are listed in Tables 4.21 and 4.23.

4.4.3 Mechanistic studies of copper(II) biosorption and desorption in fixed-bed column

To elucidate the copper(II) biosorption and desorption mechanisms of the RIM beads throughout the fixed-bed biosorption/desorption cycles, both qualitative and quantitative studies were performed. The qualitative determination was done by studying the surface chemical composition of the RIM beads using X-ray Energy Dispersive Analysis (EDAX). In view of the quantitative study, the material balance of the fixed-bed biosorption processes was calculated by determining the amount of different ions bound and released. All the details and procedures of the experiments are described in Sections 3.4.2 and 3.7.

4.4.3.1 X-ray Energy Dispersive Analysis (EDAX)

The bead samples were first collected from the RIM column for EDAX after the biosorption and desorption processes in the ten sequential cycles. The spectrum in Fig. 4.36 shows the presence of two dominant components, calcium and phosphorus, on the surface of the virgin RIM bead. These calcium and phosphorus peaks may mainly come from the alginate polymers and the cell surface of *Micrococcus luteus*.

Both the peaks were depressed after the fixed-bed biosorption in cycle 1, whereas noticeable copper peaks were displayed in the spectrum (Fig. 4.37 (a)). The conspicuous copper peaks indicate the attachment of copper ions on the bead surface. This suggests that ion exchange between calcium

ions on the virgin bead surface and copper ions in the solution might take place in the biosorption.

After the exposure of the copper-laden biosorbents to the $CaCl_2$ solution in the desorption process of cycle 1, a reverse pattern of the peaks was obtained in the spectrum (Fig. 4.37 (b)). The calcium peak re-appeared, whereas the copper peaks were reduced down to the baseline level. The result indicates that the bound copper ions on the bead surface were replaced by calcium ions in the desorbing agent during the fixed-bed desorption.

Similar patterns of the peaks were obtained in the spectra of cycles 2 to 10 (Figs. 4.38 to 4.46). The copper peaks were enhanced in the spectra of the biosorption and depressed in those of the desorption. All of them were in contrast to the patterns of the calcium peaks. These phenomena supports that the ion exchange could be one of the major mechanisms in the Cu(II) biosorption and desorption of the RIM beads in the column.

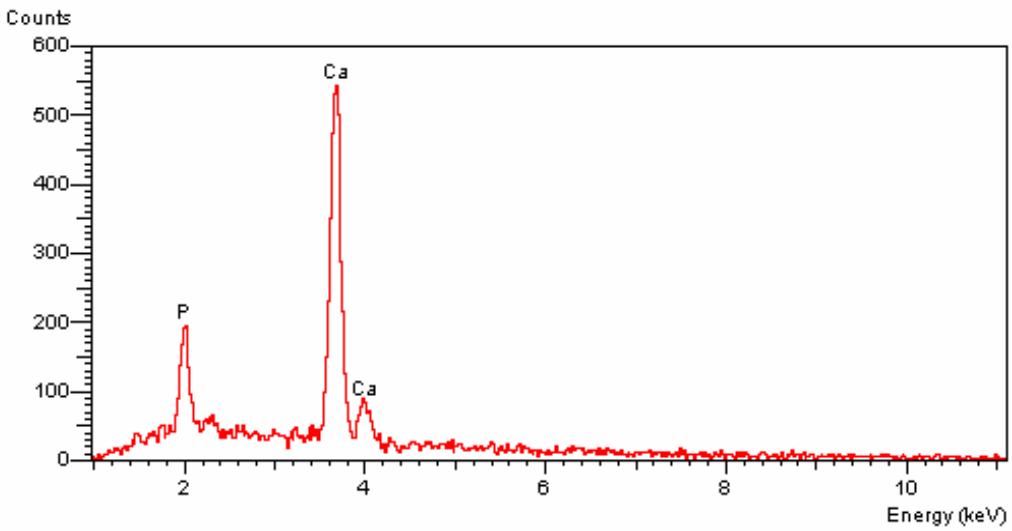

Figure 4.36. Spectrum of X-ray Energy Dispersive Analysis (EDAX) of virgin RIM bead before fixed-bed copper(II) biosorption.

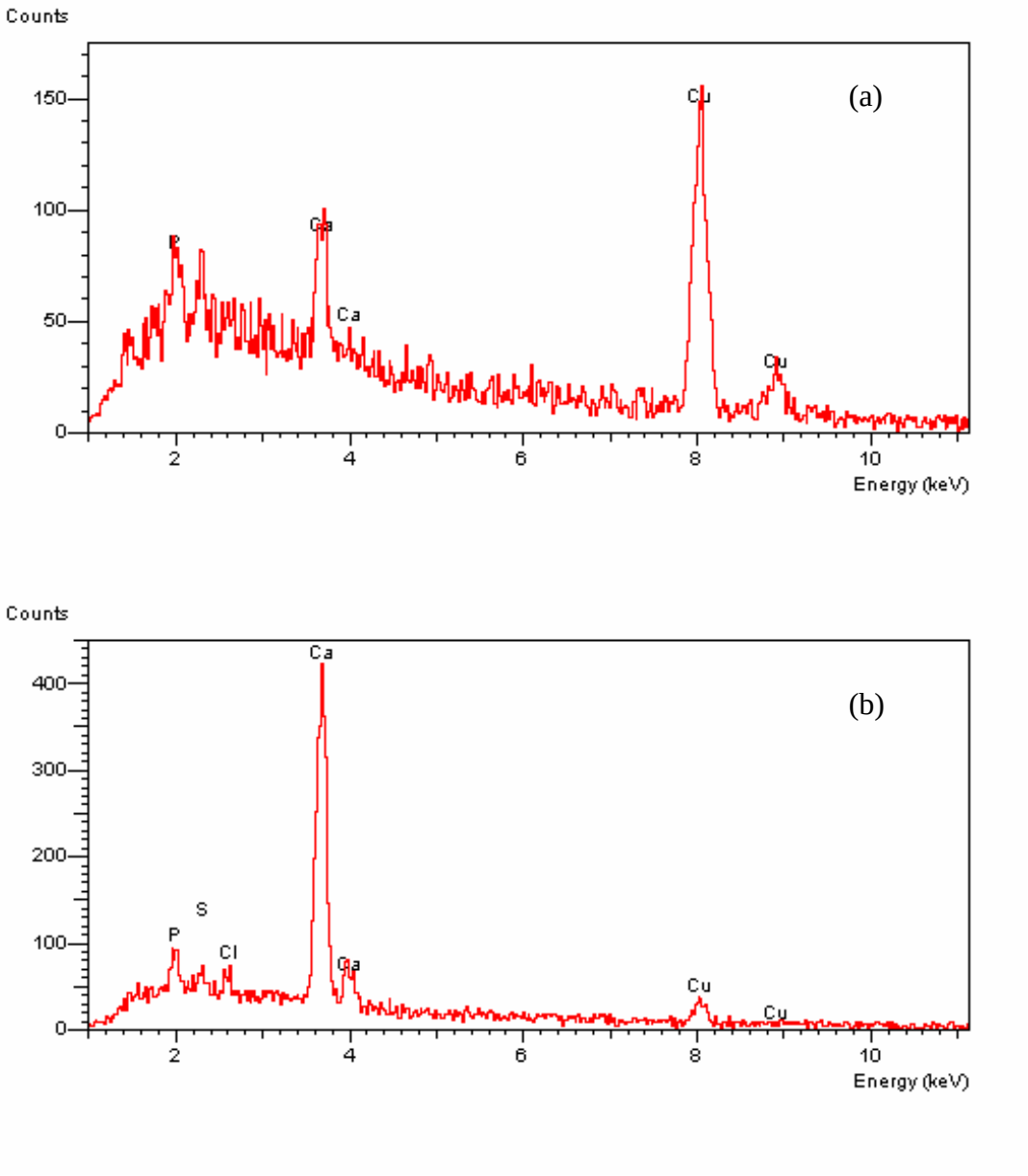

Figure 4.37. Spectra of X-ray Energy Dispersive Analysis (EDAX) of RIM bead in cycle 1: (a) after fixed-bed copper(II) biosorption; (b) after fixed-bed copper(II) desorption.

* Experimental conditions are listed in Table 4.25.

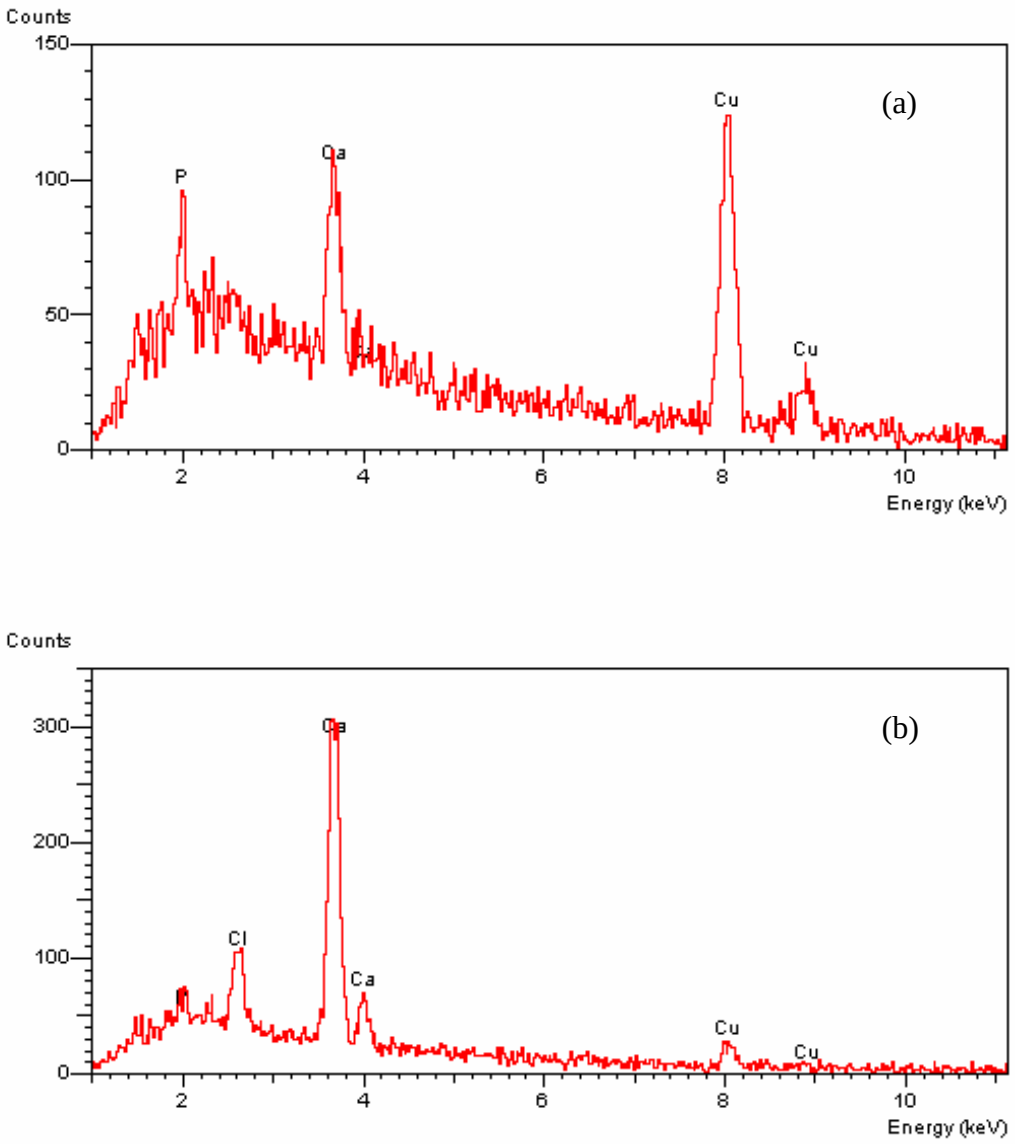

Figure 4.38. Spectra of X-ray Energy Dispersive Analysis (EDAX) of RIM bead in cycle 2: (a) after fixed-bed copper(II) biosorption; (b) after fixed-bed copper(II) desorption.

* Experimental conditions are listed in Table 4.25.

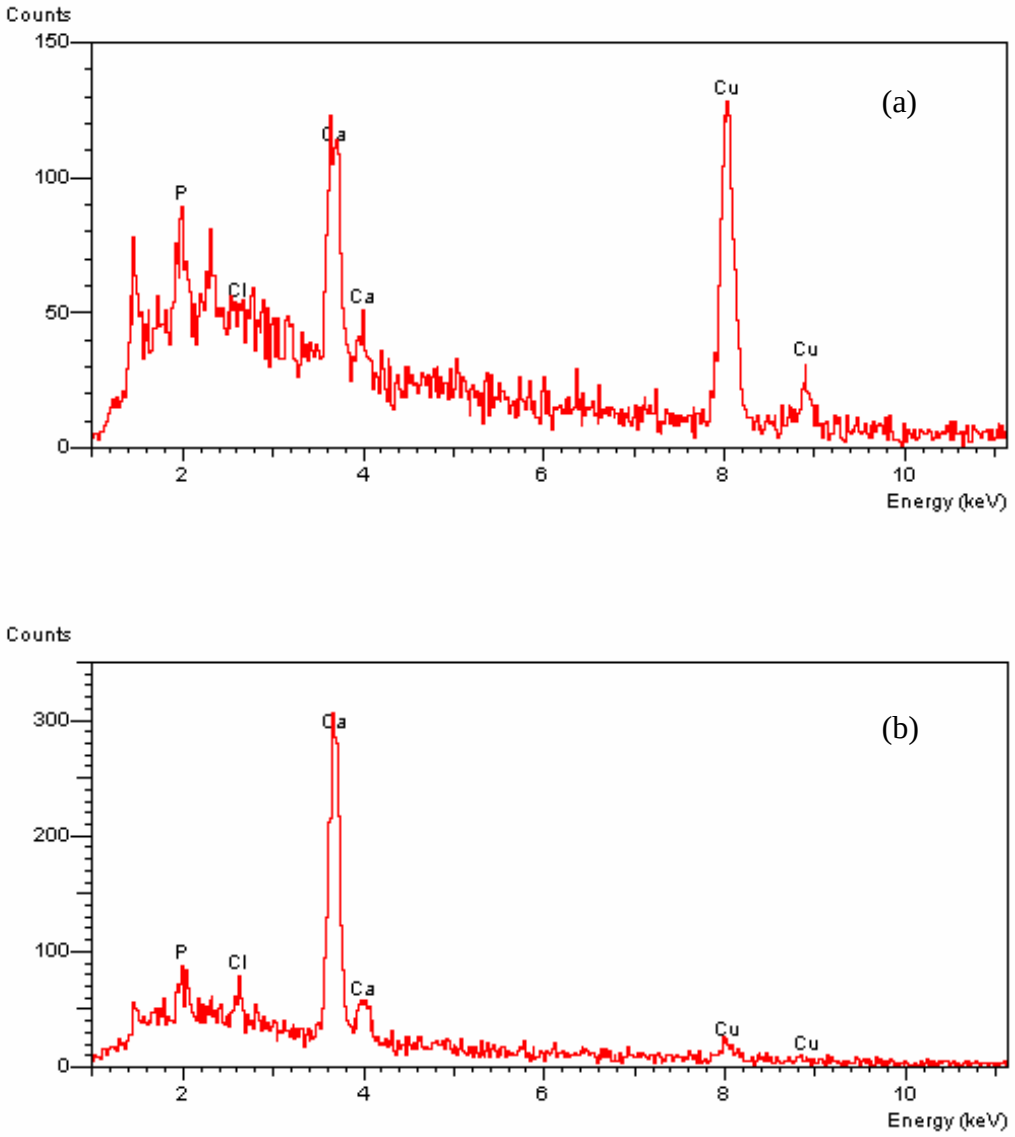

Figure 4.39. Spectra of X-ray Energy Dispersive Analysis (EDAX) of RIM bead in cycle 3: (a) after fixed-bed copper(II) biosorption; (b) after fixed-bed copper(II) desorption.

* Experimental conditions are listed in Table 4.25.

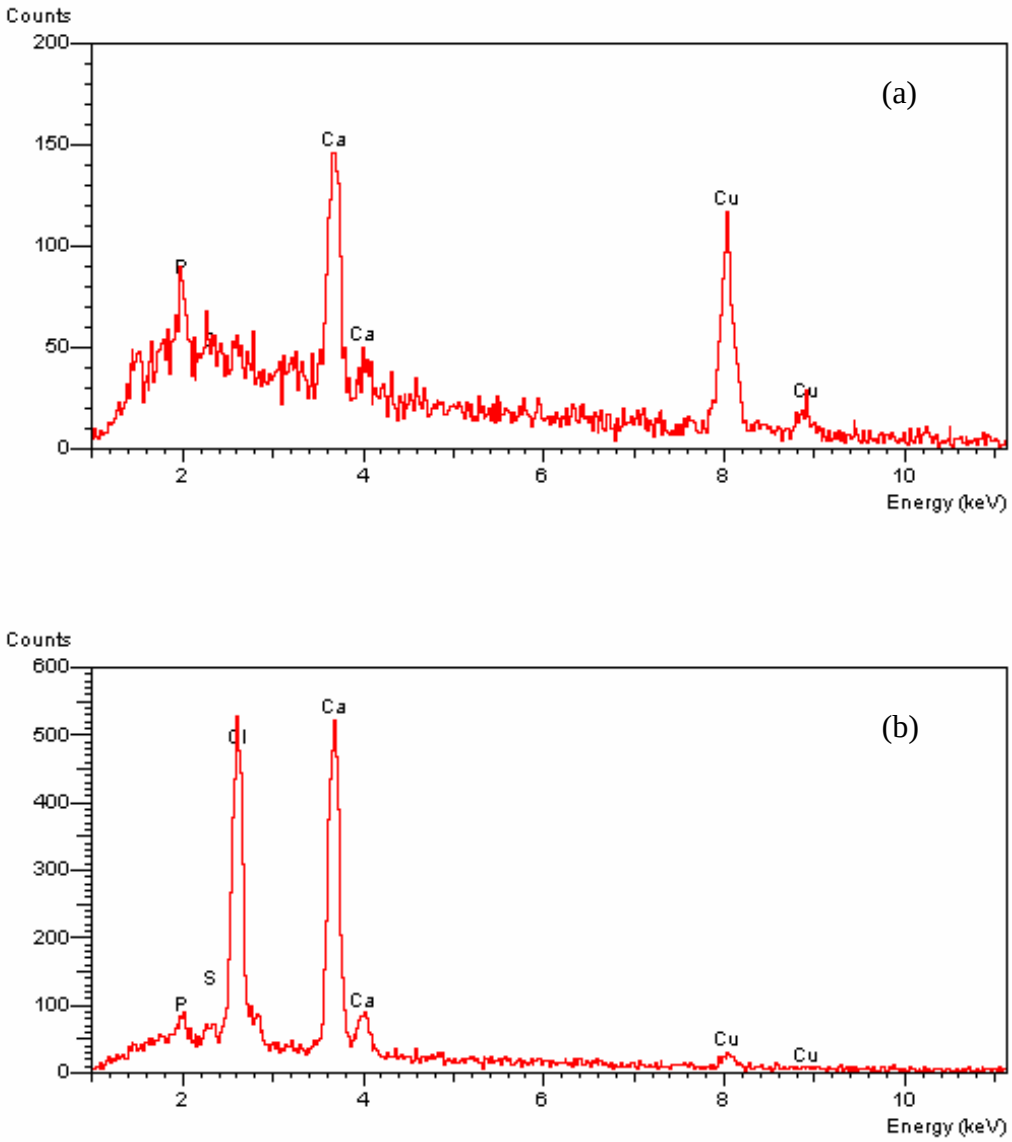

Figure 4.40. Spectra of X-ray Energy Dispersive Analysis (EDAX) of RIM bead in cycle 4: (a) after fixed-bed copper(II) biosorption; (b) after fixed-bed copper(II) desorption.

* Experimental conditions are listed in Table 4.25.

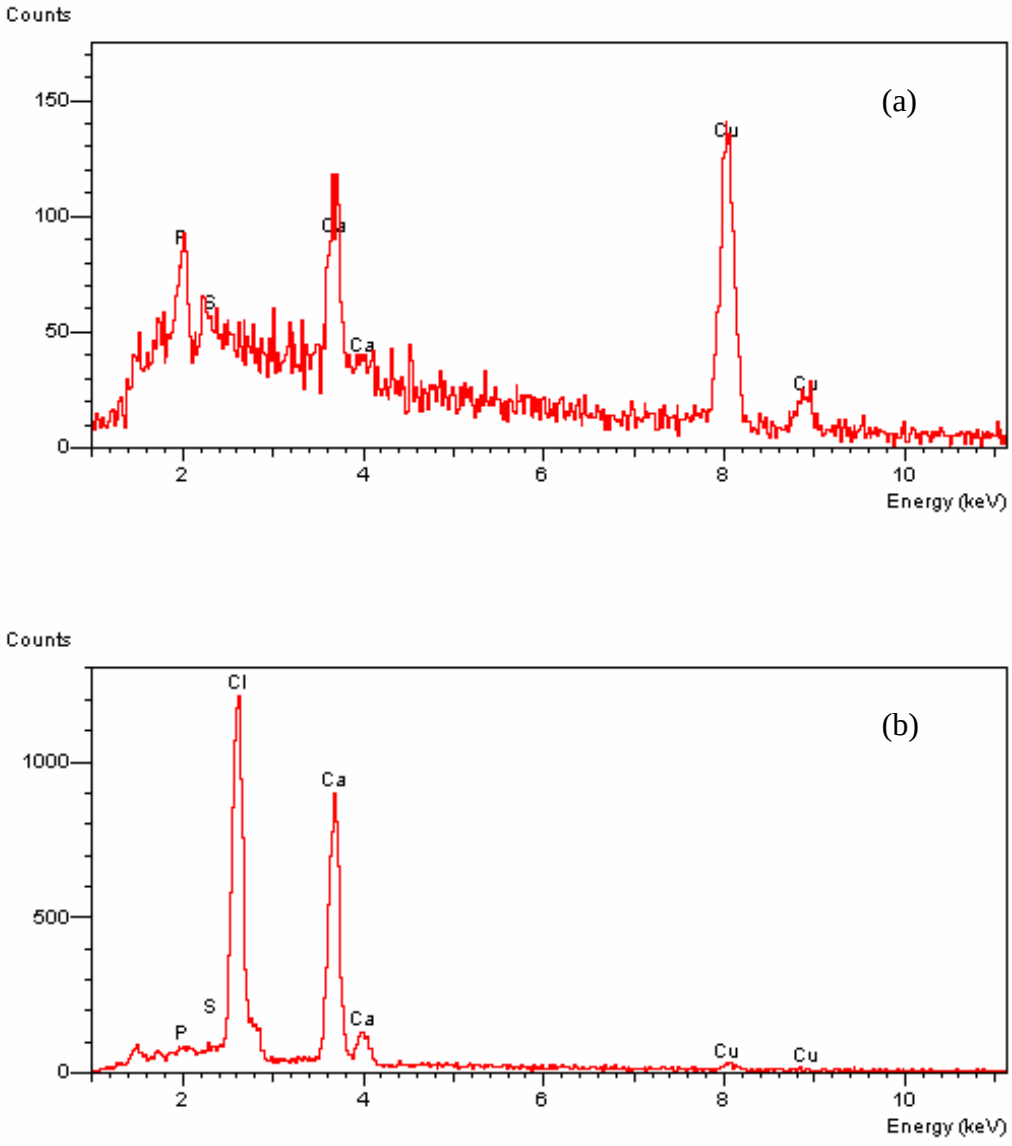

Figure 4.41. Spectra of X-ray Energy Dispersive Analysis (EDAX) of RIM bead in cycle 5: (a) after fixed-bed copper(II) biosorption; (b) after fixed-bed copper(II) desorption.

* Experimental conditions are listed in Table 4.25.

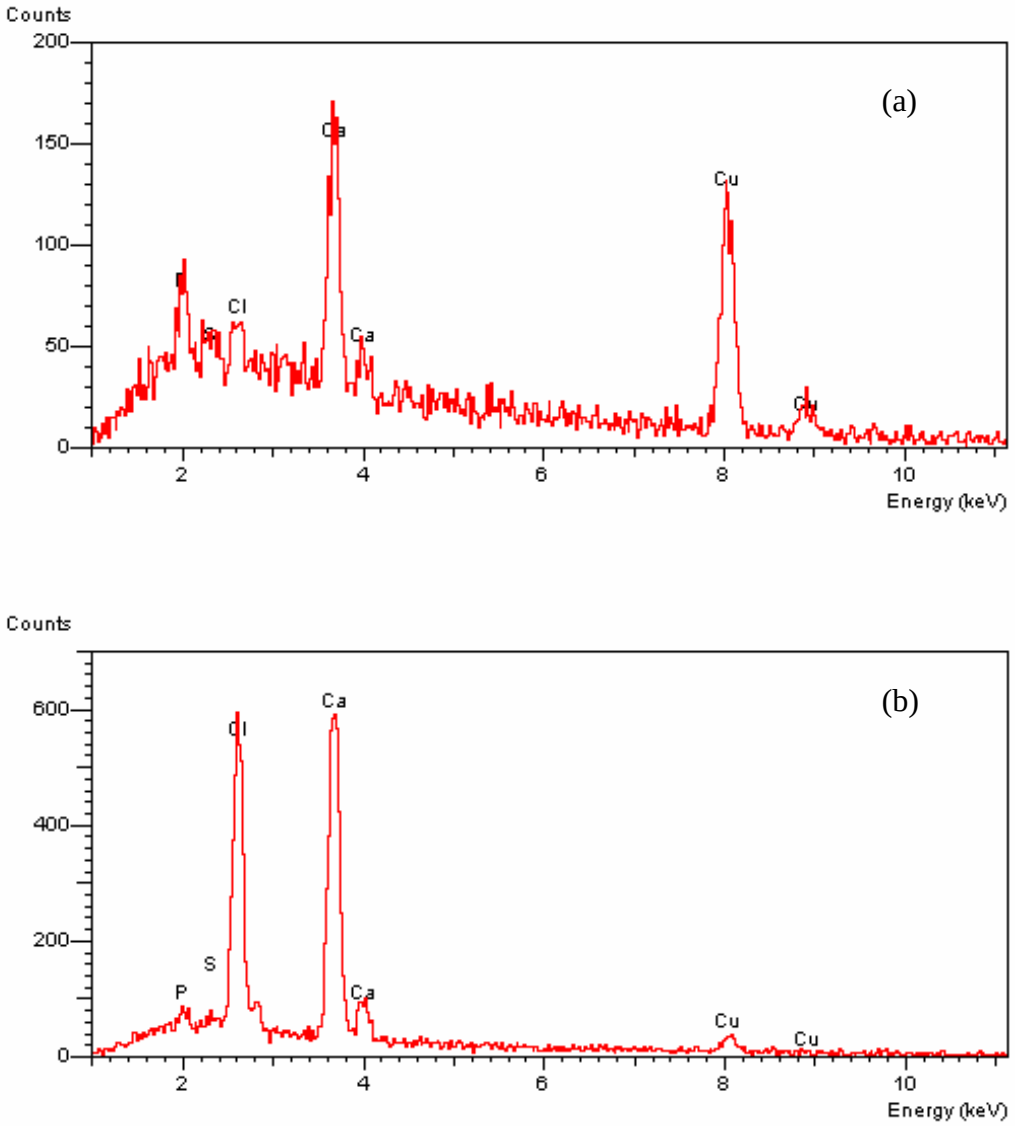

Figure 4.42. Spectra of X-ray Energy Dispersive Analysis (EDAX) of RIM bead in cycle 6: (a) after fixed-bed copper(II) biosorption; (b) after fixed-bed copper(II) desorption.

* Experimental conditions are listed in Table 4.25.

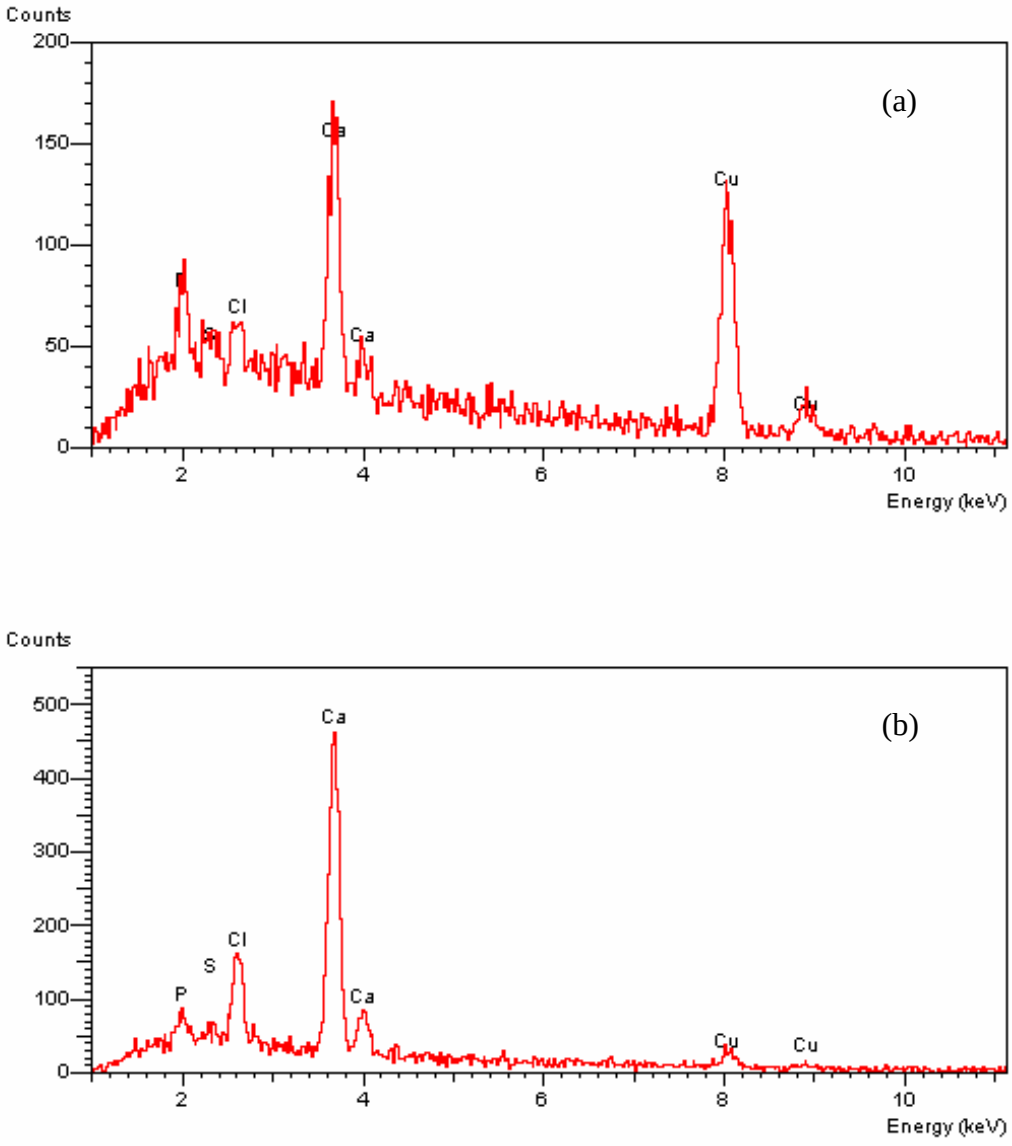

Figure 4.43. Spectra of X-ray Energy Dispersive Analysis (EDAX) of RIM bead in cycle 7: (a) after fixed-bed copper(II) biosorption; (b) after fixed-bed copper(II) desorption.

* Experimental conditions are listed in Table 4.25.

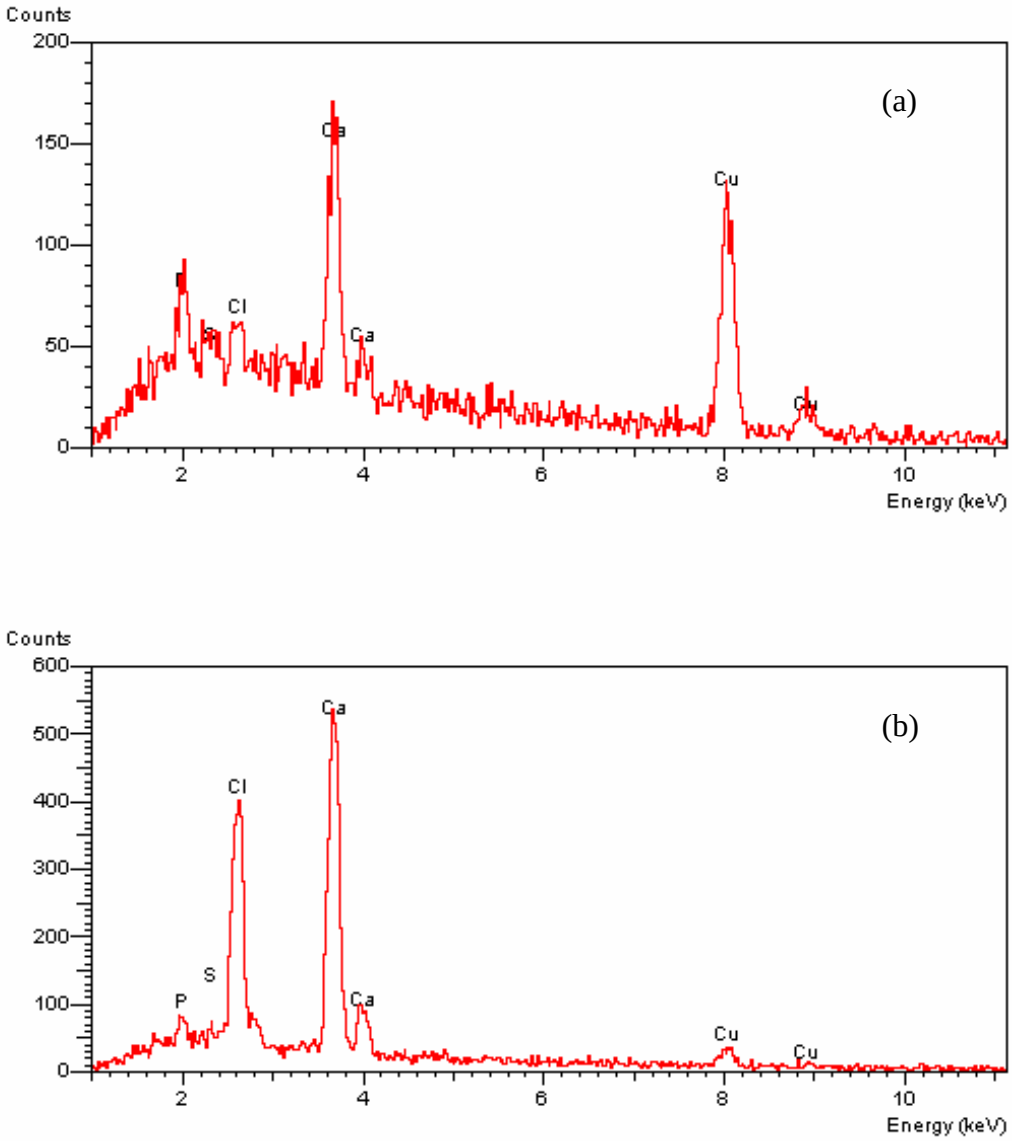

Figure 4.44. Spectra of X-ray Energy Dispersive Analysis (EDAX) of RIM bead in cycle 8: (a) after fixed-bed copper(II) biosorption; (b) after fixed-bed copper(II) desorption.

* Experimental conditions are listed in Table 4.25.

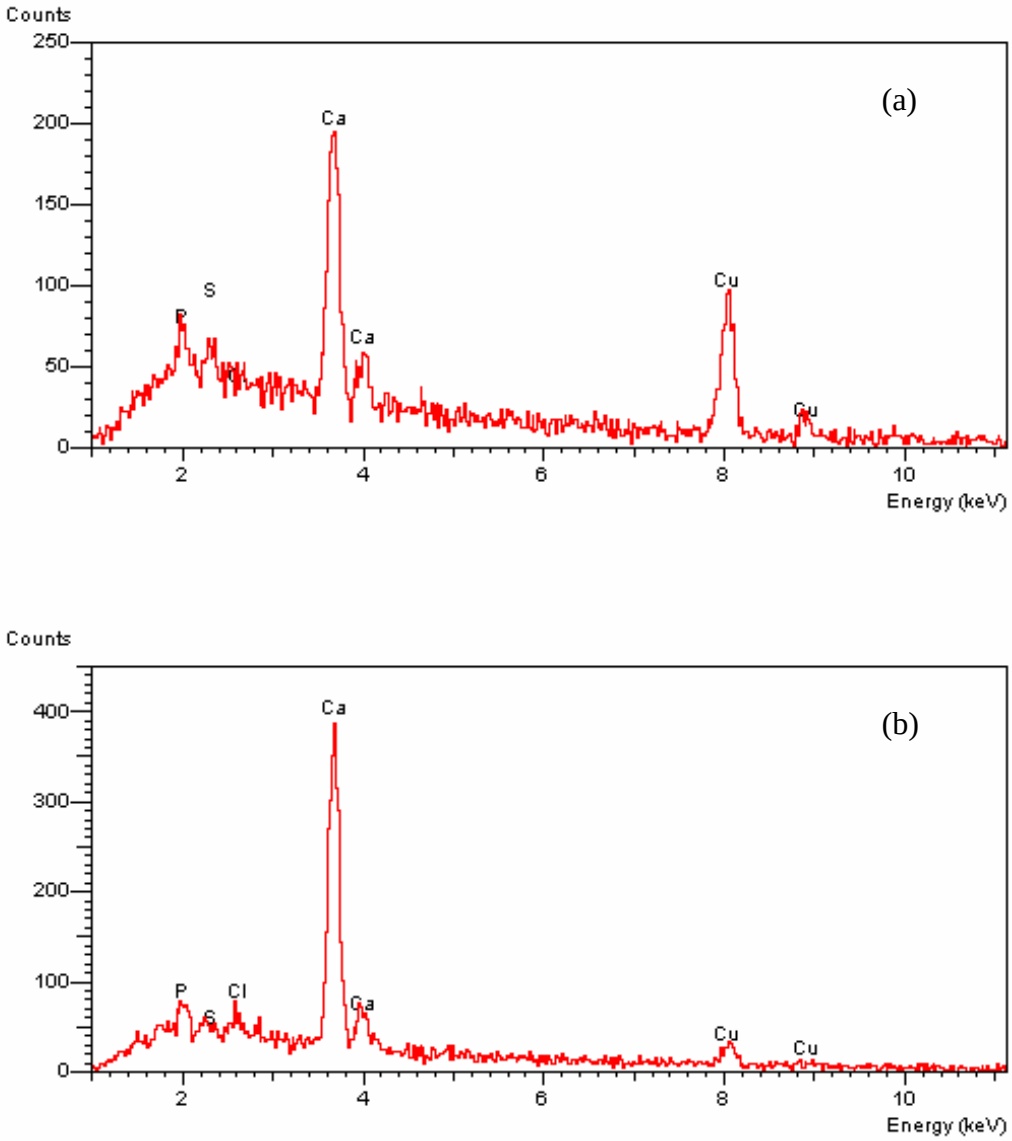

Figure 4.45. Spectra of X-ray Energy Dispersive Analysis (EDAX) of RIM bead in cycle 9: (a) after fixed-bed copper(II) biosorption; (b) after fixed-bed copper(II) desorption.

* Experimental conditions are listed in Table 4.25.

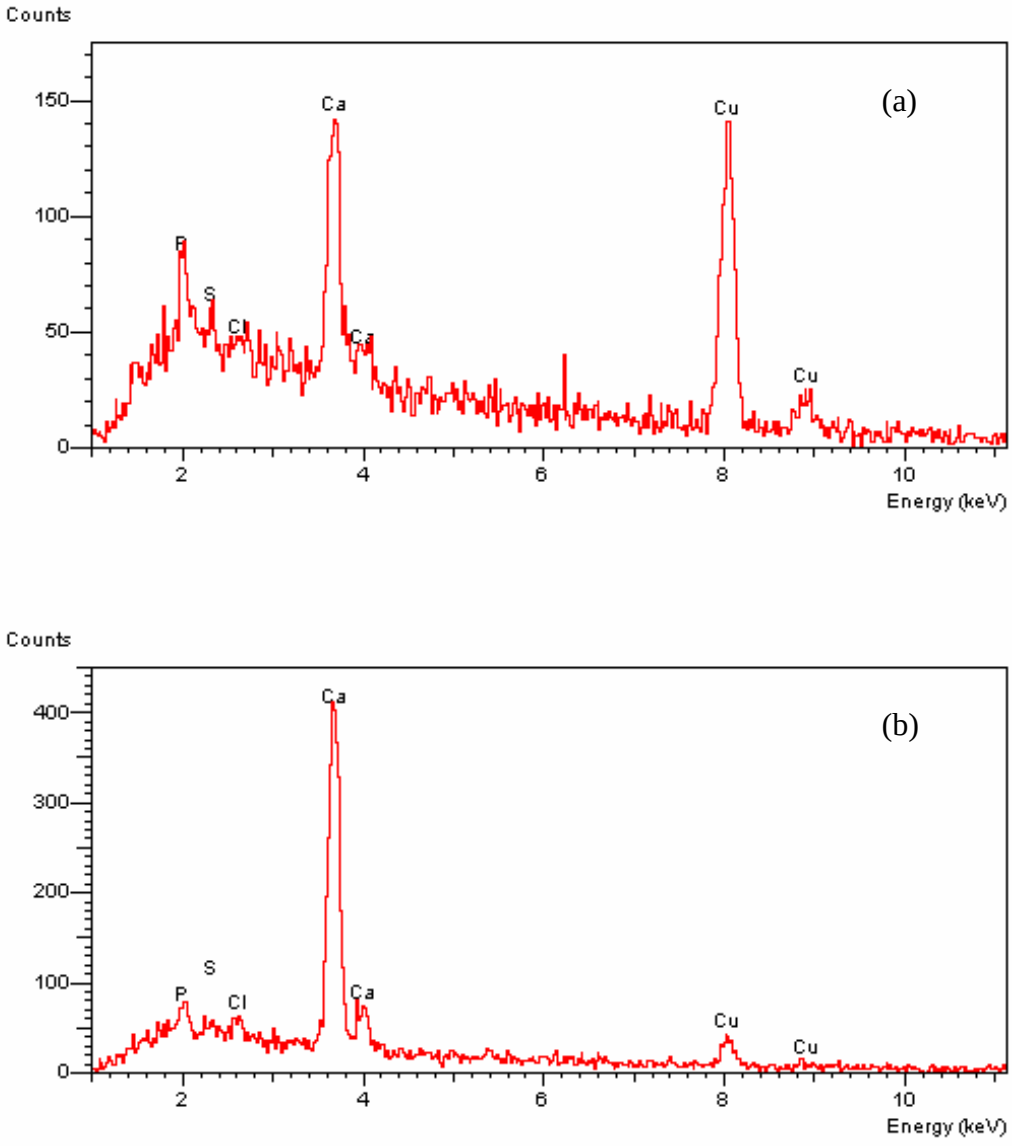

Figure 4.46. Spectra of X-ray Energy Dispersive Analysis (EDAX) of RIM bead in cycle 10: (a) after fixed-bed copper(II) biosorption; (b) after fixed-bed copper(II) desorption.

* Experimental conditions are listed in Table 4.25.

Table 4.25. Experimental conditions of sequential copper(II) biosorption and desorption in RIM column for EDAX.

Biosorption	**Desorption**
– C_o = 50 mg-Cu/L; – Q = 1 mL/min; – Z = 50 cm; – Influent pH = 5.0; – Concentration of *Micrococcus luteus* in the RIM beads = 0.133 g-cell/mL-beads; – The process was conducted up to the breakthrough level = 4 mg-Cu/L.	– C_o = 1 M $CaCl_2$; – Q = 1 mL/min; – The process was continued until 85% of copper content inside the biosorbents was desorbed.

4.4.3.2 Material balance of fixed-bed biosorption

In view of the quantitative study, the material balance of the fixed-bed biosorption processes throughout the ten biosorption/desorption cycles was calculated by considering the copper removal, proton uptake and calcium release. All these data were collected by analyzing the concentrations of these species in the effluent. The results are presented in Table 4.26.

The results demonstrate that calcium ions were released when the biosorption of copper(II) ions and protons was performed in all the ten biosorption/desorption cycles. This suggests that ion exchange is probably associated with biosorption of copper(II) ions by the RIM column. If pure ion exchange occurs, the ratio (R) of the total ion uptake to the total ion release should be in unity. As shown in Table 4.26, the values of R were close to one throughout all the ten cycles. This strongly supports that ion exchange should be the dominant mechanism of copper(II) biosorption by the RIM column.

However, this method was not appropriate to study the desorption mechanism since a high concentration of calcium ions existed in the desorption effluent. A large dilution was required to prepare the effluent samples for any quantitative analysis. A large analytical error would be resulted. The calculated amount of calcium ions adsorbed by the biosorbents would be very inaccurate. Hence, this method was not used in the mechanistic study of the fixed-bed desorption.

Table 4.26. Material balance of fixed-bed biosorption processes in ten sequential biosorption/desorption cycles.

Cycle	Copper removal (a)	Proton uptake (b)	Calcium release (c)	Material balance		R (d)
	(mmol)	(mmol)	(mmol)	Difference (e) (mmol)	% difference (f)	
1	6.11	8.33×10^{-2}	6.85	6.98×10^{-1}	10.19	0.90
2	5.00	6.05×10^{-2}	5.06	3.27×10^{-2}	0.65	0.99
3	3.79	5.07×10^{-2}	4.14	3.24×10^{-1}	7.82	0.92
4	3.05	3.71×10^{-2}	3.42	3.57×10^{-1}	10.45	0.90
5	2.72	3.54×10^{-2}	3.09	3.47×10^{-1}	11.24	0.89
6	2.72	3.16×10^{-2}	3.09	3.47×10^{-1}	11.25	0.89
7	2.78	3.16×10^{-2}	3.10	3.08×10^{-1}	9.91	0.90
8	2.54	2.97×10^{-2}	2.87	3.20×10^{-1}	11.15	0.89
9	2.58	2.25×10^{-2}	2.67	7.97×10^{-2}	2.99	0.97
10	2.50	2.59×10^{-2}	2.24	2.71×10^{-1}	12.10	1.12

- Fixed-bed biosorption conditions: C_o = 50 mg-Cu/L; Q = 1 mL/min; Z = 50 cm; Solution pH = 5.0; [*Micrococcus luteus*] = 0.133 g-cell/mL-beads; The process was conducted up to the breakthrough level (4 mg-Cu/L);
- Fixed-bed desorption conditions: C_o = 1 M $CaCl_2$; Q = 1 mL/min; The process was continued until 85% of copper content inside the biosorbents was desorbed;
- Calculations
  - (d) $R = \frac{[\text{Total ion uptake}]}{[\text{Total ion release}]} = \frac{[(a)+(b)/2]}{(c)}$;
  - (e) Difference = | (c) – (a) – [(b)/2] |;
  - (f) % difference = (d)/(c).

4.5 Simulation of copper(II) biosorption in fixed-bed column

Mathematical simulation using different fixed-bed adsorption models was carried out to describe the behaviours of copper(II) biosorption processes by the RIM column and their breakthrough profiles. The purpose of the model simulation is to give an instantaneous prediction of the process performances without conducting any experiments. This can provide great benefits and convenience in the design of scale-up fixed-bed processes.

Four mathematical models, namely the Clark model, Adams-Bohart model, Yoon and Nelson model and Thomas model, were applied to predict the breakthrough curves and determine the characteristic parameters of the column biosorption. The modeling equations are shown in Section 2.6.5. Except the Clark model, all these models would be expressed in both linearized and non-linearized forms to simulate experimental data with respect to different influent copper(II) concentrations (C_o), flow rates (Q) and bed depths (Z) (obtained from Sections 4.3.1 to 4.3.3). In the case of the Clark model, only the non-linearized simulation would be performed. All the simulated breakthrough profiles and results of the simulations are presented in Figs. 4.47 to 4.67 and Tables 4.27 to 4.38.

The applicability of the models can be evaluated from the fitting curves and the predicted results. The simulated breakthrough curves were appraised by regression coefficients (r^2) and average percentage of errors (ε%), whereas the predicted copper removals (q) and breakthrough time (t_b)

were appraised by variances (v%). A good simulation should possess a high r^2 value (close to 1) as well as low magnitudes of the variance and the average percentage of errors.

4.5.1 Clark model

The Clark model can only be expressed in a non-linearized form (Section 2.6.5.2). Different from the other fixed-bed biosorption models, it includes the Freundlich constant (n) as the critical parameter in the model equation. As shown in Figs. 4.47 to 4.49 and Tables 4.27 to 4.29, the simulations of the Clark model under different conditions of the fixed-bed biosorption could obtain good r^2 values (above 0.98) and accurate predictions of the copper removals (v% below 3). However, the simulations were especially poor at the regions of small C_e/C_o. Large average percentages of errors were found in the range from 14% to 55%. Moreover, the poorest predictions of the breakthrough time were in the cases of the shortest bed depth, the highest influent concentration as well as the fastest inlet flow rate, with the variances up to 72%, 68% and 35%, respectively. Thus, the Clark model was not a very good model for simulating the copper(II) biosorption by the RIM column.

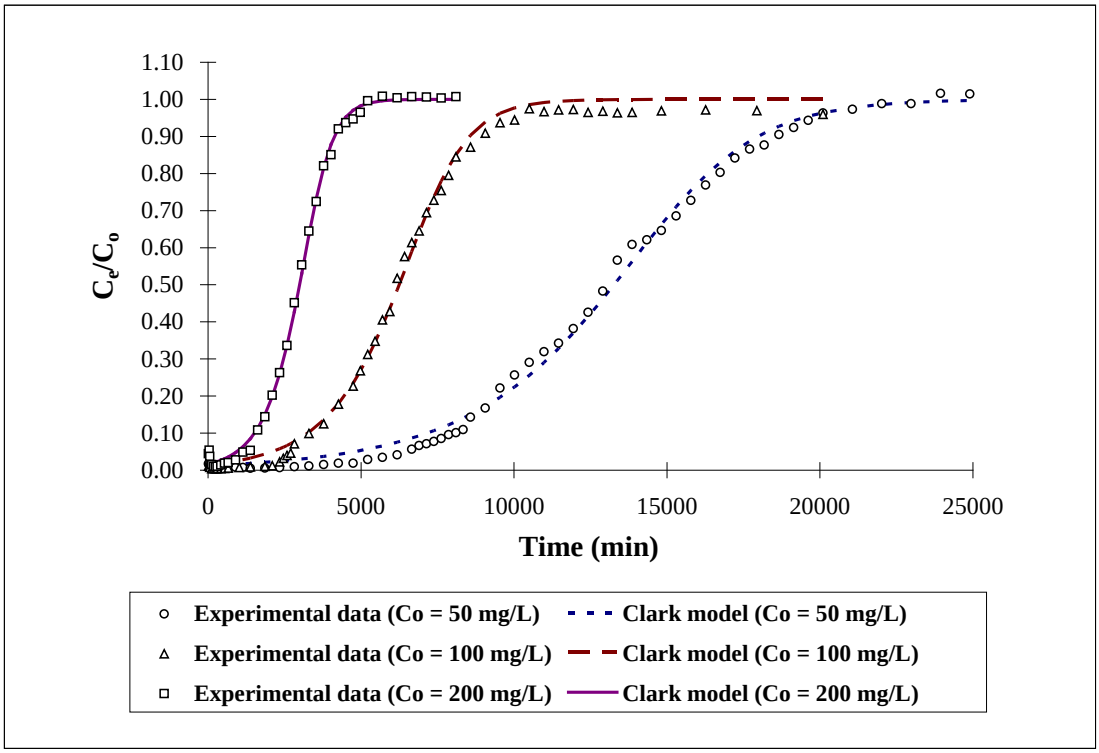

Figure 4.47. Simulation of copper(II) biosorption profiles of RIM columns at different influent copper(II) concentrations by Clark model.

* Experimental conditions are listed in Table 4.27.

Table 4.27. Parameters of Clark model for copper(II) biosorption of RIM columns at different influent copper(II) concentrations.

C_o (mg-Cu/L)		**49.88**	**98.37**	**192.77**
Z (cm)		50	50	50
Q (mL/min)		1	1	1
Volume of beads used (mL)		41.90	41.45	41.43
Freundlich constant "n"		2.79	2.79	2.79
Experimental data				
q	(mg-Cu)	649.77	610.12	561.85
	(mg-Cu/mL-beads)	15.51	14.72	13.56
	t_b (min)	7470	2594	673
Clark model				
q (mg-Cu/mL-beads)		15.31	14.36	13.42
	v%*	1.29	2.45	1.03
t_b (min)		6399	1753	218
	v%*	14.34	32.44	67.55
r^2		0.9965	0.9962	0.9988
ε%#		29.75	35.65	13.73

Calculations:

* Variance (v%) = $\frac{\left|a_{expt} - a_{model}\right|}{a_{expt}} \times 100\,\%$

Average percentage of errors (ε%) = $\frac{\sum_{i=1}^{N}\left|\frac{\left(C_e / C_o\right)_{expt} - \left(C_e / C_o\right)_{model}}{\left(C_e / C_o\right)_{expt}}\right|}{N} \times 100\,\%$

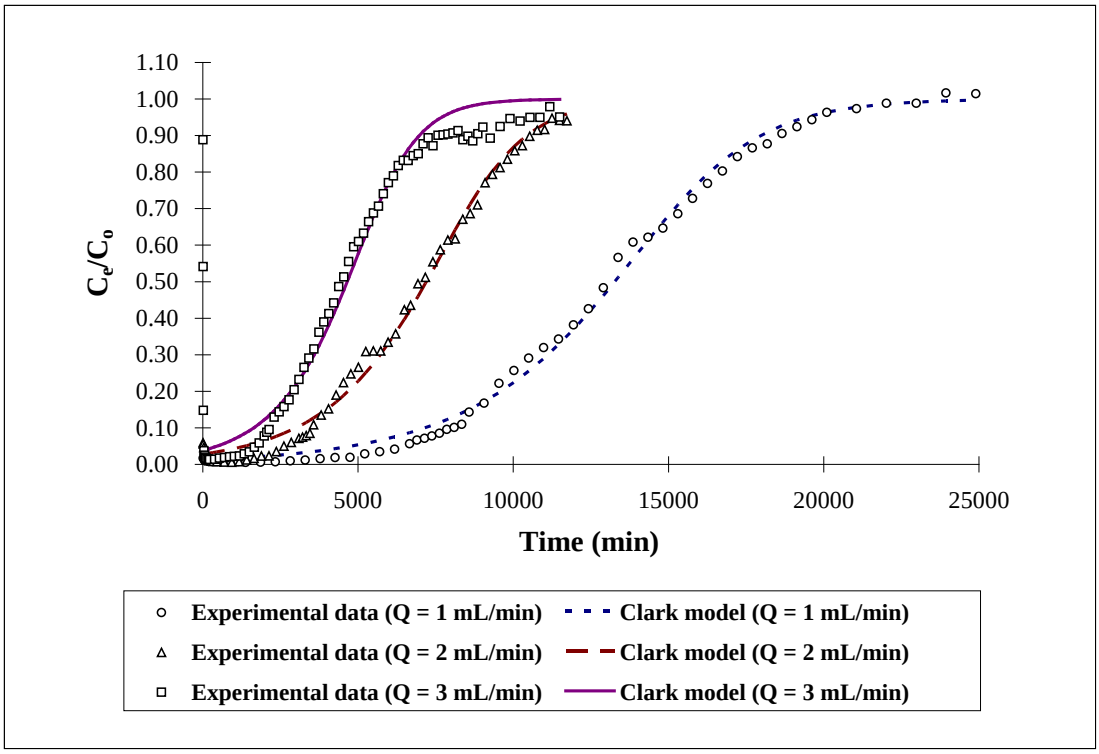

Figure 4.48. Simulation of copper(II) biosorption profiles of RIM columns under different inlet upward flow rates by Clark model.

* Experimental conditions are listed in Table 4.28.

Table 4.28. Parameters of Clark model for copper(II) biosorption of RIM columns under different inlet upward flow rates.

Q (mL/min)		**1**	**2**	**3**
Z (cm)		50	50	50
C_o (mg-Cu/L)		49.88	48.44	48.12
Volume of beads used (mL)		41.90	41.38	42.65
Freundlich constant "n"		2.79	2.79	2.79
Experimental data				
q	(mg-Cu)	649.77	675.34	666.16
	(mg-Cu/mL-beads)	15.51	16.32	15.62
	t_b (min)	7470	3405	2025
Clark model				
q (mg-Cu/mL-beads)		15.31	16.13	15.16
	v%*	1.29	1.16	2.94
t_b (min)		6399	2546	1323
	v%*	14.34	25.21	34.64
r^2		0.9965	0.9937	0.9875
ε%#		29.75	55.05	33.32

Calculations:

* Variance (v%) = $\frac{\left|a_{expt} - a_{model}\right|}{a_{expt}} \times 100\,\%$

Average percentage of errors (ε%) = $\frac{\sum_{i=1}^{N} \left| \frac{(C_e / C_o)_{expt} - (C_e / C_o)_{model}}{(C_e / C_o)_{expt}} \right|}{N} \times 100\,\%$

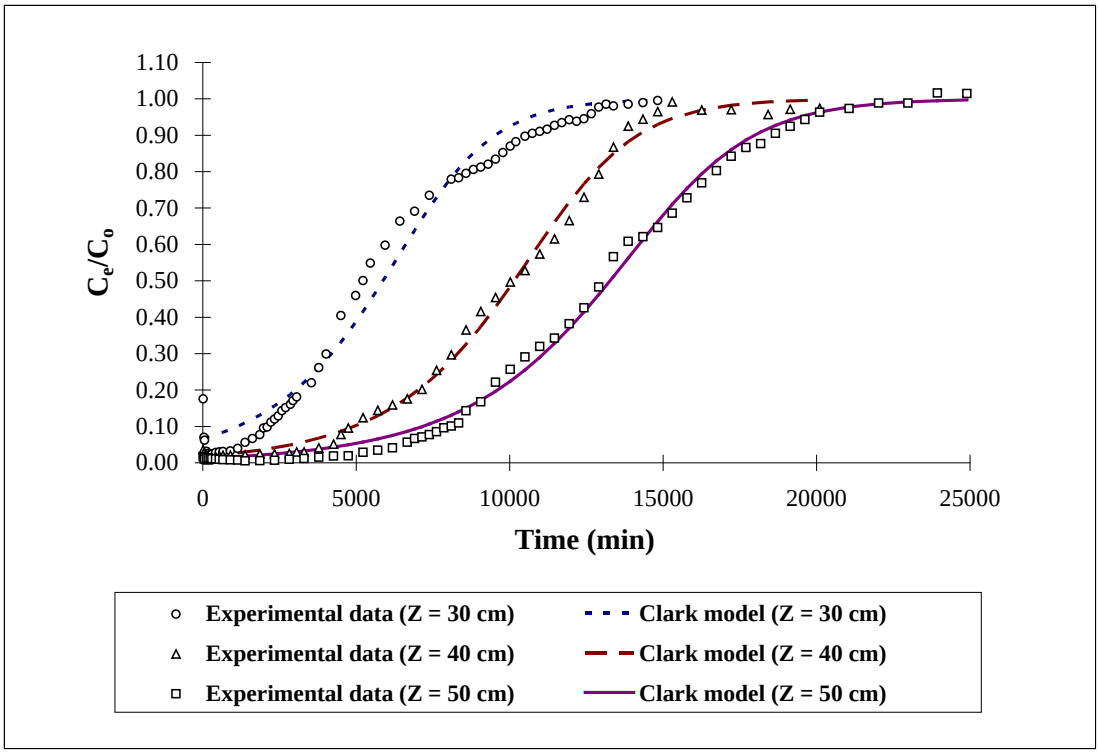

Figure 4.49. Simulation of copper(II) biosorption profiles of RIM columns with different column bed depths by Clark model.

* Experimental conditions are listed in Table 4.29.

Table 4.29. Parameters of Clark model for copper(II) biosorption of RIM columns with different column bed depths.

Z (cm)		**30**	**40**	**50**
C_o (mg-Cu/L)		49.93	49.42	49.88
Q (mL/min)		1	1	1
Volume of beads used (mL)		20.15	33.23	41.90
Freundlich constant "n"		2.79	2.79	2.79
Experimental data				
q	(mg-Cu)	283.82	481.51	649.77
	(mg-Cu/mL-beads)	14.09	14.49	15.15
t_b (min)		1878	4539	7470
Clark model				
q (mg-Cu/mL-beads)		14.10	14.49	15.31
	v%*	0.07	0.00	1.06
t_b (min)		532	4309	6399
	v%*	71.66	5.07	14.34
r^2		0.9837	0.9960	0.9965
ε%#		21.87	17.51	29.75

Calculations:

* Variance (v%) = $\frac{\left|a_{expt} - a_{model}\right|}{a_{expt}} \times 100\,\%$

Average percentage of errors (ε%) = $\frac{\sum_{i=1}^{N} \left| \frac{(C_e / C_o)_{expt} - (C_e / C_o)_{model}}{(C_e / C_o)_{expt}} \right|}{N} \times 100\,\%$

4.5.2 Adams-Bohart model

Similar to other modeling studies (Aksu and Gönen, 2004; Malkoc *et al.*, 2006; Preetha and Viruthagiri, 2007), Figs. 4.50 to 4.55 show that the Adams-Bohart model could only well describe the initial part of the breakthrough curves. The range of the simulations and the predicted results are summarized in Tables 4.30 to 4.32. Both the linearized and non-linearized simulations could obtain desirable r^2 values (above 0.93) and also well predict the copper removals and the breakthrough time (v% below 19), as presented in Tables 4.30 to 4.32. However, relatively-large average percentages of errors (ε%) were found in most of the simulations using both the linearized and non-linearized models. The average percentages of errors (ε%) were always above 15% in the linearized fittings. In the cases of the non-linearized simulations, the ε% value was up to 44% at the condition of C_o = 100 mg-Cu/L. These results degraded the reliability of the Adams-Bohart model. Thus, such model was not preferable in the simulations of copper(II) biosorption by the RIM column.

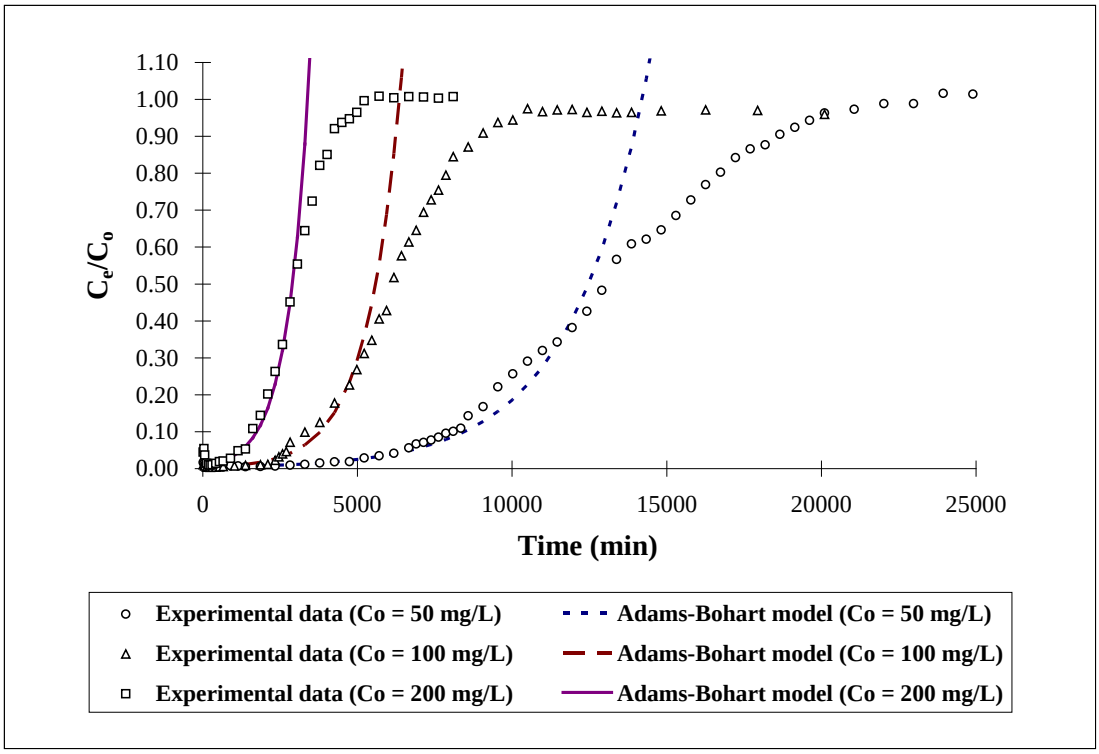

Figure 4.50. Simulation of copper(II) biosorption profiles of RIM columns at different influent copper(II) concentrations by linearized Adams-Bohart model.

* Experimental conditions are listed in Table 4.30.

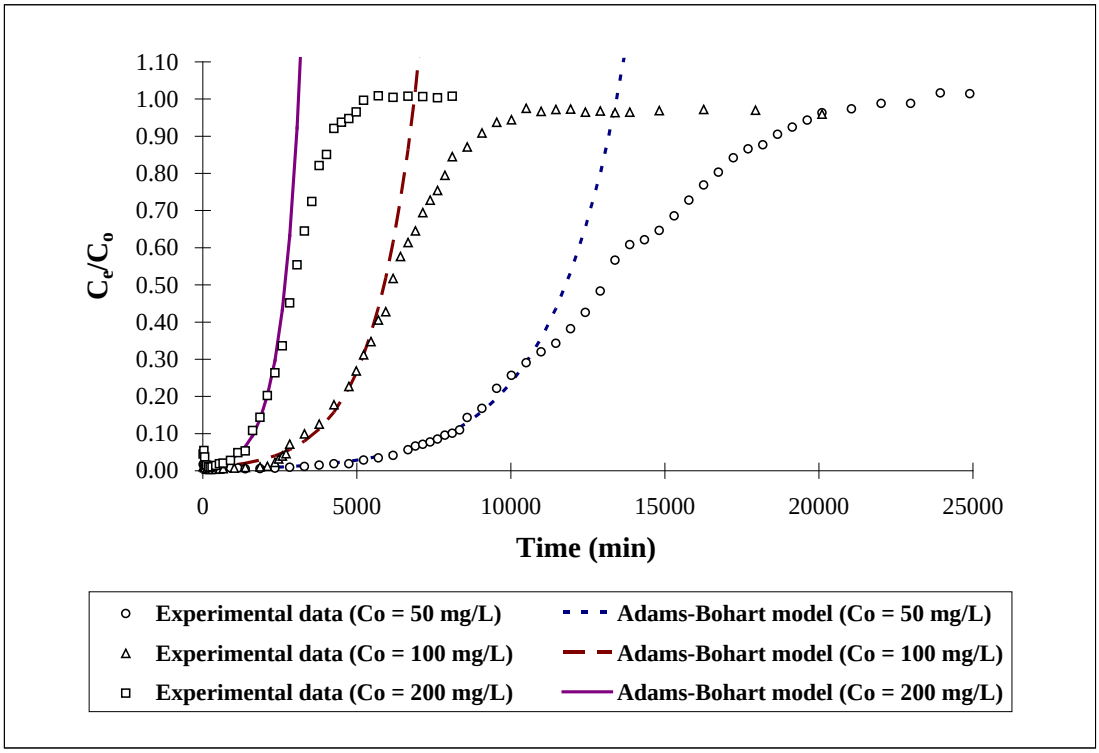

Figure 4.51. Simulation of copper(II) biosorption profiles of RIM columns at different influent copper(II) concentrations by non-linearized Adams-Bohart model.

* Experimental conditions are listed in Table 4.30.

Table 4.30. Parameters of Adams-Bohart model for copper(II) biosorption of RIM columns at different influent copper(II) concentrations.

C_o (mg-Cu/L)		**49.88**	**98.37**	**192.77**
Z (cm)		50	50	50
Q (mL/min)		1	1	1
Volume of beads used (mL)		41.90	41.45	41.43
U_o (cm/min)		1.09	1.09	1.09
Experimental data				
q	(mg-Cu)	649.77	610.12	561.85
	(mg-Cu/mL-beads)	15.51	14.72	13.56
t_b (min)		7470	2594	673
Adams-Bohart model (Linearized form)				
Modeling range (min)		13860	6420	3540
q (mg-Cu/mL-beads)		15.46	13.64	14.27
	v%*	0.32	7.34	5.24
t_b (min)		7897	2797	624
	v%*	5.72	7.83	7.28
k_{AB} (L/mg-Cu · min)		8.02×10^{-6}	9.15×10^{-6}	7.26×10^{-6}
r^2		0.9830	0.9733	0.9819
ε%#		20.73	18.94	13.51
Adams-Bohart model (Non-linearized form)				
Modeling range (min)		8580	5460	2100
q (mg-Cu/mL-beads)		14.62	14.74	13.09
	v%*	5.73	0.12	3.49
t_b (min)		7440	2349	653
	v%*	0.40	9.44	2.97
k_{AB} (L/mg-Cu · min)		8.44×10^{-6}	7.21×10^{-6}	8.18×10^{-6}
r^2		0.9812	0.9842	0.9877
ε%#		18.56	44.37	15.32

Calculations:

* Variance (v%) = $\dfrac{\left|a_{expt} - a_{model}\right|}{a_{expt}} \times 100\,\%$

Average percentage of errors (ε%) = $\dfrac{\sum_{i=1}^{N}\left|\dfrac{\left(C_e / C_o\right)_{expt} - \left(C_e / C_o\right)_{model}}{\left(C_e / C_o\right)_{expt}}\right|}{N} \times 100\,\%$

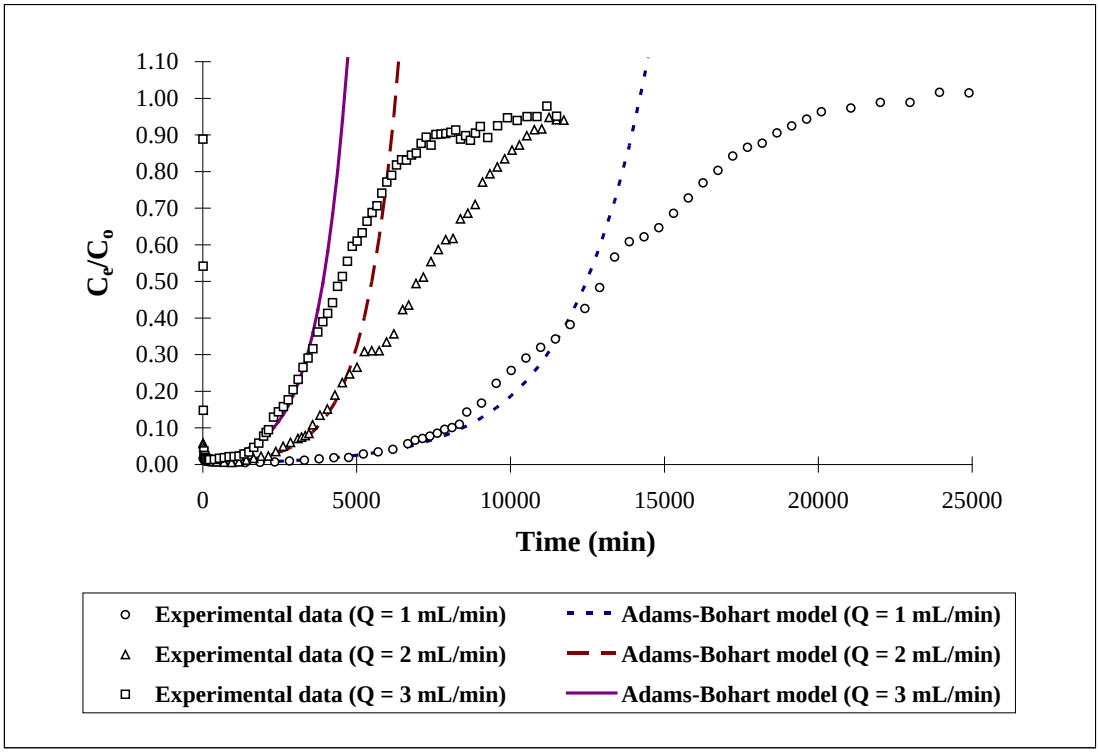

Figure 4.52. Simulation of copper(II) biosorption profiles of RIM columns under different inlet upward flow rates by linearized Adams-Bohart model.

* Experimental conditions are listed in Table 4.31.

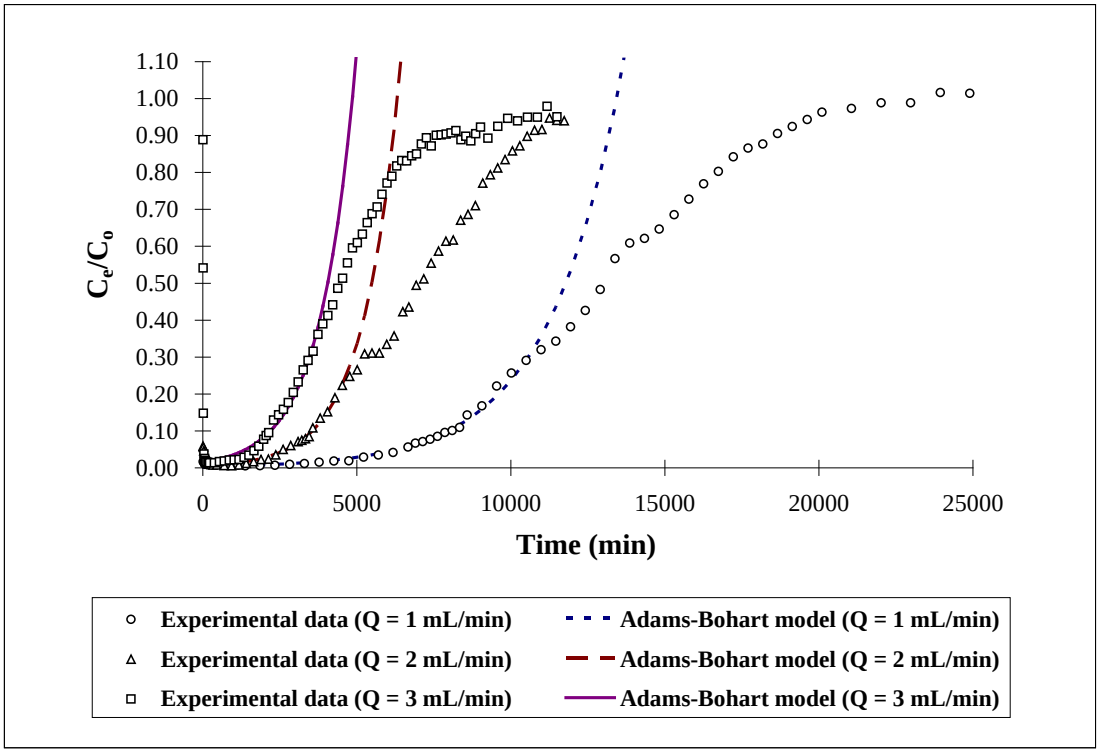

Figure 4.53. Simulation of copper(II) biosorption profiles of RIM columns under different inlet upward flow rates by non-linearized Adams-Bohart model.

* Experimental conditions are listed in Table 4.31.

Table 4.31. Parameters of Adams-Bohart model for copper(II) biosorption of RIM columns under different inlet upward flow rates.

Q (mL/min)		**1**	**2**	**3**
Z (cm)		50	50	50
C_o (mg-Cu/L)		49.88	48.44	48.12
Volume of beads used (mL)		41.90	41.38	42.65
U_o (cm/min)		1.09	2.18	3.27
Experimental data				
q	(mg-Cu)	649.77	675.34	666.16
	(mg-Cu/mL-beads)	15.51	16.32	15.62
t_b (min)		7470	3405	2025
Adams-Bohart model (Linearized form)				
Modeling range (min)		13860	5250	4380
q (mg-Cu/mL-beads)		15.46	13.24	14.50
	v%*	0.32	18.87	7.17
t_b (min)		7897	3491	2114
	v%*	5.72	2.54	4.40
k_{AB} (L/mg-Cu · min)		8.02×10^{-6}	1.86×10^{-5}	2.08×10^{-5}
r^2		0.9830	0.9760	0.9753
ε%#		20.73	16.69	12.85
Adams-Bohart model (Non-linearized form)				
Modeling range (min)		8580	4530	3740
q (mg-Cu/mL-beads)		14.62	13.35	15.30
	v%*	5.73	18.22	2.08
t_b (min)		7440	3326	1980
	v%*	0.40	2.31	2.22
k_{AB} (L/mg-Cu · min)		8.44×10^{-6}	1.72×10^{-5}	1.80×10^{-5}
r^2		0.9812	0.9924	0.9849
ε%#		18.56	17.44	21.76

Calculations:

* Variance (v%) = $\dfrac{\left|a_{expt} - a_{model}\right|}{a_{expt}} \times 100\,\%$

Average percentage of errors (ε%) = $\dfrac{\sum_{i=1}^{N}\left|\dfrac{\left(C_e/C_o\right)_{expt} - \left(C_e/C_o\right)_{model}}{\left(C_e/C_o\right)_{expt}}\right|}{N} \times 100\,\%$

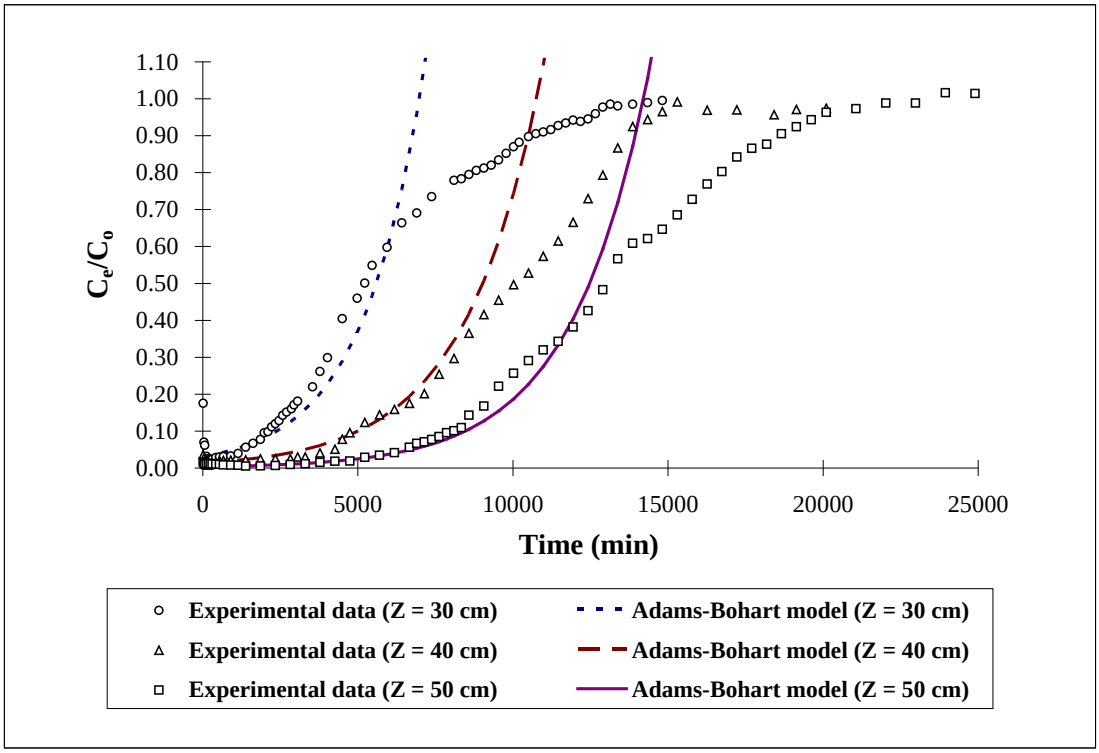

Figure 4.54. Simulation of copper(II) biosorption profiles of RIM columns with different column bed depths by linearized Adams-Bohart model.

* Experimental conditions are listed in Table 4.32.

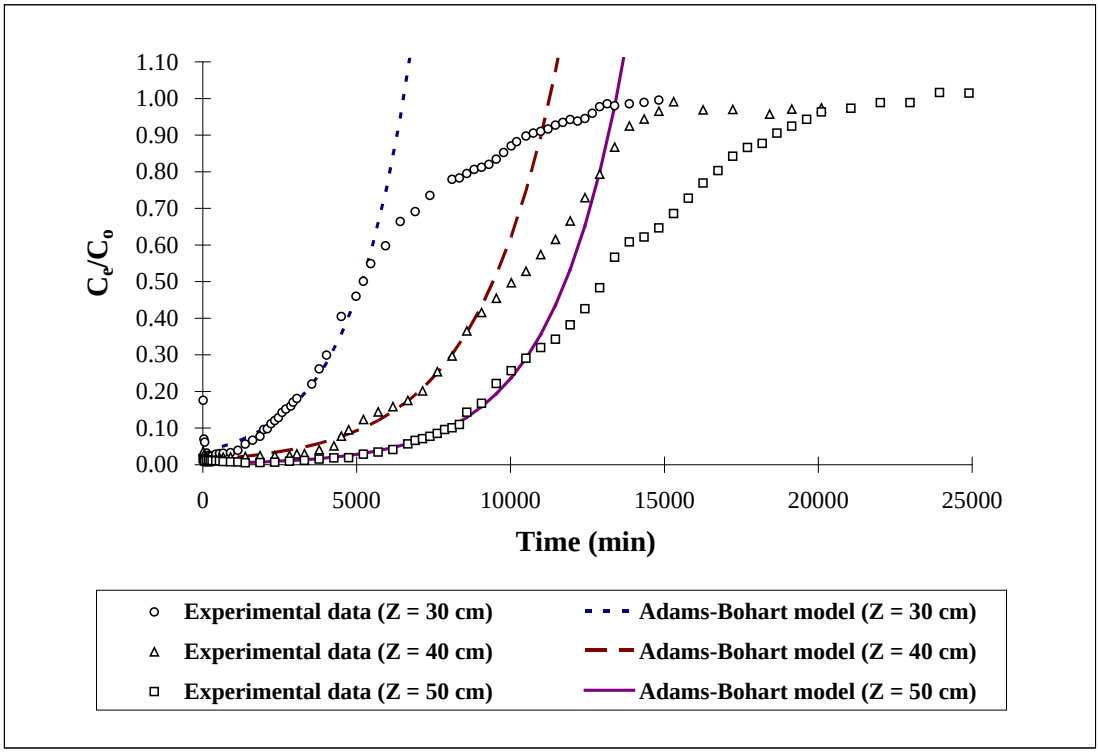

Figure 4.55. Simulation of copper(II) biosorption profiles of RIM columns with different column bed depths by non-linearized Adams-Bohart model.

* Experimental conditions are listed in Table 4.32.

Table 4.32. Parameters of Adams-Bohart model for copper(II) biosorption of RIM columns with different column bed depths.

Z (cm)		**30**	**40**	**50**
C_o (mg-Cu/L)		49.93	49.42	49.88
Q (mL/min)		1	1	1
Volume of beads used (mL)		20.15	33.23	41.90
U_o (cm/min)		1.09	1.09	1.09
Experimental data				
q	(mg-Cu)	283.82	481.51	649.77
	(mg-Cu/mL-beads)	14.09	14.49	15.51
t_b (min)		1878	4539	7470
Adams-Bohart model (Linearized form)				
Modeling range (min)		8100	11460	13860
q (mg-Cu/mL-beads)		12.68	14.51	15.46
	v%*	10.01	0.14	0.32
t_b (min)		1935	4476	7897
	v%*	3.04	1.38	5.72
k_{AB} (L/mg-Cu · min)		1.00×10^{-5}	8.09×10^{-6}	8.02×10^{-6}
r^2		0.9309	0.9705	0.9830
ε%#		19.18	23.40	20.73
Adams-Bohart model (Non-linearized form)				
Modeling range (min)		5460	9060	8580
q (mg-Cu/mL-beads)		11.85	15.19	14.62
	v%*	15.87	4.84	5.73
t_b (min)		1576	4639	7440
	v%*	16.08	2.21	0.40
k_{AB} (L/mg-Cu · min)		1.02×10^{-5}	7.67×10^{-6}	8.44×10^{-6}
r^2		0.9874	0.9910	0.9812
ε%#		18.60	20.48	18.56

Calculations:

* Variance (v%) = $\dfrac{\left|a_{expt} - a_{model}\right|}{a_{expt}} \times 100\,\%$

Average percentage of errors (ε%) = $\dfrac{\sum_{i=1}^{N}\left|\dfrac{\left(C_e / C_o\right)_{expt} - \left(C_e / C_o\right)_{model}}{\left(C_e / C_o\right)_{expt}}\right|}{N} \times 100\,\%$

4.5.3 Yoon and Nelson model

Based on the principle of the gas adsorption kinetics, Yoon and Nelson (1984) developed a mathematical model for describing the entire breakthrough profiles. It demonstrated a good agreement with the experimental results. As shown in Figs. 4.56 to 4.61 and Tables 4.33 to 4.35, both the linearized and non-linearized forms of the Yoon and Nelson model could successfully describe the whole breakthrough profiles of the biosorption using the RIM columns under different influent concentrations, flow rates and bed depths. All the r^2 values could achieve above 0.96. Also, accurate predictions of the copper removals (q) and the 50% bed exhaustion time (τ) were obtained. The variances (v%) of both the 'q' and 'τ' were almost less than 18%, except the slightly large variance of the time 'τ' (up to 28%) found in the case of Z = 30 cm. However, some outlying predictions of the breakthrough time (variances up to 41%) and large average percentages of errors (up to 31%) were found in the non-linearized simulations, whereas the variances of the breakthrough time and the average percentages of errors in the linearized model simulations were always below 5% and 17%, respectively. Thus, the linearized Yoon and Nelson model was probably applied in the simulation of copper(II) biosorption by the RIM column.

As discussed in Section 2.6.5.4, Yoon and Nelson (1984) indicated that the constant k_{YN} should be directly proportional to the influent concentration (C_o) and the flow rate (Q), but inversely proportional to the mass of sorbents (X). The sorbent mass can be further correlated with the bed depth (Z)

since more sorbents are required to construct a longer biosorbent bed. The relationship between the constant k_{YN} and the fixed-bed parameters can then be presented as below:

$$k_{YN} = k' \frac{C_o Q}{X} \approx k'' \frac{C_o Q}{Z} \qquad \text{(Equation 4.18)}$$

In view of the constants k_{YN} obtained from the linearized simulations, the trends with respect to the influent concentrations and the flow rates conformed considerately to the prediction of Equation 4.18. Larger constants k_{YN} were exhibited at the higher copper(II) concentrations and the faster flow rates (Tables 4.33 to 4.34). However, the constants were almost the same under different bed depths (Table 4.35). This deviated from the prediction of Equation 4.18 and thus demoted the reliability of the model.

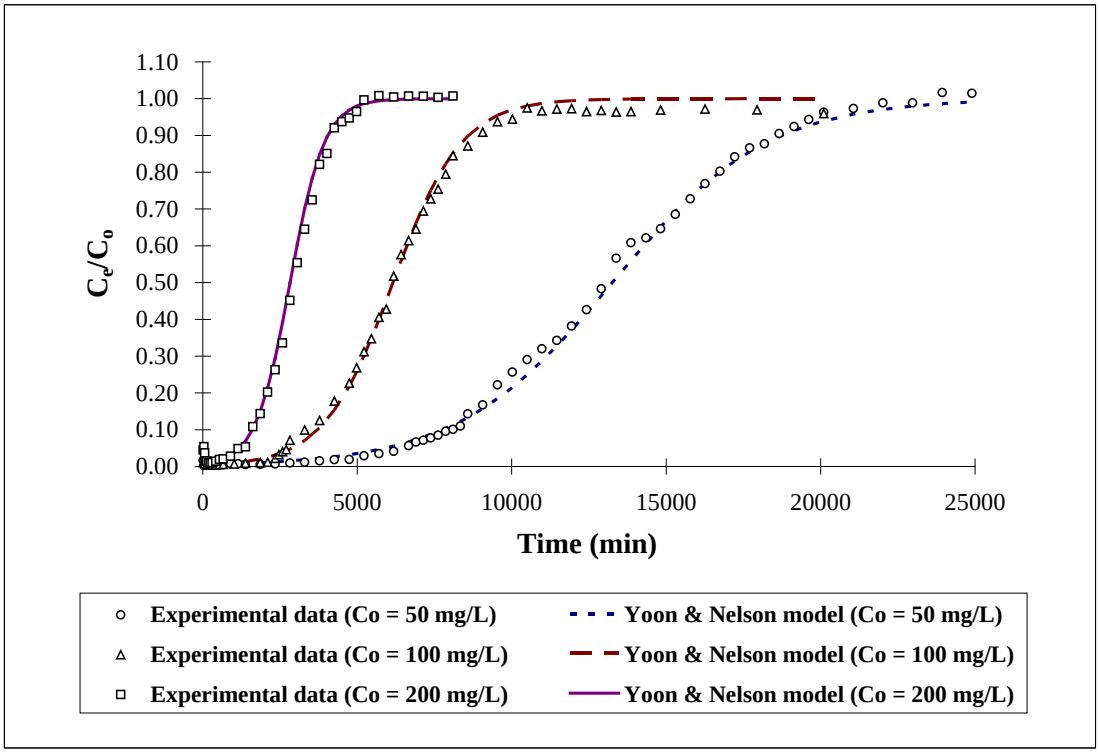

Figure 4.56. Simulation of copper(II) biosorption profiles of RIM columns at different influent copper(II) concentrations by linearized Yoon and Nelson model.

* Experimental conditions are listed in Table 4.33.

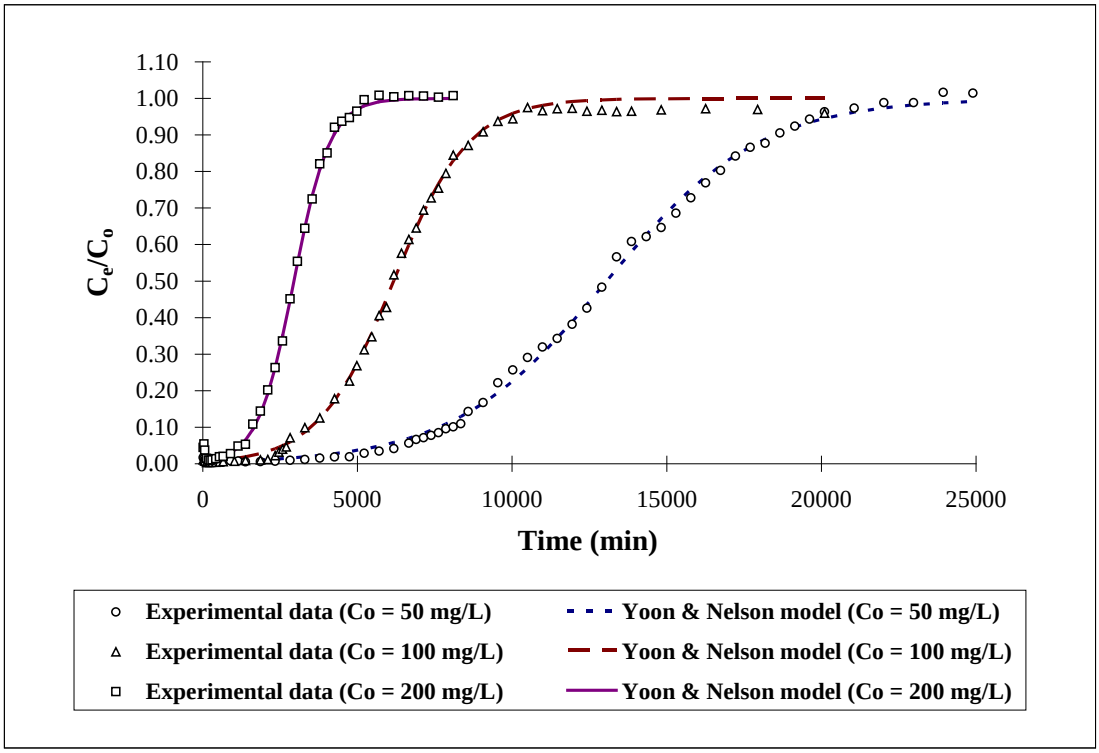

Figure 4.57. Simulation of copper(II) biosorption profiles of RIM columns at different influent copper(II) concentrations by non-linearized Yoon and Nelson model.

* Experimental conditions are listed in Table 4.33.

Table 4.33. Parameters of Yoon and Nelson model for copper(II) biosorption of RIM columns at different influent copper(II) concentrations.

C_o (mg-Cu/L)		**49.88**	**98.37**	**192.77**
Z (cm)		50	50	50
Q (mL/min)		1	1	1
Volume of beads used (mL)		41.90	41.45	41.43
Experimental data				
q	(mg-Cu)	649.77	610.12	561.85
	(mg-Cu/mL-beads)	15.51	14.72	13.56
τ (min)		12997	6133	2934
t_b (min)		7470	2594	673
Yoon and Nelson model (Linearized form)				
q (mg-Cu/mL-beads)		15.73	14.58	13.07
	v%*	1.42	0.95	3.61
τ (min)		13259	6157	2825
	v%*	2.01	0.39	3.72
t_b (min)		7140	2652	684
	v%*	4.42	2.24	1.63
k_{YN} (min^{-1})		4.00×10^{-4}	9.00×10^{-4}	1.80×10^{-3}
r^2		0.9825	0.9858	0.9856
$\varepsilon\%^{\#}$		12.59	8.42	7.54
Yoon and Nelson model (Non-linearized form)				
q (mg-Cu/mL-beads)		15.49	14.62	13.61
	v%*	0.13	0.68	0.37
τ (min)		13057	6174	2944
	v%*	0.46	0.66	0.35
t_b (min)		7020	2329	684
	v%*	6.02	10.22	1.63
k_{YN} (min^{-1})		4.05×10^{-4}	8.22×10^{-4}	1.70×10^{-3}
r^2		0.9985	0.9981	0.9995
$\varepsilon\%^{\#}$		13.17	13.30	4.82

Calculations:

* Variance (v%) = $\dfrac{\left|a_{expt} - a_{model}\right|}{a_{expt}} \times 100\,\%$

\# Average percentage of errors ($\varepsilon\%$) = $\dfrac{\sum_{i=1}^{N}\left|\dfrac{(C_e/C_o)_{expt} - (C_e/C_o)_{model}}{(C_e/C_o)_{expt}}\right|}{N} \times 100\,\%$

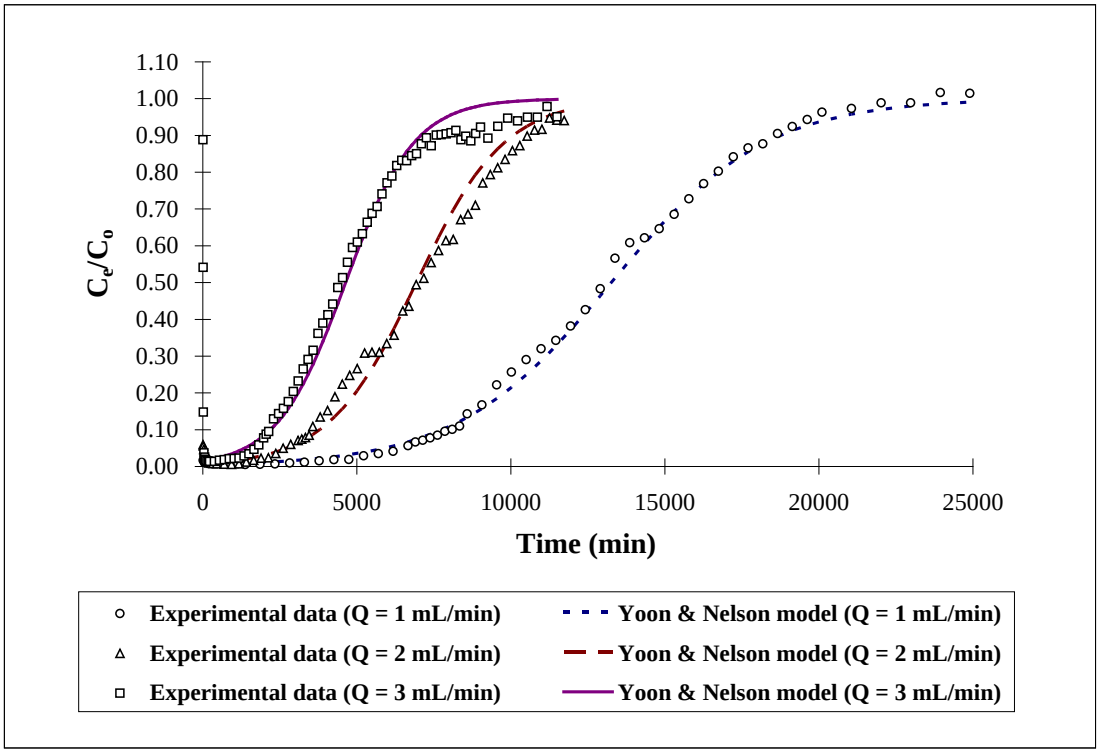

Figure 4.58. Simulation of copper(II) biosorption profiles of RIM columns under different inlet upward flow rates by linearized Yoon and Nelson model.

* Experimental conditions are listed in Table 4.34.

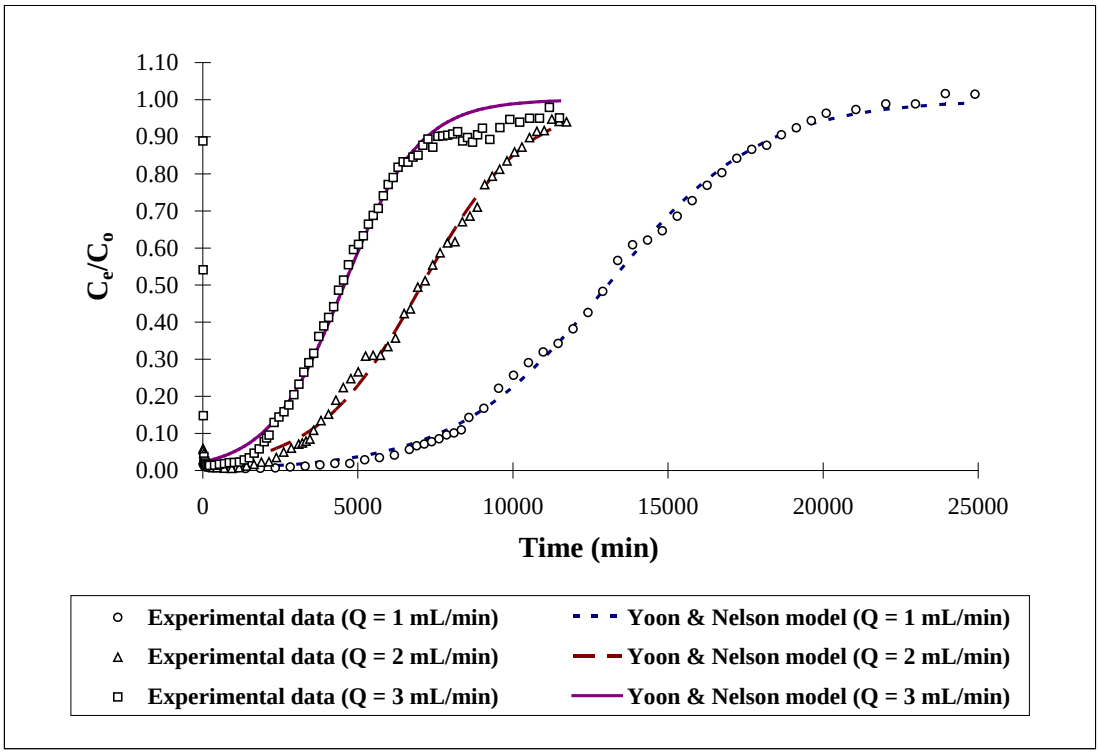

Figure 4.59. Simulation of copper(II) biosorption profiles of RIM columns under different inlet upward flow rates by non-linearized Yoon and Nelson model.

* Experimental conditions are listed in Table 4.34.

Table 4.34. Parameters of Yoon and Nelson model for copper(II) biosorption of RIM columns under different inlet upward flow rates.

Q (mL/min)		**1**	**2**	**3**
Z (cm)		50	50	50
C_o (mg-Cu/L)		49.88	48.44	48.12
Volume of beads used (mL)		41.90	41.38	42.65
Experimental data				
q	(mg-Cu)	649.77	675.34	666.16
	(mg-Cu/mL-beads)	15.51	16.32	15.62
	τ (min)	12997	7006	4461
	t_b (min)	7470	3405	2025
Yoon and Nelson model (Linearized form)				
q (mg-Cu/mL-beads)		15.73	16.09	15.63
	v%*	1.42	1.41	0.07
τ (min)		13529	6936	4636
	v%*	4.09	1.01	3.92
t_b (min)		7140	3501	1962
	v%*	4.42	2.85	3.10
k_{YN} (min^{-1})		4.00×10^{-4}	7.00×10^{-4}	9.00×10^{-4}
r^2		0.9825	0.9813	0.9755
ε%#		12.59	16.56	11.85
Yoon and Nelson model (Non-linearized form)				
q (mg-Cu/mL-beads)		15.49	16.25	15.36
	v%*	0.13	0.43	1.66
τ (min)		13057	7061	4560
	v%*	0.46	0.78	2.21
t_b (min)		7027	2981	1644
	v%*	5.93	12.44	18.81
k_{YN} (min^{-1})		4.05×10^{-4}	5.89×10^{-4}	8.25×10^{-4}
r^2		0.9985	0.9967	0.9948
ε%#		13.17	30.54	18.63

Calculations:

* Variance (v%) = $\dfrac{\left|a_{expt} - a_{model}\right|}{a_{expt}} \times 100\,\%$

Average percentage of errors (ε%) = $\dfrac{\sum_{i=1}^{N}\left|\dfrac{(C_e/C_o)_{expt} - (C_e/C_o)_{model}}{(C_e/C_o)_{expt}}\right|}{N} \times 100\,\%$

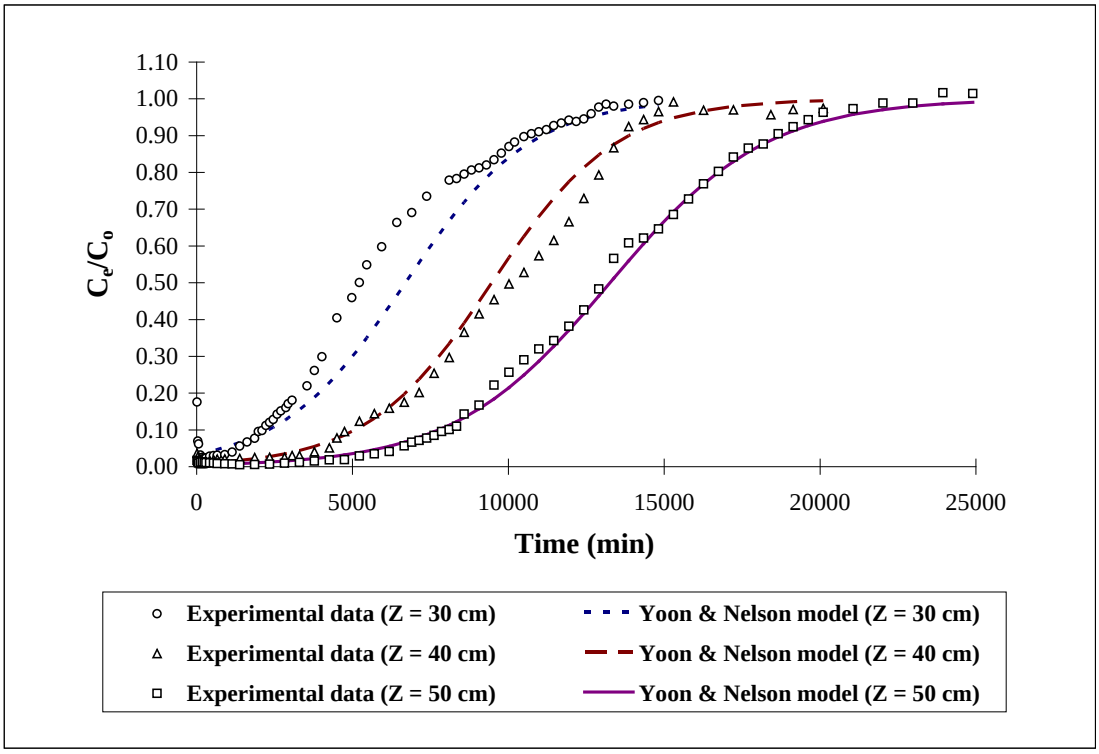

Figure 4.60. Simulation of copper(II) biosorption profiles of RIM columns with different column bed depths by linearized Yoon and Nelson model.

* Experimental conditions are listed in Table 4.35.

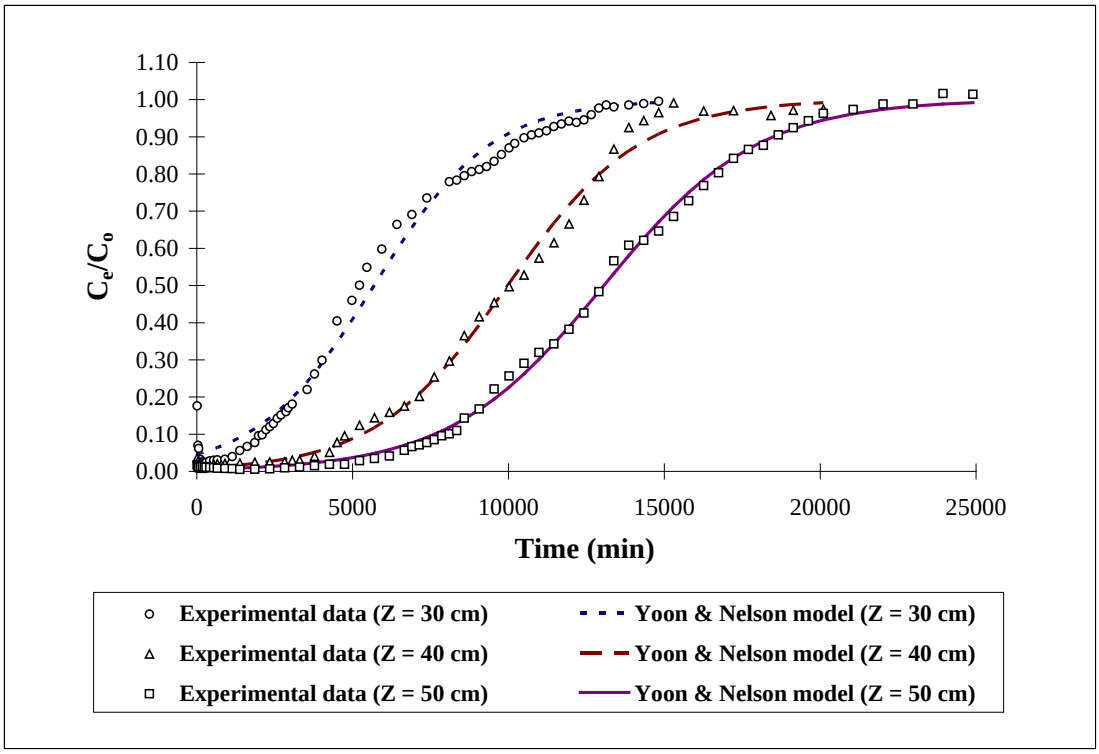

Figure 4.61. Simulation of copper(II) biosorption profiles of RIM columns with different column bed depths by non-linearized Yoon and Nelson model.

* Experimental conditions are listed in Table 4.35.

Table 4.35. Parameters of Yoon and Nelson model for copper(II) biosorption of RIM columns with different column bed depths.

Z (cm)		**30**	**40**	**50**
C_o (mg-Cu/L)		49.93	49.42	49.88
Q (mL/min)		1	1	1
Volume of beads used (mL)		20.15	33.23	41.90
Experimental data				
q	(mg-Cu)	283.82	481.51	649.77
	(mg-Cu/mL-beads)	14.09	14.49	15.51
τ (min)		5216	10070	12997
t_b (min)		1878	4539	7470
Yoon and Nelson model (Linearized form)				
q (mg-Cu/mL-beads)		16.57	13.94	15.73
	v%*	17.60	3.80	1.42
τ (min)		6697	9472	13259
	v%*	28.40	5.93	2.01
t_b (min)		1807	4607	7140
	v%*	3.80	1.50	4.42
k_{YN} (min^{-1})		5.00×10^{-4}	5.00×10^{-4}	4.00×10^{-4}
r^2		0.9790	0.9694	0.9825
$\varepsilon\%^{\#}$		15.16	11.53	12.59
Yoon and Nelson model (Non-linearized form)				
q (mg-Cu/mL-beads)		14.21	14.60	15.49
	v%*	0.85	0.76	0.13
τ (min)		5691	9973	13057
	v%*	9.11	0.96	0.46
t_b (min)		1113	4820	7020
	v%*	40.72	6.20	6.02
k_{YN} (min^{-1})		5.33×10^{-4}	4.72×10^{-4}	4.05×10^{-4}
r^2		0.9916	0.9951	0.9985
$\varepsilon\%^{\#}$		14.16	8.68	13.17

Calculations:

* Variance (v%) = $\dfrac{\left|a_{expt} - a_{model}\right|}{a_{expt}} \times 100\,\%$

$^{\#}$ Average percentage of errors ($\varepsilon\%$) = $\dfrac{\sum_{i=1}^{N}\left|\dfrac{(C_e/C_o)_{expt} - (C_e/C_o)_{model}}{(C_e/C_o)_{expt}}\right|}{N} \times 100\,\%$

4.5.4 Thomas model

Thomas model is a widely-used fixed-bed ion-exchange models that can successfully describe the entire range of the breakthrough profiles. The principle of this model is based on the concepts and assumptions of the second order kinetics, the Langmuir isotherm model and the ion-exchange theory (Thomas, 1944 and 1948). As discussed in Sections 4.2.2 and 4.2.3, the biosorption characteristics of the RIM beads demonstrated a good agreement with the pseudo-second-order kinetic model and the Langmuir isotherm model. Moreover, the results in Section 4.4.3 show that ion exchange reaction between Ca^{2+} ions on the binding sites of the RIM beads and Cu^{2+} ions in the influent solution was predominant inside the RIM column. It seems that the biosorption behaviour of the RIM column can be simulated well by the Thomas model. In order to investigate the applicability of the Thomas model, the experimental data with respect to the influent concentrations, the flow rates and the bed depths were simulated by both the linearized and non-linearized forms of the model. The simulated breakthrough profiles and the modeling parameters are presented in Figs. 4.62 to 4.67 and Tables 4.36 to 4.38.

The results show that the biosorption behaviours could be well described by both the linearized and non-linearized forms with r^2 values above 0.96. The predicted copper removals also matched with the experimental results (variances below 12%). However, poor predictions of the breakthrough time (variances up to 41%) and large average percentages of errors of the profile simulations (up to 30%) were obtained by using the

non-linearized model. By contrast, the linearized model could predict the breakthrough time with less than 10% variances and could simulate the profiles with the average percentage of errors below 16%. Accordingly, the linearized Thomas model should be more applicable than the non-linearized form.

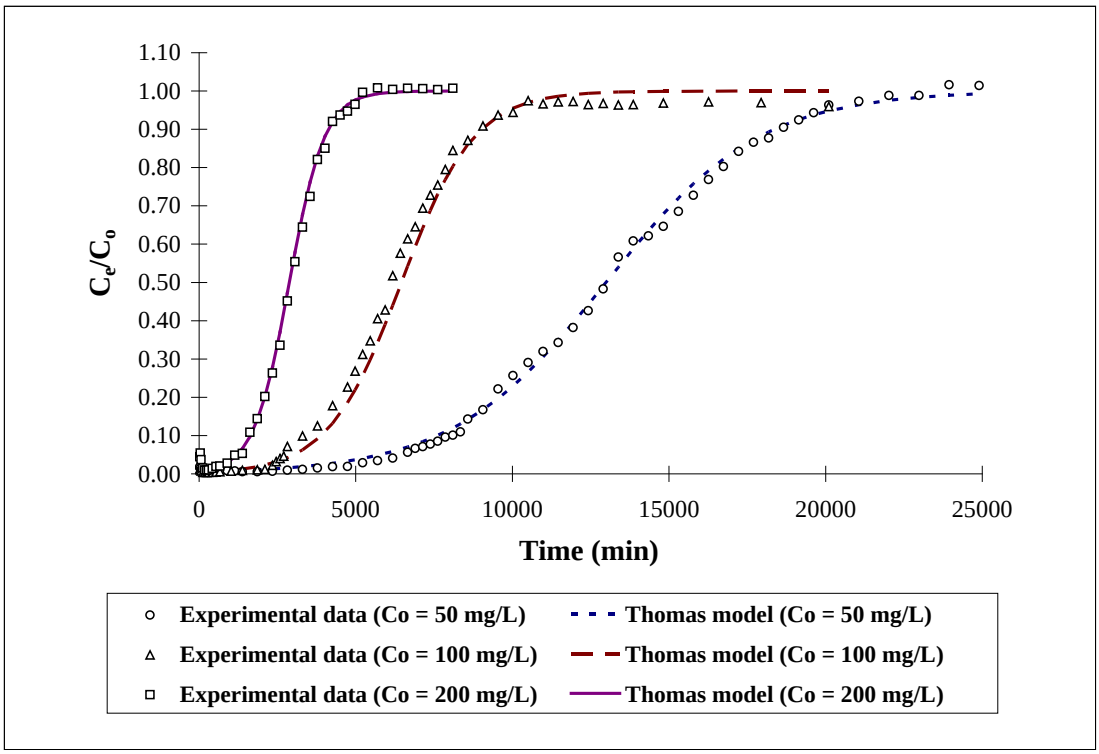

Figure 4.62. Simulation of copper(II) biosorption profiles of RIM columns at different influent copper(II) concentrations by linearized Thomas model.

* Experimental conditions are listed in Table 4.36.

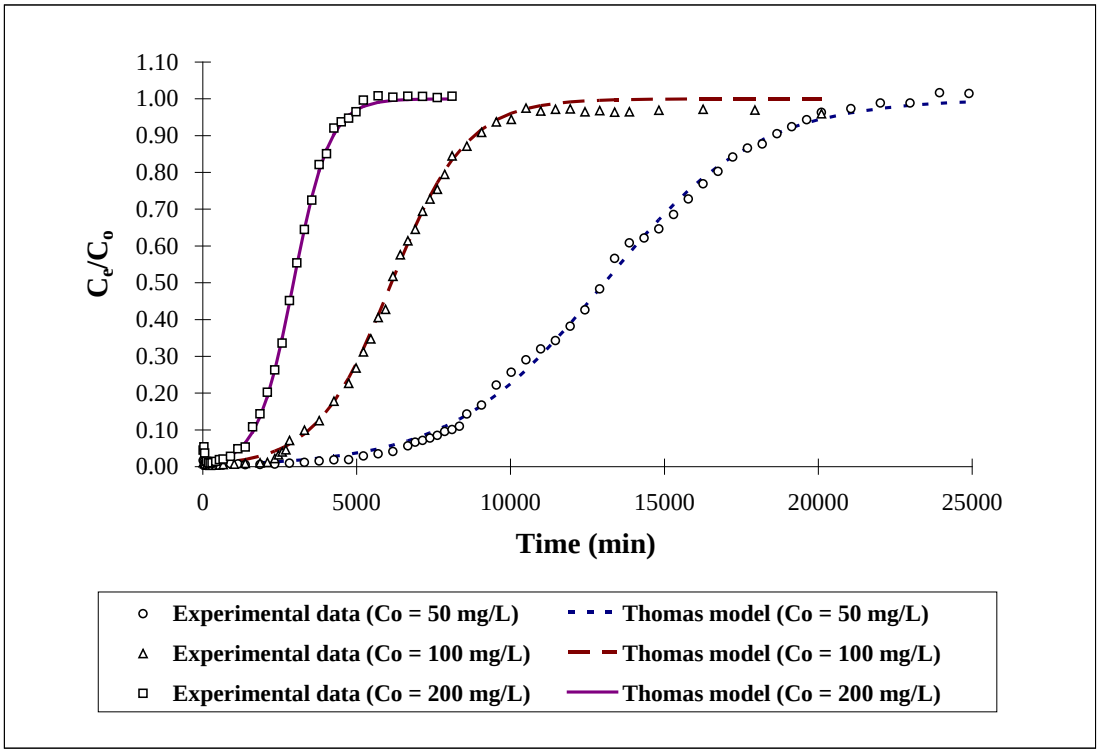

Figure 4.63. Simulation of copper(II) biosorption profiles of RIM columns at different influent copper(II) concentrations by non-linearized Thomas model.

* Experimental conditions are listed in Table 4.36.

Table 4.36. Parameters of Thomas model for copper(II) biosorption of RIM columns at different influent copper(II) concentrations.

C_o (mg-Cu/L)		**49.88**	**98.37**	**192.77**
Z (cm)		50	50	50
Q (mL/min)		1	1	1
Volume of beads used (mL)		41.90	41.45	41.43
Experimental data				
q	(mg-Cu)	649.77	610.12	561.85
	(mg-Cu/mL-beads)	15.51	14.72	13.56
V_b (L)		7.47	2.59	0.67
t_b (min)		7470	2594	673
Thomas model (Linearized form)				
q (mg-Cu/mL-beads)		15.50	15.30	13.40
	v%*	0.06	3.94	1.18
t_b (min)		7014	2776	697
	v%*	6.11	7.00	3.54
k_{Th} (mL/mg-Cu · min)		8.19×10^{-3}	8.72×10^{-3}	9.16×10^{-3}
r^2		0.9825	0.9858	0.9856
ε%#		13.28	12.51	5.83
Thomas model (Non-linearized form)				
q (mg-Cu/mL-beads)		15.54	14.56	13.70
	v%*	0.19	1.09	1.03
t_b (min)		7018	2286	683
	v%*	6.06	11.88	1.47
k_{Th} (mL/mg-Cu · min)		8.10×10^{-3}	8.35×10^{-3}	8.83×10^{-3}
r^2		0.9985	0.9981	0.9989
ε%#		13.30	14.28	4.85

Calculations:

* Variance (v%) = $\dfrac{\left|a_{expt} - a_{model}\right|}{a_{expt}} \times 100\,\%$

Average percentage of errors (ε%) = $\dfrac{\sum_{i=1}^{N}\left|\dfrac{\left(C_e/C_o\right)_{expt} - \left(C_e/C_o\right)_{model}}{\left(C_e/C_o\right)_{expt}}\right|}{N} \times 100\,\%$

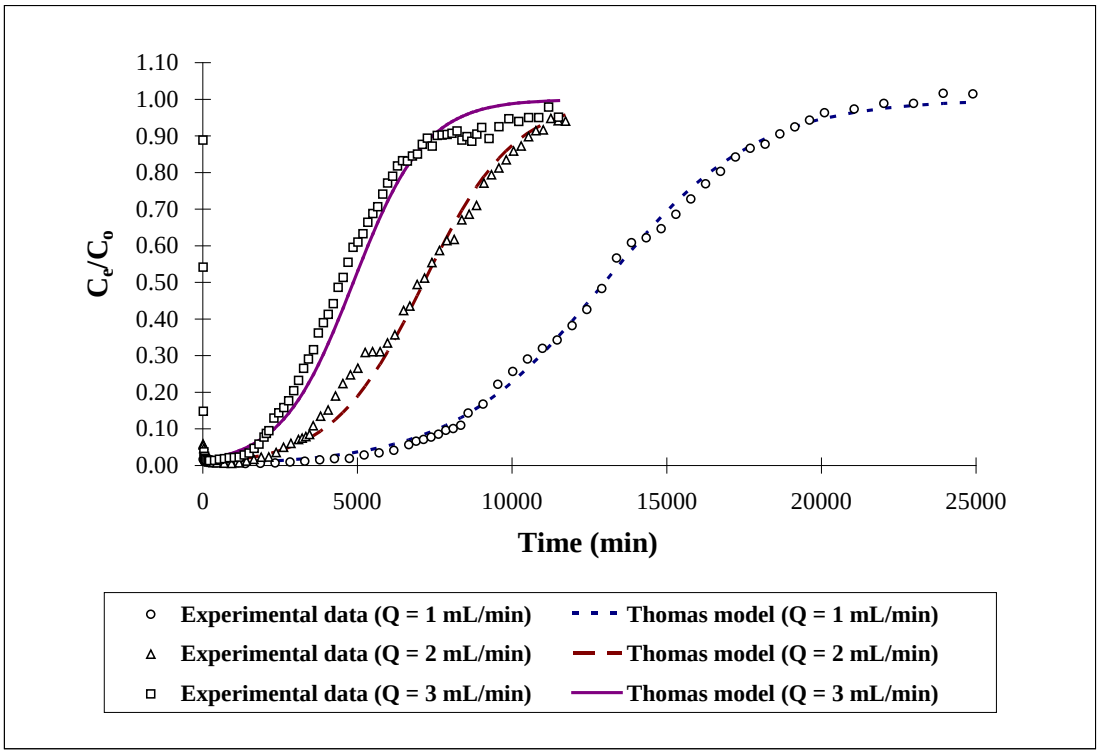

Figure 4.64. Simulation of copper(II) biosorption profiles of RIM columns under different inlet upward flow rates by linearized Thomas model.

* Experimental conditions are listed in Table 4.37.

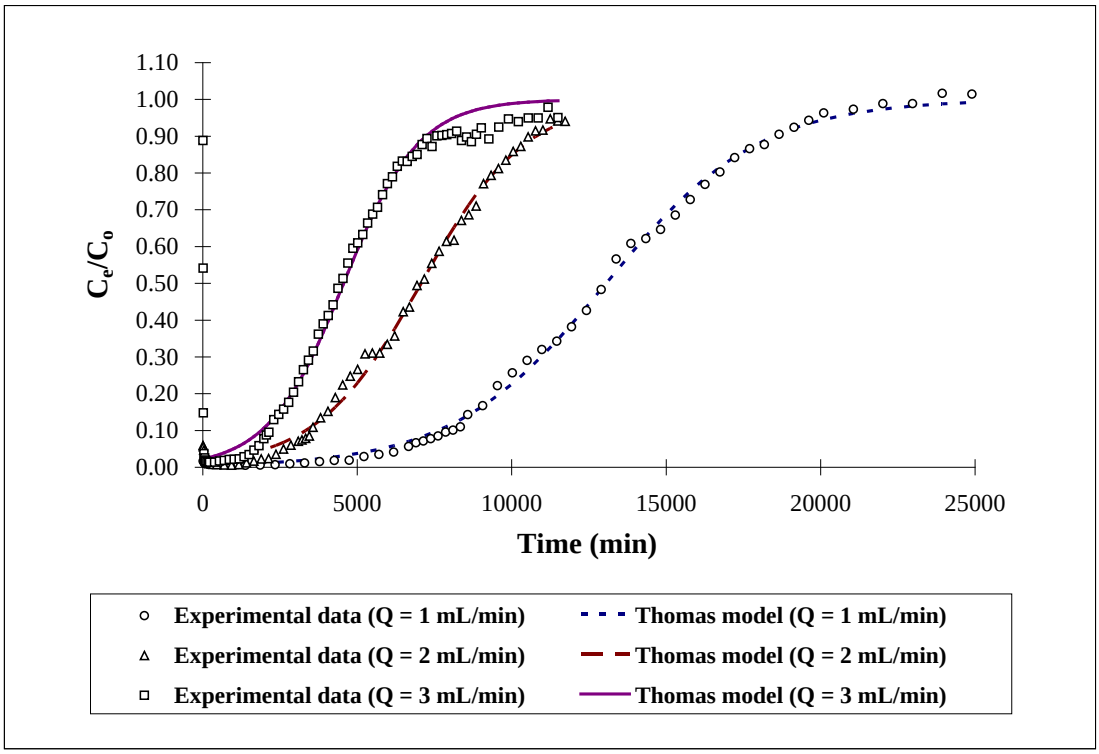

Figure 4.65. Simulation of copper(II) biosorption profiles of RIM columns under different inlet upward flow rates by non-linearized Thomas model.

* Experimental conditions are listed in Table 4.37.

Table 4.37. Parameters of Thomas model for copper(II) biosorption of RIM columns under different inlet upward flow rates.

Q (mL/min)		**1**	**2**	**3**
Z (cm)		50	50	50
C_o (mg-Cu/L)		49.88	48.44	48.12
Volume of beads used (mL)		41.90	41.38	42.65
Experimental data				
q	(mg-Cu)	649.77	675.34	666.16
	(mg-Cu/mL-beads)	15.51	16.32	15.62
V_b (mL)		7.47	6.81	6.08
t_b (min)		7470	3405	2025
Thomas model (Linearized form)				
q (mg-Cu/mL-beads)		15.50	16.70	16.50
	v%*	0.06	2.33	5.64
t_b (min)		7014	3602	2066
	v%*	6.11	5.80	2.01
k_{Th} (mL/mg-Cu · min)		8.19×10^{-3}	1.40×10^{-2}	1.78×10^{-2}
r^2		0.9825	0.9813	0.9755
ε%#		13.28	16.35	14.32
Thomas model (Non-linearized form)				
q (mg-Cu/mL-beads)		15.54	16.54	15.43
	v%*	0.19	1.35	1.21
t_b (min)		7018	2977	1648
	v%*	6.06	12.56	18.62
k_{Th} (mL/mg-Cu · min)		8.10×10^{-3}	1.22×10^{-2}	1.71×10^{-2}
r^2		0.9985	0.9966	0.9948
ε%#		13.30	30.31	18.71

Calculations:

* Variance (v%) = $\dfrac{\left|a_{expt} - a_{model}\right|}{a_{expt}} \times 100\,\%$

Average percentage of errors (ε%) = $\dfrac{\sum_{i=1}^{N}\left|\dfrac{\left(C_e / C_o\right)_{expt} - \left(C_e / C_o\right)_{model}}{\left(C_e / C_o\right)_{expt}}\right|}{N} \times 100\,\%$

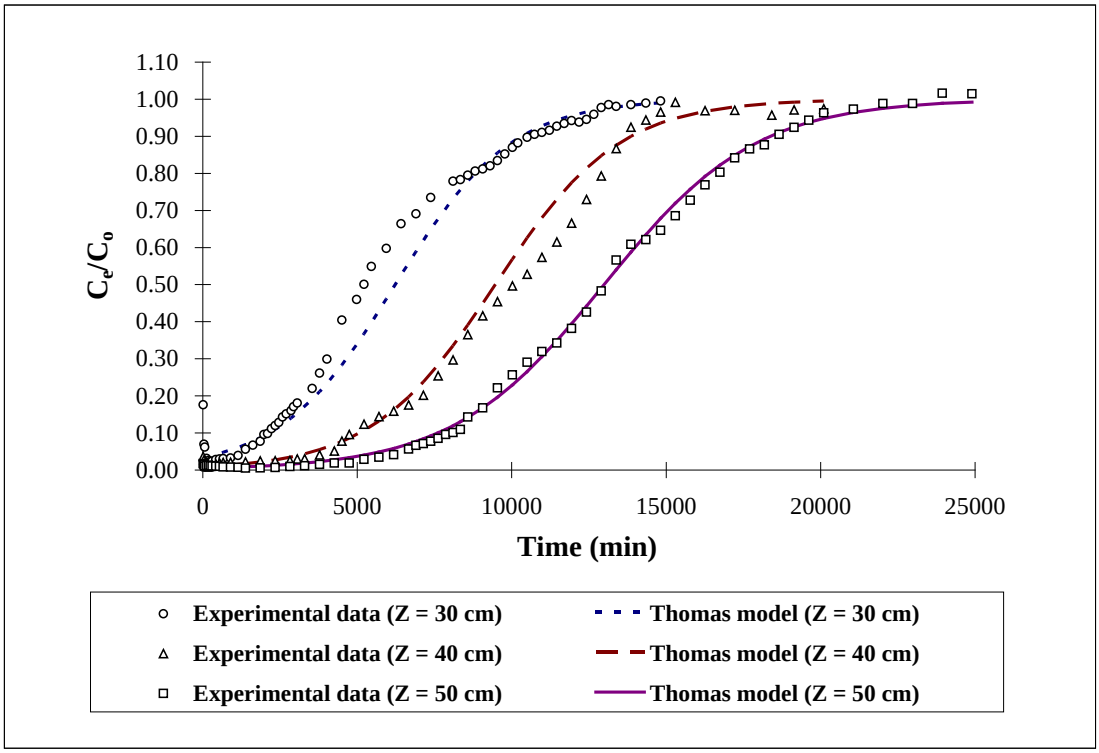

Figure 4.66. Simulation of copper(II) biosorption profiles of RIM columns with different column bed depths by linearized Thomas model.

* Experimental conditions are listed in Table 4.38.

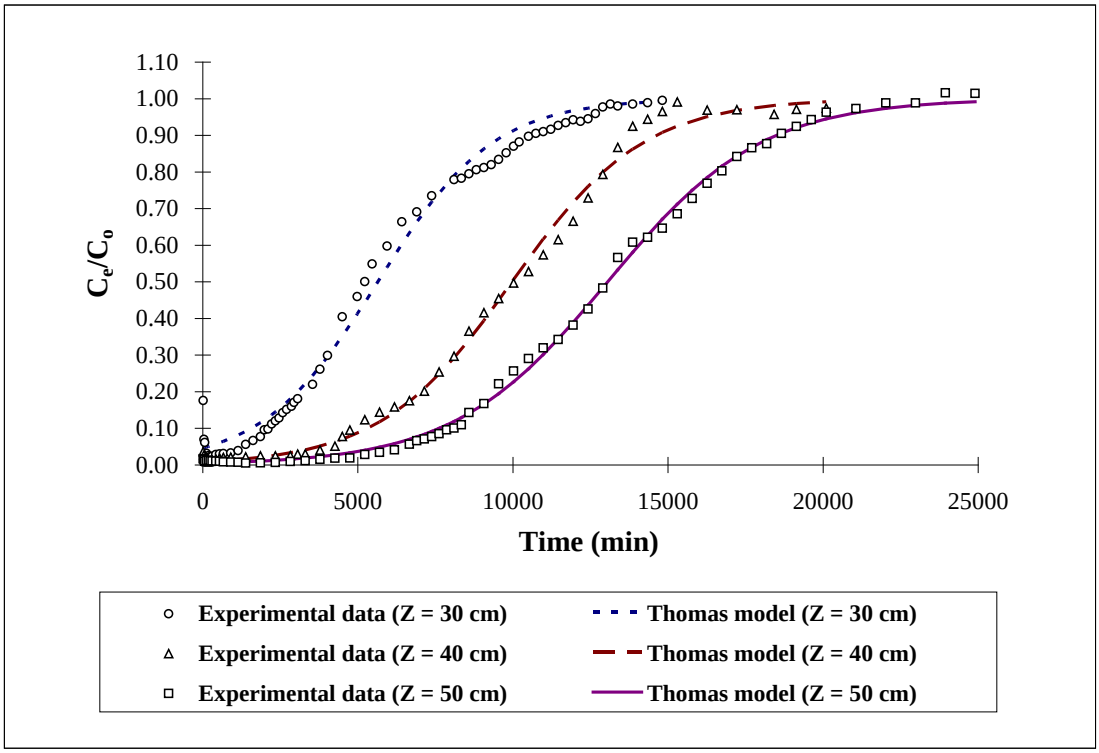

Figure 4.67. Simulation of copper(II) biosorption profiles of RIM columns with different column bed depths by non-linearized Thomas model.

* Experimental conditions are listed in Table 4.38.

Table 4.38. Parameters of Thomas model for copper(II) biosorption of RIM columns with different column bed depths.

Z (cm)		**30**	**40**	**50**
C_o (mg-Cu/L)		49.93	49.42	49.88
Q (mL/min)		1	1	1
Volume of beads used (mL)		20.15	33.23	41.90
Experimental data				
q	(mg-Cu)	283.82	481.51	649.77
	(mg-Cu/mL-beads)	14.09	14.49	15.51
V_b (L)		1.88	4.54	7.47
t_b (min)		1878	4539	7470
Thomas model (Linearized form)				
q (mg-Cu/mL-beads)		15.40	14.10	15.50
	v%*	9.30	2.69	0.06
t_b (min)		1690	4612	7014
	v%*	10.03	1.60	6.11
k_{Th} (mL/mg-Cu · min)		1.08×10^{-2}	1.01×10^{-2}	8.19×10^{-3}
r^2		0.9790	0.9694	0.9825
ε%#		11.46	12.33	13.28
Thomas model (Non-linearized form)				
q (mg-Cu/mL-beads)		13.98	14.83	15.54
	v%*	0.78	2.35	0.19
t_b (min)		1103	4818	7018
	v%*	41.28	6.14	6.06
k_{Th} (mL/mg-Cu · min)		1.08×10^{-2}	9.54×10^{-3}	8.10×10^{-3}
r^2		0.9916	0.9951	0.9985
ε%#		14.34	9.38	13.30

Calculations:

* Variance (v%) = $\dfrac{\left|a_{expt} - a_{model}\right|}{a_{expt}} \times 100\,\%$

Average percentage of errors (ε%) = $\dfrac{\sum_{i=1}^{N}\left|\dfrac{(C_e/C_o)_{expt} - (C_e/C_o)_{model}}{(C_e/C_o)_{expt}}\right|}{N} \times 100\,\%$

The parameters of the various models are summarized in Tables 4.39 to 4.42. Among these models, the linearized form of both the Thomas model and the Yoon and Nelson model could successfully simulate the entire range of the breakthrough profiles of copper(II) biosorption by RIM column. They exhibited high r^2 values and reasonably small average percentages of errors. These two simulations could also provide accurate predictions on the process performances (including both the copper removals and the breakthrough time) with small variances. Thus, the performance of Thomas model and the Yoon and Nelson model was better than other models. However, the constants k_{YN} obtained by the linearized Yoon and Nelson model could not fully conform to the theoretical principle of the model. The constant k_{YN} should be directly proportional to the influent concentration and the flow rate, but inversely proportional to the mass of sorbents. However, the calculated constants only partially followed the theoretical trends. This demoted the reliability of the Yoon and Nelson model in this study. Therefore, the linearized Thomas model was the best model for simulating the copper(II) biosorption behavior and performances of the RIM columns.

Table 4.39. Summary of parameters of Clark model for copper(II) biosorption of RIM columns with different fixed-bed conditions.

C_o (mg-Cu/L)		**49.88**	**98.37**	**192.77**	48.44	48.12	49.93	49.42
Q (mL/min)		**1**	1	1	**2**	**3**	1	1
Z (cm)		**50**	50	50	50	50	**30**	**40**
Experimental data	q (mg-Cu/mL-beads)	15.51	14.72	13.56	16.32	15.62	14.09	14.49
	t_b (min)	7470	2594	673	3405	2025	1878	4539
Clark model	q (mg-Cu/mL-beads)	15.31	14.36	13.42	16.13	15.16	14.10	14.49
	v%	1.29	2.45	1.03	1.16	2.94	0.07	0.00
	t_b (min)	6399	1753	218	2546	1323	532	4309
	v%	14.34	32.44	67.55	25.21	34.64	71.66	5.07
	r^2	0.9965	0.9962	0.9988	0.9937	0.9875	0.9837	0.9960
	ε%	29.75	35.65	13.73	55.05	33.32	21.87	17.51

Table 4.40. Summary of parameters of Adams-Bohart model for copper(II) biosorption of RIM columns with different fixed-bed conditions.

C_o (mg-Cu/L)		**49.88**	**98.37**	**192.77**	48.44	48.12	49.93	49.42
Q (mL/min)		**1**	1	1	**2**	**3**	1	1
Z (cm)		**50**	50	50	50	50	**30**	**40**
Experimental data	q (mg-Cu/mL-beads)	15.51	14.72	13.56	16.32	15.62	14.09	14.49
	t_b (min)	7470	2594	673	3405	2025	1878	4539
Adams-Bohart model (Linearized form)	Modeling range (min)	13860	6420	3540	5250	4380	8100	11460
	q (mg-Cu/mL-beads)	15.46	13.64	14.27	13.24	14.50	12.68	14.51
	v%	0.32	7.34	5.24	18.87	7.17	10.01	0.14
	t_b (min)	7897	2797	624	3491	2114	1935	4476
	v%	5.72	7.83	7.28	2.54	4.40	3.04	1.38
	k_{AB} (L/mg-Cu · min)	8.02×10^{-6}	9.15×10^{-6}	7.26×10^{-6}	1.86×10^{-5}	2.08×10^{-5}	1.00×10^{-5}	8.09×10^{-6}
	r^2	0.9830	0.9733	0.9819	0.9760	0.9753	0.9309	0.9705
	ε%	20.73	18.94	13.51	16.69	12.85	19.18	23.40
Adams-Bohart model (Non-linearized form)	Modeling range (min)	8580	5460	2100	4530	3740	5460	9060
	q (mg-Cu/mL-beads)	14.62	14.74	13.09	13.35	15.30	11.85	15.19
	v%	5.73	0.12	3.49	18.22	2.08	15.87	4.84
	t_b (min)	7440	2349	653	3326	1980	1576	4639
	v%	0.40	9.44	2.97	2.31	2.22	16.08	2.21
	k_{AB} (L/mg-Cu · min)	8.44×10^{-6}	7.21×10^{-6}	8.18×10^{-6}	1.72×10^{-5}	1.80×10^{-5}	1.02×10^{-5}	7.67×10^{-6}
	r^2	0.9812	0.9842	0.9877	0.9924	0.9849	0.9874	0.9910
	ε%	18.56	44.37	15.32	17.44	21.76	18.60	20.48

Table 4.41. Summary of parameters of Yoon and Nelson model for copper(II) biosorption of RIM columns with different fixed-bed conditions.

C_o (mg-Cu/L)		**49.88**	**98.37**	**192.77**	48.44	48.12	49.93	49.42
Q (mL/min)		**1**	1	1	**2**	**3**	1	1
Z (cm)		**50**	50	50	50	50	**30**	**40**
Experimental data	q (mg-Cu/mL-beads)	15.51	14.72	13.56	16.32	15.62	14.09	14.49
	τ (min)	12997	6133	2934	7006	4461	5216	10070
	t_b (min)	7470	2594	673	3405	2025	1878	4539
Yoon and Nelson model (Linearized form)	q (mg-Cu/mL-beads)	15.73	14.58	13.07	16.09	15.63	16.57	13.94
	v%	1.42	0.95	3.61	1.41	0.07	17.60	3.80
	τ (min)	13259	6157	2825	6936	4636	6697	9472
	v%	2.01	0.39	3.72	1.01	3.92	28.40	5.93
	t_b (min)	7140	2652	684	3501	1962	1807	4607
	v%	4.42	2.24	1.63	2.85	3.10	3.80	1.50
	k_{YN} (min^{-1})	4.00×10^{-4}	9.00×10^{-4}	1.80×10^{-3}	7.00×10^{-4}	9.00×10^{-4}	5.00×10^{-4}	5.00×10^{-4}
	r^2	0.9825	0.9858	0.9856	0.9813	0.9755	0.9790	0.9694
	ε%	12.59	8.42	7.54	16.56	11.85	15.61	11.53
Yoon and Nelson model (Non-linearized form)	q (mg-Cu/mL-beads)	15.49	14.62	13.61	16.25	15.36	14.21	14.60
	v%	0.13	0.68	0.37	0.43	1.66	0.85	0.76
	τ (min)	13057	6174	2944	7061	4560	5691	9973
	v%	0.46	0.66	0.35	0.78	2.21	9.11	0.96
	t_b (min)	7020	2329	684	2981	1644	1113	4820
	v%	6.02	10.22	1.63	12.44	18.81	40.72	6.20
	k_{YN} (min^{-1})	4.05×10^{-4}	8.22×10^{-4}	1.70×10^{-3}	5.89×10^{-4}	8.25×10^{-4}	5.33×10^{-4}	4.72×10^{-4}
	r^2	0.9985	0.9981	0.9995	0.9967	0.9948	0.9916	0.9951
	ε%	13.17	13.30	4.82	30.54	18.63	14.16	8.68

Table 4.42. Summary of parameters of Thomas model for copper(II) biosorption of RIM columns with different fixed-bed conditions.

C_o (mg-Cu/L)		**49.88**	**98.37**	**192.77**	48.44	48.12	49.93	49.42
Q (mL/min)		**1**	1	1	**2**	**3**	1	1
Z (cm)		**50**	50	50	50	50	**30**	**40**
Experimental data	q (mg-Cu/mL-beads)	15.51	14.72	13.56	16.32	15.62	14.09	14.49
	t_b (min)	7470	2594	673	3405	2025	1878	4539
Thomas model (Linearized form)	q (mg-Cu/mL-beads)	15.50	15.30	13.40	16.70	16.50	15.40	14.10
	v%	0.06	3.94	1.18	2.33	5.64	9.30	2.69
	t_b (min)	7014	2776	697	3602	2066	1690	4612
	v%	6.11	7.00	3.54	5.80	2.01	10.03	1.60
	k_{Th} (mL/mg-Cu · min)	8.19×10^{-3}	8.72×10^{-3}	9.16×10^{-3}	1.40×10^{-2}	1.78×10^{-2}	1.08×10^{-2}	1.01×10^{-2}
	r^2	0.9825	0.9858	0.9856	0.9813	0.9755	0.9790	0.9694
	ε%	13.28	12.51	5.83	16.35	14.22	11.46	12.33
Thomas model (Non-linearized form)	q (mg-Cu/mL-beads)	15.54	14.56	13.70	16.54	15.43	13.98	14.83
	v%	0.19	1.09	1.03	1.35	1.21	0.78	2.35
	t_b (min)	7018	2286	683	2977	1648	1103	4818
	v%	6.06	11.88	1.47	12.56	18.62	41.28	6.14
	k_{Th} (mL/mg-Cu · min)	8.10×10^{-3}	8.35×10^{-3}	8.83×10^{-3}	1.22×10^{-2}	1.71×10^{-2}	1.08×10^{-2}	9.54×10^{-3}
	r^2	0.9985	0.9981	0.9989	0.9966	0.9948	0.9916	0.9951
	ε%	13.30	14.28	4.85	30.31	18.71	14.34	9.38

4.6 Removal and recovery of copper from industrial electroplating wastewater

In Sections 4.3 and 4.4, the copper removal and recovery of the RIM column were studied in detail using the synthetic wastewater (pure copper(II) nitrate solution). This section will further report the applicability of the RIM column in the treatment of copper-contaminated industrial electroplating wastewater. To test the applicability, ten sequential copper(II) biosorption/desorption cycles were performed by using the RIM column. The copper discharge limit of this integrated process was set at 4 mg-Cu/L in order to meet the HKSAR government standard.

4.6.1 Compositions of industrial electroplating wastewater

The compositions of the industrial wastewater were determined before the treatment. The industrial electroplating wastewater was collected from various acid copper sulfate plating baths in the research laboratory of a local electroplating material supplier. The metal concentrations, anion contents and total organic carbon (TOC) level of the wastewater were determined by following the procedures described in Section 3.5.1.

Both direct calibration and standard addition methods were used for analyzing the metal concentrations by the flame atomic absorption spectrophotometry (FAAS). The direct calibration method is usually used for determination of dominant metal species in solution samples. The standard addition method can accurately measure trace metal contents through canceling out influences of the dominant species. The results

show that copper, lead and zinc ions were present in the original wastewater sample (Table 4.43). A high copper concentration of about 289.58 mmol/L (1.84×10^4 mg/L) was found in the wastewater, whereas the concentrations of metal species such as lead, zinc and nickel were below 0.5 mmol/L or below the lowest detection limit of the FAAS analysis.

Table 4.44 shows that sulfate, nitrate and chloride ions were present in the wastewater. A high level of sulfate ions of about 1.60×10^3 mmol/L should mainly come from copper(II) sulfate and sulfuric acid of the plating solutions. On the other hand, low concentrations of nitrate and chloride ions of about 56.39 and 0.91 mmol/L, respectively, were found in the original wastewater sample.

Since over thousands of organic additives are frequently used in the electroplating processes, it is impossible to identify all the organics present in the mixed wastewater sample and determine their levels specifically. Thus, the content of total organic carbon (TOC) was measured to represent the total amount of organics in the wastewater. Table 4.44 shows that the TOC value of the original source was about 1307.29 mg/L.

In general, industrial electroplating plants produce two major kinds of wastewater: obsolete plating solution and rinsing water. The obsolete plating solution contains a high level of copper ions. Due to economic concerns, the obsolete plating solution is usually discharged after repeated usage. To treat such wastewater, chemical precipitation together with

biosorption is recommended. The precipitation can significantly lower the copper content in the wastewater without increasing the solution volume. The biosorption process can further treat the wastewater to a level within the government discharge limit.

The rinsing water is the water used to wash the residual plating solution on the workpiece surface after the plating process. This wastewater is discharged daily in large quantities and with a relatively low copper content. It can be treated directly by the biosorption process. Thus, the integrated treatment in this study was directed to this kind of the wastewater. The original sample of the industrial electroplating wastewater was first diluted to about 50 mg-Cu/L (0.79 mmol-Cu/L) so as to simulate the condition of the rinsing water. The concentrations of the metal components, anions and organics in the diluted wastewater are listed in Tables 4.43 and 4.44. After the dilution, the levels of the trace metal species significantly decreased to below the lowest detection limit of the FAAS analysis. The concentrations of the anions were 6.11, 0.17 and 9.72×10^{-2} mmol/L with respect to sulfate, nitrate and chloride ions. The TOC level in the diluted wastewater was lowered to about 3.71 mg/L.

Table 4.43. Metal contents in industrial electroplating wastewater.

Metal ions	Concentration of metal ions			
	Original wastewater sample		Diluted wastewater*	
	Direct calibration method	Standard addition method	Direct calibration method	Standard addition method
Cu	289.58 mmol/L (1.84×10^{4} mg/L)	~	0.78 mmol/L (49.40 mg/L)	~
Pb	~	0.42 mmol/L (86.85 mg/L)	~	~
Zn	~	1.80×10^{-2} mmol/L (1.18 mg/L)	~	~
Ni	~	~	~	~
Cr	~	~	~	~
Cd	~	~	~	~
Ca	~	~	~	~
Na	~	~	~	~

Remarks:
* In order to simulate the discharged wastewater of the industrial electroplating process (after rinsing the plating workpiece), the original sample was diluted to about 50 mg-Cu/L for the column biosorption in this integrated treatment study.
~ The analyzed metal concentration is below the lowest detection limit of the flame atomic absorption spectrophotometry (FAAS).

Table 4.44. Concentrations of anions and organics in industrial electroplating wastewater.

	Original wastewater sample	**Diluted wastewater***
	Concentration of anion	
SO_4^{2-}	1.60×10^3 mmol/L (1.54×10^5 mg/L)	6.11 mmol/L (586.51 mg/L)
NO_3^-	56.39 mmol/L (3.50×10^3 mg/L)	0.17 mmol/L (10.72 mg/L)
Cl^-	0.91 mmol/L (32.1 mg/L)	9.72×10^{-2} mmol/L (3.45 mg/L)
	Total organic carbon (TOC)	
Organics	1307.29 mg/L	3.71 mg/L

Remark:
* In order to simulate the discharged wastewater of the industrial electroplating process (after rinsing the plating workpiece), the original sample was diluted to about 50 mg-Cu/L for the column biosorption in this integrated treatment study.

4.6.2 Effects of matrix components in wastewater on copper(II) biosorption

After investigating the compositions of the wastewater, three groups of matrices, including metal impurities, anions and organic additives, were identified. The effects of these matrix components on copper(II) biosorption were studied by contacting the RIM beads with the copper(II) nitrate solutions in the presence of the respective matrices.

4.6.2.1 Effect of counter cations

The results in Section 4.3.7 show that the counter metal ions could compete with copper(II) ions for the binding sites of the RIM beads, resulting in the drop of copper removal. The results also show that the RIM beads selectively bound the heavy metal ions in the following order: Pb(II) > Cu(II) >> Ni(II) > Zn(II). Such phenomena might be attributed to the electron configuration of the heavy metal ions. The pratical biosorption performance might thus be suppressed in the presence of these cations.

In view of both the original and diluted industrial wastewater, Table 4.43 shows that the concentrations of all the identified heavy metal matrices were in trace level or even below the lowest detection limit of the FAAS analysis. These trace amounts of heavy metal matrices, other than Cu(II) ions, should have a negligible influence on the copper removal in the following integrated treatment process (Section 4.6.4).

4.6.2.2 Effect of organics

In the total organic carbon analysis, about 1307.29 mg/L TOC was found in the industrial electroplating wastewater (Table 4.44). These organics might be surfactants, brighteners, leveling agents or wetting agents. They usually act as chemical modifiers in electroplating processes to enhance the plating efficiency and/or improve the workpiece properties. However, their influences on the biosorption are unknown. The batch copper(II) biosorption performance of the RIM beads was then investigated in the presence of various organics. Four common organic additives including coumarin (brightener), formaldehyde (wetting agent), urea (electroless copper plating additive) and 4-butyne-1,2-diol (brightener), were used in this study. The experimental procedures are described in Section 3.3.1.4.

Fig. 4.68 shows that the copper removals were similar in the presence or absence of the organics. Further doubling the concentrations of the organics, the RIM beads still demonstrated similar copper uptakes. All the copper removals were about 6.5×10^{-2} mmol, with less than 15% difference as compared with the case without any organics. These results demonstrate that the effect of the organics on the copper(II) biosorption was insignificant. On the other hand, the concentrations of the organics remained almost unchanged after the biosorption, with less than 13% variance (Table 4.45). This implied that there was little or even no interaction between these organic additives and the RIM beads during the copper(II) biosorption. Based on these results, it can be concluded that the

effect of organic additives on the biosorption was negligible. No additional treatment should be required to remove the organics from the wastewater before it was treated by the biosorption in the integrated fixed-bed system.

4.6.2.3 Effect of anions

As shown in Table 4.44, more than one type of anions were found in the electroplating wastewater. Sulfate ion was the dominant species. The copper(II) biosorption performance in the integrated treatment process might change in the presence of other anionic species. The effect of anions on the copper(II) biosorption should be considered before the treatment of the industrial wastewater.

In Section 4.2.5, the results show that the co-existing anions, such as sulfate and chloride, had no significant effect on copper(II) biosorption by the RIM beads. Thus, the results reported in the previous sections can be directly applied and correlated to the following integrated treatment of the electroplating wastewater.

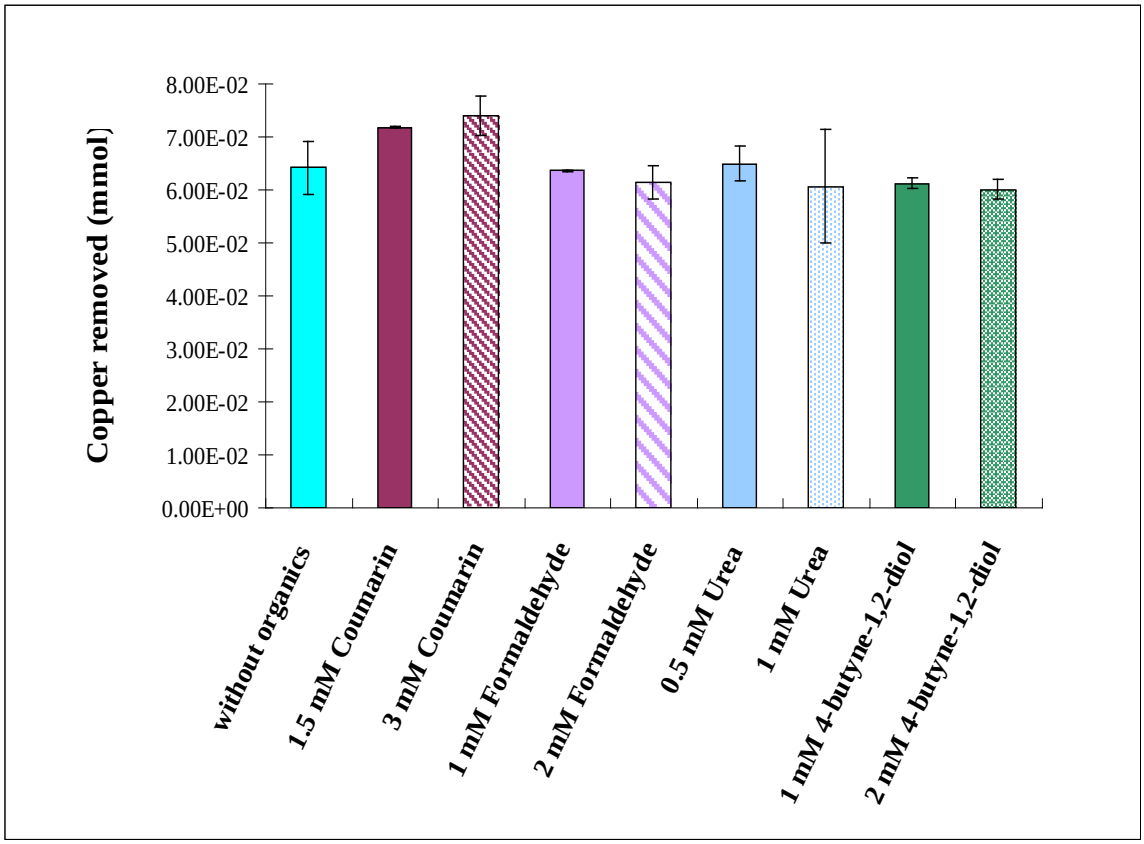

Figure 4.68. Effect of organic additives on copper(II) biosorption using RIM beads in batch system.

* Experimental conditions: Volume of the RIM beads used = 0.6 mL; [*Micrococcus luteus*] = 0.133 g-cell/mL-beads; Initial copper(II) concentration = 2 mM (in addition of various amount of different organics); Solution pH = 5.0; Volume of reaction mixture = 50 mL; Contact time = 6 h; Agitation speed = 250 rpm.

Table 4.45. Change of organic concentrations in copper(II) biosorption using RIM beads.

Organics	Organic concentration (mmol/L)		
	Initial	After biosorption	|Change| (%)
Coumarin	1.46 ± 0.01	1.43 ± 0.01	1.83 ± 0.50
	2.93 ± 0.03	2.94 ±0.00	0.23 ± 0.10
Formaldehyde	1.06 ± 0.00	1.20 ± 0.03	12.42 ± 2.88
	2.08 ± 0.01	2.26 ± 0.06	8.27 ± 2.96
Urea	0.53 ± 0.00	0.58 ± 0.01	10.53 ± 1.16
	1.02 ± 0.01	1.09 ± 0.02	6.25 ± 2.33
2-butyne-1,4-diol	1.12 ± 0.02	1.17 ± 0.08	5.03 ± 6.90
	2.19 ± 0.01	2.22 ± 0.04	1.46 ± 1.61

4.6.3 Pre-treatment of industrial electroplating wastewater

In order to maximize the treatment performance, conventional systems usually include one or multiple pre-treatment processes of wastewater. Such processes can be generally made up of two major steps: (i) eliminating matrix interferences; and, (ii) adjusting the wastewater to the optimal process conditions. In this sub-section, the pre-treatment of the industrial wastewater was examined before running the integrated treatment process.

Regarding the matrix interferences, the results in Section 4.6.2 show that the matrix components, including the metal impurities, the organic additives and the anions, had no significant effect on the copper(II) biosorption. Moreover, a large degree of dilution was carried out to adjust the copper concentration of the original wastewater sample to about 50 mg-Cu/L, which was the concentration commonly encountered in the discharge from the electroplating plants (rinsing water). This dilution procedure would greatly lower the concentrations of all the matrix components, as reported in Tables 4.43 and 4.44. The matrix influences could thus be neglected. No additional step would be required to minimize the matrix interferences.

Although the wastewater sample was diluted with a large amount of DDI water, the solution pH was still low at about 2.0. A large amount of sodium hydroxide was used to adjust the pH of the diluted industrial wastewater to the optimal level (pH 5.0) for the biosorption. It greatly increased the sodium concentration, up to about 227.3 mg Na^+/L (9.89

mmol/L). With the introduction of this NaOH pre-treated wastewater into the RIM column, swelling and blockage of the biosorbent bed were observed when the treatment volume reached 56 bed volume (Fig. 4.69). The swelling might be due to the dissolution of alginate inside the beads at such high sodium concentration. In addition, the column overshooting effect (discussed in Section 4.3.7) might further increase the sodium concentration, resulting in a serious destruction of the beads. In turn, the blockage of the column bed would occur. Hence, sodium hydroxide must be replaced for the pH adjustment of the wastewater in the integrated treatment.

Two other alkaline substitutes, lime ($CaCO_3$) and ammonia solution (NH_4OH), were used for the pH adjustment. About 246.5 mg-NH_4^+/L (13.65 mmol/L) or 204.0 mg-Ca^{2+}/L (5.09 mmol/L) were found in the diluted wastewater stocks when the pH was adjusted to 5.0. These pH-adjusted wastewater stocks were then pumped into the RIM columns for the copper removal. Fig. 4.69 shows that the copper removals and treatment volume in the three sequential biosorption/desorption cycles were much higher when NH_4OH was used, compared with $CaCO_3$. Both the copper removals and treatment volume were suppressed significantly after the first cycle in the case of using $CaCO_3$.

The difference of the treatment performances may be related to the binding affinities of Ca^{2+} and NH_4^+ ions towards the binding sites of the beads. Since calcium ion is a divalent cation, it could form a stronger

interaction with the binding sites of the beads; hence a greater competition for the binding sites would be initiated between copper and calcium ions. This resulted in an earlier breakthrough, a smaller treatment volume and lower copper removal. By contrast, even if a higher concentration of NH_4^+ ions (13.65 mmol/L) was present in the conditioned wastewater, the mono-valent NH_4^+ ions might only attach to the binding sites with a weaker interaction. The bound NH_4^+ ions could easily be displaced by fresh copper(II) ions in the influent. Thus, the copper(II) ions could compete better than the NH_4^+ ions for the binding sites. This promoted the better treatment performance of the RIM column.

To summarize, no additional process would be required to remove the matrix components before the pilot treatment of the industrial wastewater. The treatment performance was less affected when ammonia solution was used for the pH adjustment of the wastewater. Therefore, ammonia solution was chosen to replace sodium hydroxide in the subsequent integrated treatment studies.

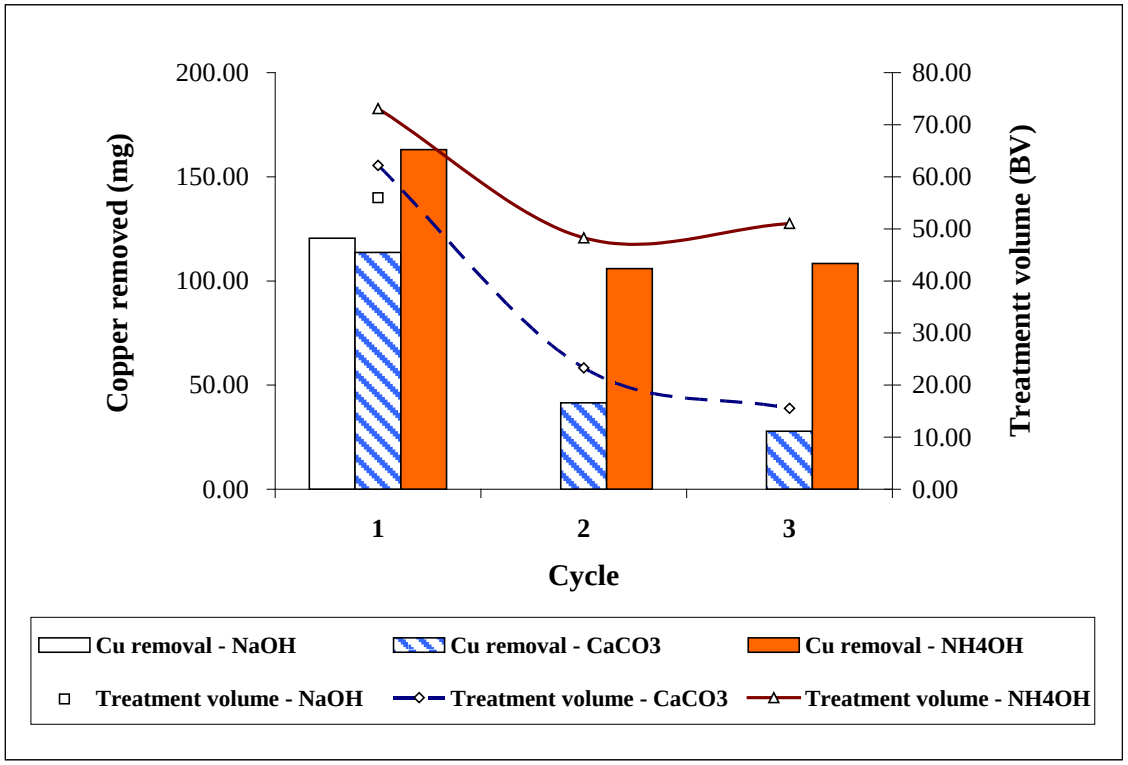

Figure 4.69. Effect of influent pH pre-treatment on copper removals and treatment volume of RIM columns in integrated treatment of industrial electroplating wastewater.

* Fixed-bed biosorption conditions: C_o = 50 mg-Cu/L; Q = 1 mL/min; Z = 50 cm; Solution pH = 5.0 (adjusted by different alkaline materials, including NaOH, $CaCO_3$ and NH_4OH); [*Micrococcus luteus*] = 0.133 g-cell/mL-beads; The process was conducted to the breakthrough level (4 mg-Cu/L);
* Fixed-bed desorption conditions: C_o = 1 M $CaCl_2$; Q = 1 mL/min; The process was continued until 85% of copper content inside the column bed was desorbed.

4.6.4 Integrated treatment by fixed-bed column

The integrated treatment of the industrial electroplating wastewater was performed by the RIM column. The industrial wastewater was diluted to 50 mg-Cu/L by DDI water and then adjusted to pH 5.0 using $25\%_{w/v}$ ammonia solution. Afterward, the pre-conditioned wastewater was applied to the copper removal process until the column breakthrough (C_e = 4 mg-Cu/L). To carry out the copper recovery (column regeneration), 1 M of $CaCl_2$ solution was introduced into the copper-laden column until 85% of copper content in the column packing was desorbed. Both the copper removal and recovery were carried out consecutively for ten cycles. The details of the whole treatment process are described in Section 3.5.2. The experimental conditions are summarized in Table 4.46. The process performances throughout the ten cycles are presented in Figs. 4.70 to 4.72 and Table 4.47.

Fig. 4.70 depicts the treatment performances of the sequential integrated column operation. The copper removals decreased after the first cycle and then remained steady in the later cycles. A similar phenomenon was also observed in the treatment volume. The decrease in the treatment performance could partly be attributed to the incomplete copper desorption in each cycle (Fig. 4.71). The incomplete desorption led to the accumulation of un-desorbed copper ions inside the column. The quantity of the free binding sites of the beads was thus reduced, resulting in the demotion of the copper removals and the treatment volume in the following cycles. This explanation could be validated by calculating the copper

accumulation in each cycle. An increasing trend of the total amount of copper(II) ions accumulated in the biosorbents was exhibited throughout the ten biosorption/desorption cycles (Table 4.47).

The performances of the integrated industrial wastewater treatment can be compared with those of the RIM column for treating the synthetic sewage, which was prepared by pure copper(II) nitrate salt (Section 4.4.2.2). Over the ten treatment cycles, the trends of the copper removals and the treatment volume in these two operations were similar (Fig. 4.70). Moreover, the efficiencies of the copper recoveries in both the operations were close to each other with more than 80% throughout all the cycles, except the first cycle (Fig. 4.71). However, lower copper removals and a smaller treatment volume were attained by the integrated industrial wastewater treatment.

The competition of NH_4^+ ions and the organic leakage from the column packing can explain the lower performances of the integrated industrial wastewater treatment. A large amount of NH_4OH was unavoidably added for the pH adjustment of the industrial wastewater. As reported in Section 4.6.3, the concentration of NH_4^+ ions was about 13.65 mmol/L (246.6 mg-NH_4^+/L). However, the copper concentration in the conditioned wastewater influent was much lower at only around 0.81 mmol/L (51.53 mg-Cu/L). Such a high concentration of NH_4^+ ions could compensate their low binding affinity towards the beads, inducing a keen competition with copper(II) ions and a fast saturation of the binding sites. As a result, lower

copper removals and a smaller treatment volume were observed in the integrated treatment process.

Secondly, Fig. 4.72 shows that a larger amount of the organics (611.08 mg) was washed into the effluent throughout the ten biosorption/desorption cycles in the integrated industrial wastewater treatment. Such organics might be active metal-binding materials of the RIM beads. The trace matrix residuals, such as surfactants and organic acids, in the industrial wastewater might promote dissolution of the active metal-binding materials of the beads. The loss of binding sites in the integrated industrial wastewater treatment then became serious. As a result, the organic leakage could cause the lower copper removals in the integrated industrial wastewater treatment.

Although the copper removals and the treatment volume in the industrial wastewater treatment were lower compared with the synthetic sewage treatment, the treatment performances of the RIM column were still steady and effective over the sequential cycles. Therefore, the RIM column could be regarded as a promising system for a large-scale treatment of the copper-laden industrial wastewater.

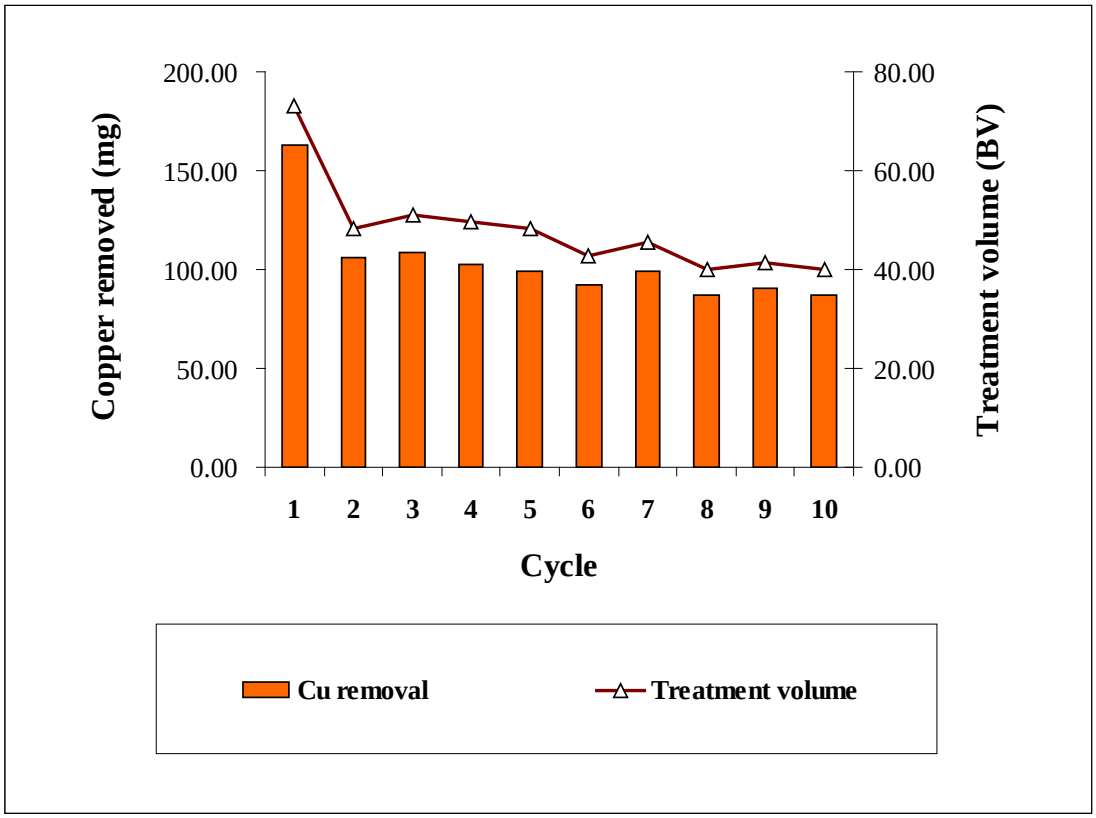

Figure 4.70. Copper removals and treatment volume of RIM column in ten sequential cycles of integrated treatment of industrial electroplating wastewater.

* Experimental conditions are listed in Table 4.46.

Table 4.46. Experimental conditions of integrated industrial wastewater treatment by RIM column (Section 4.6.4).

Biosorption	**Desorption**
– C_o = 50 mg-Cu/L (The industrial sewage was diluted from the original sewage sample collected from the electroplating material supplier); – Q = 1 mL/min; – Z = 50 cm; – Concentration of *Micrococcus luteus* in the RIM beads = 0.133 g-cell/mL-beads; – Influent pH = 5.0 (NaOH or NH_4OH was used for the pH adjustment of the industrial sewage); – The process was conducted up to the breakthrough level (4 mg-Cu/L).	– C_o = 1 M $CaCl_2$; – Q = 1 mL/min; – The process was continued until 85% of copper content inside the biosorbent was desorbed.

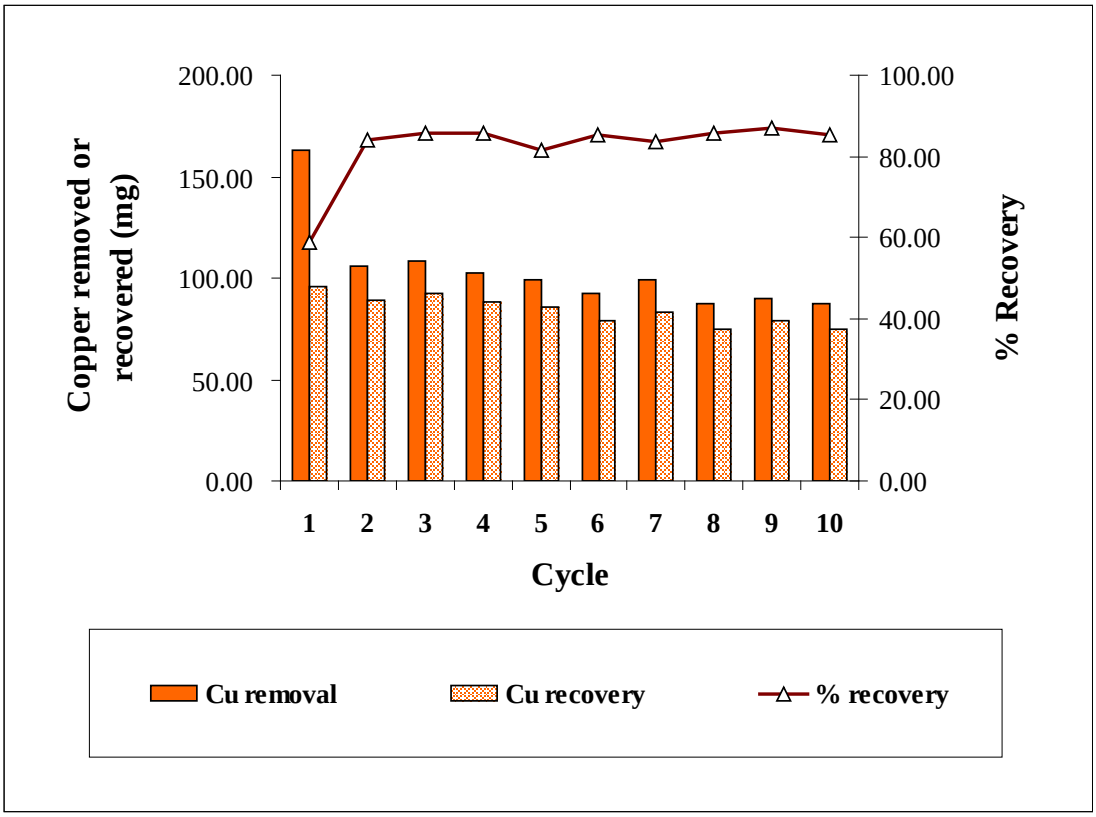

Figure 4.71. Copper removals and recoveries of RIM column in ten sequential cycles of integrated treatment of industrial electroplating wastewater.

* Experimental conditions are listed in Table 4.46.

Table 4.47. Copper removals and recoveries of RIM column in ten sequential cycles of integrated treatment of industrial electroplating wastewater.

Cycle	Biosorption		Desorption		Copper accumulation	
	Copper removal (mg) [(a)]	Performance retained (%) [(b)]	Copper recovery (mg) [(c)]	Copper recovery (%) [(d)]	Copper retained (mg) [(e)]	Net copper retained in biosorbents (mg) [(f)]
1	163.03		95.88	58.81	67.15	67.15
2	105.96	64.99	88.88	83.88	17.08	84.23
3	108.43	66.51	92.80	85.58	15.63	99.86
4	102.76	63.03	88.04	85.68	14.72	114.58
5	99.38	60.96	85.49	81.31	13.89	128.47
6	92.36	56.65	78.76	85.27	13.60	142.07
7	99.45	61.00	83.21	83.67	16.24	158.31
8	87.14	53.45	74.83	85.88	12.31	170.62
9	90.31	55.39	78.58	87.02	11.73	182.35
10	87.26	53.52	74.39	85.25	12.87	195.22

- Fixed-bed biosorption conditions: C_o = 50 mg-Cu/L; Q = 1 mL/min; Z = 50 cm; Solution pH = 5.0; [*Micrococcus luteus*] = 0.133 g-cell/mL-beads; The process was conducted up to the breakthrough level (4 mg-Cu/L);
- Fixed-bed desorption conditions: C_o = 1 M $CaCl_2$; Q = 1 mL/min; The process was continued until 85% of copper content inside the column bed was desorbed;
- Calculation:

(b) Biosorption performance retained (%) = (a) $_{\text{Cycle n}}$ / (a) $_{\text{Cycle 1}}$;
(d) Copper recovery (%) = (c) / (a);
(e) Copper accumulation (mg) = (a) – (c);
(f) Net amount of copper retained in biosorbents = $\sum_{n=1}^{10}(e)$.

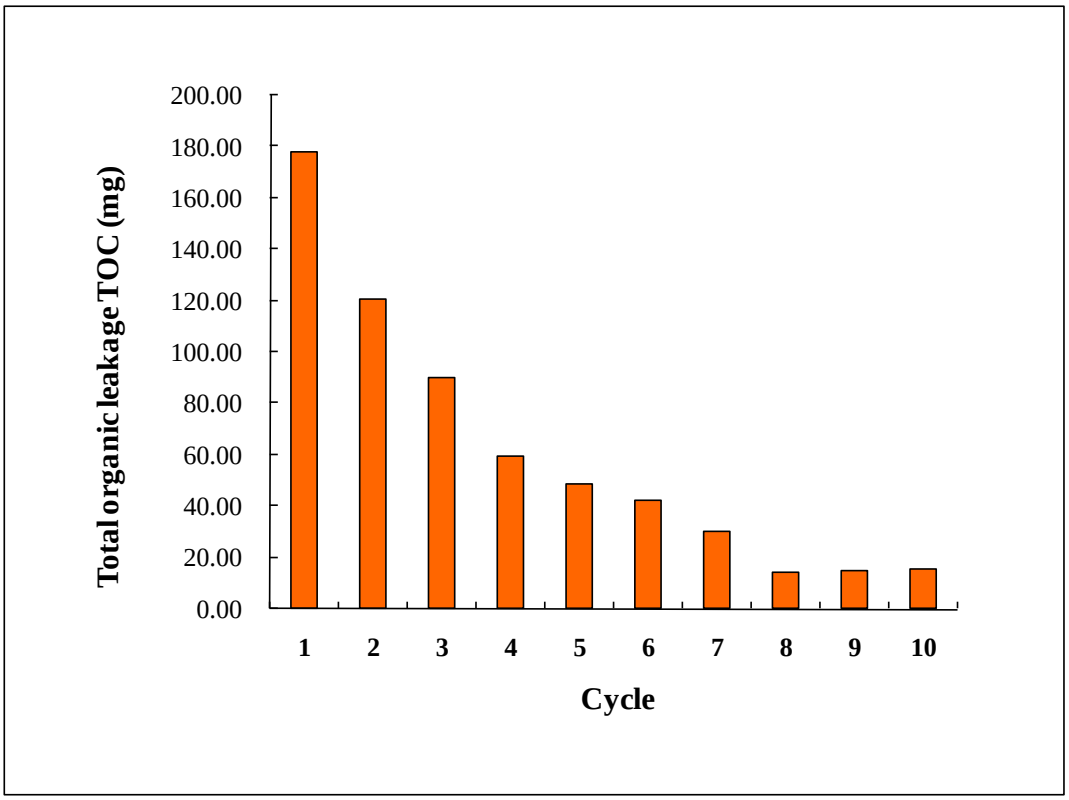

Figure 4.72. Organic leakage of RIM column in ten sequential cycles of integrated treatment of industrial electroplating wastewater.

* Experimental conditions are listed in Table 4.46.

4.7 Re-use of desorbed copper: electroplating

In the integrated treatment (Section 4.6.4), the RIM column showed reasonable efficiencies in copper removal and recovery throughout the ten sequential cycles. The biosorption/desorption process effectively converted about 20.88 L pre-conditioned industrial electroplating wastewater to 9.84 L concentrated-copper desorption effluent. Such effluent can be used again in the manufacturing process. However, there is a lack of investigation or successful demonstration on reuse of desorbed metal ions from the desorption effluent. This section reports the experimental work done to demonstrate the re-use of the desorbed copper in a practical copper electroplating process.

As described in Section 3.6.2 and Fig. 3.2, the copper(II) ions were recovered from the desorption effluent as $CuHPO_4$ salt by a two-step purification process using Na_2SO_4 and Na_2HPO_4. After the purification process, the recovered $CuHPO_4$ salt was introduced into an acid copper plating bath for carrying out the copper electroplating. The procedures and conditions of the plating process were described in Section 3.6.3 and Table 3.3. The effect of the recovered $CuHPO_4$ salt on the plating process was investigated by evaluating properties of the deposited workpiece, including the overall appearance, deposit distribution, coverage, copper purity on the deposits and electrical resistance. These properties were further compared with those of the workpieces obtained by using a conventional acid copper plating solution in order to test the feasibility of the reuse of recycled copper in the electroplating process.

4.7.1 Copper purification from fixed-bed desorption effluent

Before the electroplating studies, a purification process of the desorbed copper was developed to prepare a copper salt with a high purity in order to meet the plating requirements. The details of the process are presented in Section 3.6.2 and Fig. 3.2. This step was essential because the copper concentration in the desorption effluent was far lower than that of the desired plating solution (Table 4.48), and also a large amount of calcium ions (around 1 M) was present in the effluent. If this effluent solution, containing an insufficient amount of copper ions and high content of calcium ions, was directly applied in the plating process, serious side reactions would be induced in the copper plating bath. This might degrade the plating performances, including appearances and characteristics of the copper deposits.

To carry out the purification process, fractions of the desorption effluent with cumulative copper concentrations of up to around 200 mg-Cu/L were collected and transferred to the purification unit. After thorough mixing, the effluent mixture with about 185.00 mg-Cu/L copper concentration was treated by the two-step precipitation process, which was designed by using a computer software 'MINEQL^{+}' for metal speciation simulation (Schecher and McAvoy, 1994). During the first purification step, 482.9 g of Na_2SO_4 was added to 3.3 L of the desorption effluent to precipitate the calcium ions as $CaSO_4$. Table 4.49 shows that a large amount of calcium ions could be successfully converted to $CaSO_4$ precipitate. Such precipitate could be sold out for other laboratory and

industrial uses, such as desiccant. During the second precipitation step, 100 mL of 1 M Na_2HPO_4 solution was mixed with 3.2 L of the supernatant to precipitate the aqueous copper ions as $CuHPO_4$. An outstanding yield (1607 mg) and a high purity (89.6%) of the $CuHPO_4$ salt were obtained. Also, a good performance of copper reclamation (up to 94.00%), which involved the biosorption, desorption and purification of the copper(II) ions, was achieved.

The entire integrated treatment process of this integrated system seems to involve many steps, including fixed-bed copper biosorption, column regeneration and two-step purification. However, compared with other conventional direct precipitation methods using NaOH and Na_2HPO_4, Table 4.50 shows that the highest purity of the reclaimed copper salt was achieved in the integrated treatment system with similar performance of the copper reclamation (with about 90%). Such pure copper salt could be directly re-used in the copper plating process. Moreover, the fixed-bed copper(II) biosorption/desorption process could remove other heavy metal contaminants in the copper-laden wastewater and could produce a concentrated-copper desorption effluent with a minimal amount of metal contaminants (Section 4.3.7). By contrast, an excess amount of NaOH and Na_2HPO_4 salts was required in the direct precipitation methods in order to achieve high efficiencies of the copper reclamations. Also, a copper precipitate of low purity was resulted in the direct precipitation methods using NaOH and $NaHPO_4$. The other matrix contaminants in the wastewater such as organic additives and heavy metal contaminants could

have precipitated simultaneously, resulting in copper precipitate of low purity. The purity of the reclaimed copper was too low to be re-used in the copper plating process.

The above results demonstrate that the treatment of the industrial electroplating wastewater using the integrated system (composed of the RIM column and purification tanks) is feasible. It has a list of advantages, including a large treatment volume and high efficiencies of the copper reclamation. Moreover, the copper salt of a high purity and a large amount of $CaSO_4$ powder can be recovered. These salts can be directly reused in the electroplating process and the industrial desiccation process, respectively. These can greatly reduce the production cost of the plating process as well as the treatment cost of wastewater.

Table 4.48. Concentration of copper in industrial copper plating solution and desorption effluent of integrated treatment.

	Acid copper (sulfate) plating solution*	Desorption effluent
Copper concentration	150 – 250 g/L $CuSO_4 \cdot 5 H_2O$ (Equivalent to 38185 – 63642 mg-Cu/L)	37.16 – 158.31 mg-Cu/L (Cumulative concentration)

* Data are quoted from Dini (2000).

Table 4.49. Performances of purification units in integrated treatment system.

	Supernatant			Precipitate		Cu reclamation
	Process volume	Cu content		Powder collected	Purity	
	(L)	(mg-Cu/L)	(mg-Cu)	(mg)	(%)	(%)
Desorption effluent	3.30	185.00	610.50	--	--	--
Na_2SO_4 precipitation (the first step of purification)	3.30	181.00	597.30	479508.00 ($CaSO_4$)	68.07 ($CaSO_4$)	97.84
Na_2HPO_4 precipitation (the second step of purification)	3.20	--	--	1607.30 ($CuHPO_4$)	89.64 ($CuHPO_4$)	94.00

* The solution pH was maintained at 5.0 during both the precipitation steps.

Table 4.50. Comparisons of different conventional processes for copper removal and recovery of the industrial electroplating wastewater.

	Integrated treatment process (Biosorption-Desorption-Purification)	NaOH precipitation	Na_2HPO_4 precipitation
Cu reclamation (%)	94.00	96.25 ± 4.21	100.30 ± 1.52
Treatment volume (mL)	20880	50	50
Purity of recovered copper (%)	89.24	15.70 ± 0.75	65.04 ± 6.22

4.7.2 Optimization of copper electroplating process

As suggested by Dini (2000), quite a few benefits, including a high plating efficiency, a low production cost, a simple process control and a low susceptibility by impurities, could be obtained when using an acid copper sulfate bath for electroplating. Moreover, some desired properties of workpieces, such as an excellent coverage, a high thermal conductivity, a low electrical resistance, and good leveling and brightness properties, can be acquired by the acid copper plating. Thus, this bath is widely used to produce decorative and functional coatings on surfaces of electrical wires, steel rolls, stainless cooking vessels, machine parts and optical instruments.

Generally, the bath is composed of several major components, including copper(II) sulfate, sulfuric acid, chloride ions and organic additives. This plating process is simple to operate by controlling the current density, agitation speed and plating time. However, the concentrations of these components and the plating conditions are usually optimized in order to fulfill the specifications and requirements of the products. Hence, studies were carried out to optimize these plating parameters. The experimental procedures are described in Section 3.6.3.

4.7.2.1 Effect of copper concentration

The aim of this study was to investigate the optimal copper concentration to obtain a desirable electrodeposited workpiece without overdose. The experimental parameters are listed in Table 3.3. Copper(II)

sulfate pentahydrate ($CuSO_4 \cdot 5H_2O$) was used to prepare the plating solutions since it is the most-commonly used salt in the acid copper plating.

Figs. 4.73 (a) to (f) show the appearances of the copper-deposited workpieces obtained by the plating solutions with different copper concentrations. Generally, a relatively adequate deposit layer was obtained in the middle section of the cathode workpieces, where moderate current densities were provided. In the left edge of the cathode plates, a burning area covered with a crumbly layer of powdery copper deposits was observed. This was because high current densities in this region induced a high electropotential. This accelerated the deposition rate over the upper diffusion limit of copper ions. The insufficient supply of copper ions and accumulation of excess electropotential would be developed that initiated the electrolysis of water molecules as shown in Equation 4.19. The released hydroxide ions then precipitated copper ions to form insoluble dark powders, which were further immobilized irregularly on the deposits. As a result, the deposits revealed the dark and burned appearances together with the non-adherent and powdery natures (Pletcher and Walsh, 1990). On the other hand, no deposition occurred at the opposite edge (the right hand side) due to the presence of a low current density that was insufficient to perform the electrodepostion. In addition, the deposition efficiencies were demoted under the acid-free plating conditions in this study due to the low conductivities of the plating media, anode and cathode (Dini, 2000).

$$2\,H_2O\,(l) + 2\,e^- \leftrightarrow 2\,OH^-\,(aq) + H_2\,(g)$$

Equation 4.19. Electrolysis of water molecules (Half-cell reaction).

As the copper concentrations increased, the burning area became smaller (Figs. 4.73 (a) to (f)). This was due to an increase in the supply and diffusion rate of copper ions in the plating solutions. The electrolysis of water molecules was thus inhibited together with the formation of the copper precipitates, resulting in a reduction of the burning area. By further increasing the copper concentrations to above 250 g/L $CuSO_4 \cdot 5H_2O$, highly-porous deposits with rough surface were observed as shown in Figs. 4.73 (e) and (f). This was due to a local copper deposition (Ludwig, 2003). As the plating was performed near the solubility limit of copper sulfate, a rapid growth of giant copper crystals on the deposit nuclei would be initiated that inhibited the formation of new nuclei and limited the rearrangement of the nuclear lattice. Thus, local deposition was induced. The spongy deposit crystals with rough configurations were formed on the cathode surfaces. This phenomenon is usually called the 'spongy effect'.

In addition, some abnormal burnings occurred in the middle section of the cathode plates with moderate current densities in the cases below 150 g/L $CuSO_4 \cdot 5H_2O$ (Figs. 4.73 (a) and (b)). This might be related to the influence of agitation. The dark precipitate of copper hydroxide produced in the high current region could be carried to the middle section along the solution flow by agitation and then attached on the deposits. The abnormal burnings were thus observed.

Based on these results, relatively desirable copper deposits were only obtained by the plating processes corresponding to 150 and 200 g/L

$CuSO_4 \cdot 5H_2O$. These two concentrations were within the recommended range of the acid copper plating process (Table 2.11). Out of this concentration range (150 – 200 g/L $CuSO_4 \cdot 5H_2O$), either the burned deposits or the spongy surfaces would be unfavourably formed on the workpieces. In the case using 200 g/L of the copper salt, a broader range of current densities could be applied to obtain the desirable deposits (Table 4.51). Moreover, a better appearance of the deposit layer was observed (Fig. 4.73 (d)). The plating solution with 200 g/L $CuSO_4 \cdot 5H_2O$ was thus preferred to be used in the following studies.

(a) 50 g/L $CuSO_4 \cdot 5H_2O$

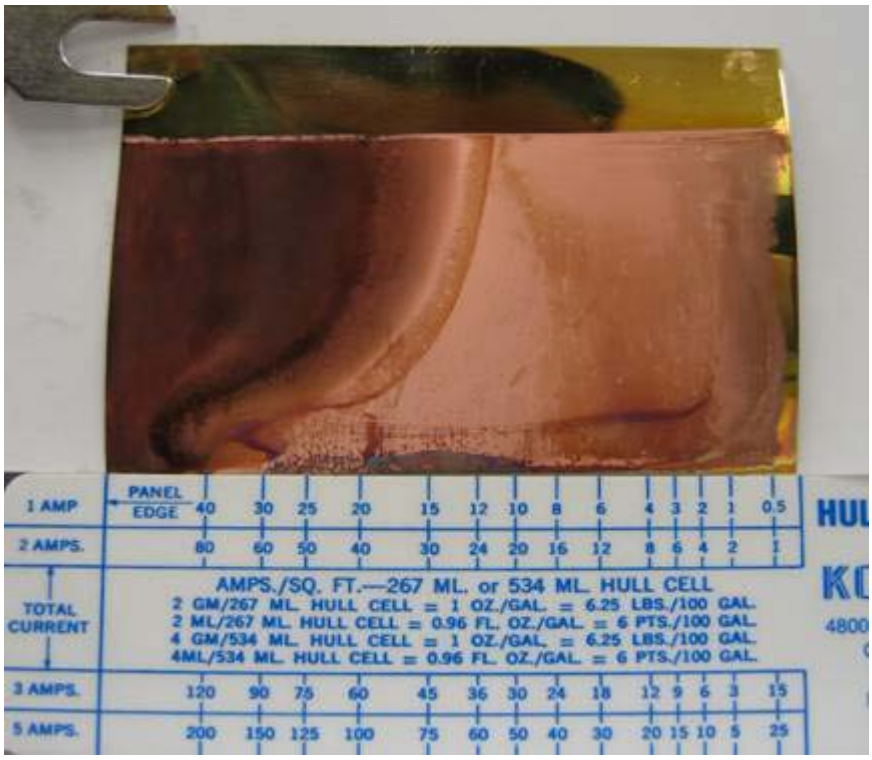

(b) 100 g/L $CuSO_4 \cdot 5H_2O$

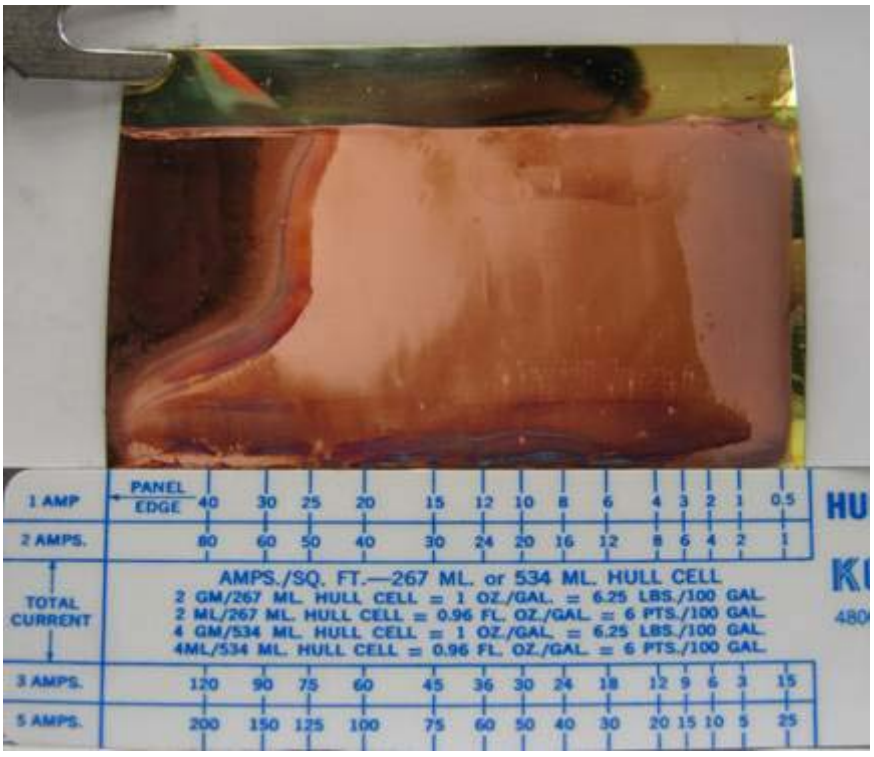

(c) 150 g/L $CuSO_4 \cdot 5H_2O$

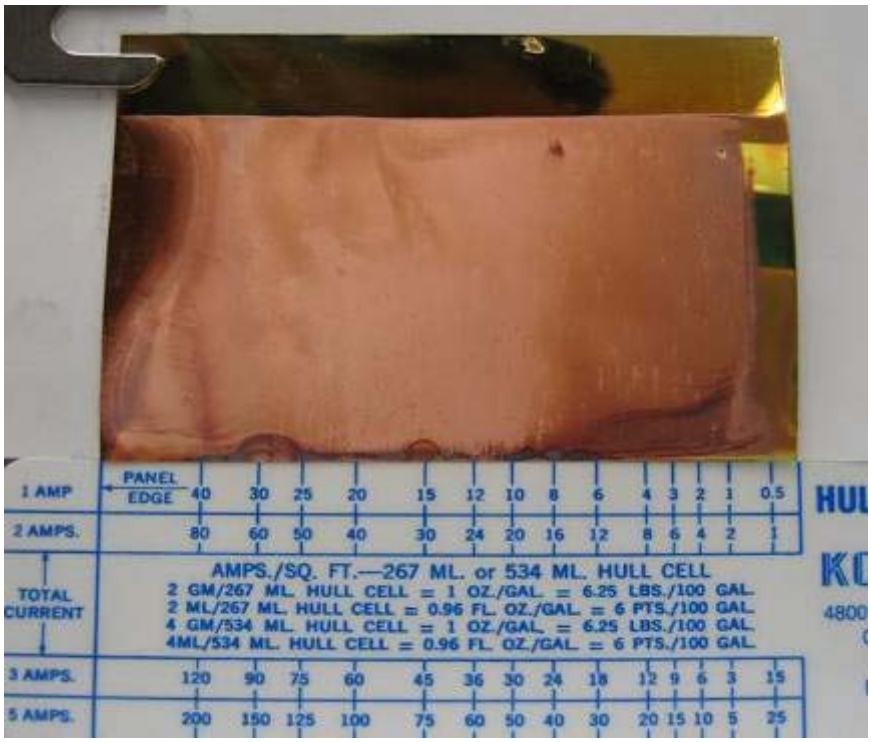

(d) 200 g/L $CuSO_4 \cdot 5H_2O$

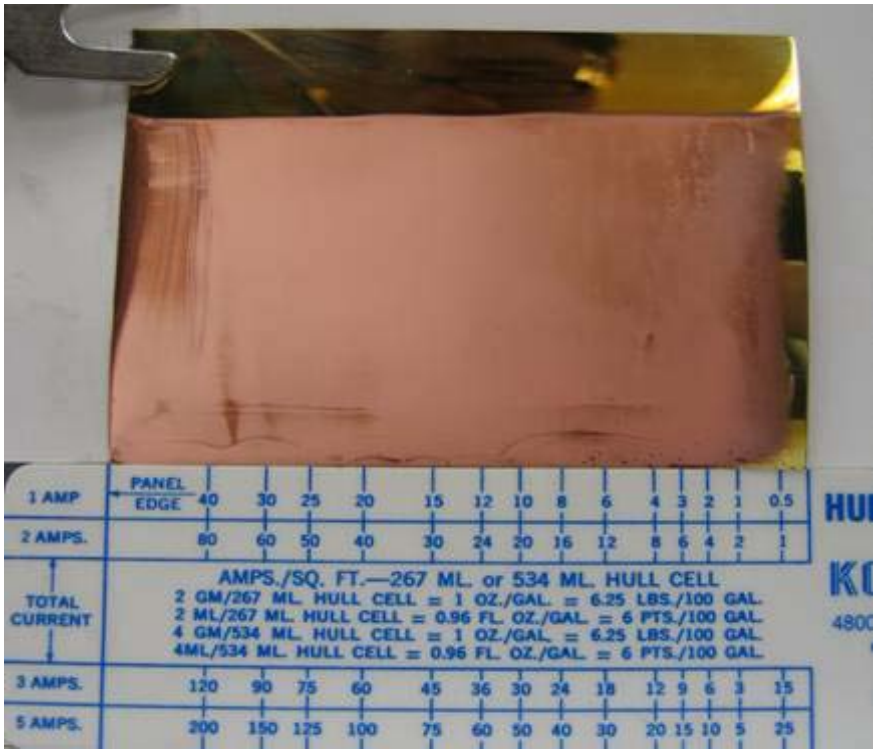

(e) 250 g/L $CuSO_4 \cdot 5H_2O$

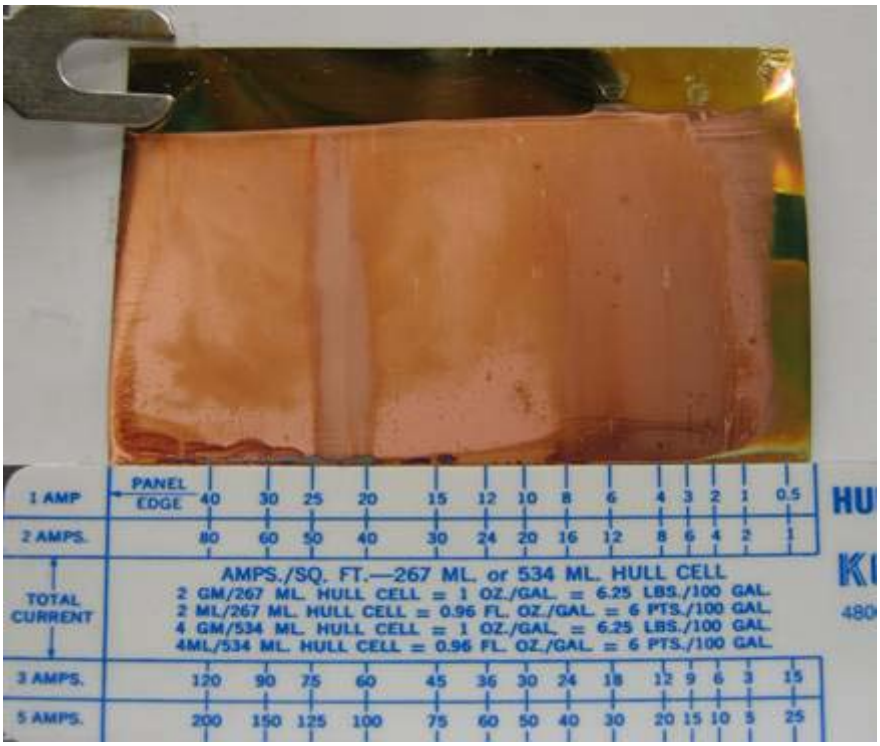

(f) 350 g/L $CuSO_4 \cdot 5H_2O$

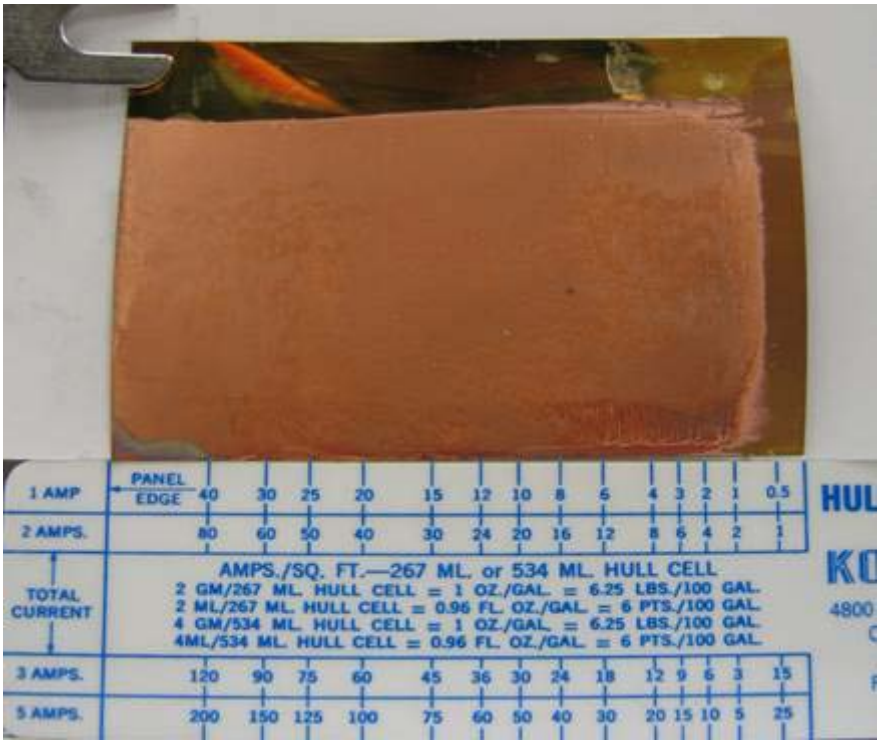

Figure 4.73. Appearances of plating workpieces in acid copper sulfate plating process with different copper concentrations: (a) 50 g/L $CuSO_4 \cdot 5H_2O$; (b) 100 g/L $CuSO_4 \cdot 5H_2O$; (c) 150 g/L $CuSO_4 \cdot 5H_2O$; (d) 200 g/L $CuSO_4 \cdot 5H_2O$; (e) 250 g/L $CuSO_4 \cdot 5H_2O$; (f) 350 g/L $CuSO_4 \cdot 5H_2O$.

* Plating conditions are listed in Table 4.51.

Table 4.51. Ranges of current densities for desirable copper depositions under different copper concentrations in plating solutions.

Concentration of $CuSO_4 \cdot 5H_2O$ (g/L)	Range of current densities
50	No acceptance
100	No acceptance
150	20 – 40 A/dm^2
200	20 – 70 A/dm^2
250	No acceptance
350	No acceptance

Remarks:

- Plating conditions: Current = 2 A; Agitation speed = 200 rpm; Plating time = 10 min (listed in Table 3.3);
- The range of current densities applied across the whole area of the workpieces was 0 – 80 A/dm^2;
- The morphological diagrams of the workpieces are displayed in Figs. 4.73 (a) to (f).

4.7.2.2 Effect of sulfuric acid concentration

Sliman *et al*. (1978) indicated that sulfuric acid in an acid copper plating could enhance the electrical conductivities of the plating solution, anode and cathode. These enhancements greatly reduced power consumption and inhibited the formation of rough and treed deposits (dendrites) at high current densities. However, as the acid concentration reached the upper limit, such benefits would be lost and the plating performances would drop seriously (Dini, 2000). In order to find out the optimal concentration of sulfuric acid, the plating experiment was performed with the conditions listed in Table 3.3.

As shown in Figs. 4.74 (a) to (g), the copper deposits displayed a better appearance in the presence of sulfuric acid. The deposit grains became fine and were evenly distributed on the workpieces, particularly in the region with low current densities (the right edge). This was because the acid could consume the excess electropotential through the reduction of protons as shown in Equation 4.20. This slowed down the copper deposition rate. The formation of the new deposit nuclei and the re-arrangement of the deposit lattices could then be carried out. The uniform distribution of the fine deposit grains would be obtained. On the other hand, no burning and agitation influence were found on the workpieces. This was also mainly attributed to the proton reduction. The reaction could successfully inhibit the electrolysis of water molecules by consuming the excess electropotential. Moreover, the acid could promote

the dissolution of the dark copper hydroxide precipitate. Thus, less or even no burned deposits could be formed on the workpieces.

$$2H^+(aq) + 2e^- \leftrightarrow H_2(g)$$

Equation 4.20. Reduction of protons (Half-cell reaction).

However, a poor coverage by the copper deposits and a low degree of the deposition were found in the high current region (left edge) under the acidic conditions (Figs. 4.74 (b) to (g)). These were related to the extensive reduction of protons, which was promoted by the excess electropotential in such region. The protons would thus compete with copper ions on the cathode surface, resulting in a strong inhibition of the copper deposition and inducing the poor coverage. As the acid concentrations were raised to 75 g/L, a yellowish brown colour was also revealed on the deposits. This might be due to the acid attack of the copper deposits. Both the yellowish appearance and the poor coverage would be worse with a further increase in the acid concentrations. As a result, the range of current densities for the desirable deposition was greatly narrowed (Table 4.52).

In the extreme case, the solubility of copper ions dramatically decreased when the plating solution was prepared by 200 g/L sulfuric acid (the highest acid concentration). A large amount of copper colloids was precipitated and suspended in the solution. The supply of copper ions was then greatly suppressed. Beside this problem, the extensive proton

reduction and the acid attack also occurred in this case. As a result, the worst deposit appearance was produced (Fig. 4.74 (g)). This indicated that 200 g/L sulfuric acid reached the upper limit of the acid concentration in this plating process.

To conclude, the optimal acid concentration should be 50 g/L sulfuric acid. Under this condition, the coverage by the copper deposits was the best and the least acid attack was found, as shown in Fig. 4.74 (c). Moreover, the desirable deposition could be produced in the broadest range of current densities (Table 4.52). Therefore, this concentration was used in the following studies.

(a) 0 g/L H_2SO_4

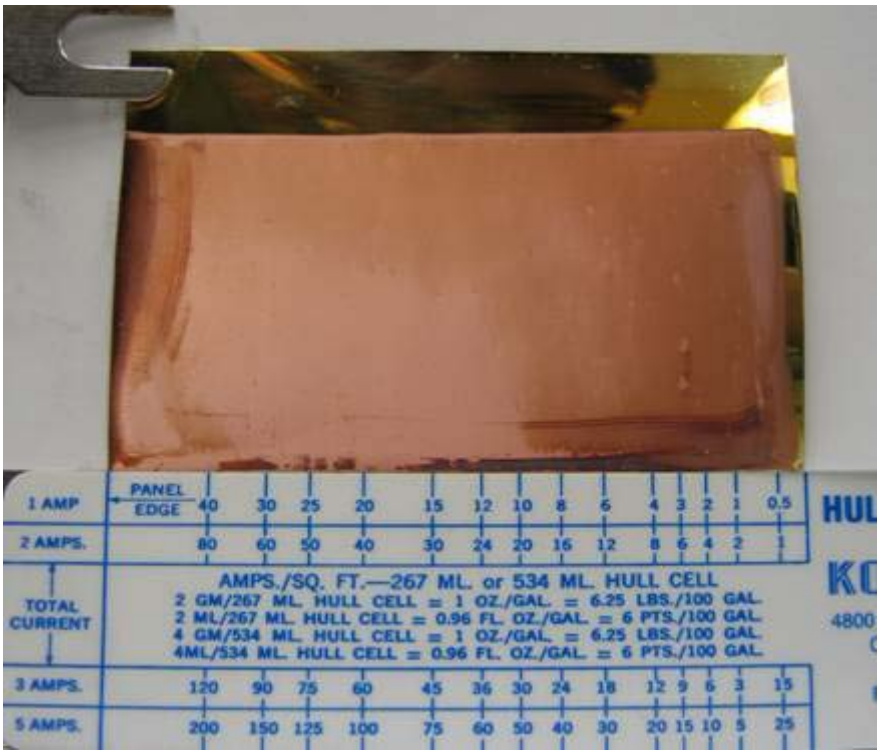

(b) 25 g/L H_2SO_4

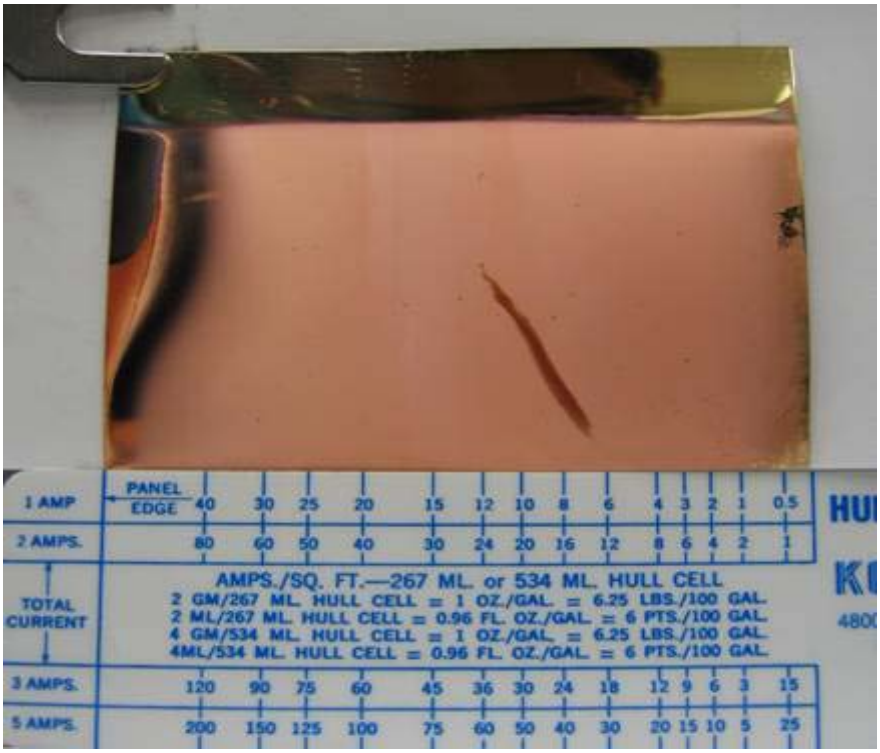

(c) 50 g/L H_2SO_4

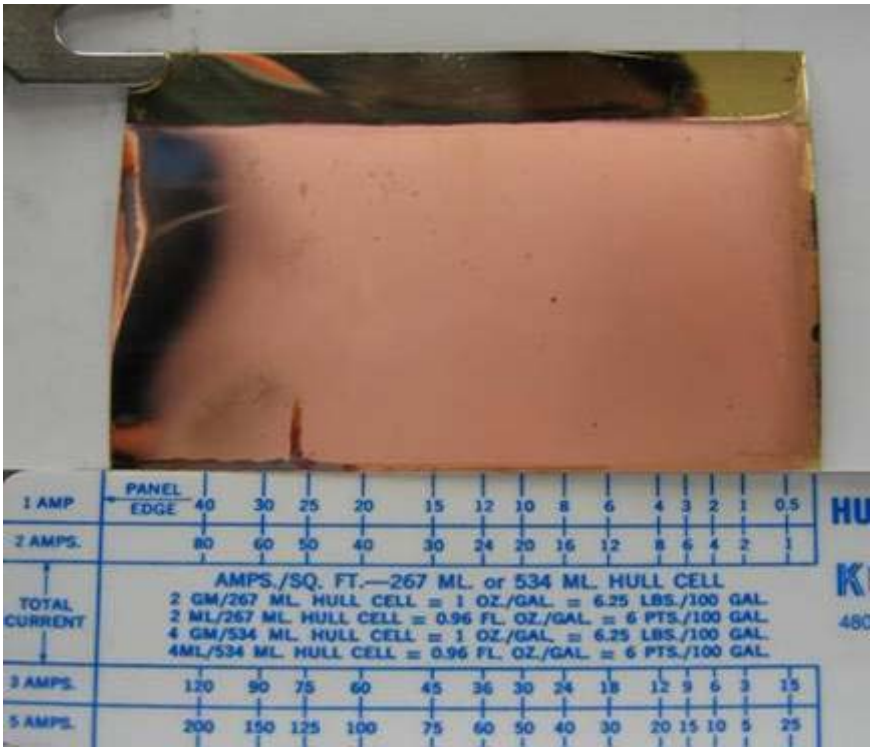

(d) 75 g/L H_2SO_4

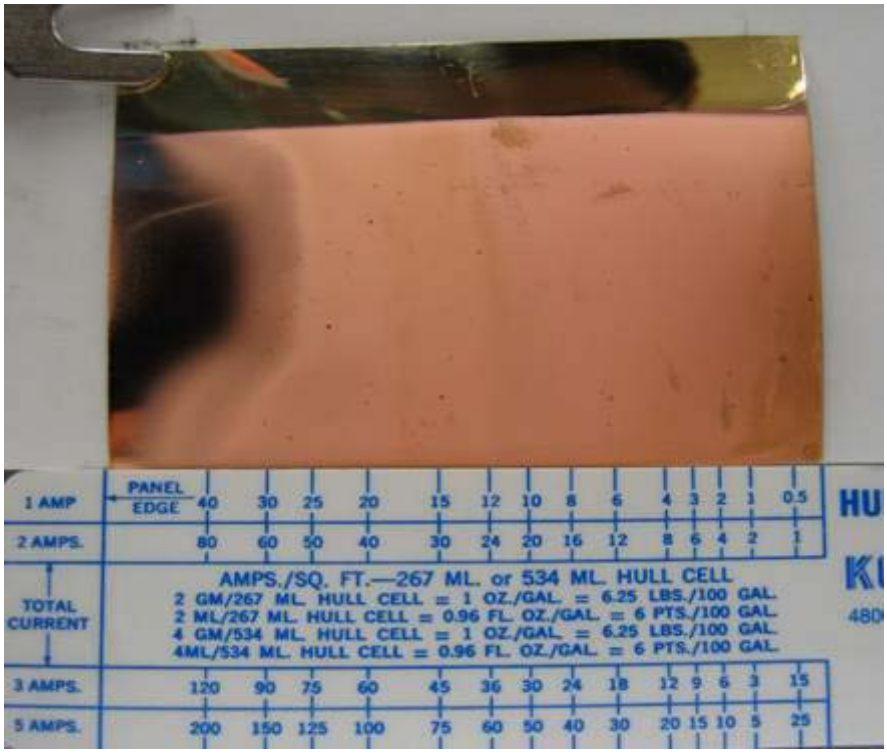

(e) 100 g/L H_2SO_4

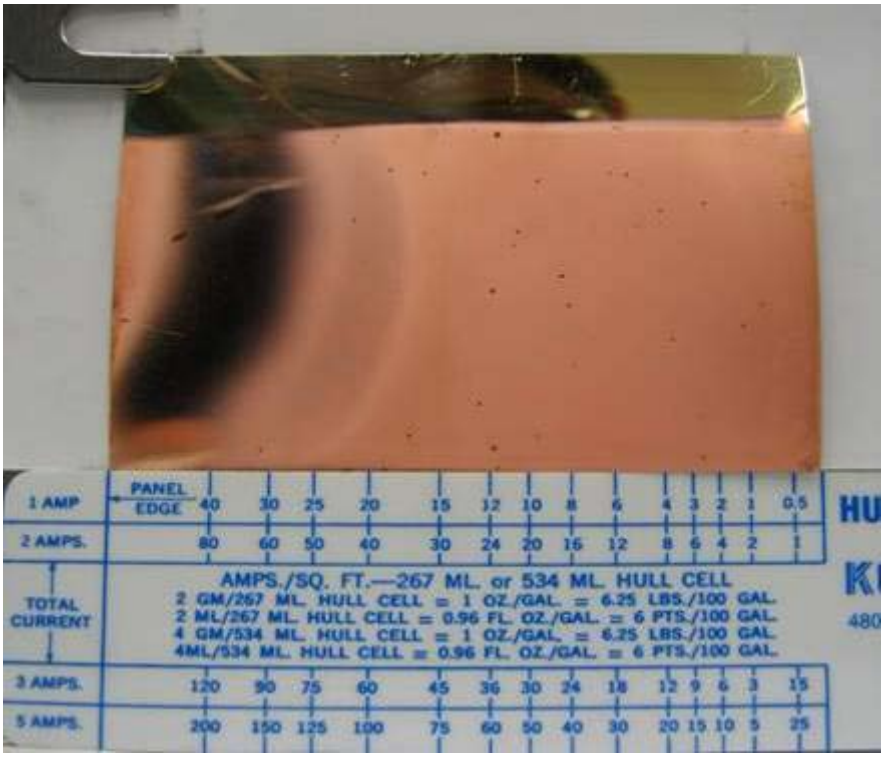

(f) 150 g/L H_2SO_4

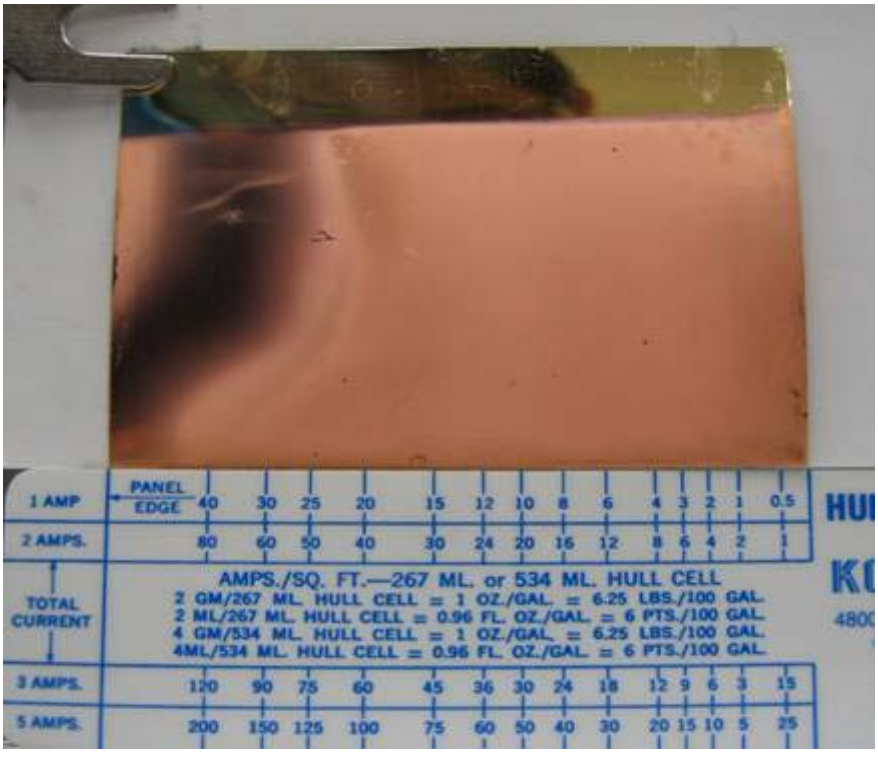

(g) 200 g/L H_2SO_4

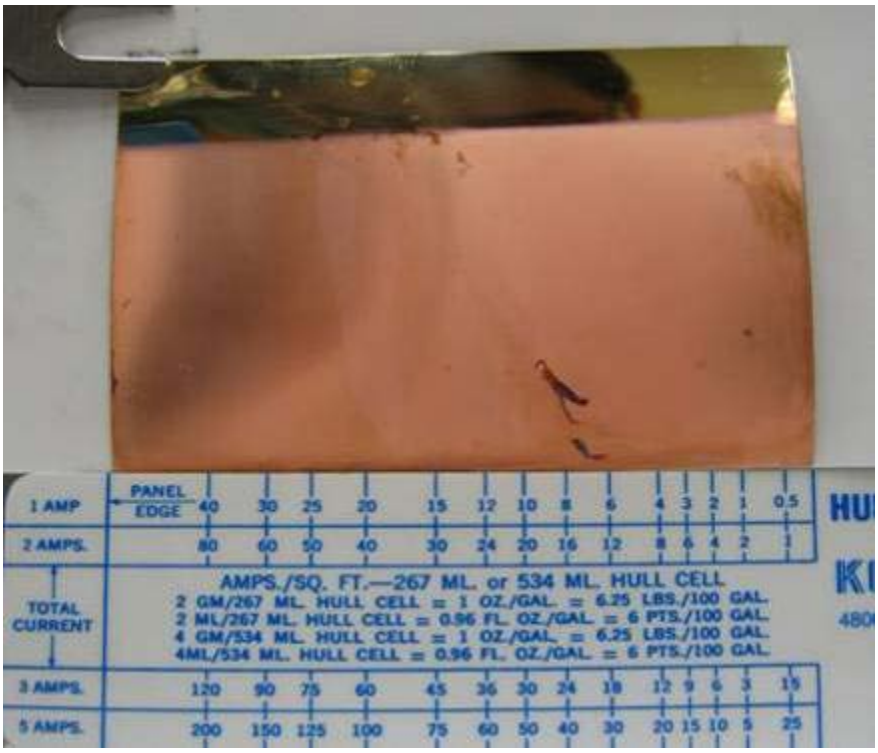

Figure 4.74. Appearances of plating workpieces in acid copper sulfate plating process with different concentrations of sulfuric acid: (a) 0 g/L H_2SO_4; (b) 25 g/L H_2SO_4; (c) 50 g/L H_2SO_4; (d) 75 g/L H_2SO_4; (e) 100 g/L H_2SO_4; (f) 150 g/L H_2SO_4; (g) 200 g/L H_2SO_4.

* Plating conditions are listed in Table 4.52.

Table 4.52. Ranges of current densities for desirable copper depositions under different concentrations of sulfuric acid in plating solutions.

Concentration of H_2SO_4 (g/L)	Range of current densities (A/dm^2)
0	20 – 70
25	2 – 60
50	2 – 60
75	4 – 50
100	3 – 35
150	4 – 30
200	No acceptance

Remarks:

- Plating conditions: Copper concentration = 200 g/L $CuSO_4 \cdot 5H_2O$; Current = 2 A; Agitation speed = 200 rpm; Plating time = 10 min (listed in Table 3.3);
- The range of current densities applied across the whole area of the workpieces was 0 – 80 A/dm^2;
- The morphological diagrams of the workpieces are displayed in Figs. 4.74 (a) to (g).

4.7.2.3 Effect of chloride concentration

Chloride concentration is one of the most important parameters in bright acid copper plating. It affects the surface appearance, structure and crystallographic orientation of the deposits. Moreover, the mechanical characteristics of the deposits, such as the microhardness, internal stress, ductility and elongation, can be significantly modified using the optimal chloride concentration. Sodium chloride salt and hydrochloric acid usually act as the chloride source. Ludwig (2003) reported that both the chloride sources could function well within the concentration range of 30 to 120 mg-Cl^-/L. Out of this range, matt deposits would be formed. In the extreme case, excess chloride could produce insoluble copper(I) chloride on the anode surface and further hinder the electroplating process. Thus, the chloride concentrations should be strictly controlled. In order to obtain a desirable plating workpiece, the chloride concentration was optimized by following the experimental conditions in Table 3.3.

Figs. 4.75 (a) to (h) show the deposit appearances obtained from the plating solutions that contained different chloride concentrations, ranging from 0 to 300 mg-Cl^-/L. In the presence of chloride ions, the plating workpieces were deposited well with a good coverage by a smooth layer of fine copper grains. This was because chloride ions could suppress the copper deposition through the formation of copper-chloride complexes, which slowed down the mass transfer rate and deposition rate of the copper species (Milad, 2001). This would inhibit the extensive growth of the giant copper crystals and promote the re-arrangement of the deposit lattices,

resulting in a better organization and a closely-packed structure of the copper deposits. Thus, a smooth deposit layer was observed. Such suppression by chloride ions could also inhibit the proton reduction through lowering the proton supply to the cathode. The competitive influence of the protons would be reduced at the high current region. As a result, a better coverage of the deposits was achieved in the presence of chloride ions. The desirable deposits could then be obtained in a broader range of current densities (Table 4.53).

When the mass transfer and the electrodeposition of copper ions and protons were inhibited by chloride ions, the excess electropotential at the high current region would promote the electrolysis of water molecules, as discussed in Section 4.7.2.1. This induced the formation of the burned and loose deposits again (Figs. 4.75 (a) to (h)). As the chloride concentrations were further increased to above 150 mg-Cl^-/L, an extension of the burning areas was observed.

On the other hand, Figs. 4.75 (a) to (h) also show that matt deposits were observed in the low current region of the workpieces as the concentration of chloride ions was raised to above 75 mg-Cl^-/L. Dini (2000) explained that the matt was related to the formation of deposit dendrites. In the low current region, the electropotential was so low that it might be insufficient to completely break down the copper-chloride complexes during the deposition. These complexes would then be immobilized together with the copper deposits. This distorted the

arrangement of the deposit grains and even promoted the formation of the treed dendrites. These caused a rough deposit surface and a dull appearance. Such undesirable matt areas were enlarged (Figs. 4.75 (d) to (h)) and the preferred range of current densities was narrowed (Table 4.53) while increasing the chloride concentration further in the plating bath. These were due to an increase in the chloride adhesion to the deposits.

Figs. 4.75 (a) to (h) show that the plating solution with 75 mg-Cl^-/L could obtain a more desirable appearance with less burning and matt area. Also, the range of current densities for the desirable deposition was among the broadest (Table 4.53). Therefore, this optimal condition was used in the following studies.

(a) 0 mg-Cl^-/L

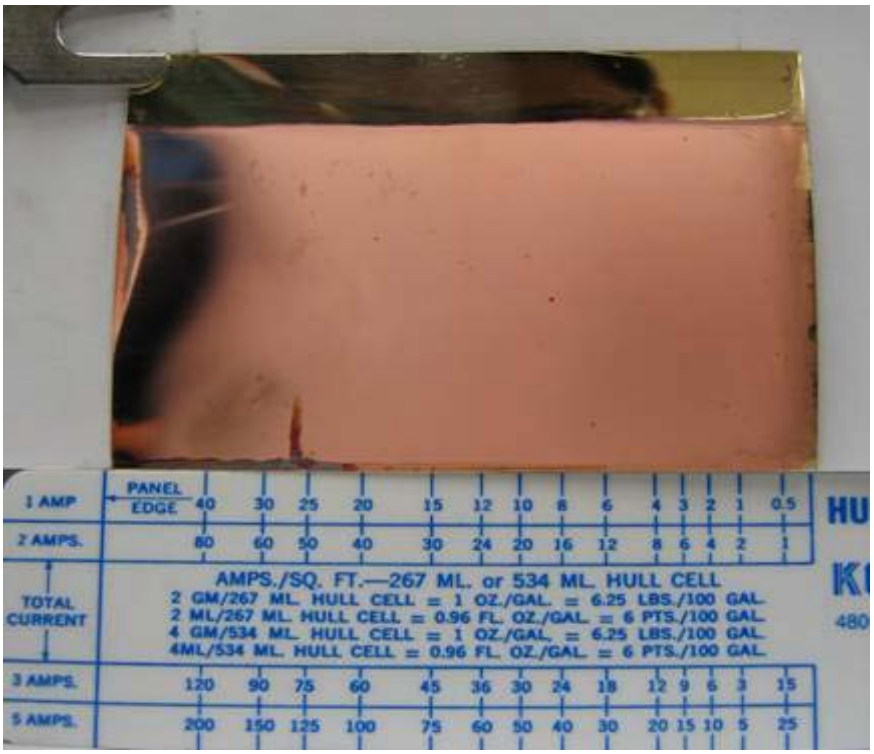

(b) 15 mg-Cl^-/L

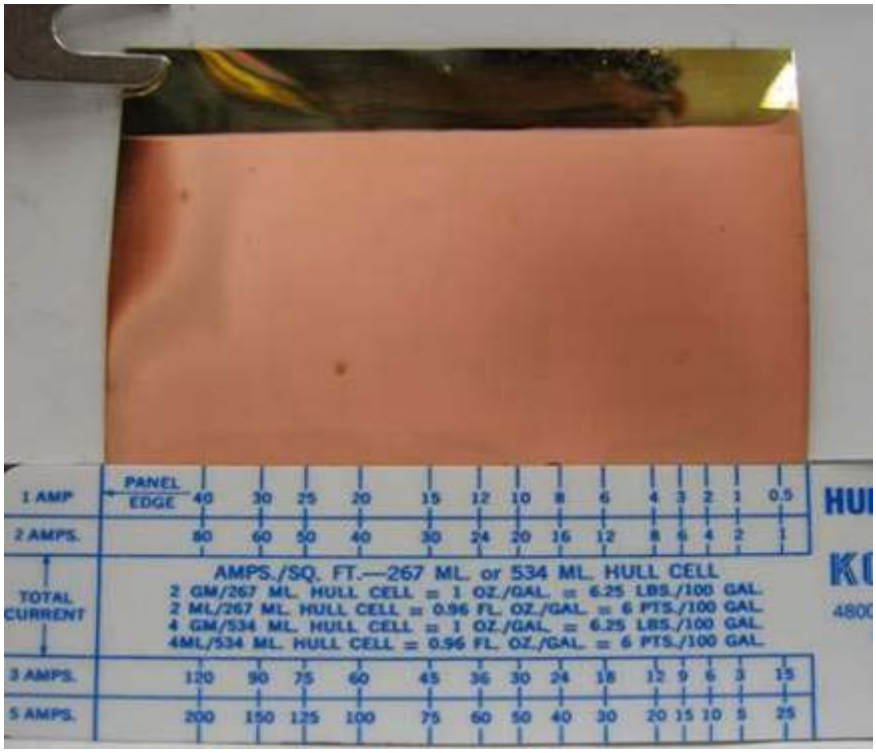

(c) 30 mg-Cl^-/L

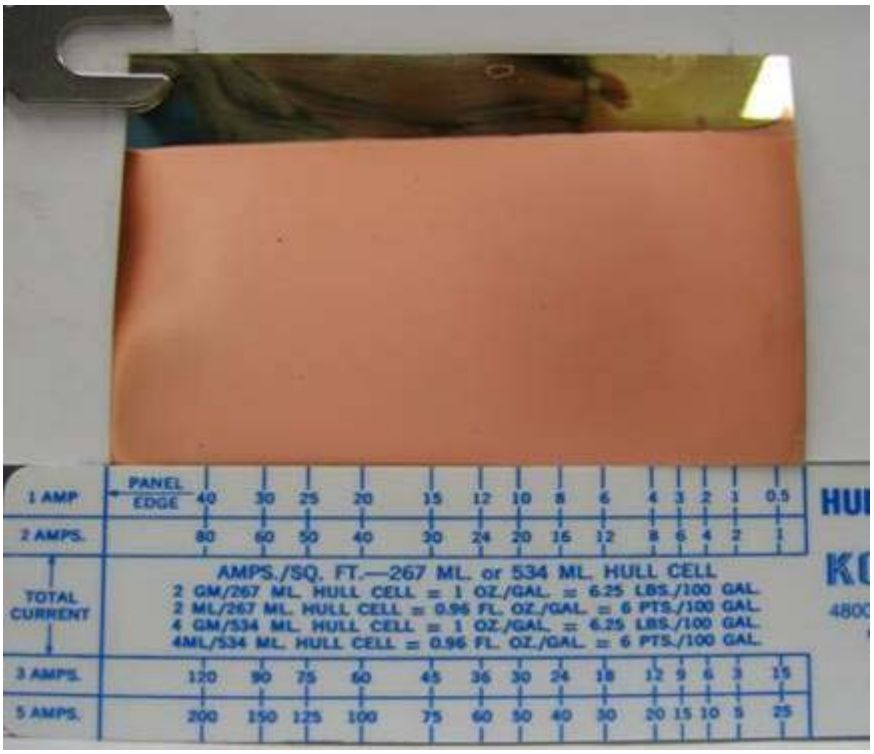

(d) 75 mg-Cl^-/L

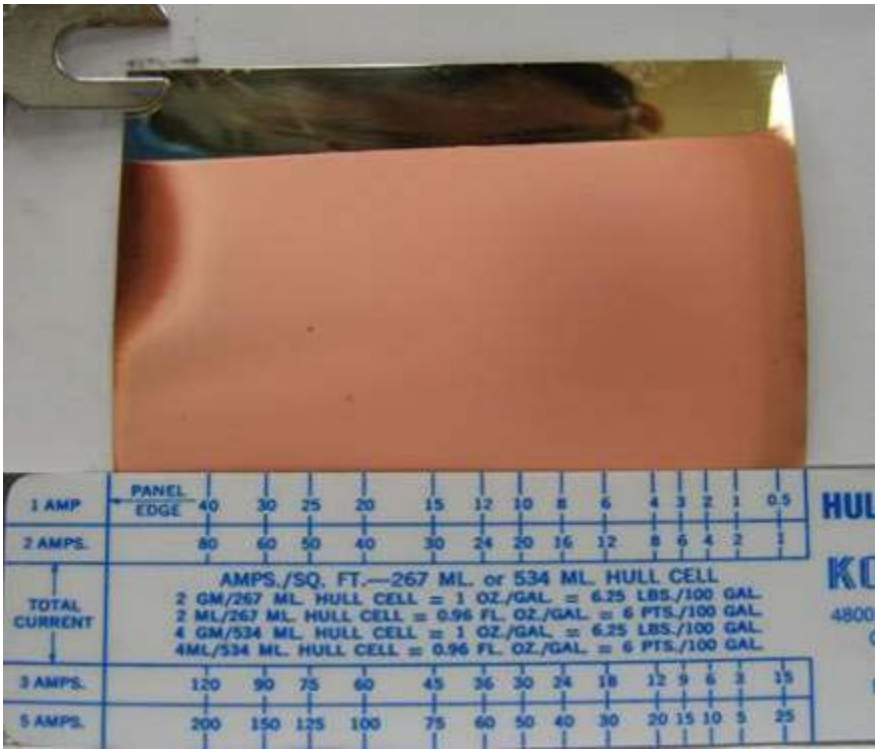

(e) 120 mg-Cl^-/L

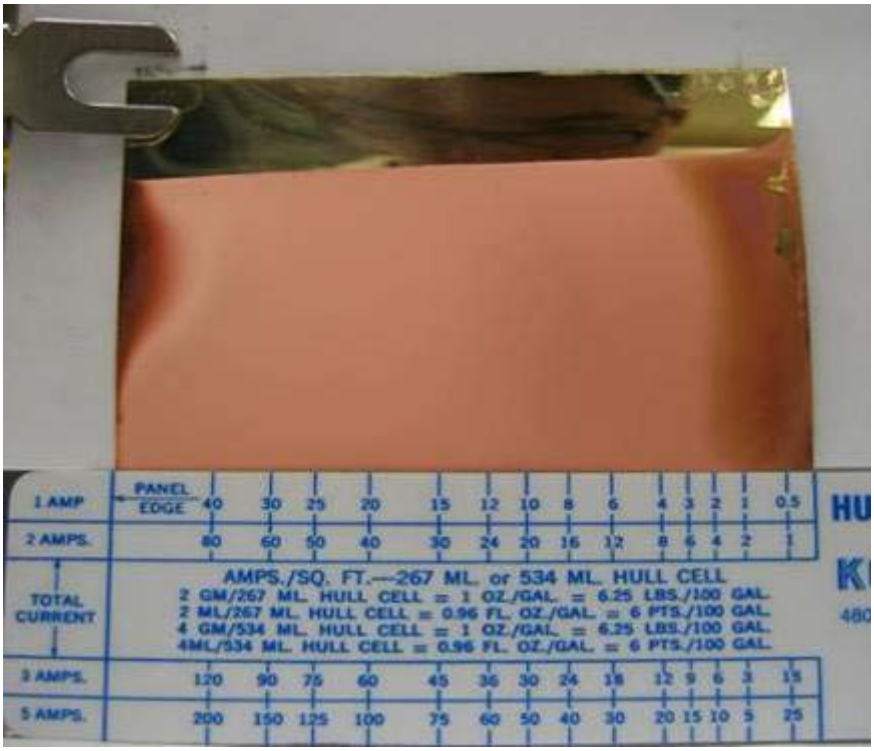

(f) 150 mg-Cl^-/L

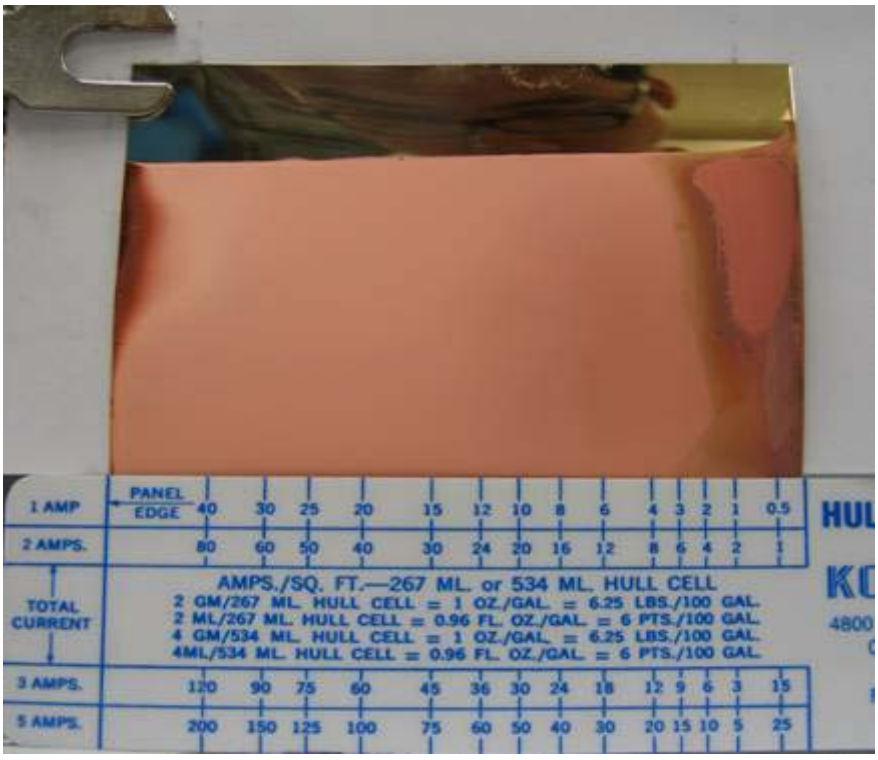

(g) 200 mg-Cl^-/L

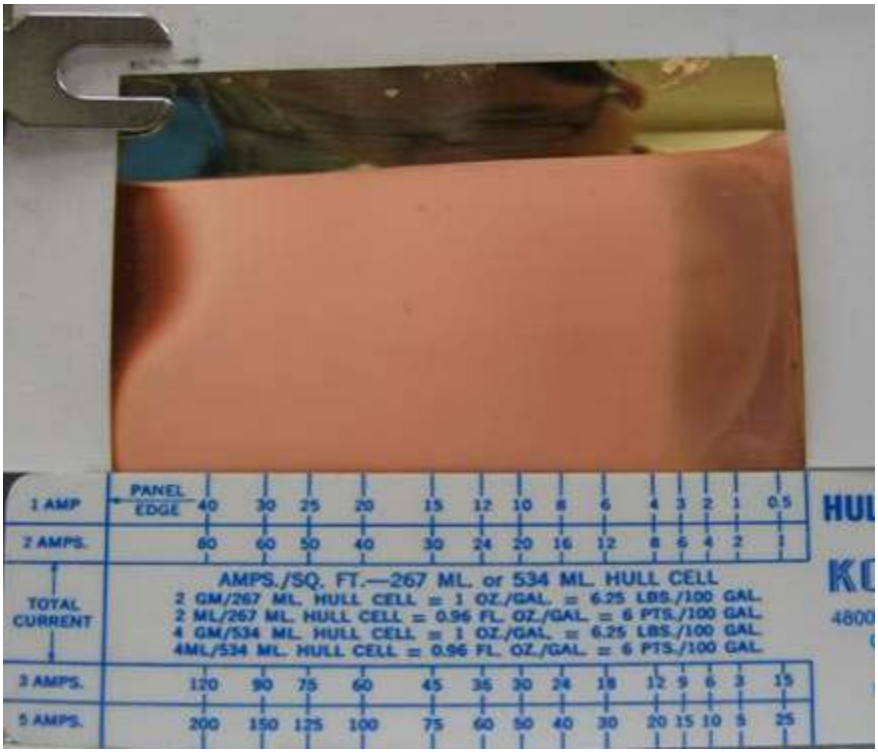

(h) 300 mg-Cl^-/L

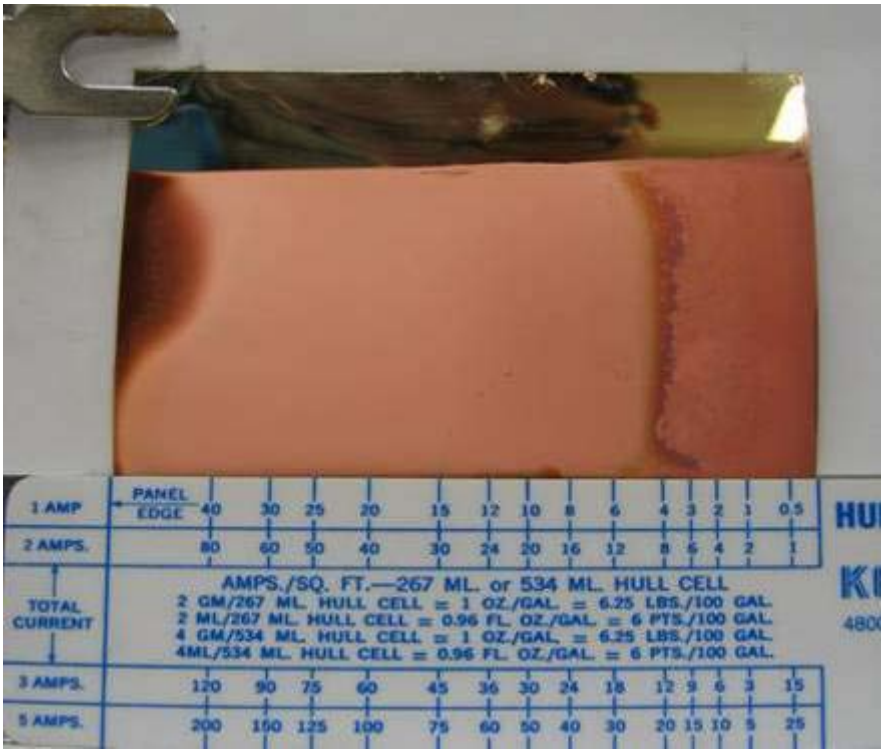

Figure 4.75. Appearances of plating workpieces in acid copper sulfate plating process with different chloride concentrations: (a) 0 mg-Cl^-/L; (b) 15 mg-Cl^-/L; (c) 30 mg-Cl^-/L; (d) 75 mg-Cl^-/L; (e) 120 mg-Cl^-/L; (f) 150 mg-Cl^-/L; (g) 200 mg-Cl^-/L; (h) 300 mg-Cl^-/L.
* Plating conditions are listed in Table 4.53.

Table 4.53. Ranges of current densities for desirable copper depositions under different chloride concentrations in plating solutions.

Concentration of chloride (mg/L)	Range of current densities (A/dm^2)
0	2 – 60
15	1 – 65
30	1 – 75
75	1.5 – 75
120	6 – 80
150	8 – 80
200	7 – 80
300	12 – 80

Remarks:

- Plating conditions: Copper concentration = 200 g/L $CuSO_4 \cdot 5H_2O$; Acid concentration = 50 g/L H_2SO_4; Current = 2 A; Agitation speed = 200 rpm; Plating time = 10 min (listed in Table 3.3);
- The range of current densities applied across the whole area of the workpieces was 0 – 80 A/dm^2;
- The morphological diagrams of the workpieces are displayed in Figs. 4.75 (a) to (h).

4.7.2.4 Effect of organic content

Organic additives are frequently used in modern electroplating. They generally act as modifiers to reduce the formation of the dendrites and enhance the brightness, hardness and smoothness of the deposit surfaces (Dini, 2000). Over hundreds of patented organic additives have been developed specifically for the acid copper plating, such as polyethylene glycol, polypropylene glycol, polyvinyl alcohol, derivatives of thiourea organic sulphur compounds, organic phosphorus compounds and organic dyesuffs (Ludwig, 2003). Such compounds are often applied individually or used in combination. In this study, the effect of organics was investigated by using a common brightener, polyvinyl alcohol (PVA) with molecular weights ranging from 30,000 to 70,000. The experimental conditions are stated in Table 3.3.

By introducing different contents of the PVA, a slight enhancement on the surface brightness of the deposits was observed (Figs. 4.76 (a) to (e)). The working principle of this polymer was similar to the suppressive function of chloride ions that lone-pair electrons in hydroxyl groups (–OH) or conjugate oxide groups ($–O^-$) of the PVA might interact with aqueous copper ions to form bulky copper-PVA intermediates. The overall mass transfer rate of copper towards the cathode would be decelerated, inducing a slower copper deposition rate. This then inhibited the extensive growth of the coarse deposit grains and promoted the deposit refinement. As a result, smooth and bright deposit layers could be obtained.

However, this brightening effect was not significantly enhanced with an increase in the PVA content. This implied that a small dose of the PVA could provide sufficient metal binding groups to effectively form the copper-polymer intermediates. Some bulky complexes and foam were observed during the plating when the PVA content increased further to 0.5%. These might be attributed to the presence of excess PVA, which might bind with the copper-PVA intermediates to form the bulky complexes and further trap air to form the foam. The complexes and foam may further attach on the surface of the workpieces, interrupt the uniform copper deposition and even induce the deposition of the copper-polymer complexes. As a result, undesirable blur-like deposit surfaces were observed (Figs. 4.76 (d) and (e)) and no acceptable range of current densities could be obtained (Table 4.54).

Furthermore, as the PVA content increased, the copper deposition was further suppressed and the electrolysis of water molecules was promoted. This induced an increase in the burning area of the deposits (Figs. 4.76 (a) to (e)). The explanation was discussed in Section 4.7.2.1.

Figs. 4.76 (a) to (e) show that the plating solution with 0.1% PVA could obtain a slightly brighter deposit with only a moderate burning. Also, no undesirable blurred appearance was found. Therefore, this condition was preferably used for further studies.

(a) 0%$_{wt}$ PVA

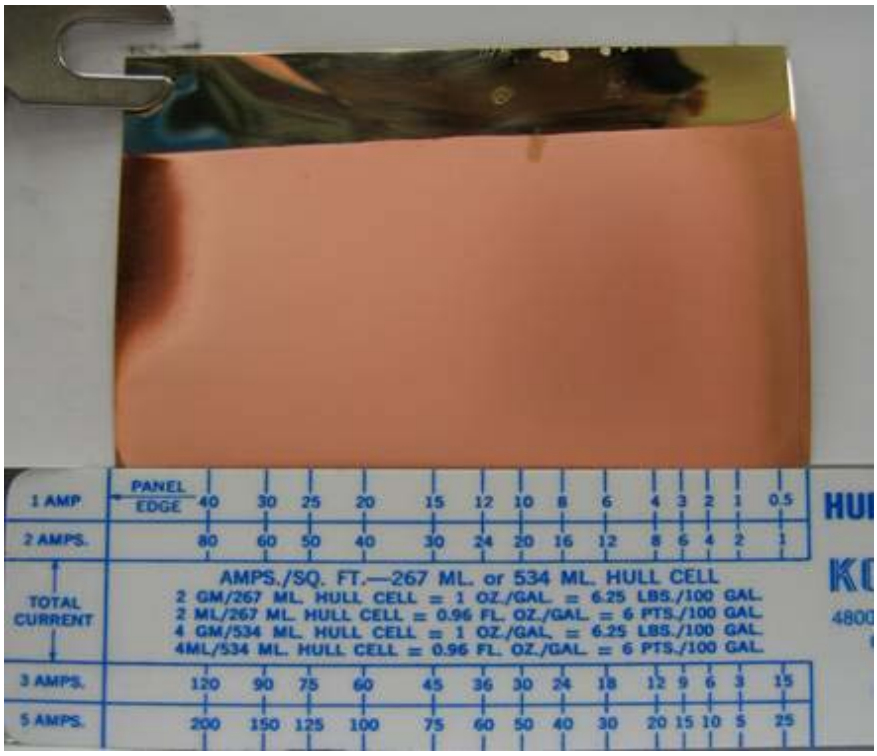

(b) 0.01%$_{wt}$ PVA

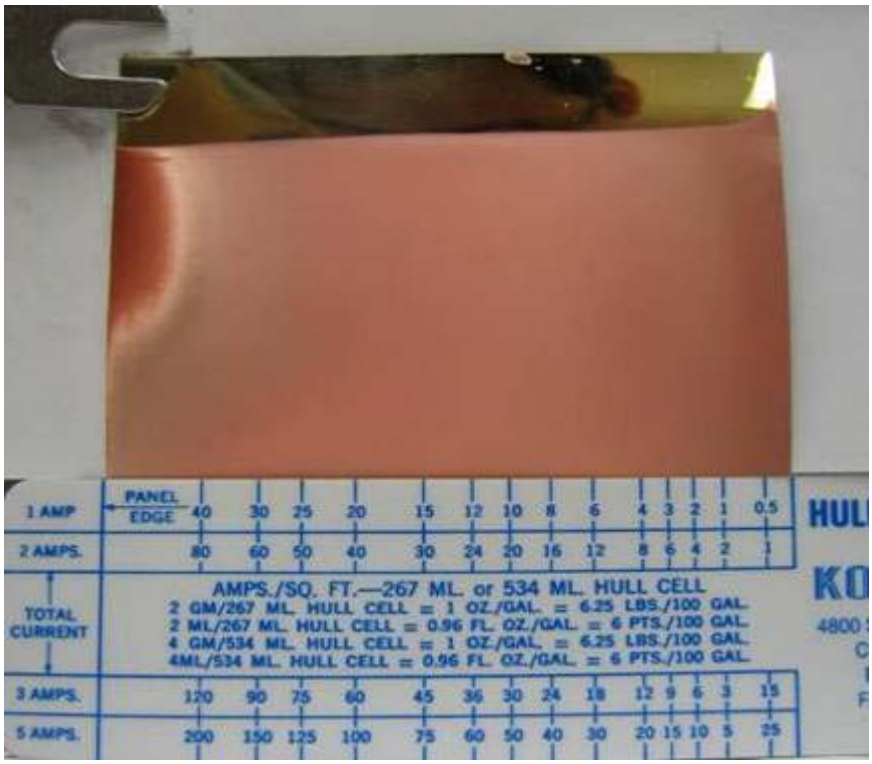

(c) 0.1%$_{wt}$ PVA

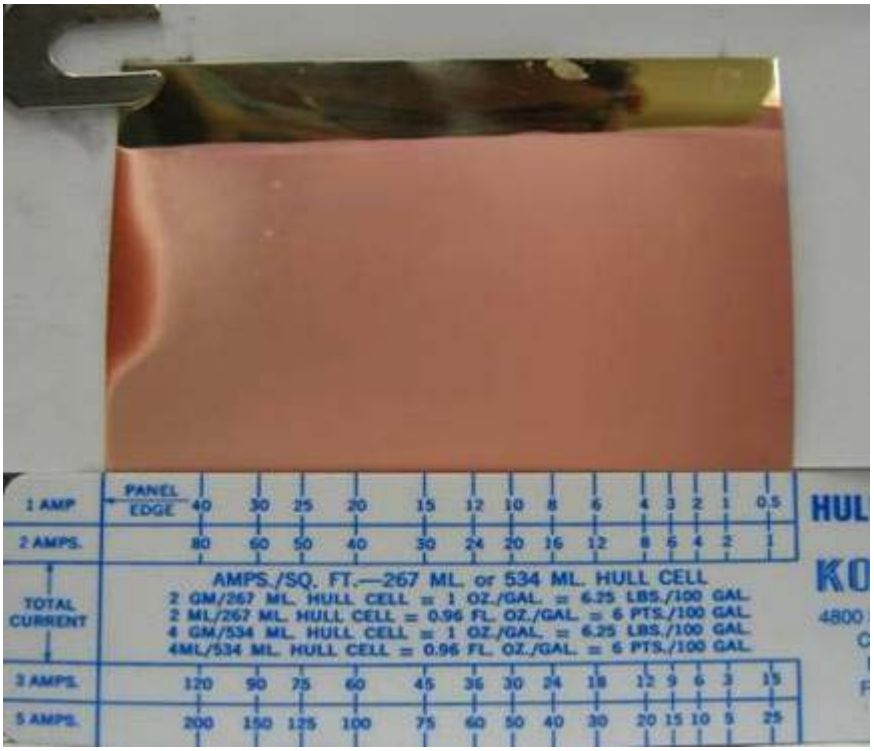

(d) 0.5%$_{wt}$ PVA

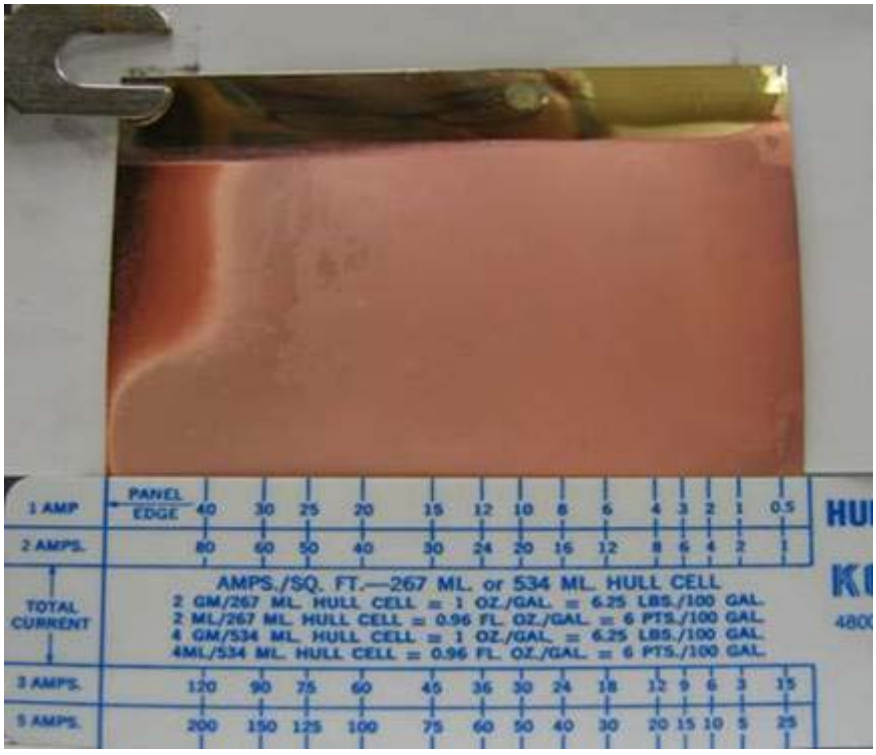

(e) 1.0%$_{wt}$ PVA

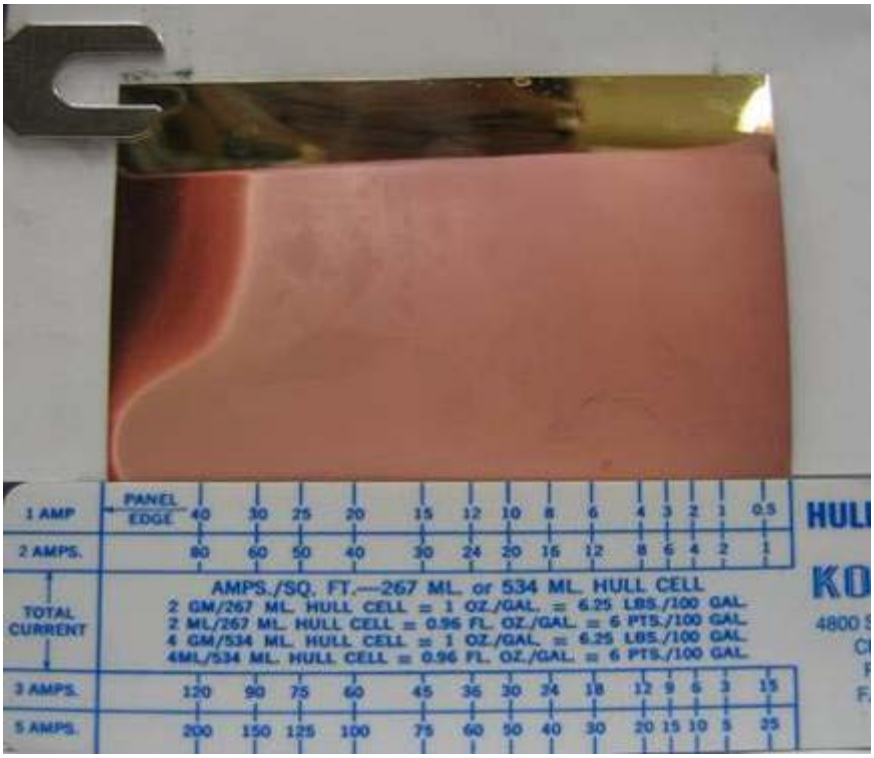

Figure 4.76. Appearances of plating workpieces in acid copper sulfate plating process with different contents of PVA: (a) 0%$_{wt}$ PVA; (b) 0.01%$_{wt}$ PVA; (c) 0.1%$_{wt}$ PVA; (d) 0.5%$_{wt}$ PVA; (e) 1.0%$_{wt}$ PVA.

* Plating conditions are listed in Table 4.54.

Table 4.54. Ranges of current densities for desirable copper depositions under different contents of PVA in plating solutions.

Content of PVA ($\%_{wt}$)	Range of current densities (A/dm^2)
0	1.5 – 70
0.01	2 – 70
0.1	2 – 70
0.5	No acceptance
1.0	No acceptance

Remarks:

- Plating conditions: Copper concentration = 200 g/L $CuSO_4 \cdot 5H_2O$; Acid concentration = 50 g/L H_2SO_4; Chloride concentration = 75 mg-Cl^-/L; Current = 2 A; Agitation speed = 200 rpm; Plating time = 10 min (listed in Table 3.3);
- The range of current densities applied across the whole area of the workpieces was 0 – 80 A/dm^2;
- The morphological diagrams of the workpieces are displayed in Figs. 4.76 (a) to (e).

4.7.2.5 Effect of current densities

As shown in the above sections, current density is one of the critical factors controlling the deposition rate and the plating performances. It generally correlates with the applied current. A larger applied current would induce a higher current density within the same area of workpieces, resulting in a faster deposition rate and a thicker deposit layer. When the current increased further, this would produce an extremely-high current density. The deposition rate might exceed the mass transfer rate of copper ions. The electrolysis of water molecules was then performed, inducing a large burning area (Ludwig, 2003). In order to obtain the optimal current density, the plating experiments would be performed by current densities ranging from 0 to 200 A/dm^2, which were provided by current at 1 to 5 A. The appearances of the copper deposits are shown in Figs. 4.77 (a) to (d), and the observed ranges of current densities for the desirable copper depositions are listed in Table 4.55.

From the figures and table, a borderline of the deposit appearances was observed on the electrodeposited workpieces at around 70 A/dm^2. At the region above this value, burned deposits were observed. By contrast, the desirable surface appearances could be obtained in the boundary below 70 A/dm^2. Within this boundary, no observable differences were found in the deposit appearances, except a slightly poor coverage by the thinner deposit layers in the current densities below 3 A/dm^2. Accordingly, the optimal range of current densities was defined as between 3 and 70 A/dm^2.

(a) 0 – 40 A/dm^2 (obtained by current at 1 A)

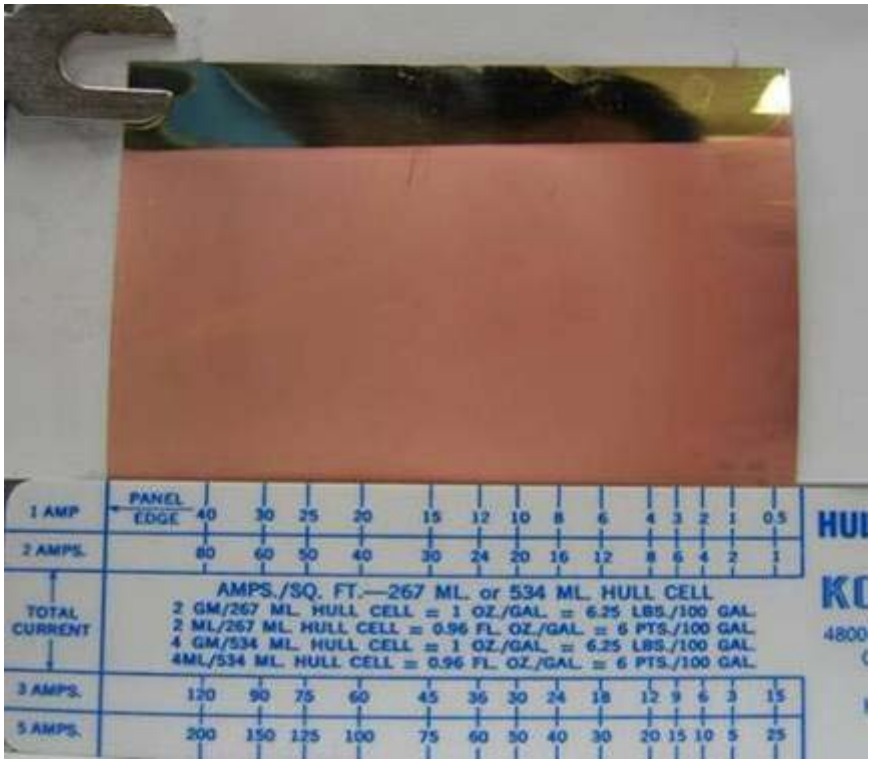

(b) 0 – 80 A/dm^2 (obtained by current at 2 A)

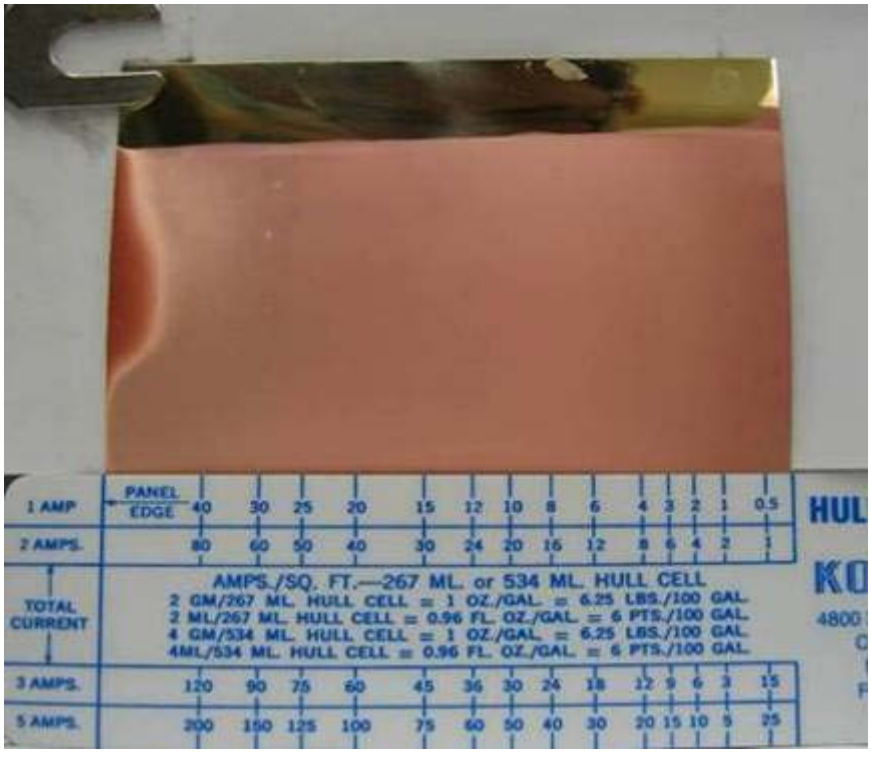

(c) 0 – 120 A/dm^2 (obtained by current at 3 A)

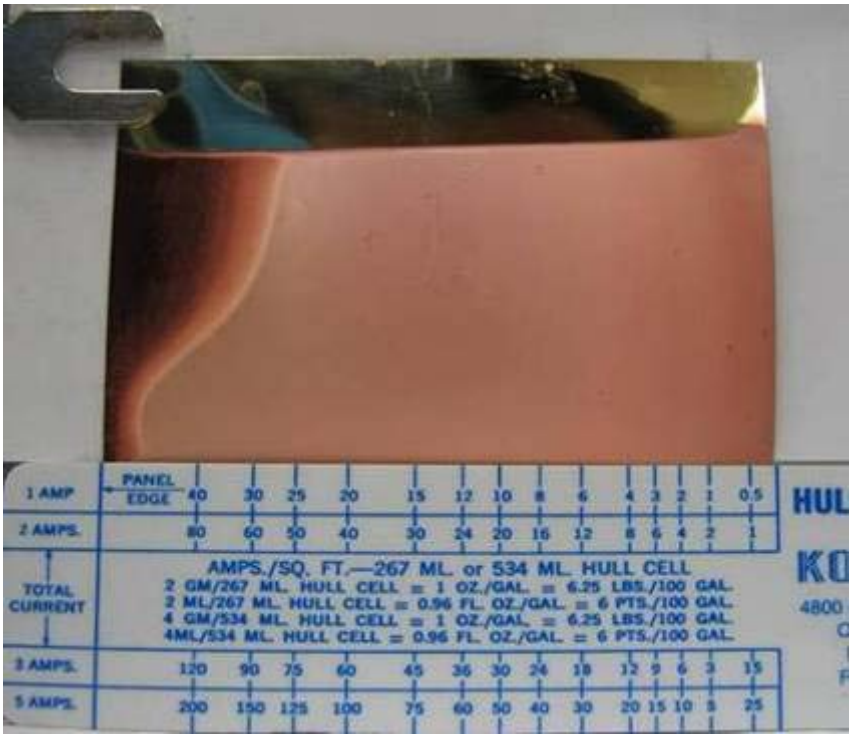

(d) 0 – 200 A/dm^2 (obtained by current at 5 A)

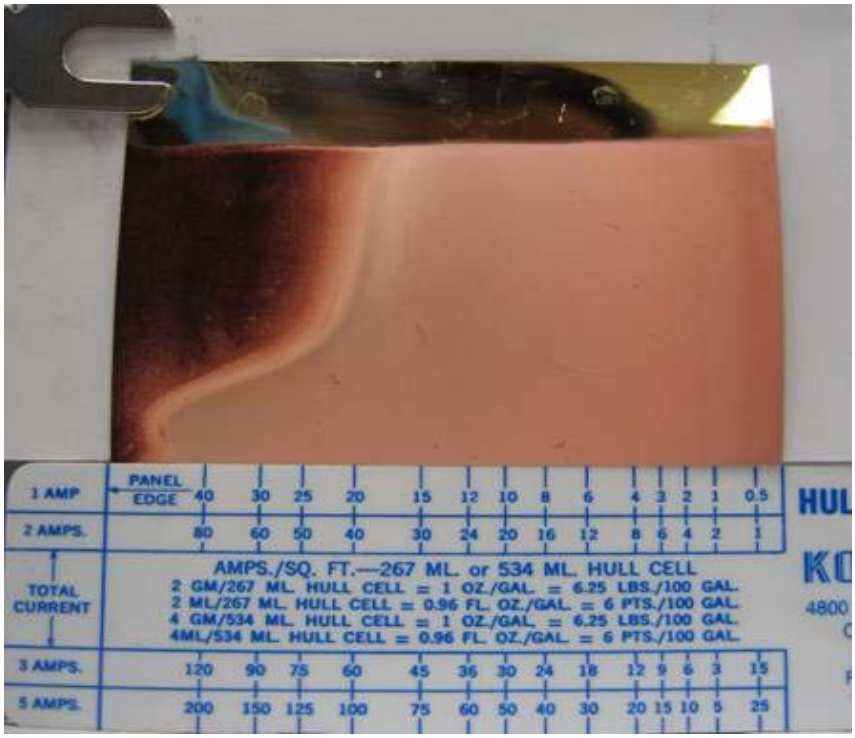

Figure 4.77. Appearances of plating workpieces in acid copper sulfate plating process under different current densities: (a) 0 – 40 A/dm^2 (obtained by current at 1 A); (b) 0 – 80 A/dm^2 (obtained by current at 2 A); (c) 0 – 120 A/dm^2 (obtained by current at 3 A); (d) 0 – 200 A/dm^2 (obtained by current at 5 A).

* Plating conditions are listed in Table 4.55.

Table 4.55. Ranges of current densities for desirable copper depositions under different current densities.

Current (A)	Range of current densities (A/dm^2)	
	Across whole workpiece	For desirable deposition
1	0 – 40	3 – above 40
2	0 – 80	2 – 70
3	0 – 120	3 – 70
5	0 – 200	3 – 75

Remarks:

- Plating conditions: Copper concentration = 200 g/L $CuSO_4 \cdot 5H_2O$; Acid concentration = 50 g/L H_2SO_4; Chloride concentration = 75 mg-Cl^-/L; Organic content = 0.1%$_{wt}$ PVA; Agitation speed = 200 rpm; Plating time = 10 min (listed in Table 3.3);
- The morphological diagrams of the workpieces are displayed in Figs. 4.77 (a) to (d).

4.7.2.6 Effect of agitation speed

Ludwig (2003) pointed out that agitation is an important factor in the plating process. It can facilitate a uniform solution movement and a rapid mass transfer at the cathode surface. Under an appropriate agitation, a uniform coating can be obtained over a wide range of current densities and less electrochemical consumption of organic additives can be resulted. Accordingly, the study was performed by varying the agitation speeds. The experimental conditions are listed in Table 3.3.

Apart from the burning area, a blur-like defect was found on the deposits obtained from the plating solution without agitation (Fig. 4.78 (a)). As shown in Figs. 4.78 (b) to (d), such defect disappeared when the plating solutions were agitated. When the agitation speed was increased up to 200 rpm, a uniform deposit layer was obtained over the region of low current densities. Table 4.56 indicates that the desirable deposition could be performed at lower current densities when the agitation was at 200 rpm or above. In the case with the fastest agitation (300 rpm), there was no observable improvement of the deposition. Therefore, the agitation speed at 200 rpm was applied in the following experiments in order to maintain an effective mass transfer of copper ions during the deposition.

(a) 0 rpm

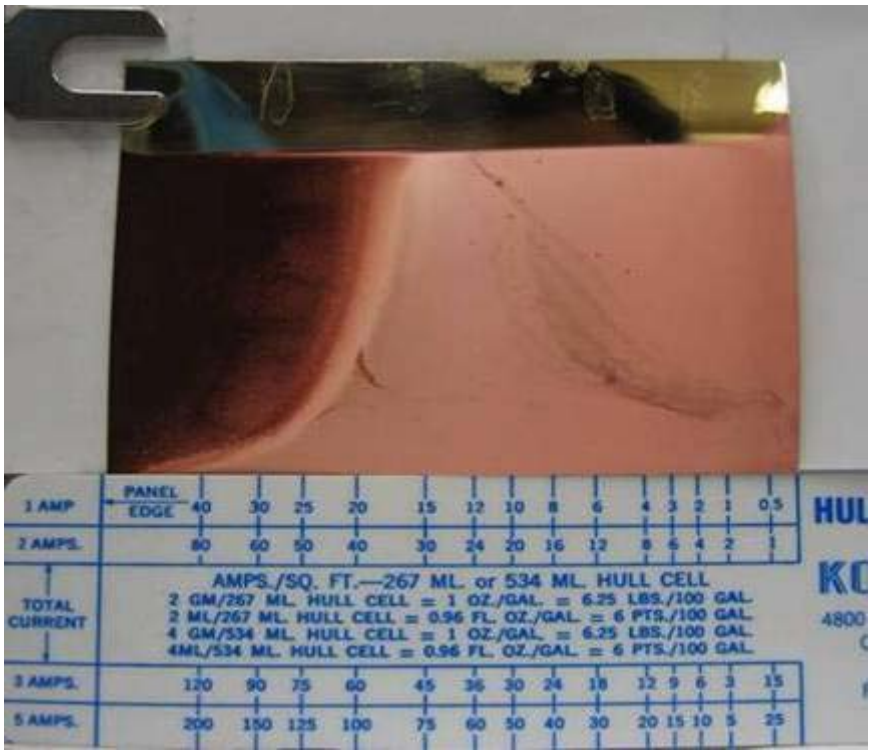

(b) 100 rpm

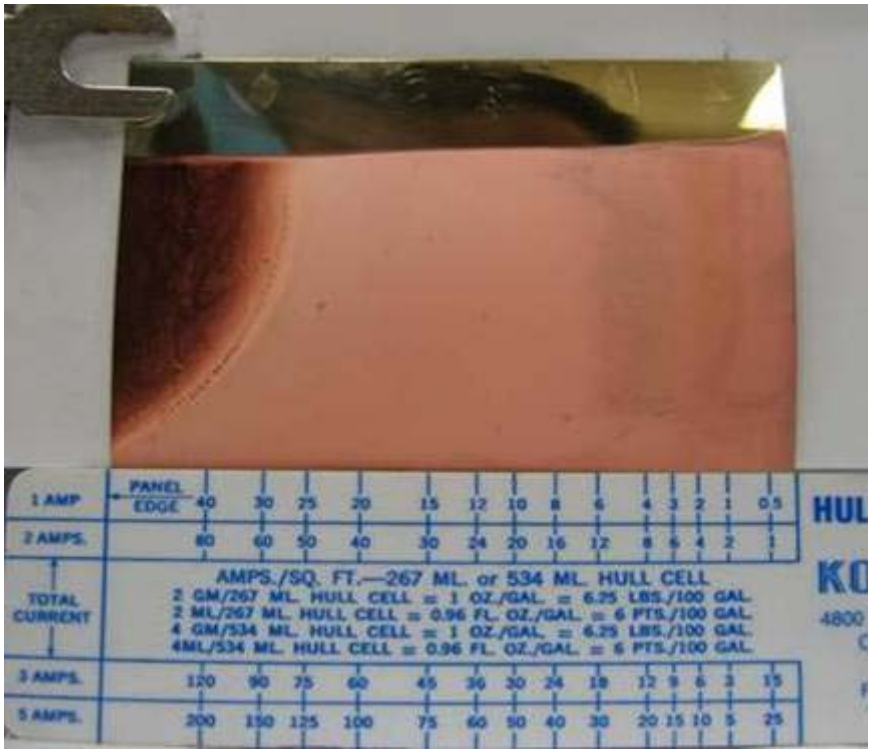

(c) 200 rpm

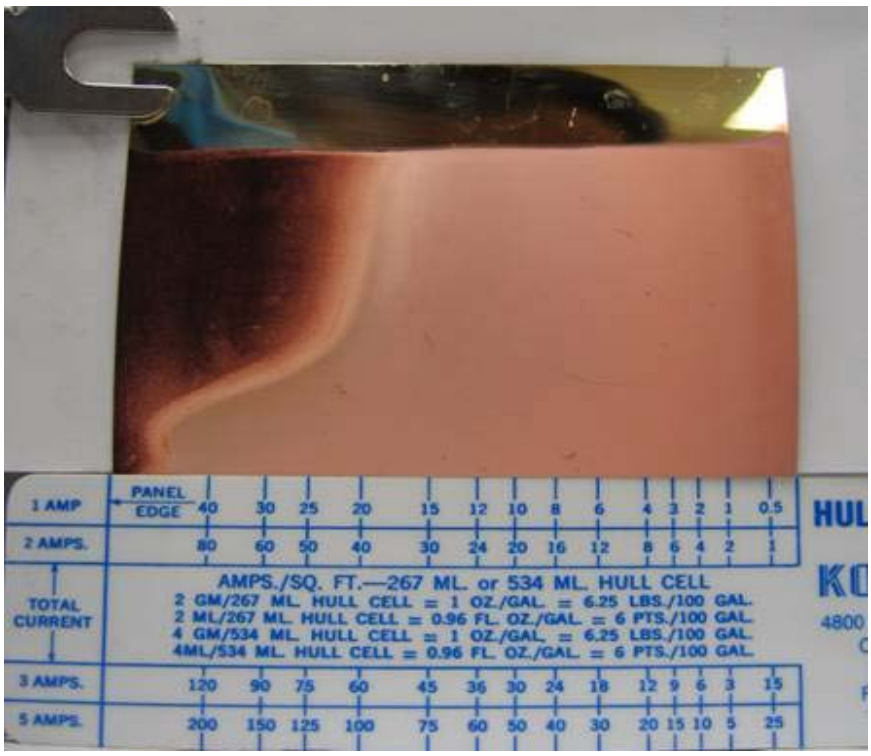

(d) 300 rpm

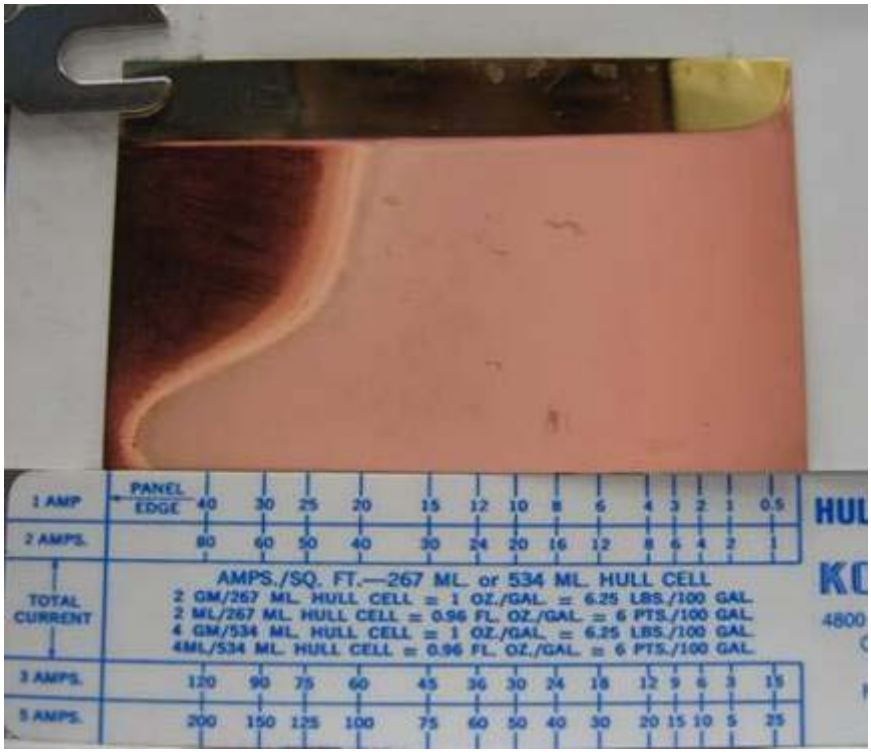

Figure 4.78. Appearances of plating workpieces in acid copper sulfate plating process under different agitation speeds: (a) 0 rpm; (b) 100 rpm; (c) 200 rpm; (d) 300 rpm.

* Plating conditions are listed in Table 4.56.

Table 4.56. Ranges of current densities for desirable copper depositions under different agitation speeds.

Agitation speed (rpm)	Range of current densities (A/dm^2)
0	No acceptance
100	45 – 125
200	5 – 75
300	5 – 75

Remarks:

- Plating conditions: Copper concentration = 200 g/L $CuSO_4 \cdot 5H_2O$; Acid concentration = 50 g/L H_2SO_4; Chloride concentration = 75 mg-Cl^-/L; Organic content = 0.1%$_{wt}$ PVA; Current = 5 A; Plating time = 10 min (listed in Table 3.3);
- The range of current densities applied across the whole area of the workpieces was 0 – 200 A/dm^2;
- The morphological diagrams of the workpieces are displayed in Figs. 4.78 (a) to (d).

4.7.2.7 Effect of plating time

In electroplating process, a longer plating time represents a higher consumption of raw materials and electricity. Both of which are major expenses of the plating process. Thus, the effect of plating time was investigated in order to appraise a minimal plating time without affecting the deposit appearance. The experiment was conducted by following the conditions listed in Table 3.3. The process time was varied from 1 to 20 min.

Figs. 4.79 (a) to (d) show the appearances of the deposits under different plating durations. By performing an one-minute process, only a thin layer of deposit was obtained, which was insufficient to shield the base of the workpiece (Fig. 4.79 (a)). As the plating time increased, a better coverage and thicker deposits were resulted. However, if the plating time increased beyond 5 min, there was no significant improvement in the deposit appearance (Figs. 4.79 (b) to (d)) or no expansion of the area covered with the desirable deposit layer (Table 4.57). This meant that the plating time could be shortened to 5 min.

(a) 1 min

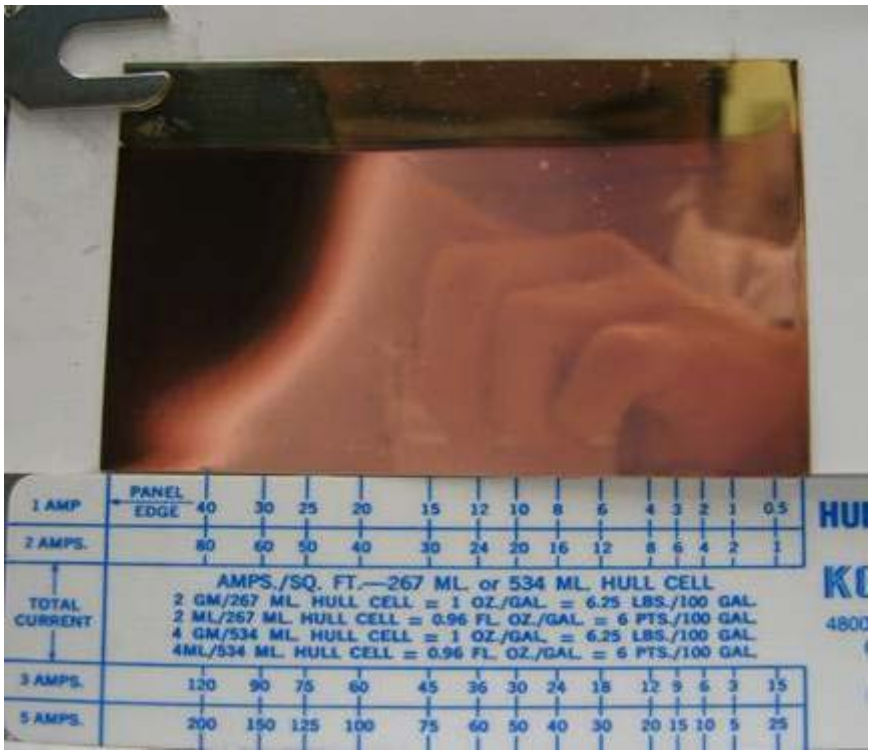
1 AMP
PANEL EDGE
40 30 25 20 15 12 10 8 6 4 3 2 1 0.5
2 AMPS.
80 60 50 40 30 24 20 16 12 8 6 4 2 1
TOTAL CURRENT
AMPS./SQ. FT.—267 ML. or 534 ML. HULL CELL
2 GM/267 ML. HULL CELL = 1 OZ./GAL. = 6.25 LBS./100 GAL.
2 ML/267 ML. HULL CELL = 0.96 FL. OZ./GAL. = 6 PTS./100 GAL.
4 GM/534 ML. HULL CELL = 1 OZ./GAL. = 6.25 LBS./100 GAL.
4ML/534 ML. HULL CELL = 0.96 FL. OZ./GAL. = 6 PTS./100 GAL.
3 AMPS.
120 90 75 60 45 36 30 24 18 12 9 6 3 15
5 AMPS.
200 150 125 100 75 60 50 40 30 20 15 10 5 25

(b) 5 min

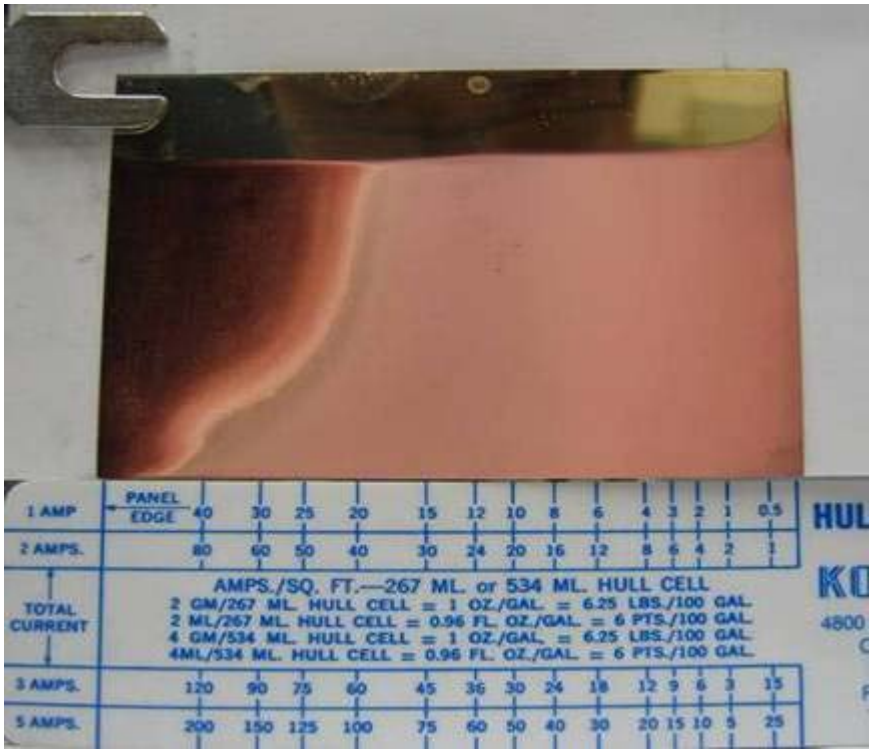
1 AMP
PANEL EDGE
40 30 25 20 15 12 10 8 6 4 3 2 1 0.5
2 AMPS.
80 60 50 40 30 24 20 16 12 8 6 4 2 1
TOTAL CURRENT
AMPS./SQ. FT.—267 ML. or 534 ML. HULL CELL
2 GM/267 ML. HULL CELL = 1 OZ./GAL. = 6.25 LBS./100 GAL.
2 ML/267 ML. HULL CELL = 0.96 FL. OZ./GAL. = 6 PTS./100 GAL.
4 GM/534 ML. HULL CELL = 1 OZ./GAL. = 6.25 LBS./100 GAL.
4ML/534 ML. HULL CELL = 0.96 FL. OZ./GAL. = 6 PTS./100 GAL.
3 AMPS.
120 90 75 60 45 36 30 24 18 12 9 6 3 15
5 AMPS.
200 150 125 100 75 60 50 40 30 20 15 10 5 25

(c) 10 min

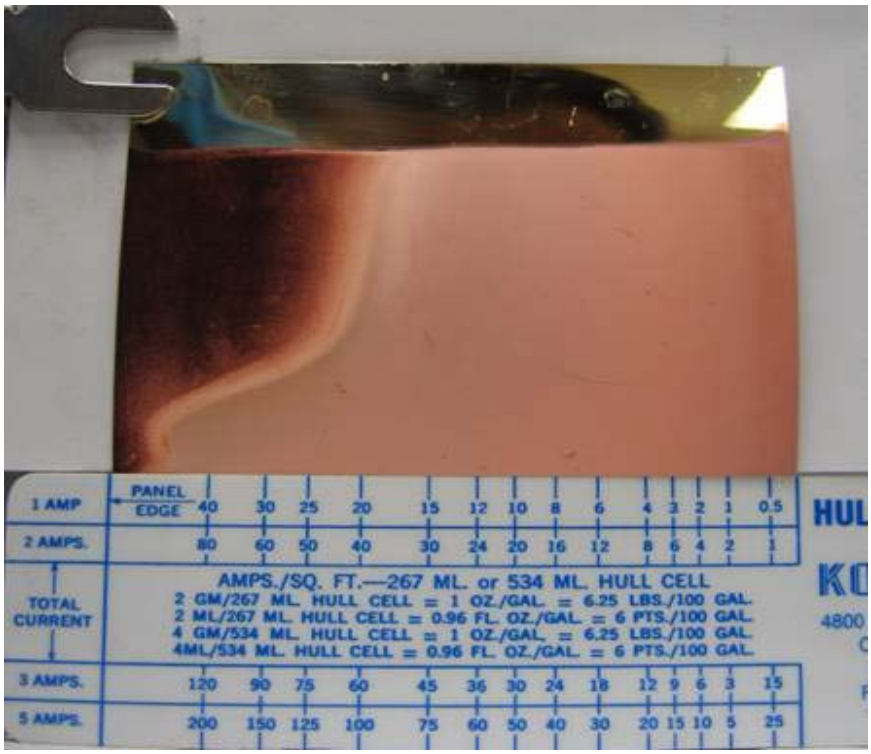

(d) 20 min

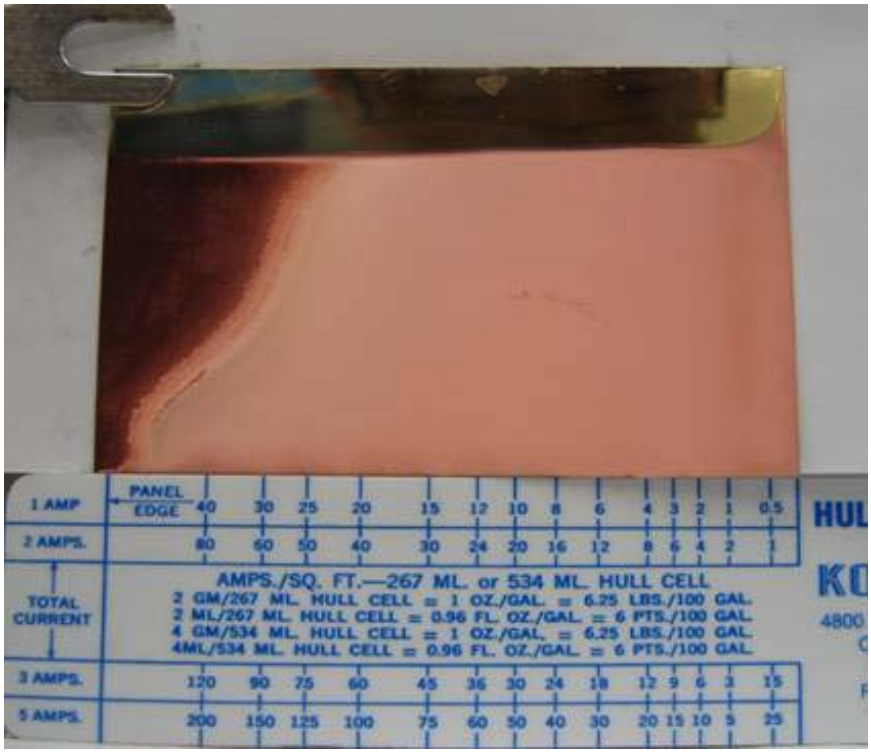

Figure 4.79. Appearances of plating workpieces in acid copper sulfate plating process under different plating time: (a) 1 min; (b) 5 min; (c) 10 min; (d) 20 min.

* Plating conditions are listed in Table 4.57.

Table 4.57. Ranges of current densities for desirable copper depositions under different plating time.

Plating time (min)	Range of current densities (A/dm^2)
1	No acceptance
5	5 – 75
10	5 – 75
20	5 – 80

Remarks:

- Plating conditions: Copper concentration = 200 g/L $CuSO_4 \cdot 5H_2O$; Acid concentration = 50 g/L H_2SO_4; Chloride concentration = 75 mg-Cl^-/L; Organic content = 0.1%$_{wt}$ PVA; Current = 5 A; Agitation speed = 200 rpm (listed in Table 3.3);
- The range of current densities applied across the whole area of the workpieces was 0 – 200 A/dm^2;
- The morphological diagrams of the workpieces are displayed in Figs. 4.79 (a) to (d).

4.7.3 Electroplating of recycled (desorbed) copper

After an in-depth investigation of the acid copper sulfate plating process, the compositions of the plating solution and the operation conditions were optimized and summarized as follows.

Optimal plating parameters:

- $CuSO_4 \cdot 5\ H_2O$: 200 g/L
- H_2SO_4: 50 g/L
- Chloride ions: 75 mg/L
- Organic additive: $0.1\%_{wt}$ PVA
- Current density: 3 – 70 A/dm^2
- Agitation speed: 200 rpm
- Plating time: 5 min

All these parameters were within the recommended ranges reported in literature as listed in Tables 2.11 and 2.12. The study was extended to the re-use of desorbed copper (obtained in Section 4.6.4) in the electroplating process. The desorbed copper was purified from the desorption effluent and converted to $CuHPO_4$ salt (Section 4.7.1). Since the effect of this recycled copper salt on the acid copper plating was unknown, the study was conducted to examine the feasibility of its use as a component in the electroplating solution. The experimental conditions are listed in Table 3.3.

The plating solutions with and without the recycled $CuHPO_4$ salt were first prepared and then applied in the plating processes. Both the solutions

contained an equivalent amount of copper ions. The copper concentration contributed by this recycled salt was about 2.5%$_{mole}$ in the solution. The appearance of the copper deposits is shown in Figs. 4.80 (a) and (b). No significant differences could be observed between the appearance of the workpieces obtained by the plating solutions with and without the recycled $CuHPO_4$. The desirable deposit appearance could be obtained in a similar range of current densities, from about 3 to 75 A/dm^2 (Table 4.58)

The deposited workpieces with the desirable appearance were further studied by a Scanning Electron Microscope (SEM) (Leica Stereoscan model 440) as shown in Figs. 4.81 (a) and (b). The micrographs with 5000X magnification show that both the plating processes with and without the addition of the recycled salt could produce a smooth layer of copper deposits with a uniform grain distribution. The size of the copper deposit grains could be measured from the micrographs under 15000X magnification (Appendix). The results are summarized in Fig. 4.82. In the presence of the recycled $CuHPO_4$ salts, slightly larger grains of about 2.50 ± 0.12 μm were deposited, whereas the grain size in the case without the salts was around 2.05 ± 0.16 μm.

To evaluate the coverage of the deposited workpieces with the desirable appearance, the X-ray Energy Dispersive Analysis (EDAX) was performed by using the Scanning Electron Microscope equipped with the X-ray Energy Dispersive Analyzer (Jeol model JSM-6490). The spectra of the EDAX are presented in Figs. 4.83 (a) to (c). The spectra illustrate that

there were strong signals of zinc and copper with an even distribution on the surface of the brass-based workpiece before the plating (substrate). After the plating processes, the peaks of zinc disappeared in the cases with and without the $CuHPO_4$ salts, and only the copper signals could be found (Figs. 4.84 and 4.85). It implies that both the plating processes could provide a good coverage of the highly-pure copper deposits.

Moreover, the results of the electrical resistivity test (Fig. 4.91) show that a slightly larger resistance was determined from the workpiece before the plating (substrate). By contrast, smaller resistances were found in the workpieces covered with copper deposits. Also, similar resistance of about 5.63 ± 0.14 ohms was determined in the cases with or without the $CuHPO_4$ salt. This indicates that the presence of the recycled salt in the plating did not alter the electrical properties of the copper deposits.

The plating solutions containing various concentrations of pure $CuHPO_4$ species ranging from 2.5 to $50.0\%_{mole}$ were applied in the plating processes to further compare the plating performances in the presence of the recycled and pure $CuHPO_4$ salts. The highest $CuHPO_4$ concontration was fixed at $50.0\%_{mole}$ since it was near the maximum limit of the solubility. Under the same $CuHPO_4$ concentration ($2.5\%_{mole}$), the plating performances in the presence of the recycled salt and the pure species were almost identical. Both could achieve: a good overall appearance in the desirable range of current densities (Figs. 4.80 (a) and (c); Table 4.58); a similar smoothness of the deposit surfaces with uniform grain distributions (Figs.

4.81 (a) and (c)); similar grain sizes of the copper deposits (Fig. 4.82); a good coverage and a high purity of copper on the deposits (Figs. 4.84 and 4.86); and, a small resistance with similar values (Fig. 4.91). All these similarities were also identified when further comparing the case of the recycled salt with those cases comprising higher concentrations of the pure species (Table 4.58 and Figs. 4.80 to 4.91). This suggests that a higher concentration of the recycled salts could be applied without any significant influence to the plating performances and the deposit properties.

As mentioned above, the plating solution containing the recycled $CuHPO_4$ salt did not significantly change the plating performances and the deposit properties, as compared with the solution containing general compositions of the acid copper plating (without $CuHPO_4$ salt) and that with an addition of various amounts of pure $CuHPO_4$ species. Except the grain size, the deposits obtained by all these cases could display almost the same characteristics, such as a good overall appearance, a high degree of surface smoothness, a uniform grain distribution, a good coverage, a high copper purity and a small resistance. These results suggest that the recycled copper in the form of $CuHPO_4$ could be successfully reused in the acid copper electroplating process. Other spectroscopic techniques, such as Atomic Force Microscopy (AFM), and some industrial standard methods for testing the quality of electroplating workpieces, such as hardness and brightness, should be used further for characterizing the deposit properties of this copper plating.

(a) 2.5%$_{mole}$ of recycled $CuHPO_4$

(b) 0%$_{mole}$ of $CuHPO_4$

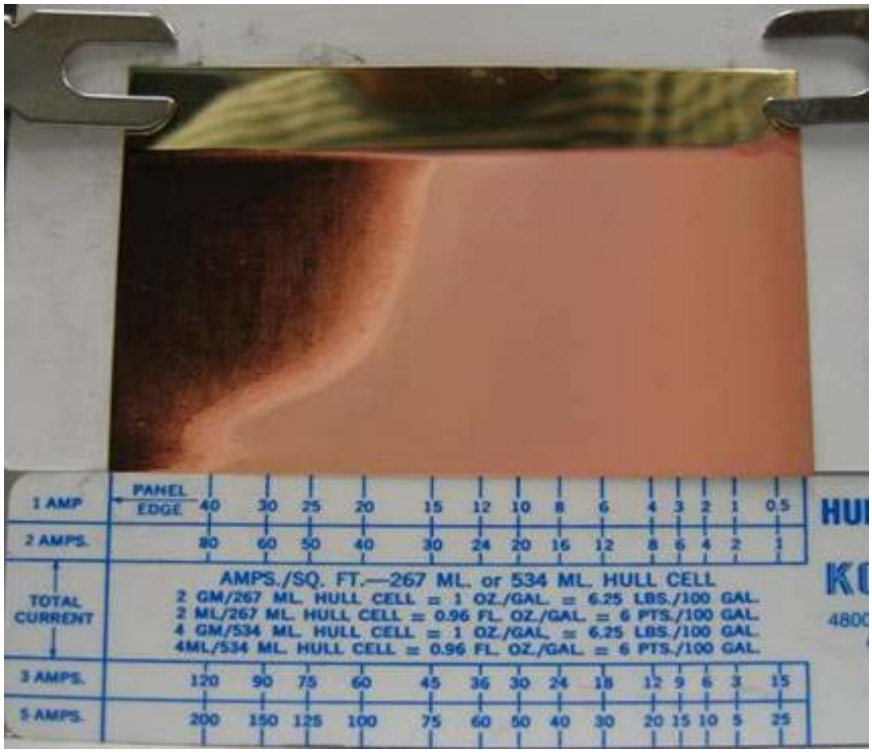

(c) 2.5%$_{mole}$ of pure $CuHPO_4$

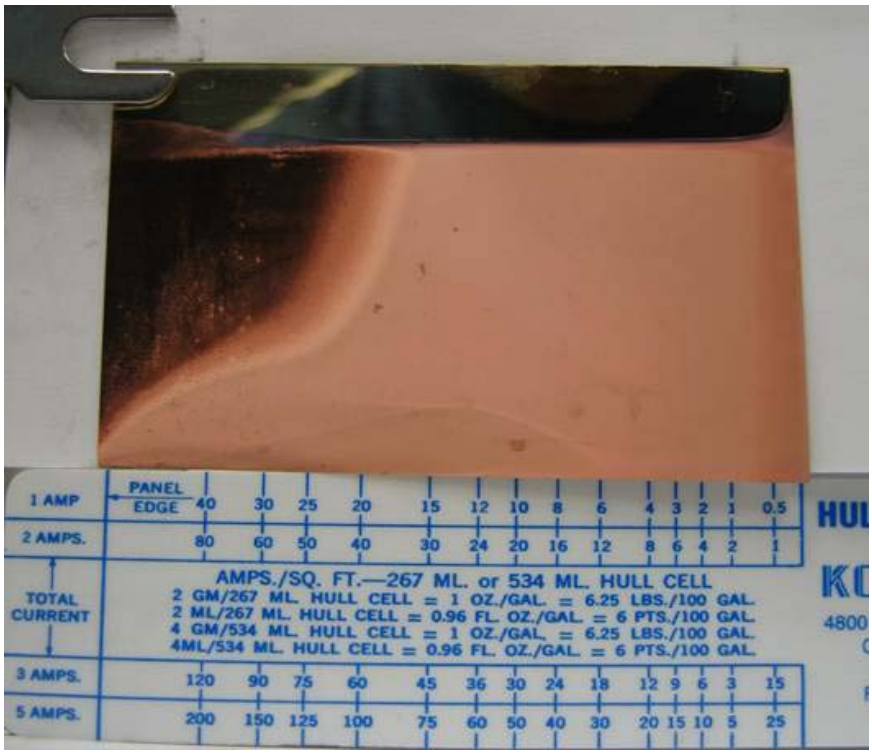

(d) 5.0%$_{mole}$ of pure $CuHPO_4$

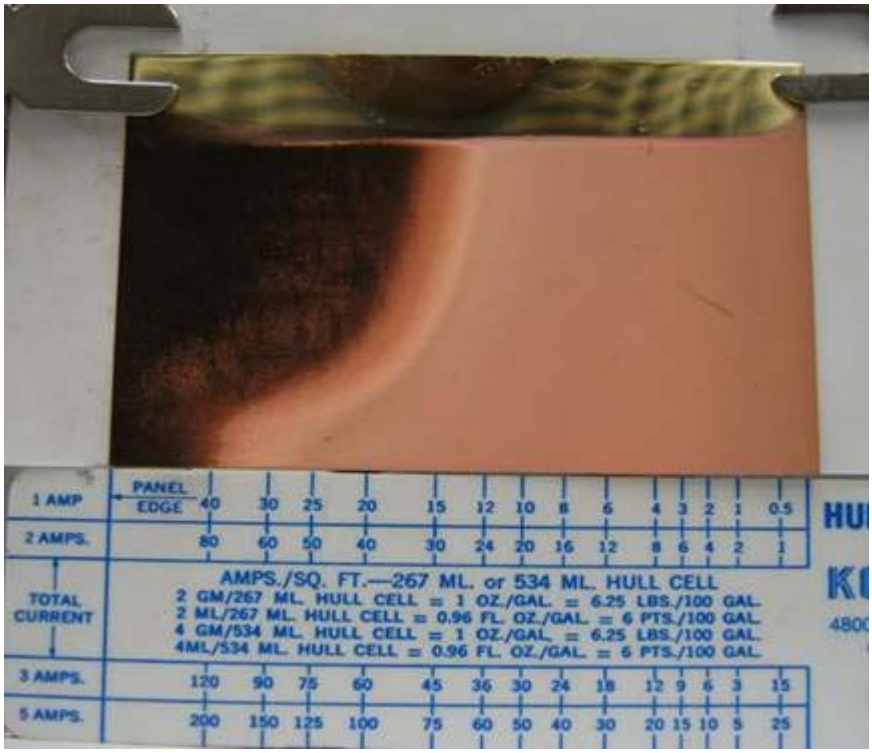

(e) 10.0%$_{mole}$ of pure $CuHPO_4$

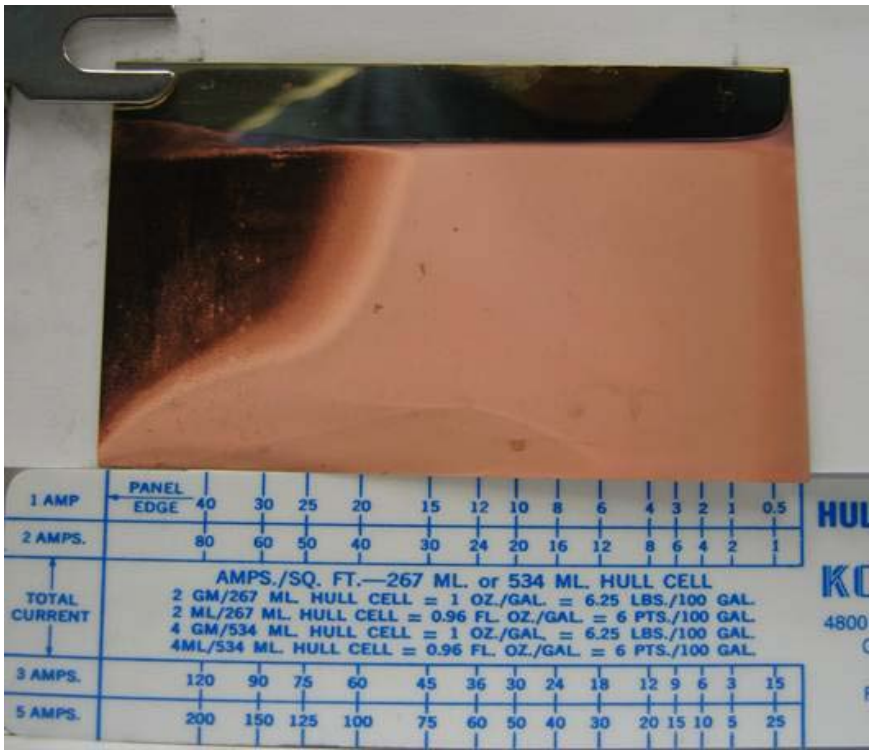

(f) 25.0%$_{mole}$ of pure $CuHPO_4$

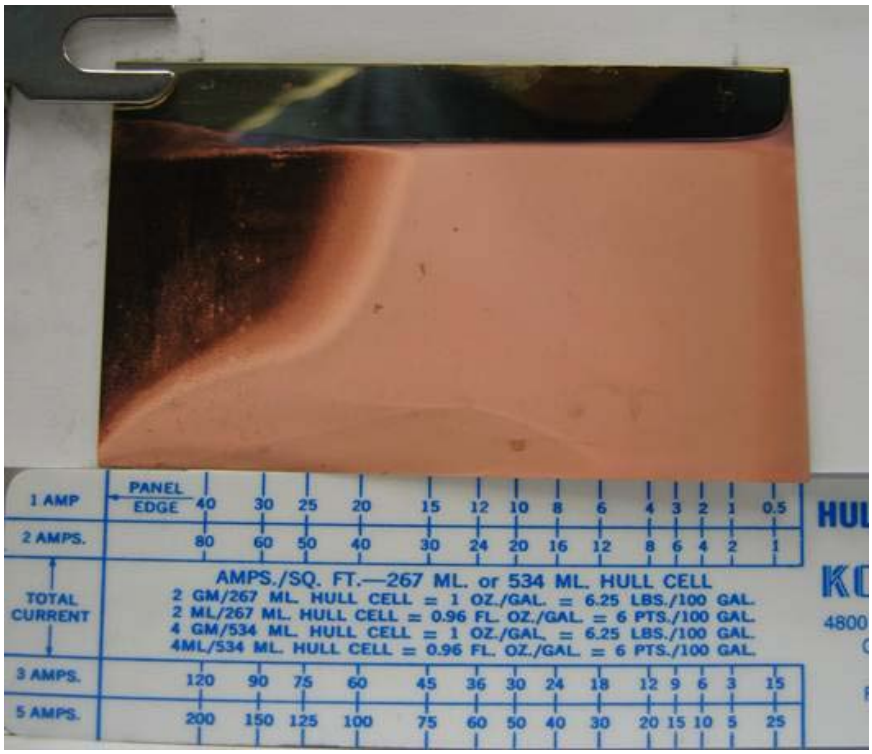

(g) 50.0%$_{mole}$ of pure $CuHPO_4$

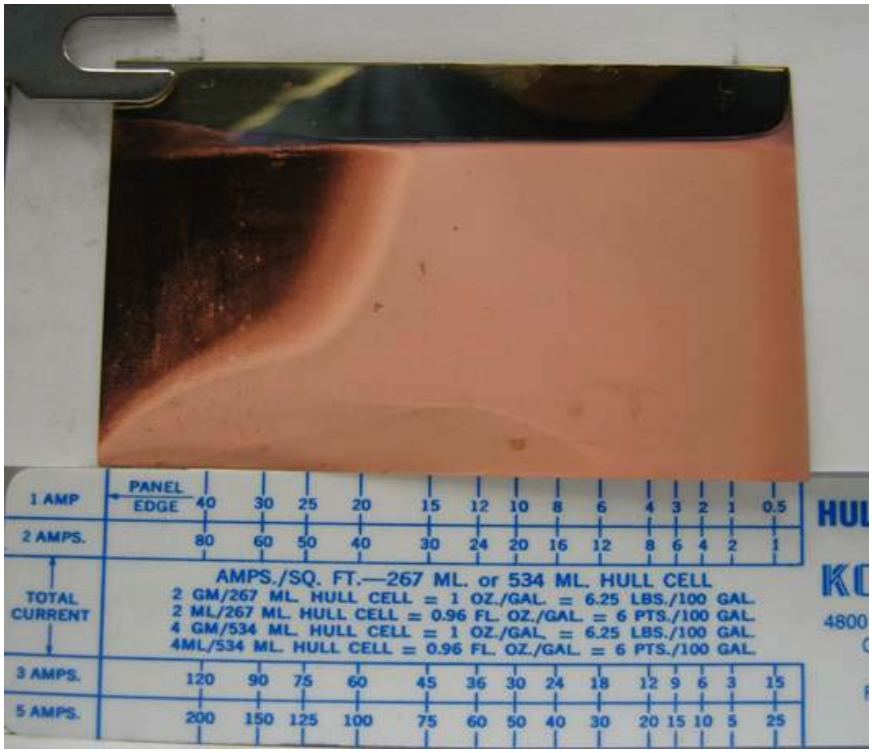

Figure 4.80. Appearances of plating workpieces in acid copper sulfate plating process under different concentrations of $CuHPO_4$ salts: (a) 2.5%$_{mole}$ of recycled $CuHPO_4$; (b) 0%$_{mole}$ of $CuHPO_4$; (c) 2.5%$_{mole}$ of pure $CuHPO_4$; (d) 5.0%$_{mole}$ of pure $CuHPO_4$; (e) 10.0%$_{mole}$ of pure $CuHPO_4$; (f) 25.0%$_{mole}$ of pure $CuHPO_4$; (g) 50.0%$_{mole}$ of pure $CuHPO_4$.

* Plating conditions are listed in Table 4.58.

Table 4.58. Ranges of current densities for desirable copper depositions under different concentrations of $CuHPO_4$ salt in plating solutions.

Contcentration of $CuHPO_4$ salt ($\%_{mole}$)	Range of current densities (A/dm^2)
Recycled $CuHPO_4$ salt	
2.5	3 – 75
Pure $CuHPO_4$ salt	
0	3 – 75
2.5	3 – 75
5.0	3 – 65
10.0	3 – 55
25.0	3 – 65
50.0	3 – 75

Remarks:

- Plating conditions: Copper concentration = 50 – 100%$_{mole}$ (100 – 200 g/L) $CuSO_4 \cdot 5H_2O$ plus 0 – 50%$_{mole}$ $CuHPO_4$ (pure or recycled salt); Acid concentration = 50 g/L H_2SO_4; Chloride concentration = 75 mg-Cl^-/L; Organic content = 0.1%$_{wt}$ PVA; Current = 5 A; Agitation speed = 200 rpm; Plating time = 5 min (listed in Table 3.3);
- The range of current densities applied across the whole area of the workpieces was 0 – 200 A/dm^2;
- The morphological diagrams of the workpieces are displayed in Figs. 4.80 (a) to (g).

(a) 2.5%$_{mole}$ of recycled $CuHPO_4$

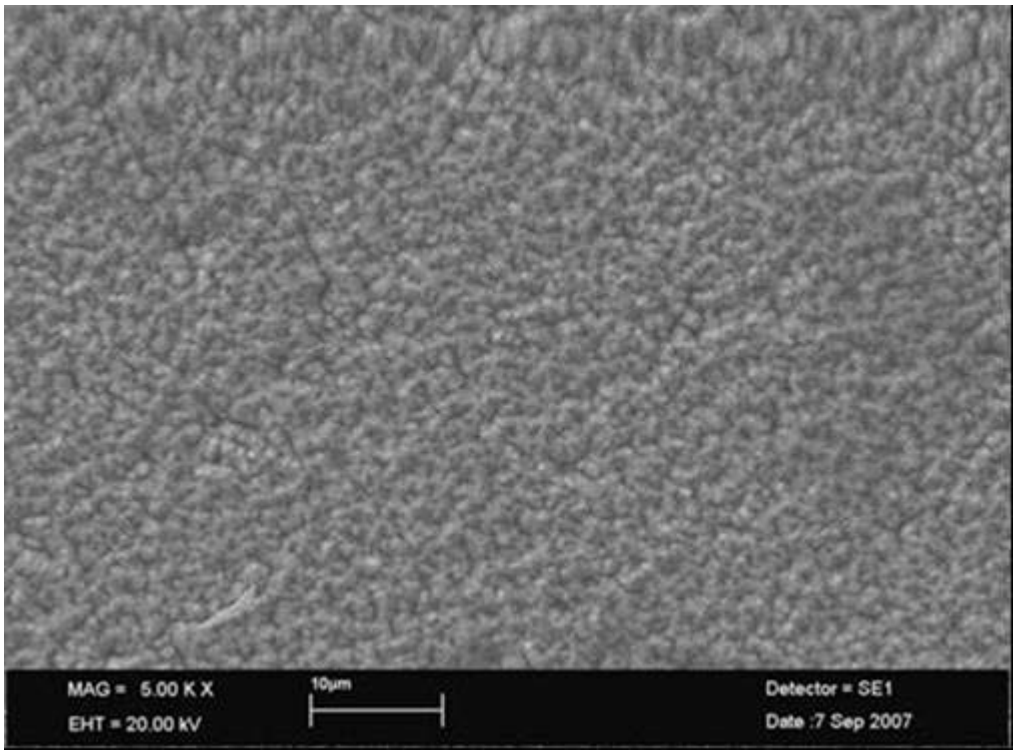

(b) 0%$_{mole}$ of $CuHPO_4$

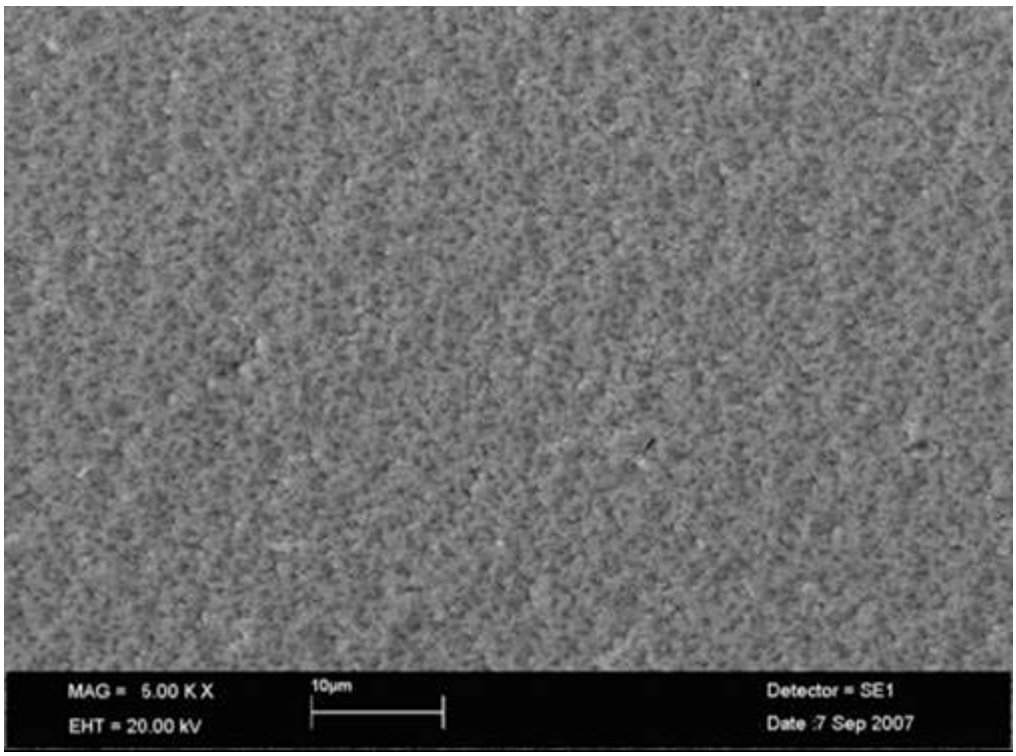

(c) 2.5%$_{mole}$ of pure $CuHPO_4$

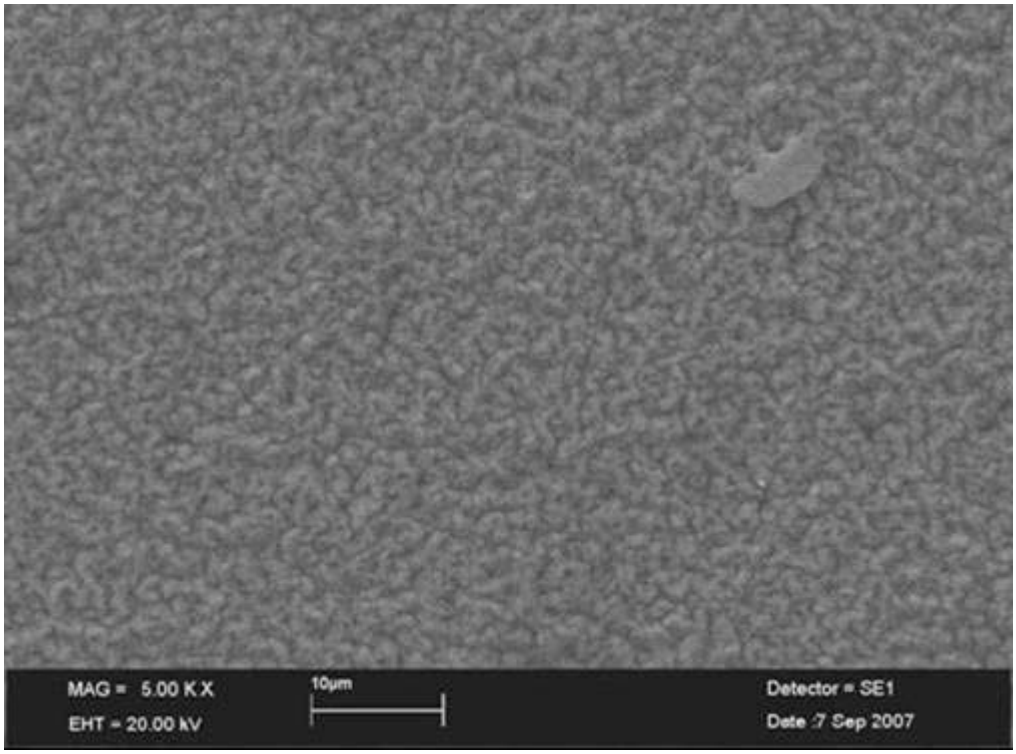

(d) 5.0%$_{mole}$ of pure $CuHPO_4$

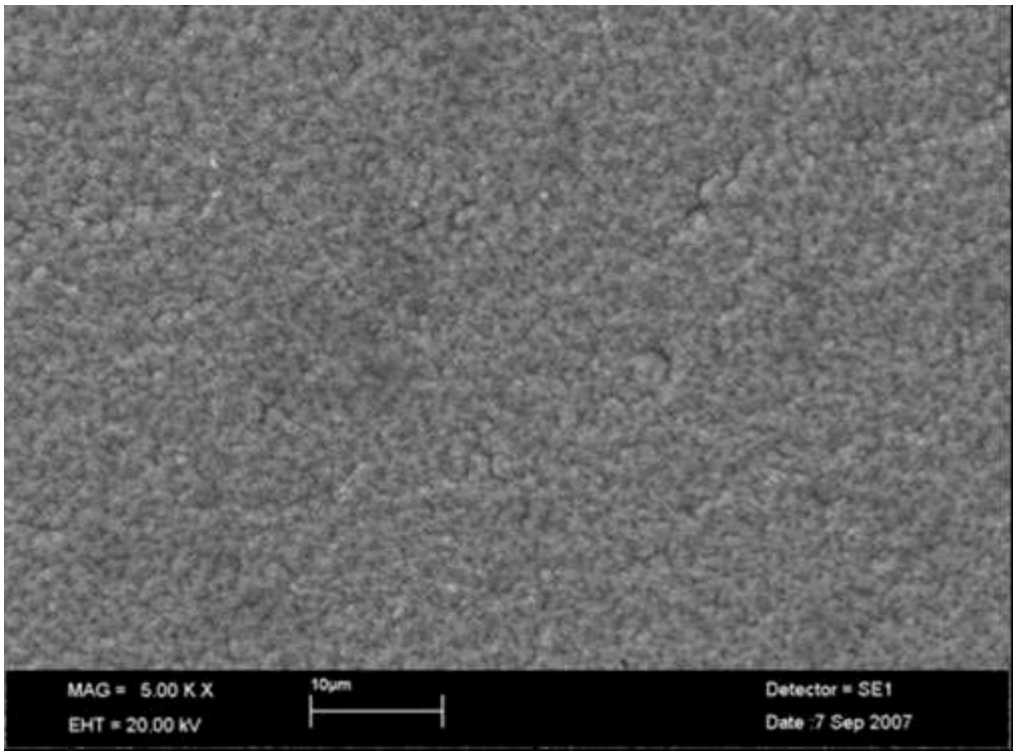

(e) 10.0%$_{mole}$ of pure $CuHPO_{4=}$

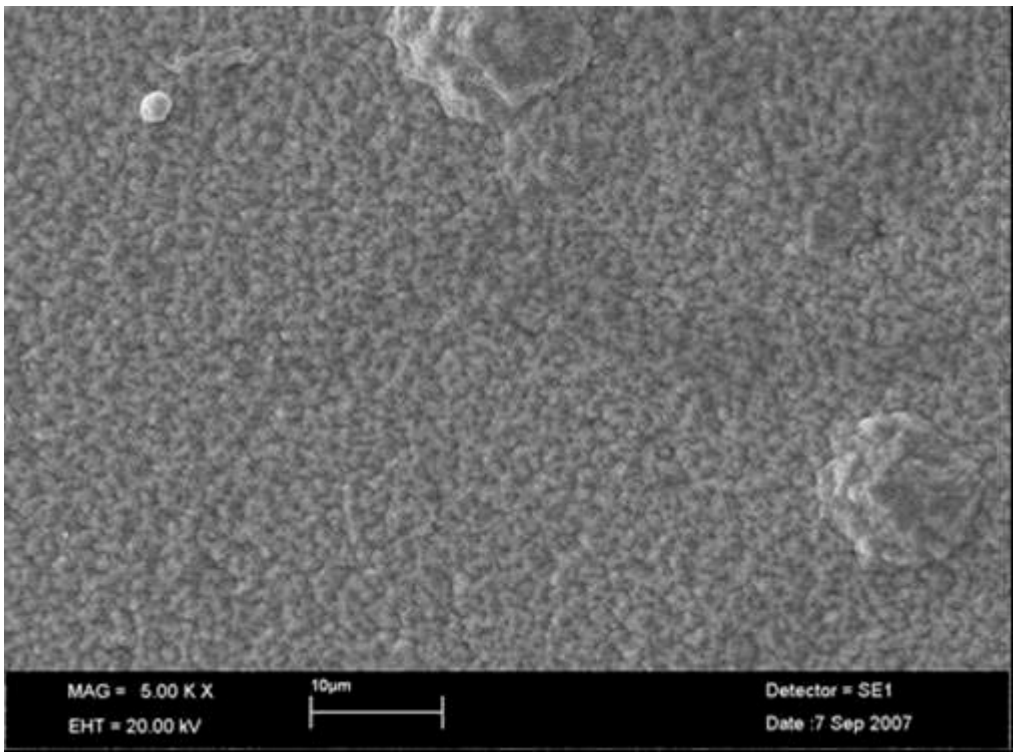

(f) 25.0%$_{mole}$ of pure $CuHPO_4$

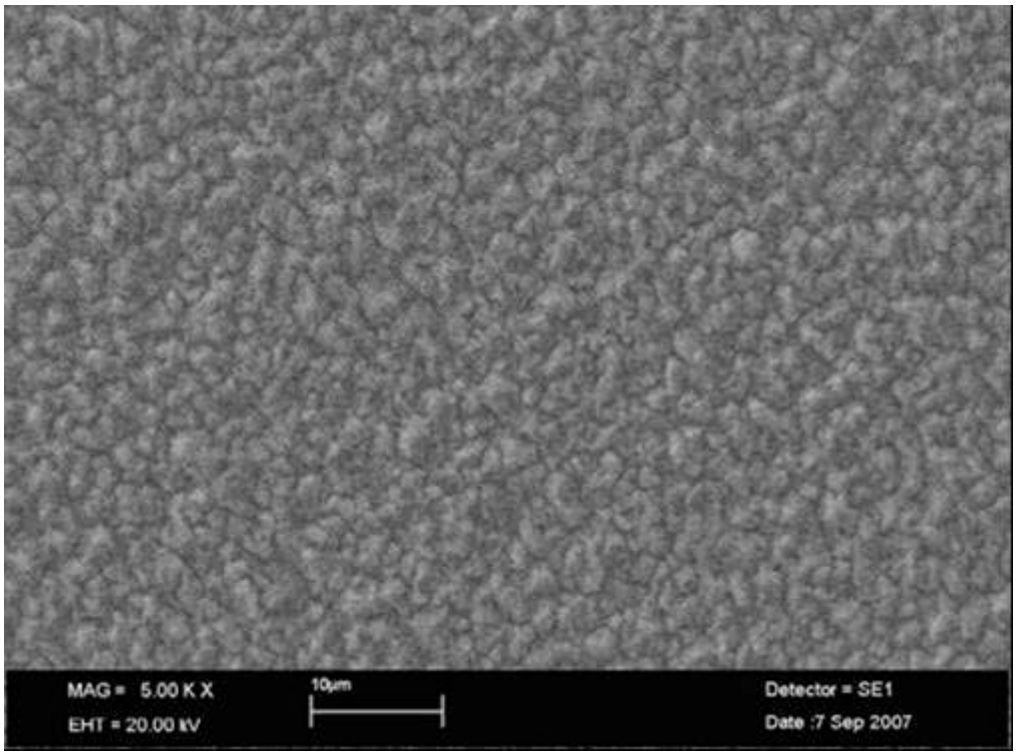

(g) 50.0%$_{mole}$ of pure $CuHPO_4$

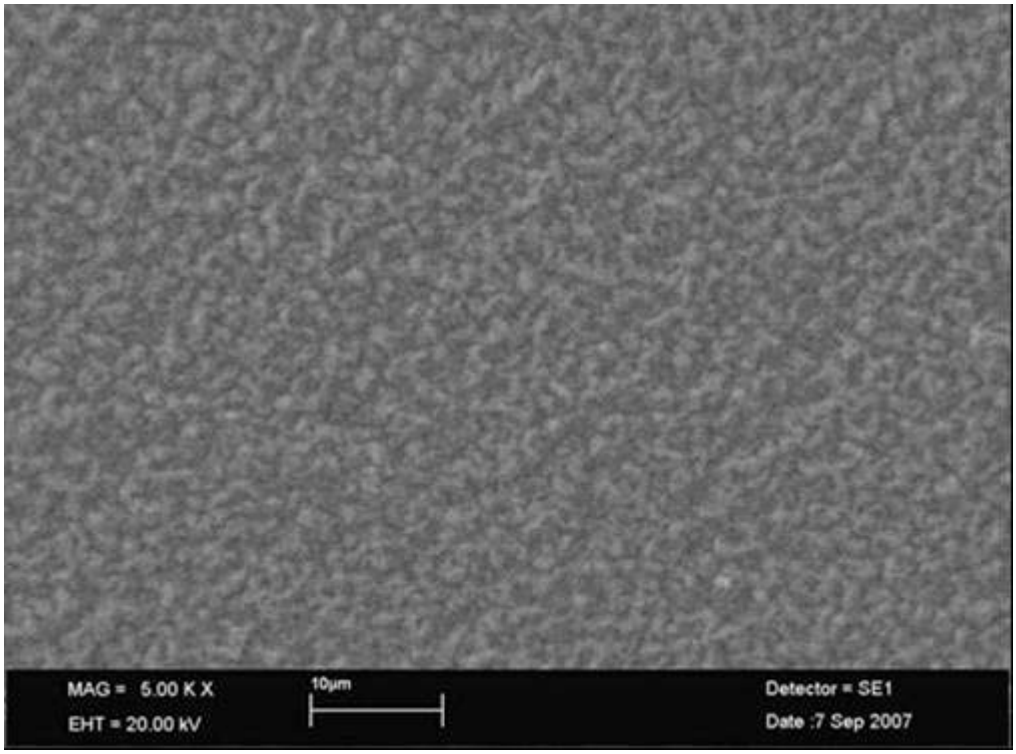

Figure 4.81. Scanning Electron Micrographs (SEMs) of copper deposits obtained by plating solutions containing different concentrations of $CuHPO_4$ salts (magnification: 5000X): (a) 2.5%$_{mole}$ of recycled $CuHPO_4$; (b) 0%$_{mole}$ of $CuHPO_4$; (c) 2.5%$_{mole}$ of pure $CuHPO_4$; (d) 5.0%$_{mole}$ of pure $CuHPO_4$; (e) 10.0%$_{mole}$ of pure $CuHPO_4$; (f) 25.0%$_{mole}$ of pure $CuHPO_4$; (g) 50.0%$_{mole}$ of pure $CuHPO_4$.

* Plating conditions are listed in Table 4.58.

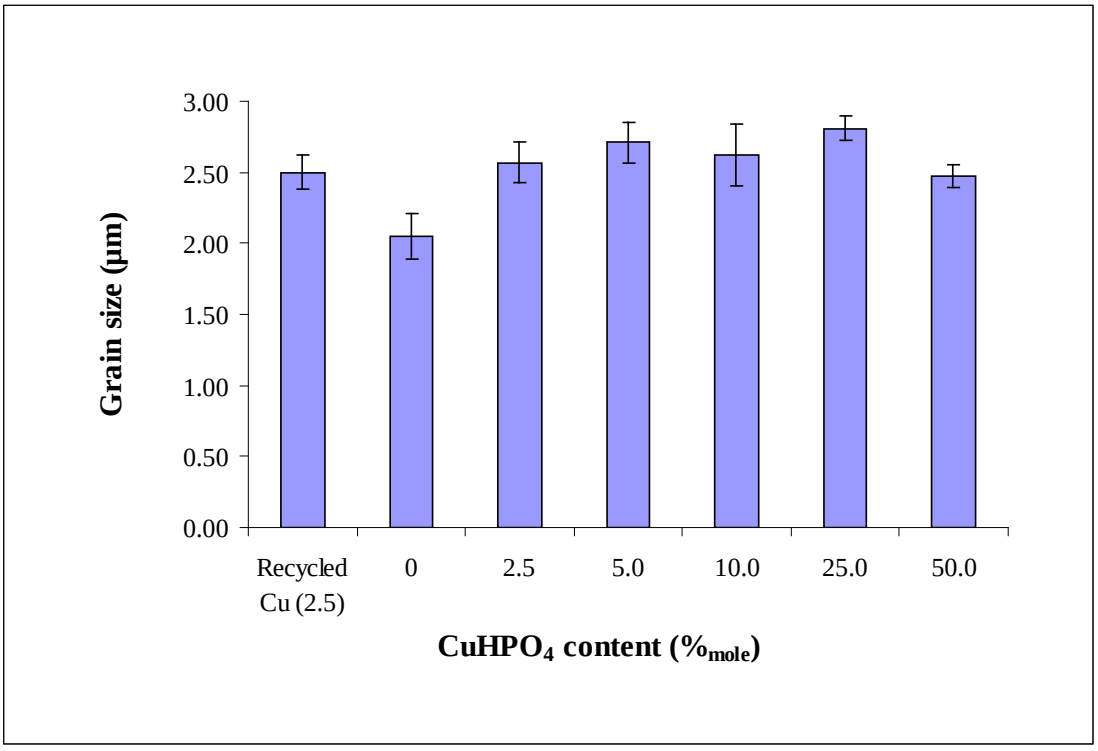

Figure 4.82. Grain size of copper deposits obtained by plating solutions containing different concentrations of $CuHPO_4$ salts.

* Plating conditions are listed in Table 4.58.

(a)

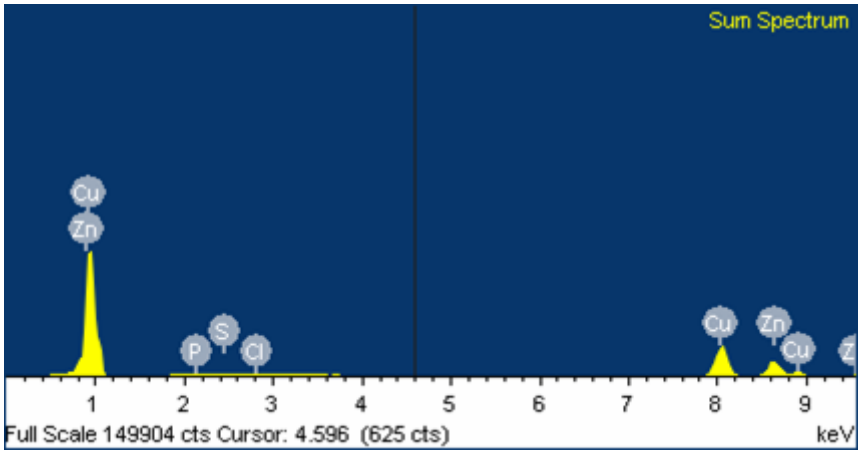

(b)

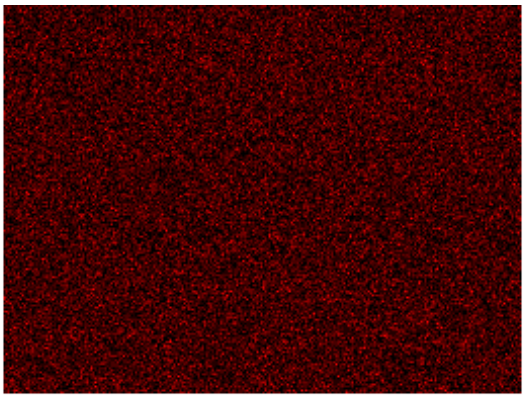

(c)

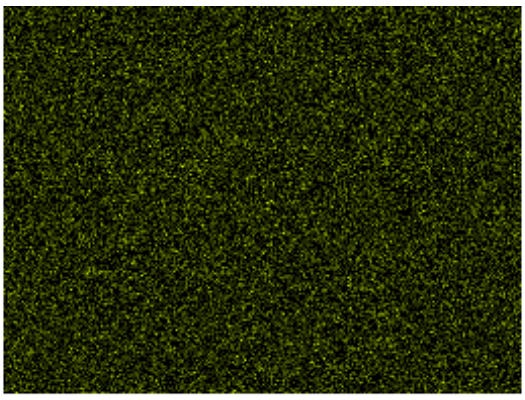

Figure 4.83. Spectra of X-ray Energy Dispersive Analysis (EDAX) of cathode workpiece (substrate) before plating: (a) overview; (b) Cu mapping; (c) Zn mapping.

(a)

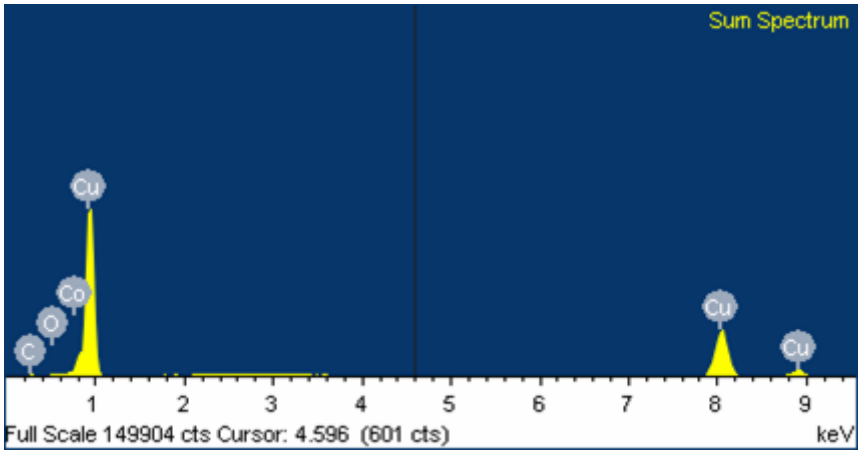

(b)

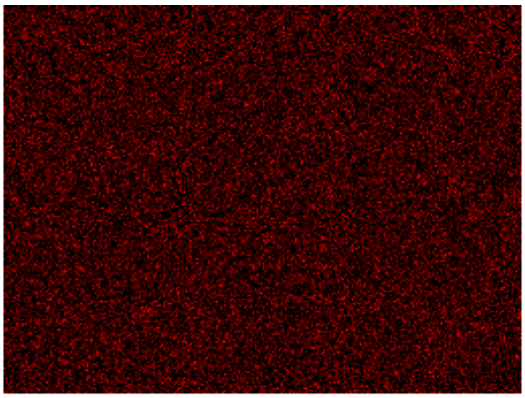

(c)

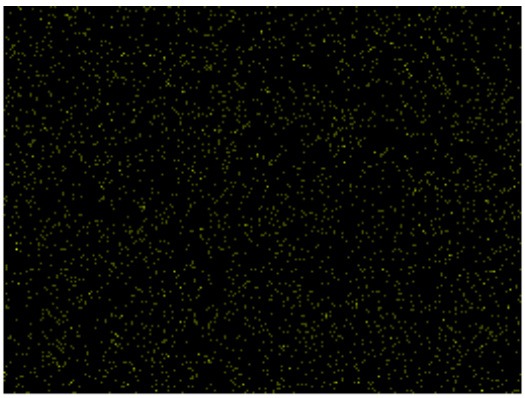

Figure 4.84. Spectra of X-ray Energy Dispersive Analysis (EDAX) of copper deposit obtained by plating solution containing 2.5%$_{mole}$ of recycled $CuHPO_4$ salt: (a) overview; (b) Cu mapping; (c) Zn mapping.

* Plating conditions are listed in Table 4.58.

(a)

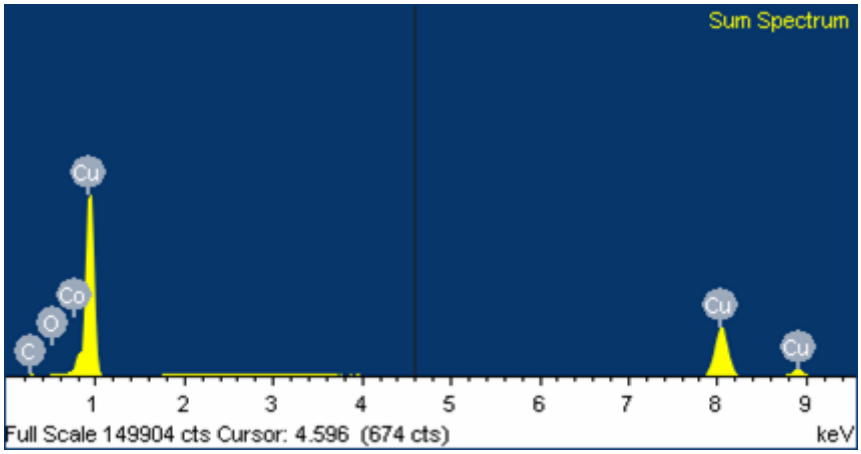

(b)

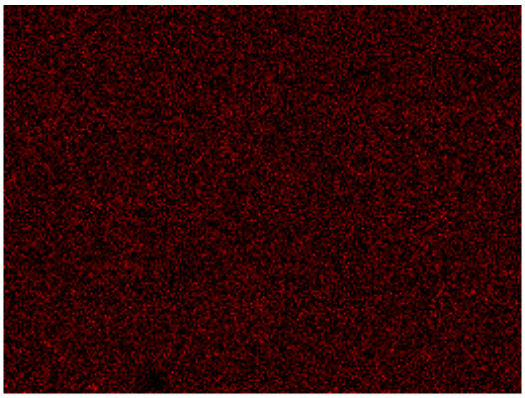

Cu Ka1

(c)

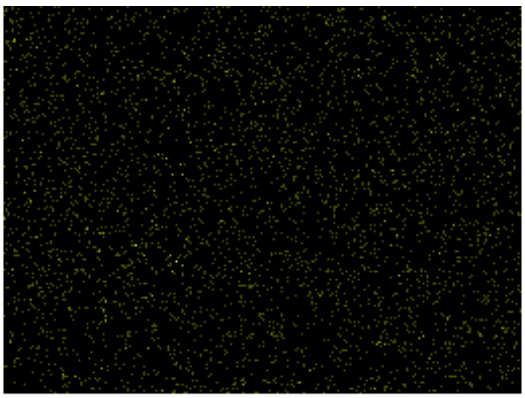

Zn Ka1

Figure 4.85. Spectra of X-ray Energy Dispersive Analysis (EDAX) of copper deposit obtained by plating solution containing $0\%_{mole}$ of $CuHPO_4$ salt: (a) overview; (b) Cu mapping; (c) Zn mapping.

* Plating conditions are listed in Table 4.58.

(a)

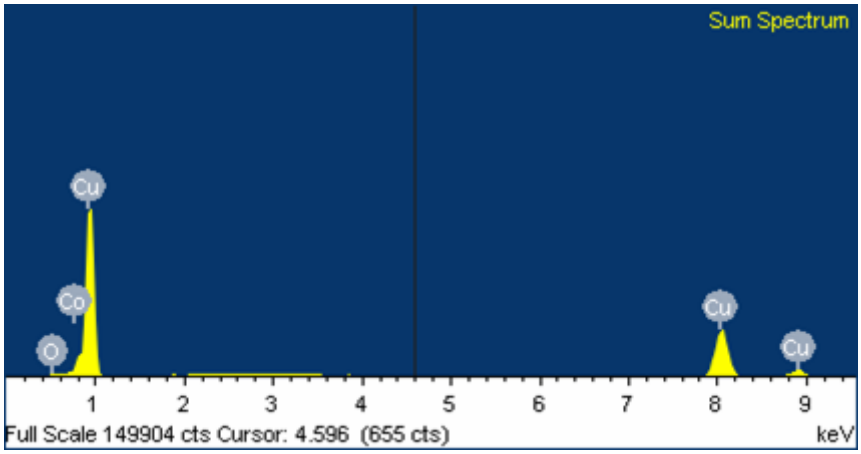

(b)

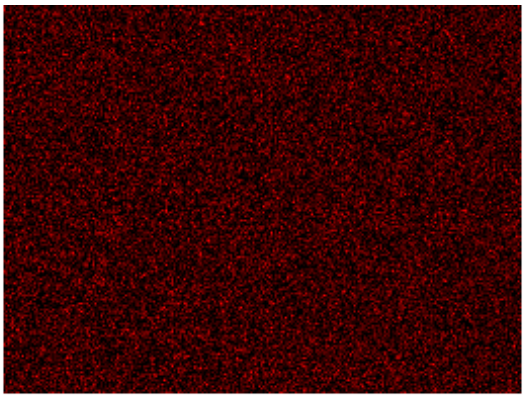

Cu Ka1

(c)

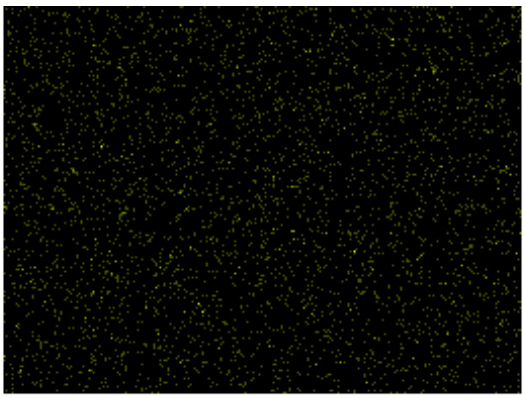

Zn Ka1

Figure 4.86. Spectra of X-ray Energy Dispersive Analysis (EDAX) of copper deposit obtained by plating solution containing 2.5%$_{mole}$ of pure $CuHPO_4$ salt: (a) overview; (b) Cu mapping; (c) Zn mapping.

* Plating conditions are listed in Table 4.58.

(a)

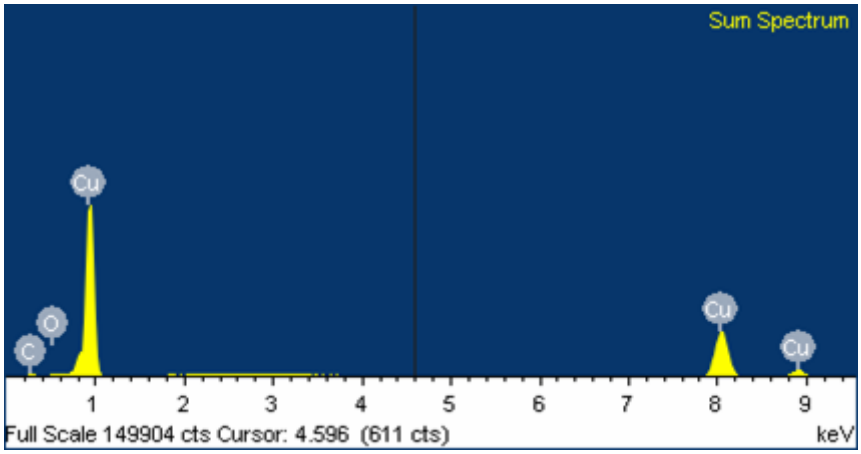

(b)

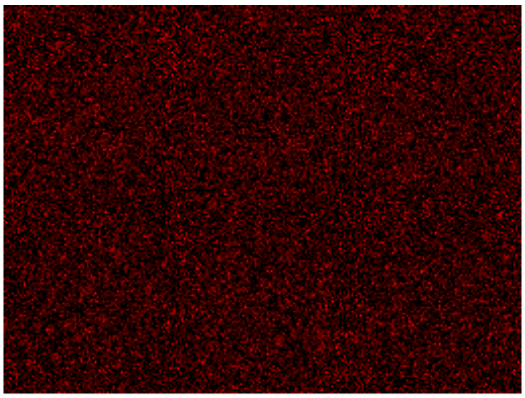

(c)

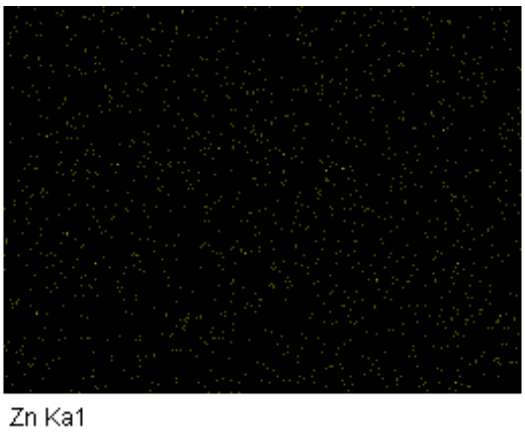

Figure 4.87. Spectra of X-ray Energy Dispersive Analysis (EDAX) of copper deposit obtained by plating solution containing 5.0%$_{mole}$ of pure $CuHPO_4$ salt: (a) overview; (b) Cu mapping; (c) Zn mapping.

* Plating conditions are listed in Table 4.58.

(a)

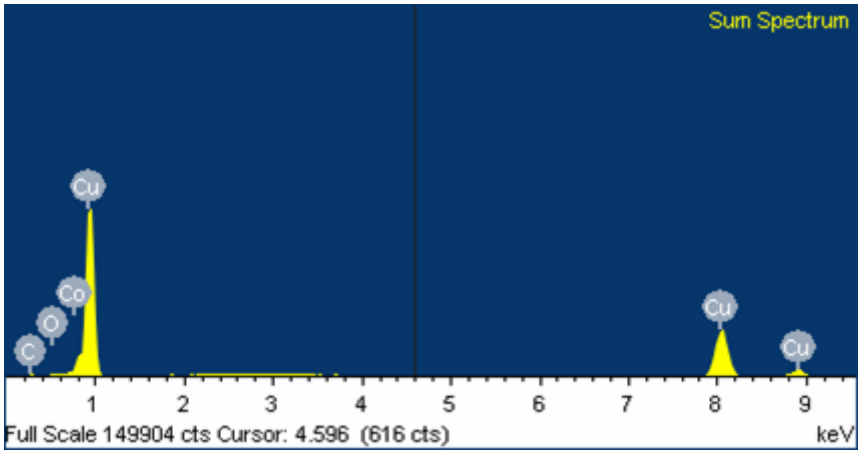

(b)

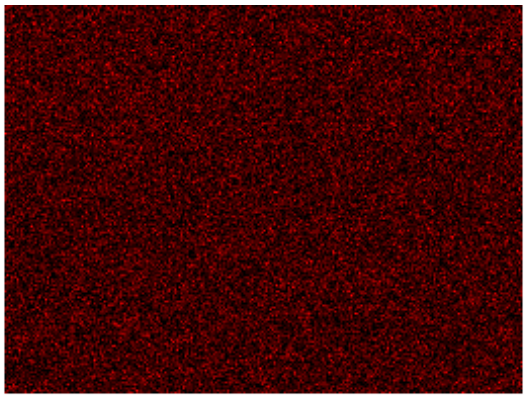

(c)

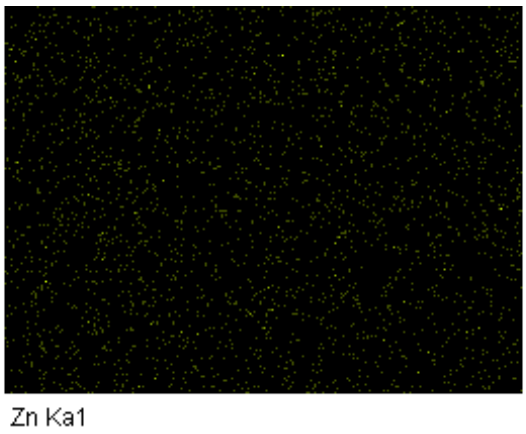

Figure 4.88. Spectra of X-ray Energy Dispersive Analysis (EDAX) of copper deposit obtained by plating solution containing 10.0%$_{mole}$ of pure $CuHPO_4$ salt: (a) overview; (b) Cu mapping; (c) Zn mapping.

* Plating conditions are listed in Table 4.58.

(a)

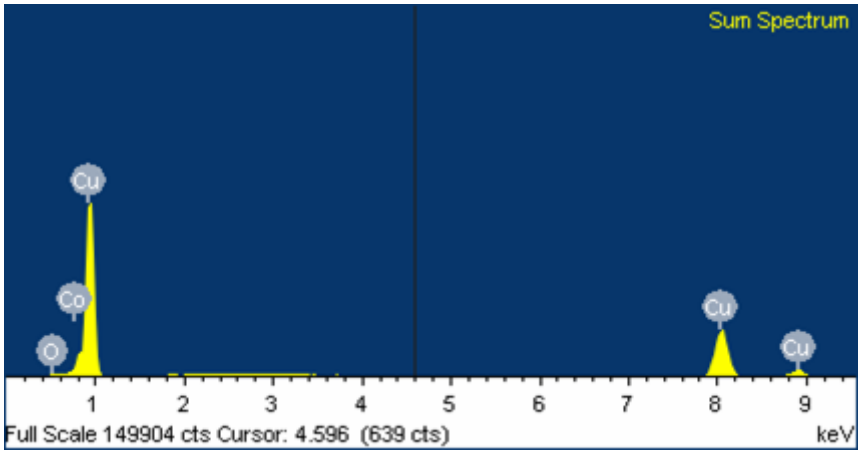

(b)

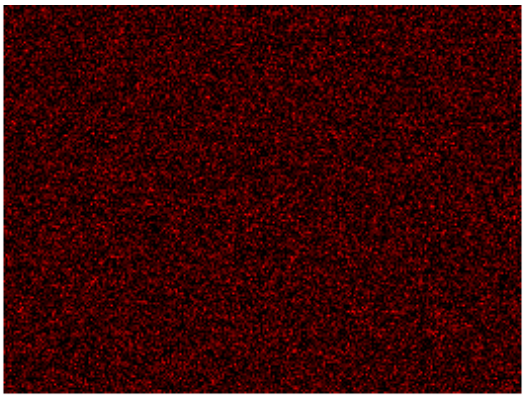

(c)

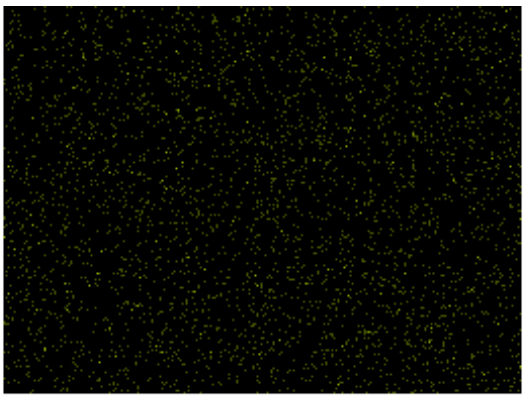

Figure 4.89. Spectra of X-ray Energy Dispersive Analysis (EDAX) of copper deposit obtained by plating solution containing 25.0%$_{mole}$ of pure $CuHPO_4$ salt: (a) overview; (b) Cu mapping; (c) Zn mapping.

* Plating conditions are listed in Table 4.58.

(a)

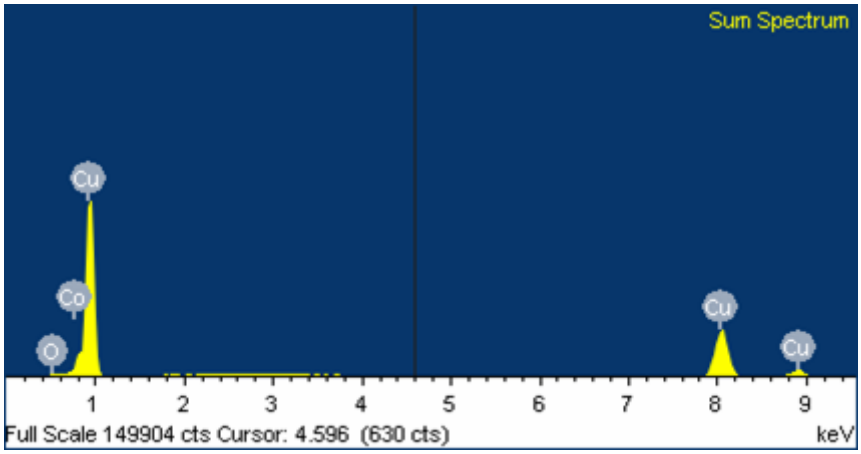

(b)

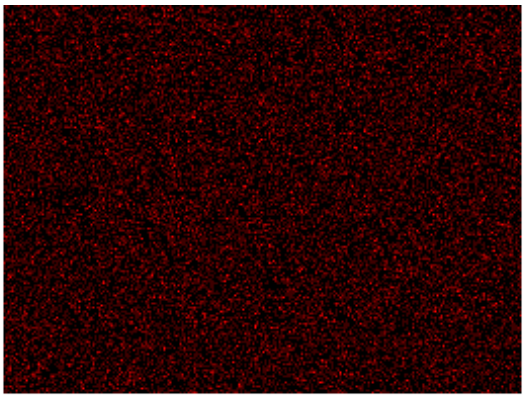

Cu Ka1

(c)

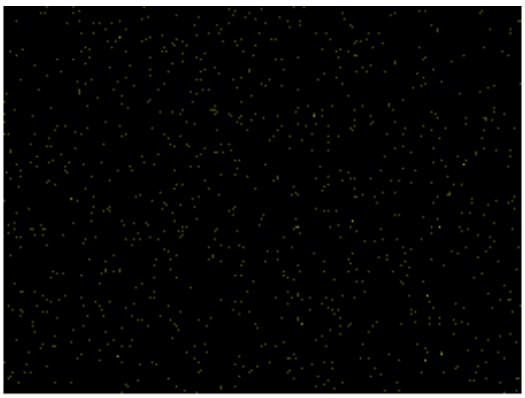

Zn Ka1

Figure 4.90. Spectra of X-ray Energy Dispersive Analysis (EDAX) of copper deposit obtained by plating solution containing 50.0%$_{mole}$ of pure $CuHPO_4$ salt: (a) overview; (b) Cu mapping; (c) Zn mapping.

* Plating conditions are listed in Table 4.58.

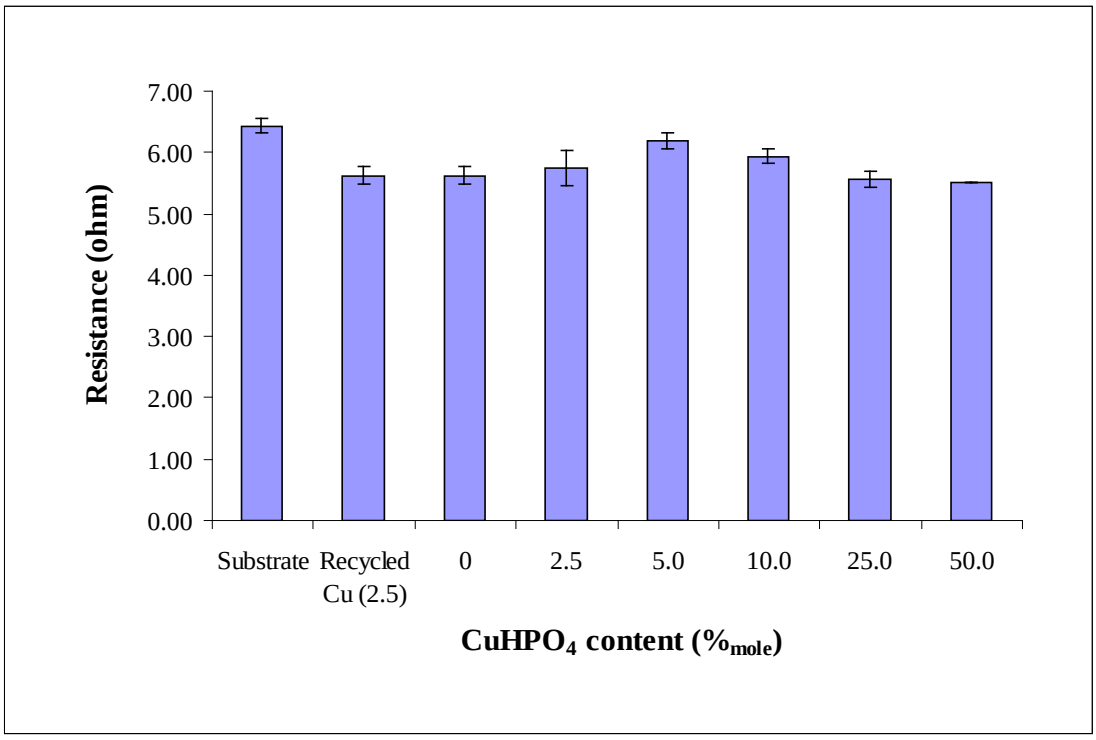

Figure 4.91. Electrical resistances of copper deposits obtained by plating solutions containing different concentrations of $CuHPO_4$ salts.

* Plating conditions are listed in Table 4.58.

Chapter 5. Conclusions

The study presented in this dissertation aimed at developing an inexpensive and effective wastewater treatment process for copper removal and recovery from industrial wastewater. *Micrococcus luteus*, an activated-sludge bacterial isolate, was investigated since it demonstrated a high copper(II) biosorption capacity in previous work. However, the suspended *M. luteus* was inefficiently separated from wastewater after the biosorption. This limited the applicability of the biomass for further recovery of the bound copper(II) ions and for reuse in the sequential wastewater treatment process. This work has examined the use of Ca-alginate/polyacrylamide gel as an immobilization matrix for the removal of copper(II) ions by *M. luteus*. A fixed-bed column reactor was then developed by using the optimized biosorbents for removal and recovery of copper(II) ions. The applicability and reusability of the column reactor were examined by consecutively treating the synthetic wastewater and the industrial electroplating wastewater. The properties of both the fixed-bed copper(II) biosorption and desorption were also characterized. To confirm the feasibility of copper recycle, the recovered copper was reused in an acid copper electroplating process.

The characteristics of Ca-alginate grafted with polyacrylamide (PAA) as immobilization matrix were examined. The results showed that this immobilization matrix could improve the copper(II) biosorption capacity of *M. luteus* and could facilitate liquid-biomass separation. These cell-immobilized Ca-alginate/PAA beads also offered a better mechanical strength and a higher uniformity than the conventional Ca-alginate beads

grafted with other polymers, such as polyvinyl alcohol and phosphorylated polyvinyl alcohol. However, shrinkage of the cell-immobilized Ca-alginate/PAA beads was observed throughout five copper(II) biosorption/desorption cycles in the batch system. This problem could not be improved by changing gelation agents of alginate (such as $BaCl_2$, $Ba(NO_3)_2$, $CaCl_2$ and $Ca(NO_3)_2$), whereas rehydration treatment (40 ^oC oven-drying followed by re-immersing in DDI water) could stabilize the beads with a smaller size and minimize the shrinkage.

The batch biosorption studies demonstrated that the rehydrated form of the Ca-alginate/PAA immobilized *M. luteus* (RIM) and the untreated beads showed similar copper(II) biosorption capacities. Both these two types of beads required 250 min to achieve 90% of total copper(II) ions sorbed. The kinetics of copper(II) biosorption by these two types of beads could well be modeled by a pseudo-second-order equation. Both the Langmuir and Freundlich isotherm models could well describe the equilibrium isotherms of these two bead types. It was showed that the immobilization matrix exerted mass transfer resistance for copper(II) biosorption by the immobilized *M. luteus*. Accordingly, the rehydration process did not significantly alter the copper(II) biosorption characteristics of the cell-immobilized beads, and the RIM beads showed stability without a significant shrinkage. This rehydrated form of the immobilized *M. luteus* (RIM) can be applied to develop effective and inexpensive biosorbents for removing and recovering copper from wastewater.

To develop a fixed-bed column reactor, the RIM beads were packed into columns with bed depths ranging from 30 to 50 cm. Influent solutions with 50 to 200 mg-Cu/L copper(II) concentrations at pH 5.0 were introduced respectively into the stationary beds of the columns with 1 to 3 mL/min inlet upward flow rates. The results showed that breakthrough of the biosorption columns (C_e = 4 mg-Cu/L) was deferred by increasing the bed depth and decreasing the influent concentration and the flow rate. The optimal conditions were found as follows: a 50 cm bed depth, a 50 mg-Cu/L influent concentration and a 1 mL/min inlet upward flow rate.

Compared to the columns packed with the untreated biosorbents, the fixed-bed columns packed with the RIM beads exhibited a higher copper removal, a larger treatment volume, and a smaller reduction in the bead volume and the bed depth. These elucidated that the RIM beads were more applicable for the copper removal.

The RIM column operated under the optimal conditions showed a greater copper(II) uptake capacity (8.67 mg-Cu/mL-beads) and a larger treatment volume (7470 mL) at the breakthrough, compared with those achieved in the continuous-stirred-tank reactor at the breakthrough (3.93 mg-Cu/mL-beads and 3660 mL) and the batch reactor at the equilibrium (4.09 mg-Cu/mL-beads and 3818 mL). It can be concluded that the fixed-bed column reactor packed with the RIM beads was an effective system for treating copper-laden wastewater.

In the binary-metal biosorption studies, overshooting effect ($C_e/C_o > 1$) was observed in the column breakthrough profiles. The overshoots of nickel and zinc were observed in the presence of Cu(II) ions, whereas Pb(II) ions promoted the copper overshoot. The metal uptakes of the binary metal systems calculated from the column data demonstrated that the binding preference of the RIM column towards different metal ions was in the following order: Pb(II) > Cu(II) >> Ni(II) > Zn(II).

A list of common desorbing agents with various concentrations was screened to determine and compare their ability of recovering copper(II) ions from the copper-laden RIM beads. The results showed that sodium salts (NaCl, $NaNO_3$ and Na_2SO_4) were poor desorbing agents (with less than 35% copper recovery). Complexing agents (Na_2H_2EDTA, Na_2NTA and $Na_5P_3O_{10}$) displayed a destructive chelating effect on the cross linkage of calcium alginate, resulting in a serious collapse of the bead structure. Strong acids (HCl, HNO_3 and H_2SO_4) exhibited over 95% copper recoveries in the batch desorption system. However, a significant drop of the biosorption performance was consecutively observed in the biosorption/desorption cycles. This may be due to the cumulative damage of the binding sites of the RIM beads caused by the strong acids. Calcium salts, $CaCl_2$ and $Ca(NO_3)_2$, demonstrated moderate desorption abilities and reasonable bead reusabilities. $CaCl_2$ was preferred since it displayed slightly better copper(II) desorption ability and bead reusability than $Ca(NO_3)_2$.

Fixed-bed desorption studies showed that the influent $CaCl_2$ concentrations and upward flow rates had no significant influence on the overall copper recovery. A moderate flow rate (1 mL/min) and a 1 M $CaCl_2$ solution were selected as the optimal column desorption conditions to ensure an efficient desorption with minimum material consumption. The results also showed that the copper recovery in the fixed-bed system was better than that in the batch reactor.

To test the reusability of the RIM fixed-bed column, a total of ten successive biosorption/desorption cycles were performed. The biosorption runs were conducted up to the breakthrough point (C_e = 4 mg-Cu/L). The desorption processes were ceased when about 85% of the bound copper in the biosorbent packing was desorbed. The results showed that the copper removal decreased at the first four cycles (especially cycle 1) and remained steady afterward. A similar trend was also found in the treatment volume. These phenomena could be explained by the incomplete desorption in each cycle. When compared with 0.2 M HCl desorbing agent, a better reusability of the column packing was achieved by using 1 M $CaCl_2$ for the copper(II) desorption.

The surface chemical composition of the RIM beads in the sequential fixed-bed biosorption and desorption was characterized by X-ray energy-dispersive analysis. The results coupled with the material balance calculation showed that the ion exchange between calcium and copper ions was one of the major mechanisms of the biosorption and desorption in the

RIM column.

Mathematical models, including the Clark model, the Admas-Bohart model, the Yoon and Nelson model and the Thomas model, were applied in this study to predict the breakthrough curves of the fixed-bed copper(II) biosorption. Both linearized and non-linearized forms of these models were used to simulate the experimental breakthrough profiles. Good simulated breakthrough curves were obtained by the models with respect to the bed depths, the flow rates and the influent copper(II) concentrations. The r^2 values of all these simulations were almost above 0.9. The linearized Thomas model offered the better simulation with large r^2 values and small average percentages of errors. It could also provide accurate predictions of the process performances (including both the copper removals and the breakthrough time) with low variances. These indicated that the linearized Thomas model was applicable to provide an accurate description of the column dynamic behaviour, which was useful for the design of wastewater treatment process.

To carry out an integrated treatment process, industrial electroplating wastewater was pre-conditioned by adjusting the copper(II) concentration and pH, and then introduced into the RIM column for ten sequential copper(II) biosorption/desorption cycles like the above reusability study. The original stock of the wastewater was collected from a local electroplating material supplier, which was mainly composed of about 18000 mg/L copper(II) ions, 154000 mg/L sulfate ions, 3500 mg/L nitrate

ions and 1307 mg/L TOC (organic additives). The studies showed that trace amounts of matrices, including counter metal ions, anions and organics, existed in the pre-conditioned wastewater and induced insignificant effects on the copper(II) biosorption. By using ammonia solution (NH_4OH) for the pH adjustment of the wastewater, the influences on the copper removal and the stability of the RIM beads could be significantly reduced as compared with NaOH and $CaCO_3$. In the sequential integrated treatment study, similar trends of the copper removals and the treatment volume were observed as compared to those of the reusability study using the synthetic copper(II) solution. The copper removal and the treatment volume decreased at the initial cycles and then remained steady afterwards. The incomplete desorption of the bound copper in the column packing should be one of the possible reasons causing the demotion of the treatment performance. Moreover, the results showed that a large amount of organics, which might be the active metal-binding molecules of the beads, was washed into the column effluent throughout the process. Further, during the pH adjustment of the wastewater, the extensive addition of ammonia solution might induce a large competition between the ammonium ions and copper ions for the binding sites. As a result, lower treatment efficiency was found as compared to that of treating the synthetic wastewater.

The applicability of the recovered copper in the desorption effluent was examined in the acid-sulfate copper electroplating process. Purification was first performed by precipitating calcium and copper ions separately

from the desorption effluent with Na_2SO_4 and Na_2HPO_4. The purified copper salt could be directly reused in the plating process. As compared with the conventional metal precipitation methods, the results showed that this three-step recycle process (biosorption-desorption-purification) was particularly effective for recovering the copper salt with a higher purity from the industrial wastewater. To study the effect of the recycled copper on the plating performance, the copper salt was introduced into the plating solution to maintain a constant copper content. As compared with the plating without the recycled copper, the deposited workpieces did not reveal any significant differences in the overall appearance, surface smoothness, distribution of copper deposits, coverage, purity of copper on the deposits and electrical resistance as shown by the scanning electron micrographs, the spectra of the X-ray energy dispersive analysis and the resistance readings of the electronic multitester. All the results suggested that the recycled copper salt could be directly utilized in the plating process; hence the production cost could be lowered.

In this research studies, the rehydrated form of the Ca-alginate/PAA immobilized *M. luteus* was successfully applied in the fixed-bed column reactor with reasonable copper removal performance, desorption efficiency and biosorbent reusability. The desorbed copper after the purification could be reused in the electroplating process without any significant influence on the plating performances and the deposit characteristics. Thus, this integrated biosorption system could be developed as a promising

technology for copper removal and recovery from industrial wastewater, and should be applied further in the practical treatment system.

Chapter 6. Future Studies

The following areas are proposed to further investigate:

(i) The copper biosorption in the fixed-bed column can be studied in multiple metal solution systems and further simulated with mathematical multi-component models;

(ii) The scale-up pilot treatment can be performed in electroplating plants in order to further confirm the applicability of the integrated process;

(iii) Other spectroscopic techniques (such as AFM) and some industrial standard methods for testing the quality of electroplating workpieces (such as hardness and brightness) can be used to investigate deposit characteristics of the copper plating and evaluate the feasibility of the copper reuse through the electroplating.

Appendix
Scanning Electron Micrographs (SEMs) of copper deposits obtained by plating solutions containing different contents of $CuHPO_4$ salts (magnification: 15000X)

(a) 2.5%$_{mole}$ of recycled $CuHPO_4$

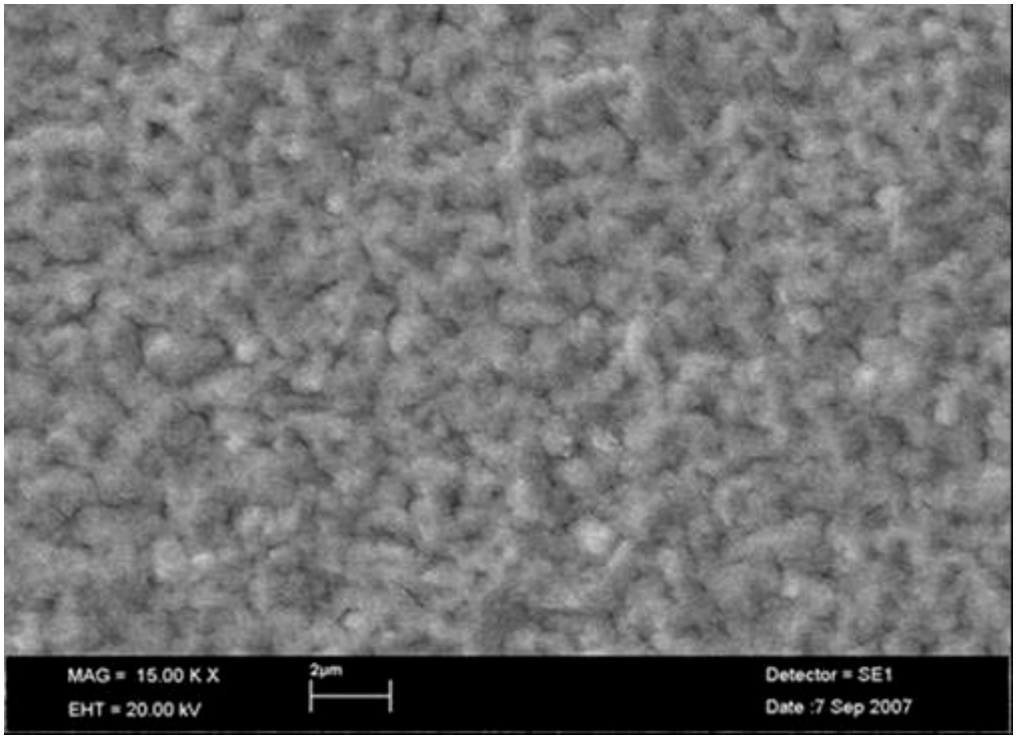

(b) 0%$_{mole}$ of $CuHPO_4$

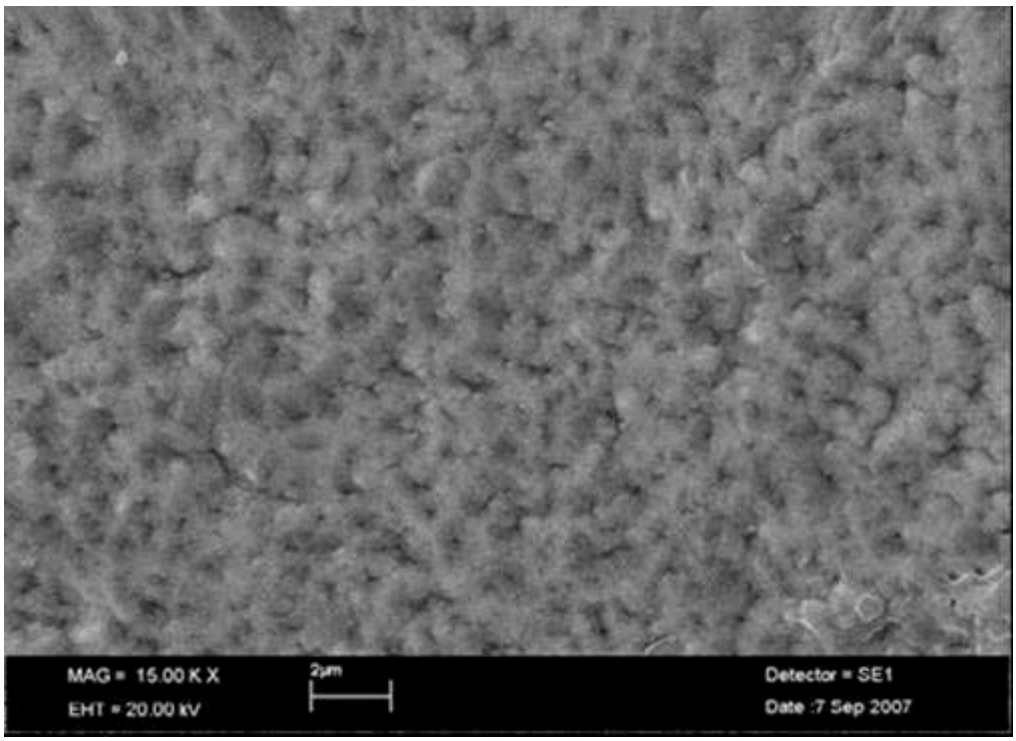

(c) 2.5%$_{mole}$ of pure $CuHPO_4$

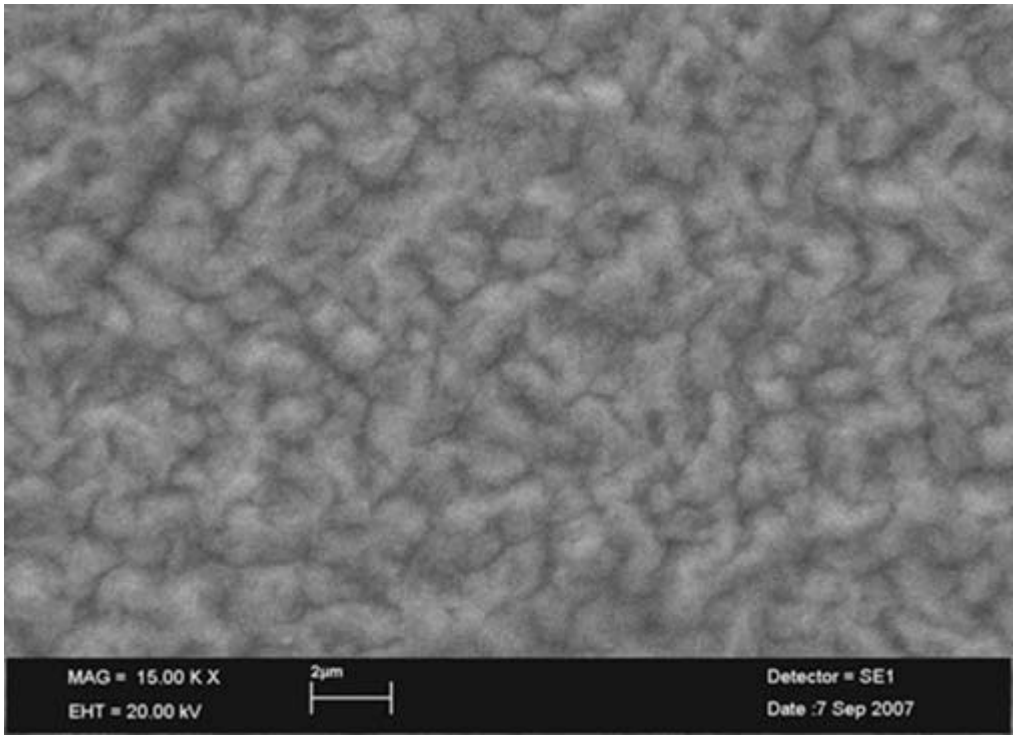

(d) 5.0%$_{mole}$ of pure $CuHPO_4$

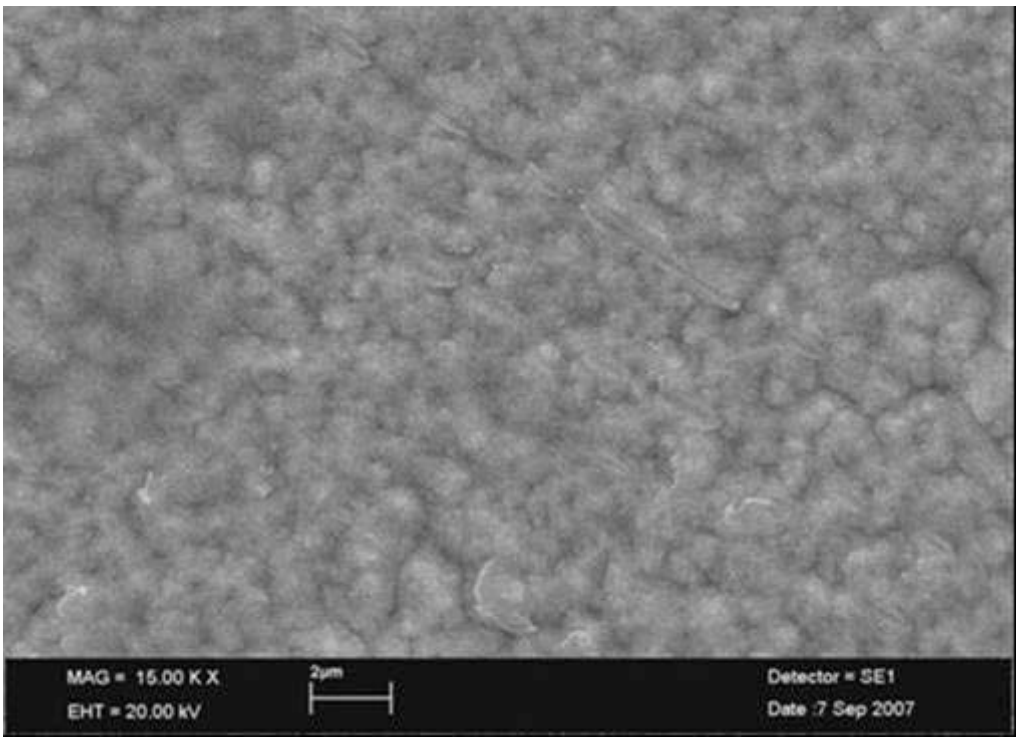

(e) 10.0%$_{mole}$ of pure $CuHPO_4$

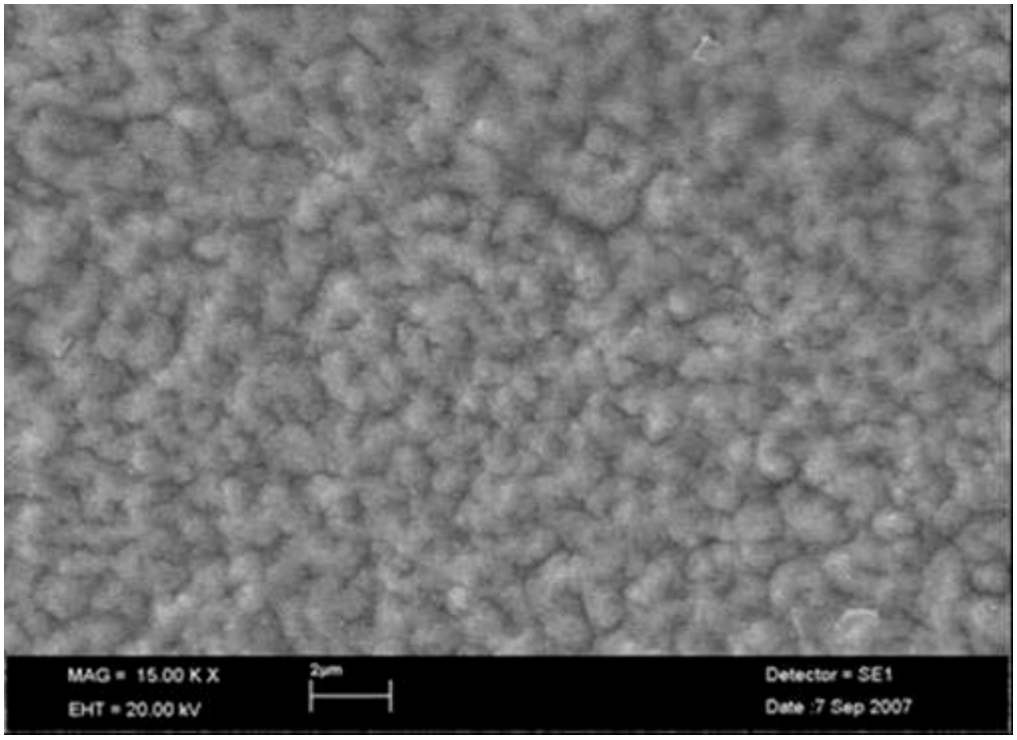

(f) 25.0%$_{mole}$ of pure $CuHPO_4$

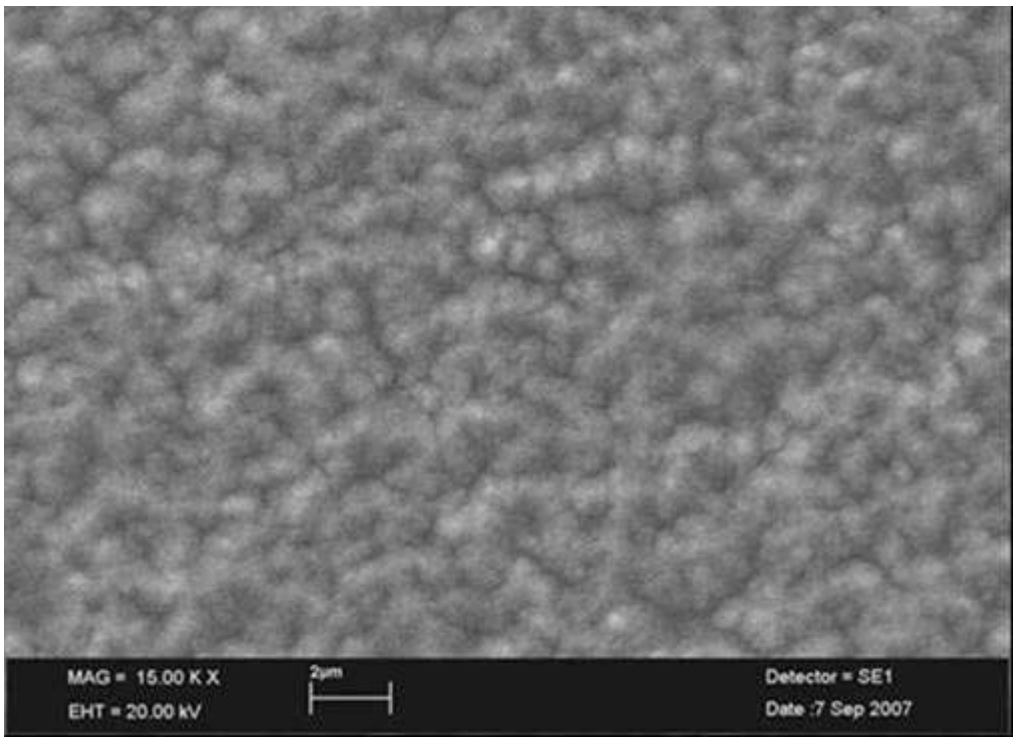

(g) 50.0%$_{mole}$ of pure $CuHPO_4$

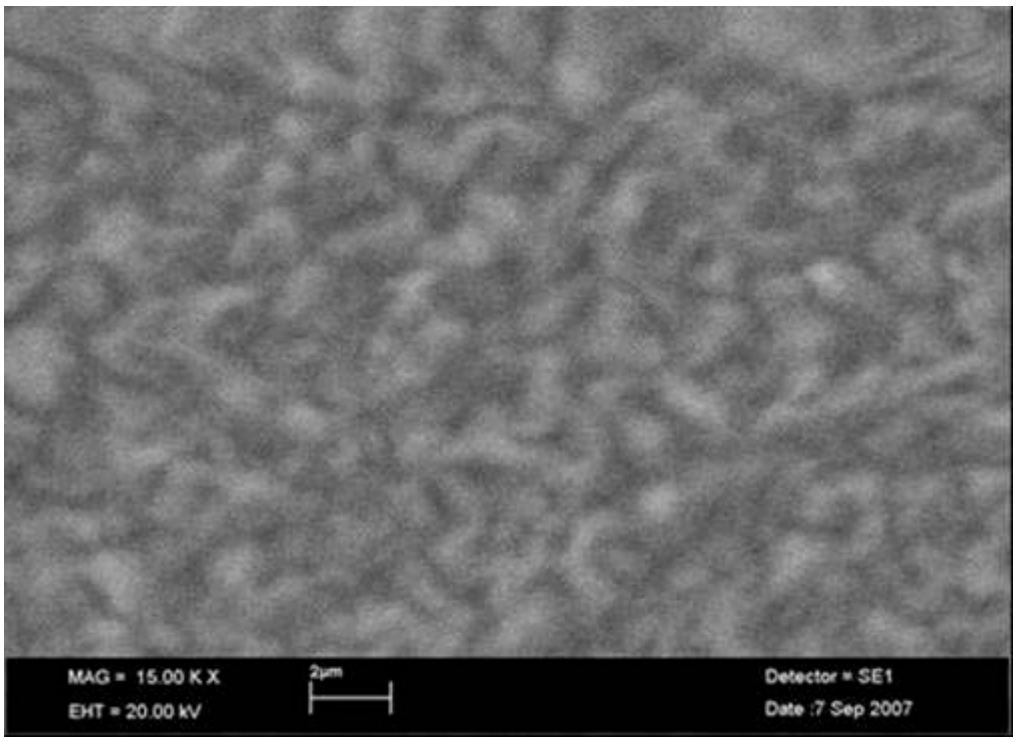

Figure A.1. Scanning Electron Micrographs (SEMs) of copper deposits obtained by plating solutions containing different concentrations of $CuHPO_4$ salts (magnification: 15000X): (a) 2.5%$_{mole}$ of recycled $CuHPO_4$; (b) 0%$_{mole}$ of $CuHPO_4$; (c) 2.5%$_{mole}$ of pure $CuHPO_4$; (d) 5.0%$_{mole}$ of pure $CuHPO_4$; (e) 10.0%$_{mole}$ of pure $CuHPO_4$; (f) 25.0%$_{mole}$ of pure $CuHPO_4$; (g) 50.0%$_{mole}$ of pure $CuHPO_4$.

* Experimental conditions are listed in Table 3.3.

References

1. Aaseth, J. and Norseth, T., (1986). Chapter 10, Copper. In Friberg, L., Nordberg, G.F. and Vouk, V.B., eds., *Handbook on the toxicology of metals, volume II,* Elsevier Science Publishers Company, New York, 233-254.

2. Agency for Toxic Substances and Disease Registry (ATSDR), (2004). *ToxFAQ™ for Strontium*. Retrieved September, 2007, from http://www.atsdr.cdc.gov/tfacts159.html.

3. Agency for Toxic Substances and Disease Registry (ATSDR), (2005). *ToxFAQ™ for Barium*. Retrieved September 11, 2007, from http://www.atsdr.cdc.gov/tfacts24.html.

4. Aharoni, C. and Suzin, Y., (1982). Application of the Elovich equation to the kinetics of occlusion, Part 1. – Homogeneous microporosity. *Journal of the Chemical Society, Faraday Transaction 1: Physical Chemistry in Condensed Phases*, **78**, (8), 2313-2320.

5. Ahluwalia, S.S. and Goyal, D., (2007). Microbial and plant derived biomass for removal of heavy metals from wastewater. *Bioresource Technology*, **98**, (12), 2243-2257.

6. Akar, T., Tunali, S. and Kiran, I., (2005). *Botrytis cinerea* as a new fungal biosorbent for removal of Pb(II) from aqueous solutions. *Biochemical Engineering Journal*, **25**, (3), 227-235.

7. Akhtar, N., Iqbal, J. and Iqbal, M., (2004). Removal and recovery of nickel(II) from aqueous solution by loofa sponge-immobilized biomass of *Chlorella sorokiniana*: characterization studies. *Journal of Hazardous Materials*, **B108**, 85-94.

8. Aksu, Z., Akpinar, D., Kabasakal, E. and Köse, B., (1999). Simultaneous biosorption of phenol and nickel(II) from binary mixtures onto dried aerobic activated sludge. *Process Biochemistry*, **35**, 301-308.

9. Aksu, Z. and Balibek, E., (2007). Chromium(VI) biosorption by dried *Rhizopus arrhizus*: Effect of salt (NaCl) concentration on equilibrium and kinetic parameters. *Journal of Hazardous Materials*, **145**, (1-2), 210-220.

10. Aksu, Z., Çağatay, Ş.Ş. and Gönen, F., (2007). Continuous fixed bed biosorption of reactive dyes by dried *Rhizopus arrhizus*: Determination of column capacity. *Journal of Hazardous Materials*, **143**, (1-2), 362-371.

11. Aksu, Z., Eğretli, G. and Kutsal, T., (1998). A competitive study of copper(II) biosorption on Ca-alginate, agarose and immobilized *C. vulgaris* in a packed-bed column. *Process Biochemistry*, **33**, 393-400.

12. Aksu, Z. and Gönen, F., (2004). Biosorption of phenol by immobilized activated sludge in a continuous packed bed: prediction of breakthrough curves. *Process Biochemistry*, **39**, (5), 599-613.

13. Al Duri, B., (1995). Chapter 7, Adsorption modeling and mass transfer. In Mckay, G., ed., *Use of Adsorbents for the Removal of Pollutants from Wastewaters*, CRC Press, Boca Raton, New York, London, Tokyo, 133-173.

14. Al-Qodah, Z., (2006). Biosorption of heavy metal ions from aqueous solutions by activated sludge. *Desalination*, **196**, (1-3), 164-176.

15. Al-Rub, F.A.A., El-Naas, M.H., Benyahia, F. and Ashour, I., (2004). Biosorption of nickel on blank alginate beads, free and immobilized algal cells. *Process Biochemistry*, **39**, (11), 1767-1773.

16. An, H.K., Park, B.Y. and Kim, D.S., (2001). Crab shell for the removal of heavy metals from aqueous solution. *Water Research*, **35**, 3551-3556.

17. Andrès, Y., MacCordick, H.J. and Hubert, J.C., (1995). Selective biosorption of thorium ions by an immobilized mycobacterial biomass. *Applied Microbiology and Biotechnology*, **44**, 271-276.

18. Ansari, M.I, and Malik, A., (2007). Biosorption of nickel and cadmium by metal resistant bacterial isolates from agricultural soil irrigated with industrial wastewater. *Bioresource Technology*, **98**, (16), 3149-3153.

19. Arıca, M.Y., Arpa, Ç., Ergene, A., Bayramoğlu, G. and Genç, Ö., (2003). Ca-alginate as a support for Pb(II) and Zn(II) biosorption with immobilized *Phanerochaete chrysosporium*. *Carbohydrate Polymers*, **52**, (2), 167-174.

20. Arıca, M.Y., Bayramoğlu, G., Yılmaz, M., Bektaş, S. and Genç, Ö., (2004). Biosorption of Hg^{2+}, Cd^{2+}, and Zn^{2+} by Ca-alginate and immobilized wood-rotting fungus *Funalia trogii*. *Journal of Hazardous Materials*, **109**, (1-3), 191-199.

21. ASTM International (ASTM), (2003). Designation: B 832-93, Standard guide for electroforming with nickel and copper. *ASTM International*, US.

22. Ayoob, S. and Gupta, A.K., (2007). Sorptive response profile of an adsorbent in the defluoridation of drinking water. *Chemical Engineering Journal*, **133**, (1-3), 273-281.

23. Babel, S. and Kurniawan, T.A., (2004). Cr(VI) removal from synthetic wastewater using coconut shell charcoal and commercial activated carbon modified with oxidizing agents and/or chitosan. *Chemosphere,* **54,** 951-967.

24. Bai, R.S. and Abraham, T.E., (2002). Studies on enhancement of Cr(VI) biosorption by chemically modified biomass of *Rhizopus nigricans*. *Water Research*, **36**, (5), 1224-1236.

25. Bai, R.S. and Abraham, T.E., (2003). Studies on chromium(VI) adsorption-desorption using immobilized fungal biomass. *Bioresource Technology*, **87**, 17-26.

26. Baik, W.Y., Bae, J.H., Cho, K.M. and Hartmeier, W., (2002). Biosorption of heavy metals using whole mold mycelia and parts of thereof. *Bioresource Technology*, **81**, 167-170.

27. Bailey, S.E., Olin, T.J., Bricka, R.M. and Adrian, D.D., (1999). A review of potentially low-cost sorbents for heavy metals. *Water Research*, **33**, 2469-2479.

28. Bajpai, S.K., Saxena, S.K. and Sharma, S., (2006). Swelling behavior of barium ion-crosslinked bipolymeric sodium alginate-carboxymethyl guar gum blend beads. *Reactive and Functional Polymers*, **66**, (6), 659-666.

29. Bajpai, S.K. and Sharma, S., (2004). Investigation of swelling/degradation behavior of alginate beads crosslinked with Ca^{2+} and Ba^{2+} ions. *Reactive and Functional Polymers*, **59**, (2), 129-140.

30. Bakkaloglu, I., Butter, T.J., Evison, L.M., Holland, F.S. and Hancock, I.C., (1998). Screening of various types biomass for removal and recovery of heavy metals (Zn, Cu, Ni) by biosorption, sedimentation and desorption. *Water Science and Technology,* **38**, (6), 269-277.

31. Belter, P.A., Cussler, E.L. and Hu, W., (1988). Chapter 6, Adsorption. *Bioseparations: Downstream Processing for Biostechnology*, John Wiley and Sons, Inc., New York, 145-179.

32. Beolchini, F., Pagnanelli, F., Toro, L. and Veglio, F., (2003). Biosorption of copper by *Sphaerotilus natans* immobilized in polysulfone matrix: equilibrium and kinetic analysis. *Hydrometallurgy*, **70**, 101-112.

33. Bilgili, M.S., (2006). Adsorption of 4-chlorophenol from aqueous solutions by xad-4 resin: isotherm, kinetic, and thermodynamic analysis. *Journal of Hazardous Materials*, **137**, (1), 257-164.

34. Bohart, G.S. and Adams, E.Q., (1920). Some aspects of the behavior of charcoal with respect to chlorine. *Journal of American Chemical Society*, **42**, 523-544.

35. Brady, D. and Duncan, J.R., (1994). Bioaccumulation of metal cations by *Saccharomyces cerevisiae*. *Applied Microbial and Biotechnology*, **41**, 149-154.

36. Brown, P., Jefcoat, I.A., Parrish, D., Gill, S. and Graham, E., (2000). Evaluation of the adsorptive capacity of peanut hull pellets for heavy metals in solution. *Advanced Environmental Research*, **4**, 19-29.

37. Butter, T.J., Evison, L.M., Hancock, I.C., Holland, F.S., Matis, K.A., Philipson, A., Sheikh, A.I. and Zoubouis, A.I., (1998). The removal and recovery of cadmium from dilute aqueous by biosorption and electrolysis at laboratory scale. *Water Research*, **32**, (2), 400-406.

38. Çabuk, A., Akar, T., Tunali, S. and Gedikli, S., (2007). Biosorption of Pb(II) by industrial strain of *Saccharomyces cerevisiae* immobilized on the biomatrix of cone biomass of *Pinus nigra*: Equilibrium and mechanism analysis. *Chemical Engineering Journal*, **131**, (1-3), 293-300.

39. Çabuk, A., Akar, T., Tunali, S. and Tabak, Ö., (2006). Biosorption characteristics of *Bacillus* sp. ATS-2 immobilized in silica gel for removal of Pb(II). *Journal of Hazardous Materials*, **136**, (2), 317-323.

40. Chang, C.C., Tseng, S.K. and Huang, H.K., (1999). Hydrogenotrophic denitrification with immobilized *Alcaligenes eutrophus* for drinking water treatment. *Bioresource Technology*, **69**, (1), 53-58.

41. Chang, J.S. and Huang, J.C., (1998). Selective adsorption/ recovery of Pb, Cu, and Cd with multiple fixed beds containing immobilized bacterial biomass. *Biotechnology Progress*, **14**, 735-741.

42. Chen, B., Chen, S. and Chang, J., (2005a). Immobilized cell fixed-bed bioreactor for wastewater decolorization. *Process Biochemistry*, **40**, (11), 3434-3440.

43. Chen, J., Tao, X., Xu, J., Zhang, T. and Liu, Z., (2005b). Biosorption of lead, cadmium and mercury by immobilized *Microcystis aeruginosa* in a column. *Process Biochemistry*, **40**, (12), 3675-3679.

44. Choy, K.K.H., Ko, D.C.K., Cheung, C.W., Porter, J.F. and Mckay, G., (2004). Film and intraparticle mass transfer during the adsorption of metal ions onto bone char. *Journal of Colloid and Interface Science*, **271**, 284-295.

45. Chu, K.H., (2002). Removal of copper from aqueous solution by chitosan in prawn shell: adsorption equilibrium and kinetics. *Journal of Hazardous Materials*, **B90**, 77-95.

46. Chu, K.H. and Hashim, M.A., (2007). Copper biosorption on immobilized seaweed biomass: Column breakthrough characteristics. *Journal of Environmental Sciences*, **19**, (8), 928-932.

47. Clark, R.M., (1987). Evaluating the cost and performance of field-scale granular activated carbon systems. *Environmental Science and Technology*, **21**, 573-580.

48. Cliff, B.,Weibel, D.E., Lockyer, N.P., Jungnickel, H., Stephens, G. and Vickerman, J.C., (2003). Detection of chlorinated pesticides on the surface of fungus using ToF-SIMS. *Applied Surface Science*, **203-204**, 710-713.

49. Cochrane, E.L., Lu, S., Gibb, S.W. and Villaescusa, I., (2006). A comparison of low-cost biosorbents and commercial sorbents for the removal of copper from aqueous media. *Journal of Hazardous Materials*, **137**, (1), 198-206.

50. Connors, K.A., (1990). Chapter 2, Simple rate equations. *Chemical Kinetics: The study of reaction rates in solution*, VCH Publishers, Inc., USA, 17-57.

51. Copper Development Association (CDA), (2007). *Annual Data 2007 Copper · Brass · Bronze, Copper Supply and Consumption 1986-2006*, Copper Development Association Inc., New York.

52. Crist, R.H., Martin, J.R., Chonko, J. and Crist, D.R., (1996). Uptake of metals on peat moss: ion-exchange process. *Environmental Science and Technology*, **30**, 2461-2456.

53. Dainty, A.L., Goulding, K.H., Robinson, P.K., Simpkins, I. and Trevan, M.D., (1986). Stability of alginate-immobilized algal cells. *Biotechnology and Bioengineering*, **28**, 210-216.

54. Das, S.K. and Guha, A.K., (2007). Biosorption of chromium by *Termitomyces clypeatus*. *Colloids and Surfaces B: Biointerfaces*, **60**, (1), 46-54.

55. Davis, T.A., Volesky, B. and Mucci, A., (2003). A review of the biochemistry of heavy metal biosorption by brown algae. *Water Research*, **37**, 4311-4330.

56. Davis, T.A., Volesky, B. and Vieira, R.H.S.F., (2000). *Sargassum* seaweed as biosorbent for heavy metals. *Water Research*, **34**, (17), 4270-4278.

57. Deng, L., Su, Y., Su, H., Wang, X. and Zhu, X., (2007). Sorption and desorption of lead (II) from wastewater by green algae *Cladophora fascicularis*. *Journal of Hazardous Materials*, **143**, (1-2), 220-225.

58. Deng, S. and Ting, Y.P., (2005). Characterization of PEI-modified biomass and biosorption of Cu(II), Pb(II) and Ni(II). *Water Research*, **39**, 2167-2177.

59. Dini, J.W., (1993). Chapter 7, Additives. *Electrodeposition: The Materials Science of Coatings and Substrates*, Noyes Publications, US, 195-248.

60. Dini, J.W., (2000). Chapter 2, Electrodeposition of copper. In Schlesinger, M. and Paunovic, M., eds., *Modern Electroplating*, 4th ed., John Wiley and Sons, Inc., 61-125.

61. Diniz, V., Weber, M.E., Volesky, B. and Naja, G., (2008). Column biosorption of lanthanum and europium by *Sargassum*. *Water Research*, **42**, (1-2), 363-371.

62. Do, D.D., (1998). Chapter 9, Analysis of adsorption kinetics in a single homogeneous particle. *Adsorption Analysis: Equilibria and Kinetics*, Imperial College Press, 519-602.

63. Dos Santos, V.A.P.M., Leenen, E.J.T.M., Rippoll, M.M., Van Der Sluis, C., Van Vliet, T., Tramper, J. and Wijiffels, R.H., (1997). Relevance of rheological properties of gel beads for their mechanical stability in bioreactors. *Biotechnology and Bioengineering*, **56**, 517-529.

64. Durney, L.J., (1984). Chapter 6, Plating bath compositions and operating conditions. *Electroplating Engineering Handbook*, 4th ed., Van Nostrand Reinhold Company, New York, 226-262.

65. Dursun, A.Y. and Aksu, Z., (2000). Biodegradation kinetics of ferrous(II) cyanide complex ions by immobilized *Pseudomonas fluorescens* in a packed column reactor. *Process Biochemistry*, **35**, 615-622.

66. Eccles, H., (1995). Removal of heavy metals from effluent streams – why select a biological process? *International Biodeterioration and Biodegradation*, **35**, (103), 5-16.

67. Eibl, R.H. and Moy, V.T., (2005). Atomic force microscopy measurements of protein-ligand interactions on living cells. *Methods of Molecular Biology*, **305**, 439-450.

68. Ellaiah, P., Prabhakar, T., Ramakrishna, B., Taleb, A.T. and Adinarayana, K., (2004). Production of lipase by immobilized cells of *Aspergillus niger*. *Process Biochemistry*, **39**, (5), 525-528.

69. El-Sikaily, A., Nemr, A.E., Khaled, A. and Abdelwehab, O., (2007). Removal of toxic chromium from wastewater using green alga Ulva lactuca and its activated carbon. *Journal of Hazardous Materials*, **148**, (1-2), 216-228.

70. Environmental Protection Agency (EPA), (2006). *Consumer Factsheet on: Copper*. Retrieved November 29, 2006, from http://www.epa.gov/safewater/dwh/c-ioc/copper.html

71. Environmental Protection Department (EPD), (2004). *Technical Memorandum - Standards for Effluents Discharged into Drainage and Sewerage Systems, Inland and Coastal Waters*, The Government of the Hong Kong Special Administrative Region, Hong Kong.

72. Environmental Protection Department (EPD), (2005). Appendix E, Summary statistics for bottom sediment quality in the Eastern Buffer and Victoria Habour WCZs, 2001 - 2005. *20 Years of Marine Water Quality Monitoring in hong Kong (1986 - 2005)*, The Government of the Hong Kong Special Administrative Region, Hong Kong, E-6.

73. Esposito, A., Pagnanelli, F., Lodi, A., Solisio, C. and Vegliò, F., (2001). Biosorption of heavy metal by *Sphaerotilus natans*: An equilibrium study at different pH and biomass concentrations. *Hydrometallurgy*, **60**, (2), 129-141.

74. Figueira, M.M., Volesky, B., Azarian, K. and Cimielli, V.S.T., (2000). Biosorption column performance with a metal mixture. *Environmental Science & Technology*, **34**, 4320-4326.

75. Figueiredo, H., Silva, B., Raposo, M.M.M., Fonseca, A.M., Neves, I.C., Quintelas, C. and Tavares, T., (2008). Immobilization of Fe(III) complexes of pyridazine derivatives prepared from biosorbents supported on zeolites. *Microporous and Mesoporous Materials*, **109**, 163-171.

76. Foulke, D.G., (1975). Chapter 9, Solution analysis. In Foulke, D.G., eds., *Electorplater's process control handbook*, Robert E Krieger Publishing Company, Malabar, Florida, 162-250.

77. Fourest, E. and Roux, J.C., (1992). Heavy metal biosorption by fungal mycelial by-products: mechanisms and influence of pH. *Applied Microbial and Biotechnology*, **37**, 399-403.

78. Fourest, E. and Roux, J.C., (1994). Improvement of heavy-metal biosorption by mycelial dead biomasses (*Rhizopus arrhizus*, *Mucor miehei* and *Penicillium chrysogneum*) – pH control and cationic activation. *FEMS Microbiology Review*, **14**, 325-332.

79. Furusawa, T. and Smith, J.M., (1973). Fluid-particle and intraparticle mass transport rates in slurries. *Industrial and Engineering Chemistry Fundamentals*, **12**, (12), 197-203.

80. Gadd, G.M., White, C. and Rome, L., (1988). Heavy metal and radionuclide uptake by fungi and yeasts. In Norris, P. R., Kew, D. P., eds., *Biohydrometallurgy*, Kelly, UK, 421-435.

81. Galiatsatou, P., Metaxas, M. and Kasselouri-Rigopoulou, V., (2002). Adsorption of zinc by activated carbons prepared from solvent extracted olive pulp. *Journal of Hazardous Materials*, **91**, (1-3), 187-203.

82. Gong, R., Ding, Y., Liu, H., Chen, Q. and Liu, Z., (2005). Lead biosorption and desorption by intact and pretreated *Spirulina maxima* biomass. *Chemosphere*, **58**, (1), 125-130.

83. Gouda, M.K., Omar, S.H., Chekroud, Z.A. and Eldin, H.M.N., (2007). Bioremediation of kerosene I: A case study in liquid media. *Chemosphere*, **69**, (11), 1807-1814.

84. Grant, G.T., Morris, E.R., Rees, D.A., Smith, P.J.C. and Thom, D., (1973). Biological interactions between polysaccharides and divalent cations: the egg-box model. *FEEBS letter*, **32**, 195-198.

85. Grimm, A., Zanzi, R., Björnbom, E. and Cukierman, A.L., (2008). Comparison of different types of biomasses for copper biosorption. *Bioresource Technology*, **99**, (7), 2559-2565.

86. Gupta, V.K., Rastogi, A., Saini, V.K. and Jain, N., (2006). Biosorption of copper(II) from aqueous solutions by *Spirogyra* species. *Journal of Colloid and Interface Science*, **296**, (1), 59-63.

87. Hahn, D., (2003). Chapter 3, The technology of electrodeposition of copper and its alloys. In Kanani, N., ed., *Electroplating and Electroless Plating of Copper and its Alloys*, Finishing Publications Ltd., UK, 51-73.

88. Hammaini, A., Ballester, A., Gonzalez, F., Blazquez, M.L. and Munoz, J.A., (1999). Activated sludge as biosorbent of heavy metals. Biohydrometallurgy and the environment toward the mining of the 21st century. *International Biohydrometallurgy symposium IBS'99*, 185-192.

89. Hammaini, A., González, F., Ballester, A., Blázquez, M.L. and Muñoz, J.A., (2007). Biosorption of heavy metals by activated sludge and their desorption characteristics. *Journal of Environmental Management*, **84**, (4), 419-426.

90. Han, M.H. and Yun, Y., (2007). Mechanistic understanding and performance enhancement of biosorption of reactive dyestuffs by the waste biomass generated from amino acid fermentation process. *Biochemical Engineering Journal*, **36**, (1), 2-7.

91. Han, R., Wang, Y., Zou, W., Wang, Y. and Shi, J., (2007). Comparison of linear and nonlinear analysis in estimating the Thomas model parameters for methylene blue adsorption onto natural zeolite in fixed-bed column. *Journal of Hazardous Materials*, **145**, (1-2), 331-335.

92. Han, R., Zhang, J., Zou, W., Shi, J. and Liu, H., (2005). Equilibrium biosorption isotherm for lead ion on chaff. *Journal of Hazardous Materials*, **125**, (1-3), 266-271.

93. Han, X., Wong, Y.S. and Tam, N.F.Y., (2006). Surface complexation mechanism and modeling in Cr(III) biosorption by a microalgal isolate, *Chlorella miniata*. *Journal of Colloid and Interface Science*, **303**, (2), 365-371.

94. Hanif, M.A., Nadeem, R., Zafar, M.N., Akhtar, K. and Bhatti, H.N., (2007). Kinetic studies for Ni(II) biosorption from industrial wastewater by *Cassia fistula* (Golden Shower) biomass. *Journal of Hazardous Materials*, **145**, (3), 501-505.

95. Hatzikioseyian, A., Mavituna, F. and Tsezos, M., (1999). Modelling of fixed bed biosorption columns in continuous metal ion removal processes. The case of single solute local equilibrium. *Process Metallurgy*, **9B**, 429-448.

96. Hawari, A.H. and Mulligan, C.N., (2006a). Biosorption of lead(II), cadmium(II), copper(II) and nickel(II) by anaerobic granular biomass. *Bioresource Technology*, **97**, (4), 692-700.

97. Hawari, A.H. and Mulligan, C.N., (2006b). Heavy metals uptake mechanisms in a fixed-bed column by calcium-treated anaerobic biomass. *Process Biochemistry*, **41**, (1), 187-198.

98. Helfferich, F., (1995). Chapter 6, Kinetics. *Ion exchange*, Dover Publication, Inc., New York, 250-322.

99. Hillman, D.C., (1995). Part 4000, Inorganic nonmetallic constituents. In Eaton, A.D., Clesceri, L.S. and Greenberg, A.E., eds., *Standard Methods for the Examination of Water and Wastewater*, 19th ed., American Public Health Association, Washington DC, US, 4:85-86.

100. Ho, Y.S. and Mckay, G., (1998). Kinetic models for the sorption of dye from aqueous solution by wood. *Process Safety and Environmental Protection*, **76**, (B), 183-191.

101. Housecroft, C.E. and Sharpe, A.G., (2005). Appendix 8, Ground state electronic configurations of the elements and ionization energies for the first five ionizations. *Inorganic Chemistry*, 2nd ed., Pearson Education Limited, England, 880-882.

102. Hu, M.Z.C. and Reeves, M., (1997). Biosorption of uranium by *Pseudomonas aeruginosa* strain CSU immobilized in a novel matrix. *Biotechnology Progress*, **13,** 60-70.

103. Ibáñez, J. P. and Umetsu, Y., (2002). Potential of protonated alginate beads for heavy metals uptake. *Hydrometallurgy*, **64**, 89-99.

104. Ibáñez, J.P. and Umetsu, Y., (2004). Uptake of trivalent chromium from aqueous ions using protonated dry alginate beads. *Hydrometallurgy*, **72**, (3-4), 327-334.

105. Igel, O. and Streup, H., (2003). Chapter 5, The applications of electrodeposited copper and copper alloy coatings. In Kanani, N., ed., *Electroplating and Electroless Plating of Copper and its Alloys*, Finishing Publications Ltd., UK, 89-122.

106. Iqbal, M., Saeed, A. and Zafar, S.I., (2007). Hybrid biosorbent: An innovative matrix to enhance the biosorption of Cd(II) from aqueous solution. *Journal of Hazardous Materials*, **148**, (1-2), 47-55.

107. Jeon, C., Park, J.Y. and Yoo, Y.J., (2002). Novel immobilization of alginic acid for heavy metal removal. *Biochemical Engineering Journal*, **11**, (2-3), 159-166.

108. Jeon, C., Yoo, Y.J. and Hoell, W.H., (2005). Environmental effects and desorption characteristics on heavy metal removal using carboxylated alginic acid. *Bioresource Technology*, **96**, (1), 15-19.

109. Kaikake, K., Hoaki, K., Sunada, H., Dhakal, R.P. and Baba, Y., (2007). Removal characteristics of metal ions using degreased coffee beans: Adsorption equilibrium of cadmium(II). *Bioresource Technology*, **98**, (15), 2787-2791.

110. Kalavathy, M.H., Karthikeyan, T., Rajgopal, S. and Miranda, L.R., (2005). Kinetic and isotherm studies of Cu(II) adsorption onto H3PO4-activated rubber wood sawdust. *Journal of Colloid and Interface Science*, **292,** 354-362.

111. Kanani, N. (2003). Chapter 7, Properties of electroless copper coatings. *Electroplating and Electroless Plating of Copper and its Alloys*, Finishing Publications Ltd., UK, 159-184.

112. Kasan, H.C., (1993). The role of waste activated sludge and bacteria in metal-ion removal from solution. *Critical Reviews in Environmental Science and Technology*, **23**, 79-117.

113. Kazy, S.K., D'Souza, S.F. and Sar, P., (2008). Uranium and thorium sequestration by a *Pseudomonas* sp.: mechanism and chemical characterization. *Journal of Hazardous Materials*, **163**, (1), 65-72.

114. Khang, D., Kim, S.Y., Liu-Snyder, P., Palmore, G.T.R., Durbin, S.M. and Webster, T.J., (2007). Enhanced fibronectin adsorption on carbon nanotube/poly(carbonate) urethane: Independent role of surface nano-roughness and associated surface energy. *Biomaterials*, **28**, (32), 4756-4768.

115. Khattar, J.I.S., Sarma, T.A. and Singh, D.P., (1999). Removal of chromium ions by agar immobilized cells of the cyanobacterium *Anacystis nidulans* in a continuous flow bioreactor. *Enzyme Microbial Technoloby*, **25**, 564-568.

116. Khoo, K.M. and Ting, Y.P., (2001). Biosorption of gold by immobilized fungal biomass. *Biochemical Engineering Journal*, **8**, (1), 51-59.

117. Ko, D.C.K., Porter, J.F., Mckay, G., (2000). Optimised correlations for the fixed-bed adsorption of metal ions on bone char. *Chemical Engineering Science*, **55**, 5819-5829.

118. Kokate, A.V., Suryavanshi, U.B. and Bhosale, C.H., (2006). Structural, compositional and optical properties of electrochemically deposited stoichiometric CdSe thin films from non-aqueous bath. *Solar Energy*, **80**, (2), 156-160.

119. Kratochvil, D., Volesky, B. and Demopoulos, G., (1997). Optimizing Cu removal/ recovery in a biosorption column. *Water Research*, **31**, 2327-2339.

120. Kundu, S. and Gupta, A.K., (2007). As(III) removal from aqueous medium in fixed bed using iron oxide-coated cement (IOCC): Experimental and modeling studies. *Chemical Engineering Journal*, **129**, (1-3), 123-131.

121. Kuyucak, N. and Volesky, B., (1989). Accumulation of cobalt by marine alga. *Biotechnology and Bioengineering*, **33**, 809-814.

122. Lafouresse, M.C., Heard, P.J. and Schwarzacher, W., (2007). Surface roughness analysis of electrodeposited Cu. *Electrochimica Acta*, **53**, (1), 229-232.

123. Lázaro, N., Sevilla, A.L., Morales, S. and Marqués, A.M., (2003). Heavy metal biosorption by gellan gum gel beads. *Water Research*, **37**, (9), 2118-2126.

124. Leung, W.C., Chua, H. and Lo, W., (2001). Biosorption of heavy metals by bacteria isolated from activated sludge. *Applied Biochemistry and Biotechnology*, **91-93**, 171-184.

125. Li, B., Lin, A. and Gan, F., (2006). Preparation and characterization of Cr–P coatings by electrodeposition from trivalent chromium electrolytes using malonic acid as complex. *Surface and Coatings Technology*, **201**, (6), 2578-2586.

126. Li, H., Liu, T., Li, Z. and Deng, L., (2008). Low-cost supports used to immobilize fungi and reliable technique for removal hexavalent chromium in wastewater. *Bioresource Technology*, **99**, (7), 2234-2241.

127. Liu, Y. and Xu, H., (2007). Equilibrium, thermodynamics and mechanisms of Ni^{2+} biosorption by aerobic granules. *Biochemical Engineering Journal*, **35**, (2), 174-182.

128. Lo, W., Chua, H., Wong, M.F. and Yu, P., (2002). Bacterial biosorbent for removing and recovering copper from electroplating effluents. *Water Science and Technology*, **47**, (1), 251-256.

129. Low, K.S., Lee, C.K. and Ng, A.Y., (1999). Column studies on the sorption of Cr(VI) using quaternized rice hulls. *Bioresource Technology*, **68**, 205-208.

130. Lu, S., Gibb, S.W. and Cochrane, E., (2007). Effective removal of zinc ions from aqueous solutions using crab carapace biosorbent. *Journal of Hazardous Materials*, **149**, (1), 208-217.

131. Lu, Y. and Wilkins, E., (1996). Heavy metal removal by caustic-treated yeast immobilized in alginate. *Journal of Hazardous Materials*, **49**, (2-3), 165-179.

132. Ludwig, H., (2003). Chapter 2, Electrodeposition of copper and its alloys. In Kanani, N., ed., *Electroplating and Electroless Plating of Copper and its Alloys*, Finishing Publications Ltd., UK, 21-50.

133. Macaskie, L.E., Wates, J.M. and Dean, A.C.R., (1986). Cadmium accumulation by a *Citrobacter* sp. immobilized on gel and solid supports: applicability to the treatment of liquid wastes containing heavy metal cations. *Biotechnology and Bioengineering*, **30**, 66-73.

134. Mack, C.L., Wilhelmi, B., Duncan, J.R. and Burgess, J.E., (2008). A kinetic study of the recovery of platinum ions from an artificial aqueous solution by immobilized *Saccharomyces cerevisiae* biomass. *Minerals Engineering*, **21**, (1), 31-37.

135. Majumda, S.S., Das, S.K., Saha, T., Panda, G.C., Bandyopadhyoy, T. and Guha, A.K., (2008). Adsorption behavior of copper ions on *Mucor rouxii* biomass through microscopic and FTIR analysis. *Colloids and Surfaces B: Biointerfaces*, **63**,138-145.

136. Malkoc, E., Nuhoglu, Y. and Dundar, M., (2006). Adsorption of chromium(VI) on pomace—An olive oil industry waste: Batch and column studies. *Journal of Hazardous Materials*, **138**, (1), 142-151.

137. Martínez, M., Miralles, N., Hidalgo, S., Fiol, N., Villaescusa, I. and Poch, J., (2006). Removal of lead(II) and cadmium(II) from aqueous solutions using grape stalk waste. *Journal of Hazardous Materials*, **133**, (1-3), 203-211.

138. Mckay, G., Yee, T.F., Nassar M.M. and Magdy, Y., (1998). Fixed-bed adsorption of dyes on Bagasse ptih. *Adsorption science and Technology*, **16**, (8), 623-639.

139. Mellah, A. and Chegrouche, S., (1997). The removal of zinc from aqueous solutions by natural bentonite. *Water Research*, **31,** 621-629.

140. Menter, P., (2000). *Acrylamide Polymerization – A Practical Approach*. From http://www.biocompare.com/techart.asp?id=1089

141. Milad, G., (2001). Chapter 29, Electroplating. In Coombs, C.F., ed, *Printed Circuits Handbook*, 5th ed, McGraw-Hill Companies, Inc., 29.1-29.30.

142. Mohan, D. and Singh, K.P., (2002). Single- and multi-component adsorption of cadmium and zinc using activated carbon derived from bagasse—an agricultural waste. *Water Research*, **36**, 2304-2318.

143. Mohan, S.V., Ramanaiah, S.V., Rajkumar, B. and Sarma, P.N., (2007). Removal of fluoride from aqueous phase by biosorption onto algal biosorbent *Spirogyra* sp.-IO2: Sorption mechanism elucidation. *Journal of Hazardous Materials*, **141**, (3), 465-474.

144. Mohan, S.V., Ramanaiah, S.V. and Sarma, P.N., (2008). Biosorption of direct azo dye from aqueous phase onto *Spirogyra* sp. I02: Evaluation of kinetics and mechanistic aspects. *Biochemical Engineering Journal,* **38**, (1), 61-69.

145. Moreira, S.M., Moreira-Santos, M., Guilhermino, L. and Ribeiro, R., (2006). Immobilization of the marine mircoalga *Phaeodactylum tricornutum* in alginate for in situ experiments: Bead stability and suitbility. *Enzyme and Microbial Technology,* **38**, 135-141.

146. Murphy, V., Hughes, H. and McLoughlin, P., (2007). Cu(II) binding by dried biomass of red, green and brown macroalgae. *Water Research*, **41**, (4), 731.

147. Mutlu, M., Sağ, Y. and Kutsal, T., (1997). The adsorption of copper(II) by *Z. ramigera* immobilized on Ca-alginate in packed bed column: a dynamic approach by stimulus-response technique and evaluation of adsorption data by moment analysis. *The Chemical Engineering Journal*, **65**, 81-86.

148. Naddafi, K., Nabizadeh, R., Saeedi, R., Mahvi, A.H., Vaezi, F., Yaghmaeian, K., Ghasri, A. and Nazmara, S., (2007). Biosorption of lead(II) and cadmium(II) by protonated *Sargassum glaucescens* biomass in a continuous packed bed column. *Journal of Hazardous Materials*, **147**, (3), 785-791.

149. Naja, G. and Volesky, B., (2006). Multi-metal biosorption in a fixed-bed flow-through column. *Colloids and Surfaces A: Physicochemical and Engineering Aspects,* **281**, (1-3), 194-201.

150. Namasivayam, C. and Sangeetha, D., (2006). Recycling of agricultural solid waste, coir pith: Removal of anions, heavy metals, organics and dyes from water by adsorption onto ZnCl2 activated coir pith carbon. *Journal of Hazardous Materials,* **135,** 449-452.

151. Nestle, N. and Kimmich, R., (1996). Heavy metal uptake of alginate gels studied by NMR microscopy. *Colloids Surface A: Physicochemical Engineering Aspects,* **115,** (30), 141-147.

152. Nichols, R.J., Beckmann, W. and Meyer, H., (1992). An in situ scanning tunnelling microscopy study of bulk copper deposition and the influence of an organic additve. *Journal of Electroanalytical Chemistry*, **330**, 381-394.

153. Nikolić, N.D., Popov, K.I., Pavlović, L.J. and Pavlović, M.G., (2006). Morphologies of copper deposits obtained by the electrodeposition at high overpotentials. *Surface and Coatings Technology*, **201**, 560-566.

154. Oliveira, W.E., Franca, A.S., Oliveira, L.S. and Rocha, S.D., (2008). Untreated coffee husks as biosorbents for the removal of heavy metals from aqueous solutions. *Journal of Hazardous Materials*, **152**, (3), 1073-1081.

155. Önal, S., Baysal, Ş.H. and Ozdemir, G., (2007). Studies on the applicability of alginate-entrapped *Chryseomonas luteola* TEM 05 for heavy metal biosorption. *Journal of Hazardous Materials*, **146**, (1-2), 417-420.

156. Padmavathy, V., Vasudevan, P. and Dhingra, S.C., (2003). Thermal and spectroscopic studies on sorption of nickel(II) ions on protonated baker's yeast. *Chemosphere*, **52**, 1807-1817.

157. Pagnanelli, F., Trifoni, M., Beolchini, F., Esposito, A., Toro, L. and Vegliò, F., (2001). Equilibrium biosorption studies in single and multi-metal systems. *Process Biochemistry*, **37**, (2), 115-124.

158. Pamukoglu, M.Y. and Kargi, F., (2006). Batch kinetics and isotherms for biosorption of copper(II) ions onto pre-treated powdered waste sludge (PWS). *Journal of Hazardous Materials*, **138,** (3), 479-484.

159. Pan, J., Ge, X., Liu, R. and Tang, H., (2006). Characteristic features of *Bacillus cereus* cell surfaces with biosorption of Pb(II) ion by AFM and FT-IR. *Colloids and Surfaces B: Biointerfaces*, **52**, 89-95.

160. Park, H.G., Kim, T.W., Chae, M.Y. and Yoo, I., (2007). Activated carbon-containing alginate adsorbent for the simultaneous removal of heavy metals and toxic organics. *Process Biochemistry*, **42**, (10), 1371-1377.

161. Pavez, J., Silva, J.F. and Melo, F., (2005). Effects of alginic acid from marine algae on calcium carbonate electrodeposited coating. *Journal of Crystal Growth*, **282**, (3-4), 438-447.

162. Peter, J., Hutter, W., Stöllnberger, W. and Hampel, W., (1996). Detection of chlorinated and brominated hydrocarbons by an ion sensitive whole cell biosensor. *Biosensors and Bioelectronics*, **11**, (12), 1215-1219.

163. Pletcher, D. and Walsh, F.C., (1990). Chapter 8, Metal finishing. *Industrial Electrochemistry*, 2nd ed., Chapman and Hall, New York, 385-449.

164. Pradhan, S., Singh, S. and Rai, L.C., (2007). Characterization of various functional groups present in the capsule of *Microcystis* and study of their role in biosorption of Fe, Ni and Cr. *Bioresource Technology*, **98**, (3), 595-601.

165. Preetha, B. and Viruthagiri, T., (2007). Batch and continuous biosorption of chromium(VI) by *Rhizopus arrhizus*. *Separation and Purification Technology*, **57**, (1), 126-133.

166. Quintelas, C., Fernandes, B., Castro, J., Figueiredo, H. and Tavares, T., (2008). Biosorption of Cr(VI) by a *Bacillus coagulans* biofilm supported on granular activated carbon (GAC). *Chemical Engineering Journal*, **136**, (2-3), 195-203.

167. Rangsayatorn, N., Pokethitiyook, P., Upatham, E.S., and Lanza, G.R., (2004). Cadmium biosorption by cells of *Spirulina platensis* TISTR 8217 immobilized in alginate and silica gel. *Environmental International*, **30**, 57-63.

168. Rao, M.M., Rao, G.P.C., Seshaiah, K., Choudary, N.V. and Wang, M.C., (2008). Activated carbon from *Ceiba pentandra* hulls, an agricultural waste, as an adsorbent in the removal of lead and zinc from aqueous solutions. *Waste Management*, **28**, (5), 849-858.

169. Reddad, Z., Gerente, C., Andres, Y. and Cloire, L.P., (2002). Adsorption of several metal ions onto a low-cost biosorbent: kinetic and equilibrium studies. *Environmental Science and Technology*, **36**, 2067-2073.

170. Rehim, S.S.A.E., Sayyah, S.M. and Deeb, M.M.E., (2000). Electroplating of copper films on steel substrates from acidic gluconate baths. *Applied Surface Science*, **165**, 249-254.

171. Romera, E., González, F., Ballester, A., Blázquez, M.L. and Muñoz, J.A., (2007). Comparative study of biosorption of heavy metals using different types of algae. *Bioresource Technology*, **98**, (17), 3344-3353.

172. Saeed, A., Iqbal, M. and Akhtar, M.W., (2005). Removal and recovery of lead(II) from single and multimetal (Cd, Cu, Ni, Zn) solutions by crop milling waste (black gram husk). *Journal of Hazardous Materials*, **117**, (1), 65-73.

173. Safranek, W.H., (1986). Chapter 7, Copper. *The Properties of Electrodeposited Metals and Alloys*, 2nd ed., American Elsevier Publishing Co., Inc., New York, 99-140.

174. Sağ Y. and Aktay, Y. (2001). Application of equilibrium and mass transfer models to dynamic removal of Cr(VI) ions by chitin in packed column reactor. *Process Biochemistry*, **36**, 1187-1197.

175. Şahin, Y. and Öztürk, A., (2005). Biosorption of chromium(IV) ions from aqueous solution by the bacterium *Bacillus thuringiensis*. *Process Biochemistry*, **40**, 1895-1901.

176. Sakurai, A. and Sakakibara, M., (1999). Production of 4,5-dihydroxyphthalate by *Pseudomonas testosteroni* immobilized in alginate gel beads. *Biochemical Engineering Journal*, **3**, (3), 235-238.

177. Sankararamakrishnan, N., Sharma, A.K. and Sanghi, R., (2007). Novel chitosan derivative for the removal of cadmium in the presence of cyanide from electroplating wastewater. *Journal of Hazardous Materials*, **148**, (1-2), 353-359.

178. Santos, S., Machado, R., Correia, M.J.N. and Carvalho, J.R., (2004). Treatment of acid mining waters. *Minerals Engineering*, **17**, (2), 225-232.

179. Sawalha, M.F., Peralta-Videa, J.R., Romero-González, J. and Gardea-Torresdey, J.L., (2006). Biosorption of Cd(II), Cr(III), and Cr(VI) by saltbush (*Atriplex canescens*) biomass: Thermodynamic and isotherm studies. *Journal of Colloid and Interface Science*, **300**, (1), 100-104.

180. Schecher, W.D. and McAvoy, D.C., (1994). *MINEQL$^+$: A Chemical Equilibrium Program for Person Computers, version 3.0*. Environmental Research Software, Hallowell, Maine.

181. Šćiban, M., Klašnja, M. and Škrbić, B., (2006). Modified softwood sawdust as adsorbent of heavy metal ions from water. *Journal of Hazardous Materials*, **136**, (2), 266-271.

182. Selatnia, A., Madani, A., Bakhti, A.Z., Kertous, L., Mansouri, Y. and You, R., (2004). Biosorption of Ni^{2+} from aqueous solution by a NaOH-treated bacterial dead *Streptomyces rimosus* biomass. *Minerals Engineering*, **17**, (7-8), 903-911.

183. Sharma, D.C. and Forster, C.F., (1995). Column studies into the adsorption of chromium(VI) using *Sphagnum* moss peat. *Bioresource Technology*, **52**, 261-267.

184. Sheng, P.X., Ting, Y., Chen, J.P. and Hong, L., (2004). Sorption of lead, copper, cadmium, zinc, and nickel by marine algal biomass: characterization of biosorptive capacity and investigation of mechanisms. *Journal of Colloid and Interface Science*, **275**, (1), 131-141.

185. Sheng, P.X., Wee, K.H., Ting, Y.P. and Chen, J.P., (2008). Biosorption of copper by immobilized marine algal biomass. *Chemical Engineering Journal*, **136**, (2-3), 156-163.

186. Silman, H., Isserlis, G. and Averill, A.F., (1978). Chapter 8, Copper and brass plating. *Protective and Decorative Coatings for Metals*, Finishing Publications Ltd., UK, 301-322.

187. Simmons, P. and Singleton, I., (1996). A method to increase silver biosorption by an industrial strain of *Saccharomyces cerevisiae*. *Applied Microbiology and Biotechnology*, **45**, 278-285.

188. Sing, C. and Yu, J., (1998). Copper adsorption and removal from water by living mycelium of white-rot fungus *Phanerochaete chrysosporium*. *Water Research*, **32**, (9), 2746-2752.

189. Skoog, D.A., Holler, F.J. and Nieman, T.A., (1998). *Principles of Instrumental Analysis*, 5th ed., Harcourt Brace College Publishers, Florida.

190. Skountzou, P., Soupioni, M., Bekatorou, A., Kanellaki, M., Koutinas, A.A., Marchant, R. and Banat, I.M., (2003). Lead(II) uptake during baker's yeast production by aerobic fermentation of molasses. *Process Biochemistry*, **38**, (10), 1479-1482.

191. Slejko, F.L., (1985). *Adsorption technology: A Step-by-Step Approach to Process Evaluation and Application*, Marcel Dekker, Inc., New York, USA.

192. Smidsrød, O. and Skjåk-Bræk, G., (1990). Alginate as immobilization matrix for cells. *Trends in Biotechnology*, **8**, 71-78.

193. Southichak, B., Nakano, K., Nomura, M., Chiba, N. and Nishimura, O., (2006). *Phragmites australis*: A novel biosorbent for the removal of heavy metals from aqueous solution. *Water Research*, **40**, (12), 2295-2302.

194. Srikrajib, S., Tongta, A., Thiravetyan, P. and Sivaborvorn, K., (1999). Cadmium removal by the dry biomass of *Sargassum polycystum*. *Process Metallurgy*, **9**, (2), 419-427.

195. Stokke, B., Smidsrød, O, Bruheim, P. and Skjåk-Bræk, G., (1991). Distribution of urinate residues in alginate chains in relation to alginate gelling properties. *Macromolecules*, **24**, 4637-4645.

196. Strandbergy, G.W., Shumate II, S.E. and Pattott, J.R., (1985). Microbial cells as biosorbents for heavy metals: Accumulations of uranium by *Saccharomyces cerevisiae* and *Pseudomonas aeruginosa*. *Applied and Environmental Microbiology*, **41**, 237-245.

197. Subramanian, K. and Nageswar, S., (1980). The electrodeposition of copper onto a copper single-crystal (111) plane in the presence of sulphaguanidine. *Surface Technology*, **10**, (1), 7-12.

198. Tanaka, H. and Irie, S., (1988). Preparation of stable alginate gel beads in electrolyte solutions using Ba^{2+} and Sr^{2+}. *Biotechnology Technique*, **2**, (2), 115-120.

199. Texier, A.C., Andrès, Y., Faur-Brasquet, C. and Le Cloirec, P., (2002). Fixed-bed study for lanthanide (La, Eu, Yb) ions removal from aqueous solutions by immobilized *Pseudomonas aeruginosa*: experimental data and modelization. *Chemosphere*, **47**, 333-342.

200. Think & Tinker Ltd., (2007). *Hull Cell Analysis of Acid Copper Plating Baths*. Retrieved January 24, 2007, from http://www.thinktink.com/stack/volumes/volvi/hullcell.htm.

201. Thomas, A.D., Volesky, B. and Mucci, A., (2003). A review of the biochemistry of heavy metal biosorption by brown algae. *Water Research*, **37**, 4311-4330.

202. Thomas, H.C., (1944). Heterogeneous ion exchange in a flowing system. *Journal of American Chemistry Society*, **66**, 1664-1666.

203. Thomas, H.C., (1948). Chromatography: a problem in kinetics. *Annals of the New York Academy of Sciences*, **49**, 161-182.

204. Thornton *et al*., (2000). *Scanning Probe Microscopy Training Notebook, Version 3.0*. Digital Instruments, Veeco Metrology Group.

205. Tien, C., (1994). Chapter 5, Adsorbent transport: its adsorption and rates. In Tien, C. eds., *Adsorption Calculation and Modeling*, Butterworth-Heinemann, 71-86.

206. Tiwari, D., Kim, H. and Lee, S., (2007). Removal behavior of sericite for Cu(II) and Pb(II) from aqueous solutions: Batch and column studies. *Separation and Purification Technology*, **57**, (1), 11-16.

207. Tobin, J.M. and Roux, J.C., (1998). *Mucor* biosorbent for chromium removal from tanning effluent. *Water Research*, **32**, (5), 1407-1416.

208. Torres, M.R., Sousa, A.P.A., Filho, E.A.T.S., Melo, D.F., Feitosa, J.P.A., de Paula, R.C.M. and Lima, M.G.S., (2007). Extraction and physicochemical characterization of *Sargassum vulgare* alginate from Brazil. *Carbohydrate Research*, **342**, (14), 2067-2074.

209. Trelles, J.A., Fernández-Lucas, J., Condezo, L.A. and Sinisterra, J.V., (2004). Nucleoside synthesis by immobilised bacterial whole cells. *Journal of Molecular Catalysis B: Enzymatic*, **30**, (5-6), 219-227.

210. Trimukhe, K.D. and Varma, A.J., (2008). A morphological study of heavy metal complexes of chitosan and crosslinked chitosans by SEM and WAXRD. *Carbohydrate Polymers*, **71**, (4), 698-702.

211. Tripler, A.B., (1974). Appendix. In Lowenheim, F.A., ed., *Modern Electroplating, 3rd ed*, John Wiley and Sons, Inc., New York, 777.

212. Tsai, W.T., Chang, C.Y., Ho, C.Y. and Chen, L.Y., (1999). Simplified description of adsorption breakthrough curves of 1,1-dichloro-1-fluoroethane (HCFC-141b) on activated carbon with temperature effect. *Journal of Colloid and Interface Science*, **214**, (2), 455-458.

213. Valdman, E., Erijman, L., Pessoa, F.L.P. and Leite, S.G.F., (2001). Continuous biosorption of Cu and Zn by immobilized waste biomass *Sargassum* sp. *Process Biochemistry*, **36**, 869-873.

214. Vas'ko, V.A., Tabakovic, I., Riemer, S.C. and Kief, M.T., (2004). Effect of organic additives on structure, resistivity, and room-temperature recrystallization of electrodeposited copper. *Microelectronic Engineering*, **75**, (1), 71-77.

215. Vaughan, T., Seo, C.W. and Marshall, W.E., (2001). Removal of selected metal ions from aqueous solution using modified corncobs. *Bioresource Technology*, **78**, 133-139.

216. Veglio', F. and Beolchini, F., (1997). Removal of metals by biosorption: a review. *Hydrometallurgy*, **44**, 301-316.

217. Veglio', F., Esposito, A. and Reverberi, A.P., (2002). Copper adsorption on calcium alginate beads: equilibrium pH-related models. *Hydrometallurgy*, **65**, 43-57.

218. Vijayaraghavan, K., Han, M.H., Choi, S.B. and Yun, Y., (2007). Biosorption of Reactive black 5 by *Corynebacterium glutamicum* biomass immobilized in alginate and polysulfone matrices. *Chemosphere*, **68**, (10), 1838-1845.

219. Vijayaraghavan, K., Jegan, J., Palanivelu, K. and Velan, M., (2005a). Batch and column removal of copper from aqueous solution using a brown marine alga *Turbinaria ornate*. *Chemical Engineering Journal*, **106**, (2), 177-184.

220. Vijayaraghavan, K., Jegan, J., Palanivelu, K. and Velan, M., (2005b). Biosorption of copper, cobalt and nickel by marine green alga *Ulva reticulata* in a packed column. *Chemosphere*, **60**, (3), 419-426.

221. Vijayaraghavan, K., Palanivelu, K. and Velan, M., (2005c). Crab shell-based biosorption technology for the treatment of nickel-bearing electroplating industrial effluents. *Journal of Hazardous Materials*, **119**, (1-3), 251-254.

222. Vijayaraghavan, K., Palanivelu, K. and Velan, M., (2006). Biosorption of copper(II) and cobalt(II) from aqueous solutions by crab shell particles. *Bioresource Technology*, **97**, (12), 1411-1419.

223. Vijayaraghavan, K. and Prabu, D., (2006). Potential of *Sargassum wightii* biomass for copper(II) removal from aqueous solutions: Application of different mathematical models to batch and continuous biosorption data. *Journal of Hazardous Materials*, **137**, (1), 558-564.

224. Volesky, B., (1987). Biosorbent for metal recovery. *Trends In Biotechnology*, **5**, 96-101.

225. Volesky, B., (2001). Detoxification of metal-bearing effluents: biosorption for the next century. *Hydrometallurgy*, **59**, 203-216.

226. Volesky, B., (2003). *Sorption and Biosorption*, BV Sorbex Inc., Montreal – St. Lambert, Que., Canada.

227. Volesky, B. and Holan, Z.R., (1995). Biosorption of heavy metals. *Biotechnology Progress*. **11**, 235-250.

228. Volesky, B., Weber, J. and Park, J.M., (2003). Continuous-flow metal biosorption in a regenerable *Sargassum* column. *Water Research*, **37**, (2), 297-306.

229. Wang, J., (2002). Biosorption of copper(II) by chemically modified biomass of *Saccharomyces cerevisiae*. *Process Biochemistry*, **37**, 847-850.

230. Wang, Y., Chang, H., Wertheim, D.F., Jones, A.S., Jackson, C. and Coombes, A.G.A., (2007). Characterisation of the macroporosity of polycaprolactone-based biocomposites and release kinetics for drug delivery. *Biomaterials*, **28**, (31), 4619-4627.

231. West, P., (2007). *Introduction to Atomic Force Microscopy: Theory, Practice and Applications*. From http://www.AFMUniversity.org/

232. Wilson, K., Yang, H., Seo, C.W. and Marshall, W.E., (2006). Select metal adsorption by activated carbon made from peanut shells. *Bioresource Technology*, **97**, 2266-2270.

233. Wong, M.F., (2001). *Removal and Recovery of Copper(II) ions from Industrial Wastewater by Bacteria Isolated from Activated Sludge*. MPhil thesis, Department of Civil and Structural Engineering, The Hong Kong Polytechnic University, Hong Kong SAR.

234. World Health Organization (WHO), (2003). *Zinc in Drinking-water*, World Health Organization, Geneva.

235. World Health Organization (WHO), (2004). *Copper in Drinking-water*, World Health Organization, Geneva.

236. World Health Organization (WHO), (2005). *Nickel in Drinking-water*, World Health Organization, Geneva.

237. Wright, M.R., (2004). Chapter 3, The Kinetic Analysis of Experimental Data. *An Introduction to Chemical Kinetics*, John Wiley and Sons Ltd., England, 43-98.

238. Wu, J. and Yu, H., (2008). Biosorption of 2,4-dichlorophenol from aqueous solutions by immobilized *Phanerochaete chrysosporium* biomass in a fixed-bed column. *Chemical Engineering Journal*, **138**, (1-3), 128-135.

239. Yan, G. and Virarghavan, T., (2001). Heavy metal removal in a biosorption column by immobilized *M. rouxii* biomass. *Bioresource Technology*, **78**, 243-249.

240. Yetis, U., Dolek, A., Dilek, F.B. and Ozcengiz, G., (2000). The removal of Pb(II) by *Phanerochaete chrysosporium*. *Water Research*, **34**, (16), 4090-4100.

241. Yin, H., He, B., Peng, H., Ye, J., Yang, F. and Zhang, N., (2008). Removal of Cr(VI) and Ni(II) from aqueous solution by fused yeast: study of cation release and biosorption mechanism. *Journal of Hazardous Materials*, **158**, 568-576.

242. Yoon, Y.H. and Nelson, J.H., (1984). Application of gas adsorption kinetics I. A theoretical model for respirator cartridge service life. *American Industrial Hygiene Association Journal*, **45**, (8), 509-516.

243. Zainal, Z., Kassim, A., Hussein, M.Z. and Ching, C.H., (2004). Effect of bath temperature on the electrodeposition of copper tin selenide films from aqueous solution. *Materials Letters*, **58**, (16), 2199-2202.

244. Zhang, Y. and Banks, C., (2006). A comparison of the properties of polyurethane immobilised *Sphagnum* moss, seaweed, sunflower waste and maize for the biosorption of Cu, Pb, Zn and Ni in continuous flow packed columns. *Water Research*, **40**, (4), 788-798.

245. Zhao, Y., Qian, Y., Pang, D., Zhu, B. and Xu, Y., (2007). Porous membranes modified by hyperbranched polymers II: Effect of the arm length of amphiphilic hyperbranched-star polymers on the hydrophilicity and protein resistance of poly(vinylidene fluoride) membranes. *Journal of Membrane Science*, **304**, (1-2), 138-147.

246. Zhou, D., Zhang, L. and Guo, S., (2005). Mechanisms of lead biosorption on cellulose/chitin beads. *Water Research*, **39**, (16), 3755-3762.

247. Zhu, C., Luan, Z., Wang, Y. and Shan, X., (2007). Removal of cadmium from aqueous solutions by adsorption on granular red mud (GRM). *Separation and Purification Technology*, **57**, (1), 161-169.

248. Ziagova, M., Dimitriadis, G., Aslanidou, D., Papaioannou, X., Tzannetaki, E.L. and Liakopoulou-Kyriakides, M., (2007). Comparative study of Cd(II) and Cr(VI) biosorption on *Staphylococcus xylosus* and *Pseudomonas* sp. in single and binary mixtures. *Bioresource Technology*, **98**, (15), 2859-2865.

249. Zouboulis, A.I., Matis, K.A., Loukidou, M. and Sebesta, F., (2003). Metal biosorption by PAN-immobilized fungal biomass in simulated wastewaters. *Colloids Surface A: Physicochemical Engineering Aspects*, **212**, 185-195.

250 Zulfadhly, Z., Mashitah, M.D. and Bhatia, S., (2001). Heavy metals removal in fixed-bed column by the macro fungus *Pycnoporus sanguineus*. *Environmental Pollution*, **112**, (3), 463-470.